

University of Windsor

Scholarship at UWindor

Electronic Theses and Dissertations

Theses, Dissertations, and Major Papers

2016

HEAT TRANSFER IN SQUEEZE CASTING OF LIGHT ALLOYS

Xuezhi Zhang

University of Windsor

Follow this and additional works at: <https://scholar.uwindsor.ca/etd>

Recommended Citation

Zhang, Xuezhi, "HEAT TRANSFER IN SQUEEZE CASTING OF LIGHT ALLOYS" (2016). *Electronic Theses and Dissertations*. 5878.

<https://scholar.uwindsor.ca/etd/5878>

This online database contains the full-text of PhD dissertations and Masters' theses of University of Windsor students from 1954 forward. These documents are made available for personal study and research purposes only, in accordance with the Canadian Copyright Act and the Creative Commons license—CC BY-NC-ND (Attribution, Non-Commercial, No Derivative Works). Under this license, works must always be attributed to the copyright holder (original author), cannot be used for any commercial purposes, and may not be altered. Any other use would require the permission of the copyright holder. Students may inquire about withdrawing their dissertation and/or thesis from this database. For additional inquiries, please contact the repository administrator via email (scholarship@uwindsor.ca) or by telephone at 519-253-3000ext. 3208.

HEAT TRANSFER IN SQUEEZE CASTING OF LIGHT ALLOYS

By

Xuezhi Zhang

A Dissertation

Submitted to the Faculty of Graduate Studies

through the Department of Mechanical, Automotive & Materials Engineering

in Partial Fulfillment of the Requirements for

the Degree of Doctor of Philosophy

at the University of Windsor

Windsor, Ontario, Canada

2016

© 2016 Xuezhi Zhang

HEAT TRANSFER IN SQUEEZE CASTING OF LIGHT ALLOYS

By

Xuezhi Zhang

APPROVED BY:

D. Chen, External Examiner

Department of Mechanical and Industrial Engineering, Ryerson University

A. Fartaj

Department of Mechanical, Automotive & Materials Engineering

R. Bowers

Department of Mechanical, Automotive & Materials Engineering

X. Nie

Department of Mechanical, Automotive & Materials Engineering

H. Hu, Advisor

Department of Mechanical, Automotive & Materials Engineering

6 May 2016

DECLARATION OF CO-AUTHORSHIP/PREVIOUS PUBLICATION

I. CO-AUTHORSHIP DECLARATION

I hereby declare that this dissertation incorporates material that is result of joint research. In all cases, the key ideas, primary contributions, experimental designs, data analysis and interpretation, were performed by the author and Dr. H. Hu as advisor, and the contribution of co-authors in Chapters 3 to 9 was primarily through the provision of experiment preparations. I certify that, with the above qualification, this dissertation, and the research to which it refers, is the product of my own work.

I am aware of the University of Windsor Senate Policy on Authorship and I certify that I have properly acknowledged the contribution of other researchers to my thesis, and have obtained written permission from each of the co-authors to include the above material(s) in my thesis.

II. DECLARATION OF PREVIOUS PUBLICATION

This dissertation includes seven original papers that have been previously published/submitted for publication in peer reviewed journals/conference proceedings, as follows:

CHAPTER 3	Xuezhi Zhang , Alfred Yu and Henry Hu. (2014). Characterization of Local Cavity Pressures in Squeeze Casting of Magnesium Alloy AM50. <i>Advanced Materials Research</i> . 936: 1666-1670.	Published
CHAPTER 4	Xuezhi Zhang , Li Fang and Henry Hu. (2016). Solidification and Microstructure Refining Phenomena of Squeeze Cast Mg Alloy AJ62. <i>Material Science Forum</i> .	Accepted
CHAPTER 5	Xuezhi Zhang , Li Fang, Bojun Xiong, Henry Hu, Xueyuan Nie, and Jimi Tjong. (2015). Determination of Heat Transfer Coefficients by Energy Balance Method in Squeeze Casting of Magnesium Alloy AJ62 with Variation in Wall Thicknesses. <i>Proceedings of Mg 2015. The 10th</i>	Published

	<i>International Conference on Magnesium Alloys and Their Applications</i> , Jeju, Korea, Republic of, 2015-10-13 (569-575).	
CHAPTER 6	Xuezhi Zhang , Li Fang and Henry Hu. (2015). Interfacial Heat Transfer of Squeeze Casting of Wrought Aluminum Alloy 5083 with Variation in Wall Thicknesses. <i>Journal of Advances in Materials and Processing Technologies</i> .	Accepted
CHAPTER 7	Xuezhi Zhang , Li Fang, Zhizhong Sun, Henry Hu. (2015). Interfacial Heat Transfer in Squeeze Casting of Magnesium Alloy AM60 with Variation of Applied Pressures and Casting Wall-thicknesses. <i>Journal of Heat and Mass Transfer</i> . 51(1):1-13.	Published
CHAPTER 8	Xuezhi Zhang , Li Fang, Henry Hu, Xueyuan Nie, and Jimi Tjong. (2015). Estimation of Heat Transfer Coefficient in Squeeze Casting of Wrought Al Alloy 7075 by the Polynomial Curve Fitting Method. <i>Light Metals 2015. TMS 2015 144th Annual Meeting & Exhibition</i> , Orlando, United States, 2015-03-18 (257-261).	Published
CHAPTER 9	Xuezhi Zhang , Li Fang, Henry Hu, Xueyuan Nie, Jimi Tjong. (2016). Determination of metal/die interfacial heat transfer coefficients in squeeze casting of wrought aluminum alloy 7075 with variations in section thicknesses and applied pressures, <i>Journal of Heat Transfer</i> .	Submitted

I hereby certify that I have obtained a written permission from the copyright owner(s) to include the above published material(s) in my dissertation. I certify that the above material describes work completed during my registration as graduate student at the University of Windsor.

I declare that, to the best of my knowledge, my dissertation does not infringe upon anyone's copyright nor violate any proprietary rights and that any ideas, techniques, quotations, or any other material from the work of other people included in my dissertation, published or otherwise, are fully acknowledged in accordance with the standard referencing practices. Furthermore, to the extent that I have included copyrighted material that surpasses the bounds of fair dealing within the meaning of the Canada Copyright Act, I certify that I have

obtained a permission from the copyright owner(s) to include such material(s) in my dissertation.

I declare that this is a true copy of my dissertation, including any final revisions, as approved by my dissertation committee and the Graduate Studies office, and that this dissertation has not been submitted for a higher degree to any other University or Institution.

ABSTRACT

In automotive industry, the weight reduction in vehicles can be achieved by using new designed lighter engineering materials such as aluminum or magnesium alloys. To maintain the same performance as reducing the weight of the vehicles, high strength material has to be used. This study was aimed to develop a solution for casting high strength wrought aluminum alloys and magnesium alloys. Some critical process parameters need to be precisely pre-determined. The interfacial heat transfer coefficient is one of the most important factor.

At beginning of this study, an experiment has been carried out to characterize the pressure distribution in the die cavity during squeeze casting of magnesium alloy AM50. This experiment aimed to reveal the changes of pressure distribution with the cavity geometry as well as the local cavity pressure at various locations during the solidification process. To understand the solidification and microstructure refining phenomena, squeeze casting of magnesium alloy AJ62 were performed under an applied pressure 60 MPa by using the simple cylindrical mold.

A more complex shape casting mold with five different section thicknesses (2, 4, 8, 12 and 20 mm) was then developed. Wrought aluminum alloys 5083, 7075 and magnesium alloy AM60, AJ62 were squeeze casted under different applied pressures of 30, 60 and 90 MPa. With measured temperature, heat fluxes and interfacial heat transfer coefficients were determined using the inverse method. By observing the IHTC versus time curve profiles, the IHTC peak values of each step were found to increase accordingly as the applied pressure increased. In comparison with the thinner steps, the relatively thicker steps

attained higher heat fluxes IHTCs values due to high local pressures and high melt temperature.

Finally, the empirical equation relating IHTCs to the local pressures and solidification temperature at the casting surface were derived for wrought aluminum alloy 7075 and magnesium alloy AM60. For magnesium alloy AM60, the calculated IHTC values by using the inverse method were integrated into the casting simulation software (MAGMASoft) to simulate the solidification process of the 5-step casting. The results indicated that the numerical calculated temperatures were in good agreement with the experimental measured temperatures.

DEDICATION

I would like to dedicate this dissertation to my parents for their unconditional love, support and encouragement.

I also would like to thank my wife, and my daughter. Their love and support enable me to go through the difficult time and finally complete this dissertation.

ACKNOWLEDGEMENTS

This study could not have been done without the financial support from the Natural Sciences and Engineering Research Council of Canada (NSERC), and Ontario Centre of Excellence (OCE).

I would like to thank my doctoral advisor, Dr. Henry Hu, for his valuable suggestions and excellent supervision of this research work during my study.

Many thanks to my committee members (Dr. A. Fartaj, Dr. R. Bowers and Dr. X. Nie) for their helpful comments and careful review of this work.

I would like to thank Mr. Andy Jenner, Mr. Li Fang, Mr. Junxiang Zhou, from University of Windsor for their assistance with the experiments.

Finally, I am thankful to the faculty, staff and graduate students at the Department of Mechanical, Automotive and Materials Engineering of the University of Windsor, particularly my colleagues in the Light Metals Casting lab, for their support and encouragement.

TABLE OF CONTENTS

DECLARATION OF CO-AUTHORSHIP/PREVIOUS PUBLICATION	III
ABSTRACT	VI
DEDICATION	VIII
ACKNOWLEDGEMENTS	IX
LIST OF TABLES	XVIII
LIST OF FIGURES	XIX
NOMENCLATURE	XXVI
CHAPTER 1	1
1. INTRODUCTION.....	1
2. OBJECTIVES	5
3. DISSERTATION OUTLINE	5
REFERENCES	9
CHAPTER 2	10
LITERATURE REVIEW	10
1. WROUGHT ALUMINUM ALLOYS	10
2. PROCESSING OF WROUGHT ALUMINUM ALLOYS.....	12
3. HEAT TRANSFER IN SQUEEZE CASTING.....	15
4. INTERFACIAL HEAT TRANSFER COEFFICIENT	17

4.1 Analytical interfacial heat transfer	19
4.2 Numerical analysis of interfacial heat transfer	21
4.3 Interfacial heat transfer from various casting experiments	22
5. MATHEMATICAL MODELLING	25
5.1 Direct problem.....	25
5.2 Inverse problem	26
6. SUMMARY	28
REFERENCE	29
CHAPTER 3	34
CHARACTERIZATION OF LOCAL CAVITY PRESSURES IN SQUEEZE	
CASTING OF MAGNESIUM ALLOY AM50	34
1. INTRODUCTION.....	35
2. THEORETICAL CONSIDERATIONS	36
2.1 Thermal Contraction.....	36
2.2 Hydrostatic deformation	37
2.3 Plastic Deformation	37
2.4 Elastic Deformation.....	38
2.5 Friction between casting and the mold	39
3. EXPERIMENTAL SETUP AND PROCEDURES	41
4. RESULTS AND DISCUSSIONS	44

4.1 Pressure distribution on the surface of a cylindrical casting	44
4.2 Pressure distribution change with time.....	46
4.3 Variation of Pressure Transfer Rate and Temperature	48
4.4 Pressure variation in different die cavity configurations.....	49
5. CONCLUSIONS	50
REFERENCES.....	52
CHAPTER 4.....	54
A STUDY OF SOLIDIFICATION AND MICROSTRUCTURE REFINING PHENOMENA OF SQUEEZE CAST MAGNESIUM ALLOY AJ62 WITH VARIATION IN APPLIED PRESSRUES	54
1. INTRODUCTION.....	54
2. EXPERIMENTAL PROCEDURES	56
2.1 Material.....	56
2.2 Squeeze casting.....	57
3. RESULTS AND DISCUSSION	58
3.1 Effect of applied pressure on liquidus and solidus temperature	58
3.2 Pressure loss during solidification.....	62
3.3 Effect of applied pressure on microstructure.....	63
4. CONCLUSIONS	66
REFERENCES.....	68

CHAPTER 5	70
DETERMINATION OF HEAT TRANSFER COEFFICIENTS BY ENERGY	
BALANCE METHOD IN SQUEEZE CASTING OF MAGNESIUM ALLOY AJ62	
WITH VARIATION IN WALL THICKNESSES	70
1. INTRODUCTION.....	70
2. EXPERIMENTAL PROCEDURE.....	71
2.1 Experimental setup and sensor installation	71
3.2 Casting Process.....	74
3.3 Determination of IHTC	76
4. RESULTS AND DISCUSSION	77
4.1 Experimental cooling curve.....	77
4.2 Heat flux (q) and IHTC (h) curves	79
5. CONCLUSIONS	82
REFERENCES.....	84
CHAPTER 6	86
INTERFACIAL HEAT TRANSFER OF SQUEEZE CASTING OF WROUGHT	
ALUMINUM ALLOY 5083 WITH VARIATION IN WALL THICKNESSES	
1. INTRODUCTION.....	86
2. EXPERIMENTAL PROCEDURE.....	89
2.1 Material and squeeze casting.....	89

2.2 Experimental measurements of temperatures and pressures	90
2.3 Inverse algorithm for the IHTC	92
3. RESULTS AND DISCUSSIONS	96
4. CONCLUSIONS	102
REFERENCES	103
CHAPTER 7	105
INTERFACIAL HEAT TRANSFER IN SQUEEZE CASTING OF MAGNESIUM ALLOY AM60 WITH VARIATION OF APPLIED PRESSURES AND CASTING WALL-THICKNESSES	105
1. INTRODUCTION.....	105
2. EXPERIMENTAL DESIGN.....	109
3. INVERSE ALGORITHM FOR THE IHTC	114
4. NUMERICAL SIMULATION FOR IHTC VERIFICATION	115
5. RESULTS AND DISCUSSION	118
5.1 Pressure Effect on IHTCs	118
5.2 Effect of Casting Wall Thicknesses on IHTCs.....	123
5.3 IHTC Empirical Equations	125
5.4 IHTC Verification.....	127
6. CONCLUSIONS	132
REFERENCES	134

CHAPTER 8.....	137
ESTIMATION OF HEAT TRANSFER COEFFICIENT IN SQUEEZE CASTING	
OF WROUGHT ALUMINUM ALLOY 7075 BY THE POLYNOMIAL CURVE	
FITTING METHOD	137
1. INTRODUCTION.....	137
2. EXPERIMENTAL PROCEDURES	140
2.1 Die Design.....	140
2.2 Casting Process.....	142
2.3 Heat Transfer Model.....	143
2.4 Polynomial Curve Fitting	145
3. RESULTS AND DISCUSSION	147
3.1 Cooling curves.....	147
3.2 Heat Flux and IHTC Curves.....	148
4. CONCLUSION	152
REFERENCES.....	153
CHAPTER 9	155
DETERMINATION OF METAL/DIE INTERFACIAL HEAT TRANSFER	
COEFFICIENTS IN SQUEEZE CASTING OF WROUGHT ALUMINUM ALLOY	
7075 WITH VARIATIONS IN SECTION THICKNESSES AND APPLIED	
PRESSURES	155
1. INTRODUCTION.....	156

2. EXPERIMENTAL PROCEDURE.....	159
2.1 Material and squeeze casting	159
2.2 Experimental measurements of temperatures and pressures	161
3. INVERSE ALGORITHM.....	163
4. RESULTS AND DISCUSSION	169
4.1 Determination of heat fluxes and IHTCs.....	169
4.3 Application of the determined IHTCs	177
5. CONCLUSIONS	181
REFERENCES.....	183
CHAPTER 10	185
DISSERTATION CONCLUSIONS	185
CHAPTER 11	189
FUTURE WORKS.....	189
APPENDICES	190
APPENDIX A	190
COPYRIGHT RELEASES FROM PUBLICATIONS	190
APPENDIX B	204
MATLAB SOURCE CODE OF INVERSE MODELING METHOD	204
PUBLICATIONS	214
OTHER PUBLICATIONS.....	216

VITA AUCTORIS218

LIST OF TABLES

Table 2- 1: Precipitation hardening heat treatment stages. [4].....	11
Table 4- 1: Chemical composition of magnesium alloy AJ62. (wt. %).....	56
Table 4- 2: Thermal-physical parameters of magnesium alloy AJ62.	56
Table 5- 1: Thermophysical properties of magnesium alloy AJ62.	75
Table 6- 1: Chemical composition of wrought aluminum alloy 5083 (wt. %).	89
Table 6- 2: Thermal-physical parameters of wrought aluminum alloy 5083.	89
Table 7- 1: Thermophysical properties of magnesium alloy AM60.	110
Table 7- 2: Parameters for filling simulation.	116
Table 7- 3: Parameters for solidification simulation.	116
Table 7- 4: Initial and boundary conditions for simulation.	118
Table 8- 1: Thermo-physical parameters of Al 7075-T6 alloy.	140
Table 8- 2: Chemical composition of Al7075 alloy (in weight percent).	140
Table 9- 1: Chemical composition of wrought aluminum alloy 7075 (wt. %)	160
Table 9- 2: Thermal-physical parameters of wrought aluminum alloy 7075.	160

LIST OF FIGURES

Figure 2- 1: Classification of wrought aluminum alloys [1].	10
Figure 2- 2: Schematic drawing illustrate the three stages of solidification process at metal/mold interface.	13
Figure 2- 3: One dimensional wall with boundary conditions.....	25
Figure 3- 1: Scheme diagram showing the locations in which pressure transducers and thermal couples are embedded in the system, (a) top view, and (b) cross-section view. ..	41
Figure 3- 2: Initial pressure distributions on the casting surface under applied pressure of (a) 70 MPa and (b) 35 MPa.....	44
Figure 3- 3: Cooling curves at two locations in a cylindrical casting under applied pressure of 70 MPa.	45
Figure 3- 4: Local Pressure change with time on (a) the top surface, (b) side surface of a cylindrical casting under applied pressure of 70 MPa.	47
Figure 3- 5: Initial local pressure transfer rates on the top and side surfaces of a cylindrical squeeze casting of magnesium alloy AM50A.	48
Figure 3- 6: Three different cavities, (a) A1, (b) A2, (c) A3.	49
Figure 3- 7: Pressure development at the mid-side surface in different cavities under an applied pressure of 35 MPa.....	50
Figure 4- 1: Schematic diagram showing the squeeze casting and data acquisition system.	57

Figure 4- 2: schematic diagram showing the locations of pressure and temperature sensors in a cylindrical casting.	58
Figure 4- 3: Typical cooling curves of magnesium alloy AJ62 solidified under applied pressures of 0, 30, 60 and 90 MPa.	60
Figure 4- 4: Measured and calculated liquidus temperature of magnesium alloy AJ62 with variation in applied pressures.	61
Figure 4- 5: Measured local pressure curves during the solidification of magnesium alloy AJ62 under applied hydraulic pressure of 30, 60 and 90 MPa.	62
Figure 4- 6: Optical micrographs showing the grain size of the magnesium alloy AJ62 under applied hydraulic pressure of (a) 0 (b) 30 (c) 60 and (d) 90 MPa, the samples are heat treated (T4) and etched by 5% Nitric acid (HNO ₃).....	65
Figure 4- 7: Grain size measurements of the magnesium alloy AJ62 under applied pressure of 0, 30, 60 and 90 MPa.....	66
Figure 5- 1: Graphical illustrations showing a 5-step die connecting to temperature sensor units (TSUs) and a data acquisition system.	72
Figure 5- 2: Configuration of (a) a 5-step casting solid model and (b) a temperature sensor unit.	73
Figure 5- 3: (a) a 75 tons hydraulic press and (b) schematic diagram of the squeeze casting machine, 1) upper die, 2) lower die and 3) piston.	75
Figure 5- 4: Schematic drawing showing the temperature distribution at the metal/die interface.....	77

Figure 5- 5: Typical temperature versus time curves (Step 5, 60 MPa) at the metal surface and various positions inside the die (2 and 4 mm).	78
Figure 5- 6: Interfacial heat flux (q) and heat transfer coefficient (IHTC) curves for step 5 with an applied pressure of 60 MPa.	80
Figure 5- 7: Heat flux (q) curves for steps 1 to 5 estimated by the energy balance method.....	81
Figure 5- 8: Heat transfer coefficient (IHTC) curves for step 1 to step 5 estimated by the energy balance method for magnesium alloy AJ62 under an applied pressure of 60 MPa.	81
Figure 6- 1: Graphical installations of temperature sensor units (TSUs), pressure sensor units (PSUs) and data acquisition system.	91
Figure 6- 2: (a) 3-D model showing the front view, (b) side view and (c) isometric view of the 5-step casting. (d) 5-step casting solidifying under applied pressure of 60 MPa. ...	91
Figure 6- 3: Configuration of installation of the K-type thermocouples, the unit is in millimeters.	92
Figure 6- 4: Flow chart of the inverse algorithm for IHTC estimation at the metal die interface.....	96
Figure 6- 5: Measured temperature and local pressure versus time curves for step 5 (20 mm) under applied pressure of 60 MPa.	98
Figure 6- 6: Temperature, interfacial heat transfer coefficient (IHTC) and heat flux versus time curves for step 5 (20 mm) under applied pressure of 60 MPa.	98

Figure 6- 7: Variation of interfacial heat transfer coefficient (IHTC) and local pressure (LP) peak values with different cross section thicknesses of the five step casting	99
Figure 6- 8: Interfacial heat transfer coefficient (IHTC) versus time curves for all five steps (2, 4, 8, 10 and 20 mm) under applied pressure of 60 MPa	101
Figure 6- 9: Interfacial heat transfer coefficient curve versus section thickness in 10 second.	101
Figure 7- 1: a) side view, b) front view and c) isometric view of 5-step casting 3-D model with the round-shape gating system.....	109
Figure 7- 2: (a) An electric resistance furnace with SF ₆ gas protection, and (b) a 75-ton vertical hydraulic press.	110
Figure 7- 3: Configuration of upper-dies and geometric installation of thermocouples and pressure transducers.	111
Figure 7- 4: The left and right halves of the 5-step squeeze casting die, (a) five steel pins with the holes in their center for the insertion of the thermocouples to measure the casting temperatures, and (b) the installation of the fifteen thermocouples (TS 1-15) for the die temperature measurement.	112
Figure 7- 5: A typical 5-step squeeze casting solidifying under an applied pressure of 60MPa, (a) front view, (b) side view and (c) isometric view.	113
Figure 7- 6: X-ray radiosopic examination showing the soundness of the step castings under the applied pressures of (a) 60 MPa and (b) 0 MPa.....	119

Figure 7- 7: Typical temperature versus time curves (Step 4, 30 MPa) at metal surface, die surface, and various positions inside the die; The interfacial heat flux(q) and the heat transfer coefficient (IHTC) curves estimated by inverse method (Step 4, 30 MPa).....	120
Figure 7- 8: Typical local pressure distributions and IHTC curve at the casting-die interface of step 4 under the applied hydraulic pressures of 30, 60, 90 MPa.	121
Figure 7- 9: Typical effects of applied pressures on the heat transfer coefficients varying with casting surface temperature at the step 4.	122
Figure 7- 10: Interfacial heat transfer coefficients (IHTC) curves of 5 steps under the applied pressure of 30 MPa.....	123
Figure 7- 11: The peak IHTC values of 5 steps estimated by the inverse method with the applied pressures of 30, 60 and 90 MPa.	124
Figure 7- 12: A typical experimental cooling curve at the center of Step 5 (AM60) under an applied pressure of 60 MPa.....	128
Figure 7- 13: Temperature distribution inside the 5-step casting (80% solidified) of AM60 simulated with the input of HTCs, (a) 7000 W/m ² K, (b) Yu's research, and (c) the Inverse algorithms.....	129
Figure 7- 14: Comparison of the experimental and computational cooling curves at the center of Step 5 under an applied pressure of 60 MPa, (a) the entire cooling period, and (b) the enlarged solidification region.	130
Figure 8- 1: a) 3-D model of step casting mold, and b) side view and c) front view of 5-step casting sample of Al 7075 by squeeze casting under an applied pressure of 60 MPa.	140

Figure 8- 2: a) side view and b) front view of the step die illustrating the locations of the thermocouples in each step.	141
Figure 8- 3: Schematic diagram of squeeze casting machine 1) upper die, 2) lower die and 3) piston.....	143
Figure 8- 4: Polynomial curve fitting with the temperature readings from step 2 at 1.1 seconds after pressurized solidification.	146
Figure 8- 5: Typical temperature versus time curve (step 2, 60 MPa) at the casting metal surface, die surface and various positions inside the die.	147
Figure 8- 6: Interfacial heat flux (q) and interfacial heat transfer coefficient (IHTC) curves for step 2 with the applied pressure of 60 MPa.	149
Figure 8- 7: Heat flux (q) curves for steps 1-5 estimated by the extrapolated fitting method.....	150
Figure 8- 8: Interfacial eat transfer coefficient (IHTC) curves for step 1-5 estimated by extrapolated fitting method.	151
Figure 9- 1: Graphical installations of temperature sensor units (TSUs), pressure sensor units (PSUs) and data acquisition system.	162
Figure 9- 2: 3-D model showing the (a) front view (b) side view and (c) isometric view of the 5-step casting.	162
Figure 9- 3: Configuration of installation of the K-type thermocouples, the unit is in millimetres.	163
Figure 9- 4: One-dimension inverse heat conduction problem to be solved for heat transfer coefficient.	164

Figure 9- 5: Flow chart of the inverse algorithm for IHTC estimation at the metal/die interface.....	167
Figure 9- 6: 5-step squeeze castings with the applied pressures of (a) 30, (b) 60 and (c) 90 MPa.....	170
Figure 9- 7: Typical temperature, heat flux and IHTC versus time curves of step 2.....	170
Figure 9- 8: The residual error between the measured and calculated temperatures evaluated by the inverse method at position $T_2=4$ mm.....	171
Figure 9- 9: Local pressure and IHTC versus time curves, with the applied pressures of 30, 60 and 90 MPa for step 2 with the section thickness of 4 mm.	172
Figure 9- 10: Typical IHTC and local pressure curves for 5-step casting under the applied pressure of 60 MPa.....	174
Figure 9- 11: The peak IHTC values and local pressures for the casting under the applied hydraulic pressure of 60 MPa varied with the different wall thickness of steps 1 to 5. ..	175
Figure 9- 12: The peak IHTC values versus applied pressures for steps 1 to 5.....	176
Figure 9- 13: IHTC derived from the inverse method data applied to MAGMAsoft simulation for step 2.....	178
Figure 9- 14: IHTC derived from the inverse method data applied to MAGMAsoft simulation for step 5.....	178
Figure 9- 15: Comparison of the experimental and computational cooling curve at the center of step 2 under an applied pressure of 60 MPa.	180
Figure 9- 16: Comparison of the experimental and computational cooling curve at the center of step 5 under an applied pressure of 60 MPa.	181

NOMENCLATURE

A	Surface area
B	Calculated temperature
C_p	Heat capacity
D	Diameter
E	Young's modulus
F_0	Fourier number
j	Future time
h	Heat transfer coefficient
H	Enthalpy
K	Thermal conductivity
L	Length
P	Pressure
$P_{applied}$	Applied hydraulic pressure
P_{local}	Measured local pressure at each step
q	Heat flux
r, z	Cylindrical co-ordinate direction
R	Radius
T	Temperature
T_c	Casting temperature
T_d	Die surface temperature
T_i	Initial die temperature
T_l	Liquidus temperature
T_0	Initial temperature

T_s	Solidus temperature
T_∞	Ambient temperature
t	Time
x	Location
x_0	Thermocouple location
Y	Measured temperature

Greek Symbols

α	Thermal expansion coefficient
ε	Strain
σ	Stress
ν	Poisson's ratio
ϕ	Sensitivity coefficient
$\Delta\theta$	Time step for heat flux
Δt	Time step for temperature
ρ	Density

Superscripts

j	Future time
p	Time step

Subscripts

$1, 2, 3$	Principal Stress directions
b	Bulk
c	Casting

d	Die
n	Grid point
w	Mold wall
x, y, z	Direction

CHAPTER 1

1. INTRODUCTION

With increasingly stringent government regulations and growing market demand, lighter vehicles and engine downsizing has become an urgent and essential task for the automotive industry. The weight reduction in vehicles can be achieved by new designed lighter engineering materials such as aluminum or magnesium alloys. Traditionally, passenger vehicle engine output is much more powerful than required for average driving usage. To deliver such high power using a large engine indicates that almost all of the time the engine is operating at a tiny fraction of its maximum power and therefore inefficiently. To improve its efficiency, engine downsizing has become an established trend in the automotive industry in the past few years. Downsizing is referred to as the installation of a small engine in a vehicle which meets the performance aspirations of a driver by designing the engine to operate at extremely high powers when needed. The most common approach to achieving this goal is through turbocharging and/or supercharging the engine. Both techniques compress the air entering the engine, allowing more fuel to be burnt and more power to be generated.

In the past few years, the development and application of three cylinder engines have attracted great interest from researchers and designers in the automotive industry. The basic advantage of a three-cylinder engine over a four-cylinder is that it is inherently more fuel efficient (as there is one cylinder less of volume of fuel to burn). The smaller the engine

size, the less fuel it will burn making the system more fuel efficient. However, to maintain the engineering performance and output horsepower of downsized engines, high strength materials must be employed.

It is well known that aluminum weighs only one-third of iron. Thus, to further reduce the weight of engines, high strength aluminum alloys and their compatible manufacturing processes need to be developed. Generally, there are two balancing strategies for light weighting:

- 1) reducing weight of body and chassis components through advanced materials and;
- 2) developing light materials for engine and powertrain.

The first strategy is of replacing heavy low/mild carbon steels with high strength steel, aluminum or fiber-reinforced polymer composites. The properties and manufacturing of these materials are well established, and research and development activities have been placed on cost-effective processes for joining and recycling them. The second strategy is longer and targets a 50-70% weight reduction for some engine components through use of materials such as aluminum and magnesium alloys. However, more extensive R&D is needed to better understand the properties of these materials and reduce their manufacturing costs.

Increases in magnesium alloys for automotive application have driven the increasing in demand for the magnesium alloys, especially for manufacture of die-cast components. According to Australian Magnesium Corp Ltd (AMC), die-cast magnesium automotive components consume about 150,000 tons/year of magnesium alloys. It has seen a 30% increase over the last eight years, and has been forecast to continue to grow at a rate of 3% annually. This substantial and sustained increase in magnesium consumption has led to

significant changes in the magnesium manufacturing industry and has encouraged suppliers to develop their processes and alloys and identify potential future applications of magnesium for both cast and wrought products [1].

Wrought components are generally shaped by conventional methods such as forging/rolling, which are high-energy intensive processes. Squeeze casting is an economical, single-step near-net shaping process and has advantages of manipulating the microstructure within the material thereby isotropic properties can be achieved in the components. Besides, wrought grade alloys cannot usually be produced by conventional casting processes to attain the same level of tensile properties. However, progress in casting methods in recent years has made it possible to produce wrought alloy by squeeze casting techniques [2].

Squeeze casting is a general term to specify a fabrication technique where, liquid metal is fed into a permanent die and pressure is applied via a hydraulic ram until solidification is complete. Squeeze casting is also known as liquid metal forging, squeeze forming, extrusion casting and pressure crystallization. It is a casting process in which liquid metal solidifies under the direct action of pressure. The major advantages of squeeze casting: 1) produced parts are free of gas porosity or shrinkage porosity; 2) feeders or risers are not required and therefore less metal wastage occurs; 3) alloy fluidity (castability) is not critical in squeeze casting as both common casting alloys and wrought alloys can be squeeze cast to net shape with the aid of pressure; 4) squeeze castings can have enhanced mechanical properties as wrought products. On the other hand, some results show that the mechanical properties of squeeze casting alloys increase; the grain size and the dendrite arm spacing decrease and more dendrites appear with the increase of applied pressure [3].

Squeeze casting offers high metal yield, no or minimum gas or shrinkage porosity, excellent surface finish and low operating costs. This process provides probably the most effective and efficient route to produce near net-shape components and metal matrix composites for engineering application. Among all of the casting techniques available today, squeeze casting has greater potential to create less defective cast component. Since the as-fabricated components can be readily used in service or after a minor post-fabrication treatment, squeeze casting is regarded as a net or near net-shape fabrication route.

The majority of components are currently squeeze-cast from conventional Al-Si casting alloys such as A356. It has been reported that the pressure applied during squeeze casting also alloys wrought Al alloys, particularly the heat-treatable 2000 (Al-Cu), 5000 (Al-Mn-Mg), 6000 (Al-Si-Mg), and 7000 (Al-Zn-Cu-Mg) group, to be cast to shape to give high-strength, ductile components [4-6].

Extensive effort has been made for the last forty years to determine the precise interfacial heat fluxes and IHTC at the mold/metal interface. Meantime, many casting simulation models have also been developed. Mathematical modelling has changed the way that the traditional foundry works. Instead of experiment trails, casting simulation helps to do the analysis and optimization in advance of the casting process. The casting simulation also helps to make the production more efficient and cost effective by shortening development time, detect product defects prior to the real casting process. The accurate modeling of the metal casting processes requires reliable knowledge of the interfacial heat transfer coefficient (IHTC) at the mold/metal interface as a function of both time and location. IHTC is an important factor which determines the quality of the product due to influence of the thermal history of the casting on the microstructures of the final product.

2. OBJECTIVES

In the present work, the major effort was placed into analyzing and accurately determining the interfacial heat transfer coefficients (IHTCs) for simulating squeeze casting of light metals such as wrought aluminum alloys and magnesium alloys. The objectives of this work were:

1. To develop an experimental tooling for local pressure measurement during squeeze casting of wrought aluminum and magnesium alloys;
2. To develop an experimental tooling for temperature gradient measurement in order to estimate the IHTCs at the metal/mold interface;
3. To investigate and select modeling techniques to accurately determining IHTCs at the metal/mold interface; and
4. To investigate the relationship between the IHTCs, local pressures and section wall thicknesses of the squeeze castings.
5. To understand non-equilibrium solidification behaviour and grain structure evolution of magnesium alloy AJ62 under various applied pressures.

3. DISSERTATION OUTLINE

This work embodied in this dissertation is described in a total of ten chapters:

In Chapter 1, introductory remarks are provided, the objectives and a general description of the outline of the work is presented.

In Chapter 2, a literature review for this work is carried out. Squeeze casting of the wrought aluminum alloys and magnesium alloys were investigated. Various IHTC estimation methods are presented. The inverse Heat Conduction Problem (IHCP) method is explained in detail.

In Chapter 3, an attempt has been made in characterizing the pressure distribution in the die cavity during squeeze cast of magnesium alloy AM50. In squeeze casting processes, cavity pressures directly affect the heat transfer coefficients between casting and mold, and subsequently the solidification behavior of castings. For process optimization, it is very important to understand the distribution of applied pressure in a die cavity. In this work, piezo-electric quartz pressure transducer was integrated into a die cavity with different geometrical shapes. The experiments have been carried out to reveal that the pressure distribution changes with the cavity geometry. Also, the change of the local cavity pressures at various locations in the duration of casting solidification was observed.

In Chapter 4, thermal and pressure sensors were employed to evaluate the evolutions of temperature and pressure distributions in a cylindrical squeeze casting. Investigation on the non-equilibrium solidification phenomena and microstructure development of magnesium alloy AJ62 under various applied pressures has been carried out.

In Chapter 5, with the 75-ton hydraulic press machine and P20 steel die mold, a 5-step casting of magnesium alloy AJ 62 with wall thicknesses of 2, 4, 8, 12 and 20 mm was prepared by squeeze casting technique under an applied pressure of 60 MPa in a hydraulic press. The interfacial heat transfer coefficient (IHTC) between the die and casting was determined from the temperature measurement inside the casting and throughout the die at a distance of 2,4 and 6 mm to the die surface. The temperature readings were recorded by

fine Type-K thermocouples. Based on the thermal gradient, the heat flux (q) and IHTC were evaluated using the energy balance method.

In Chapter 6, a 5-step squeeze casting experiment using aluminum wrought alloy 5083 with applied hydraulic pressure of 60 MPa has been designed and conducted. The temperature profiles inside the die and casting were measured. Based on the temperature measurements of the casting at each step and the temperature at difference distance underneath the die surface (2, 4 and 6 mm) of each step, the inverse method of heat conduction was introduced and applied in determining of heat flux and heat transfer coefficient at the metal/mold interface.

In Chapter 7, a 5-step castings of magnesium alloy AM60 with different wall-thicknesses (2, 4, 8, 12, 20 mm) were poured under various hydraulic pressures (30, 60, and 90 MPa) using an indirect squeeze casting process. Thermal histories throughout the die wall and the casting surface have been recorded by fine Type-K thermocouples. The in-cavity local pressures measured by pressure transducers were explored at the casting-die interfaces of 5 steps. The metal/mold IHTC in the 5-step casting were determined based on experimental thermal histories data. The empirical equations relating the IHTCs to the local pressures and the solidification temperature at the casting surface were developed based on the multivariate linear and polynomial regression.

In Chapter 8, a 5-step casting mold was employed with section thicknesses of 2, 4, 8, 12 and 20 mm. Wrought aluminum alloy 7075 was squeeze cast under an applied pressure of 60 MPa in a hydraulic press. The temperature at the die surface was estimated by the polynomial extrapolation method, which required the temperature values at different locations inside the die. With the temperature measurements and the estimated die surface

temperatures, the heat flux and interfacial heat transfer coefficient were calculated at the metal/mold interface.

In Chapter 9, a 5-step casting was designed for numerical determination of casting thickness-dependant IHTCs, in which cross-section thicknesses of 2, 4, 8, 12 and 20 mm were included. Squeeze casting experiments were performed under the applied hydraulic pressures of 30, 60 and 90 MPa. Based on the temperature measurements of the casting at each step and the temperatures at difference depths underneath the die surface (2, 4 and 6 mm) of each step, the inverse method was applied in determining of heat fluxes and heat transfer coefficients at the metal/mold interface when heat conduction took place during the pressurized solidification of wrought aluminum alloy 7075. The influence of the casting section thicknesses and the applied hydraulic pressures on the heat transfer coefficients was investigated.

In Chapter 10, important conclusions drawn from the preceding chapters are summarized, together with suggestions for future work to original knowledge.

REFERENCES

- [1] MAG TECH 1: Magnesium alloys and processing technologies for light weight transport applications. 2004. Retrieved from http://www.improve.it/metro/file.php?file=/1/Papers/Aluminium_and_Magnesium_Foundry_Alloys/mg.pdf, 2016.
- [2] Souissi, N., Souissi, S., Niniven, C. L., Amar, M. B., Bradai, C., Elhalouani, F. Optimization of squeeze casting parameters for 2017 A wrought Al alloy using Taguchi method. *Metals*. 2014; 4(2):141-54.
- [3] Zhong, Y., Su, G., Yang, K. Microsegregation and improved methods of squeeze casting 2024 aluminium alloy. *J Mater Sci Technol* 2003; 19(5), 413–6.
- [4] Kim, S. W., Durrant, G., Lee, J. H., Cantor, B. The microstructure of direct squeeze cast and gravity die cast 7050 (Al-6.2Zn-2.3Cu-2.3Mg) wrought Al alloy. *J Mater Synth Process* 1998; 6(2), 75–87.
- [5] Lee, J. H., Kim, H. S., Hong, S. I., Won, C. W., Cho, S. S., Chun, B. S. Effect of die geometry on the microstructure of indirect squeeze cast and gravity die cast 5083 wrought Al alloy and numerical analysis of the cooling behavior. *J Mater Process Technol* 1999; (96), 188–97.
- [6] Manson-Whitton C. D. J. Cantor, B., Clinch, M. O., Reilly, K. A., Schumacher, Q. P. Squeeze casting of a conventionally wrought aluminum alloy, *Light Metal – Warrendale – Proceedings* 2003, 1023–32.

CHAPTER 2

LITERATURE REVIEW

1. WROUGHT ALUMINUM ALLOYS

Main alloying elements in wrought aluminum alloys are Cu, Mg, Zn, Si, and Mn; various alloying systems can be realized by combining these elements and others. Figure 2.1 provides an outline of aluminum alloys, which can be classified into non-heat treatable types and heat-treatable ones where age hardening can be effectively used [1].

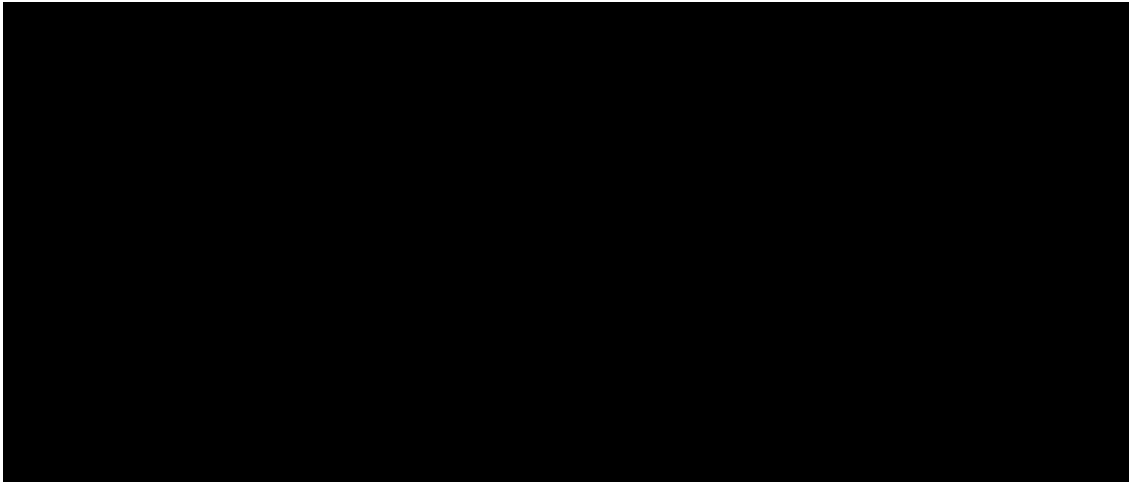


Figure 2- 1: Classification of wrought aluminum alloys [1].

Non-heat-treatable type alloys can be strengthened by alloying Mg, Mn, Si, etc., which can form a strain field for the difference in atomic radius with one of aluminum. When dislocations move on a slip plane, the strain field obstruct movement. This phenomenon is termed solid solution strengthening. Meanwhile, solute atoms lock the dislocation

movement and the phenomenon is termed a pinning effect. Also, annealed alloys (dislocation density $\sim 10^8/\text{cm}^2$) can be strengthened by cold working for increasing dislocation density (dislocation density $\sim 10^{10-12}/\text{cm}^2$), and called work hardening. This type of aluminum alloys consists of 1000, 3000, 4000, and 5000 series alloys according to their chemical composition [2].

Heat-treatable type alloys usually contain elements such as Cu, Mg, Si, and Zn, which have high solid solubility at high temperatures, but rather lower solubility at room temperature. When an alloy is quenched from high temperature (solution treatment) and aged (T6 treatment), precipitations like the Guinier-Preston (GP) zone and intermediate phase appear [3]. Accordingly, alloys can be strengthened by suppressing dislocation movement with precipitates (precipitation hardening) are, for instance in 2000, 6000 and 7000 series alloys. The precipitation hardening heat treatment involves stages, which listed in the table below.

Table 2- 1: Precipitation hardening heat treatment stages [4]

Solution treatment (T4)	<ul style="list-style-type: none"> • Part is heated to a temperature above the solvus temperature in order to dissolve the second phase in the solid solution. • The part is held at this temperature for a time varying from 1 hour to 20 hrs until the dissolving is accomplished. • The temperature and the soaking time of solution treatment should not be too high to prevent excessive growth of the grains.
-------------------------	--

Quenching	<ul style="list-style-type: none"> • Quenching is carried out in water, water-air mixture or sometimes in air. • Objective of the quenching operation is to obtain supersaturated solid solution at room temperature. • Since the second phase remains dissolved at this stage, hardness of the quenched alloy is lower than after age precipitation, however higher than hardness of the alloy in annealed state.
Aging (T5)	<ul style="list-style-type: none"> • Depending on the temperature at which this operation is carried out, aging may be artificial or natural.

Among these alloys, high strength 2000 and 7000 series alloys are notable for application to aircraft for their strength characteristics. For automotive industrial application, various casting alloys are used for engine parts and wheels. As wrought material, 5000 and 6000 series alloys are mainly applied as extruded or rolled products. In the case of wrought alloys, characteristics of fatigue, fracture toughness, creep, and resistance to stress corrosion cracking are considered to be the most important factors.

2. PROCESSING OF WROUGHT ALUMINUM ALLOYS

Wrought components are generally shaped by conventional methods such as forging/rolling, which are high-energy intensive process. Squeeze casting is an economical, single-step near-net shaping process and have advantages of manipulating the microstructure within the material thereby isotropic properties can be achieved in

components. Besides, wrought grade alloys cannot usually be produced by conventional casting processes to attain the same level of tensile properties. However, progress in casting methods in recent years has made it possible to produce wrought alloy by squeeze casting techniques [5].

Basically, there are three stages during solidification processes.

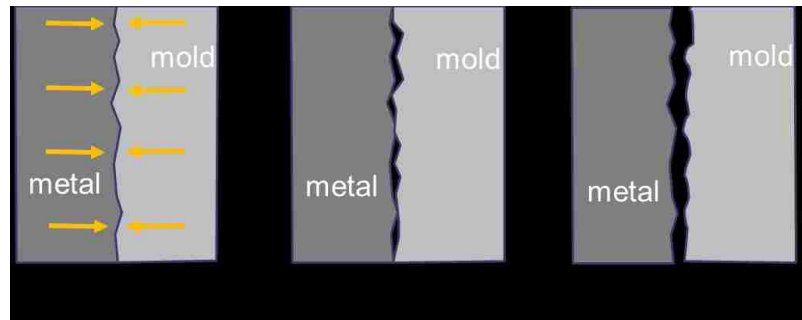


Figure 2- 2: Schematic drawing illustrating the three stages of solidification process at metal/mold interface.

- **Stage 1**, at the beginning of solidification, the contact between molten metal and mold can be assumed good. Heat transfer is made through conduction from molten metal to the die.
- **Stage 2**, as solid layer forms, the metal shrinks away from the die and a discontinuous air gap forms. So, the die and solid metal becomes partial contact. The heat transfer is made through metal/mold conduction at the contact surface and through radiation at the air gap.
- **Stage 3**, the solidified metal pulls away completely from the mold wall and the heat transfer is made only through the air gap.

To eliminate the pull-away action in stage 3, external force can be employed to keep the metal in contact with the mold as long as possible during the solidification process (stage 1). Squeeze casting technique could be one option to accomplish this task.

Squeeze casting is a general term to specify a fabrication technique where, liquid metal is fed into a permanent die and pressure is applied via a hydraulic ram until solidification is complete. Squeeze casting is also known as liquid metal forging, squeeze forming, extrusion casting and pressure crystallization. It is a casting process in which liquid metal solidifies under the direct action of pressure. The major advantages of squeeze casting: 1) produced parts are free of gas porosity or shrinkage porosity; 2) feeders or risers are not required and therefore less metal wastage occurs; 3) alloy fluidity (castability) is not critical in squeeze casting as both common casting alloys and wrought alloys can be squeeze cast to net shape with the aid of pressure; 4) squeeze castings can have enhanced mechanical properties as wrought products. On the other hand, some results show that the mechanical properties of squeeze casting alloys increase; the grain size and the dendrite arm spacing decrease and more dendrites appear with the increase of applied pressure [6].

Squeeze casting offers high metal yield, no or minimum gas or shrinkage porosity, excellent surface finish and low operating costs. This process provides probably the most effective and efficient route to produce near net-shape components and metal matrix composites for engineering application. Since the as-fabricated components can be readily used in service or after a minor post-fabrication treatment, squeeze casting is regarded as a net or near net-shape fabrication route.

The majority of components are currently squeeze-cast from conventional Al-Si casting alloys such as A356. Squeeze casting of wrought Al alloys, particularly the heat-treatable

2000 (Al-Cu), 5000 (Al-Mn-Mg), 6000 (Al-Si-Mg), and 7000 (Al-Zn-Cu-Mg) group has been attempted to make light weight high-strength and ductile materials. For example, it has been reported that the squeeze cast 7010 alloy has a UTS of 551 MPa and a ductility of 12.2%, similar to the UTS and ductility of the same alloy in the wrought condition. The tensile properties of the squeeze cast alloy have been shown to be grain-size dependent, fine grain structure always resulting in a higher tensile strength and ductility [7-9].

3. HEAT TRANSFER IN SQUEEZE CASTING

For conventional forming process such as forging or welding, the shapes of the product cannot be economically formed in one piece in a single process. With casting process, it is possible to fabricate large and intricate shapes in one operation. The inefficiency of casting operations of the past has been improved significantly upon through numerous innovations that have taken place so that precision cast components can be produced as reported by Higgins [10]. One method that has gained acceptability in casting processes is the squeeze casting [11]. Squeeze casting is one of the improved casting techniques used for the production of engineering components mostly in non-ferrous metals by the application of external pressures on the cast metal to eliminate defects associated with shrinkage cavities and/or gas porosity. By squeeze casting operation, the liquid molten metal is compressed under pressures inside the mould cavity of a re-usable metal mould, usually made of steel. Squeeze casting offers considerable saving in cost for large production quantities when the size of the casting is not very large. Das and Chatterjee [12] reported that the permanent-mold casting method becomes impracticable when large castings and alloys with high

melting temperature applied. On the other hand, the mold used in squeeze casting process apart from being re-usable and its economic advantage has the advantage of producing good surface finish, close dimensional tolerance and defect free products [12].

The solidification process of the molten aluminum in the steel mold takes a complex form. All mechanisms of heat transfer are involved and the solidifying metal undergoes state and phase changes during solidification of metals [12, 13]. The final structure and properties of the cast alloy rely on the casting parameters such as applied pressure, die temperature and pouring temperature of the liquid metals [14].

Kim and Lee [15] studied time varying heat transfer coefficients between a tube-shaped casting and metal molds. They found that the heat transfer coefficients at the interface of the inner mould decreased temporarily and then increased, while the one at the outer interface of the mold decreased monotonously to a quasi-steady state.

Browne and O'Mahoney [16] carried out experimental determinations of interface heat transfer coefficients relating to solidification range, metallostatic head, investment shell thickness, pre-heat and interface geometry and concluded that effect of metallostatic head was only significant for long freezing-range alloys while increasing shell mould thickness and pre-heat also had effects that were alloy dependent.

Maeng [17] investigated the effect of processing parameters on the microstructure and mechanical properties of modified B390 alloy in direct squeeze casting by using commercial finite volume method code for heat transfer analysis, and MAGMAsoft for cooling curves. In this model, the heat transfer was considered constant for a specific applied pressure.

Krishna [18] estimated the IHTC for A356 during an indirect squeeze casting process. They calculated temperature histories inside the die and casting with varied IHTC values, and chose the best correlation one between measured and calculated values. The authors concluded that there was a critical value of squeeze pressure beyond which the heat transfer did not significantly improve.

4. INTERFACIAL HEAT TRANSFER COEFFICIENT

As well as the delivery of liquid metal, heat transfer between a solidifying casting and the mold is another critical factor for achievement of high quality in the final product. When liquid metal is infiltrated into the mold cavity, heat is simultaneously transferred from the cast to the mold. It is important to understand the heat transfer behaviour at the metal/mold interface. It determines the quality of the product because the thermal history of the casting greatly influences the microstructures of the final product.

For any newly developed material, the most common industry practice is to assume IHTC values as constant during the casting cycle, although some modellers have used time or temperature dependent values. These coefficients are only roughly estimated based on engineering judgement. Variations in IHTC over the surface of the casting are generally not accounted for, except by rough estimates. In the case of squeeze casting, metal-mold heat transfer, as for example, indicated by solidification time, applied pressure and casting section thicknesses, are very sensitive to the interfacial heat transfer coefficient. A quantitative basis for establishing IHTC's is needed by the industry.

The IHTC essentially quantifies the resistance of heat flow from the casting to the mold. In reality, the surface of the casting and the mold are not perfectly flat. As the contact pressure at the metal/mold interface becomes reasonable high, most of the energy transfer via a limited number of actual contact spots. The heat flow transferring from the casting to the mold can be characterized by a macroscopic average metal/mold interfacial heat transfer coefficient (IHTC) according to the following Equation 2-1:

$$h = \frac{q}{A(T_{cs} - T_{ds})} \quad 2-1$$

where, h : the interfacial heat transfer coefficient;

q : the average heat flux at the metal/mold interface;

A : the cross-section area;

T_{cs} : the casting surface temperature, and

T_{ds} : the casting surface temperature and die surface temperature, respectively.

From Equation 2-1, the higher the value of h , the more heat transfer from the casting to the mold and the greater the heat flux from the casting to its surroundings. The quantification of heat flux in terms of a heat transfer coefficient requires that the heat capacity is zero so that the thermal diffusivity is infinite, and consequently heat fluxes entering and leaving the interface are equal. The heat transfer coefficient shows a high value in the initial stage of solidification, the result of the good surface conformity between the liquid core and the solidified shell. As solidification progresses, the mould expands due to the absorption of heat and the solid metal shrinks during cooling. As a result, a gap develops because

pressure becomes insufficient to maintain a conforming contact at the interface. Once the air gaps forms, the heat transfer across the interface decreases rapidly and a relatively constant value of h is attained. During the subsequent stage of solidification, a slight drop in the interfacial heat transfer coefficient with time can be observed. This might be caused by the growth of oxide films on chill and mould surfaces, and by a reduction in the thermal conductivity of the interfacial gas with declining temperature [19].

4.1 Analytical interfacial heat transfer

Extensive effort has been made for the last forty years to determine the precise interfacial heat fluxes and heat transfer coefficients at the metal/mold interface. Among the mathematical methods described in the literature, there are three main groups could be found, which are purely analytical, empirical, and numerical methods based on the methods of finite difference or finite element.

- *purely analytical techniques*, the assumption of a constant interfacial heat transfer coefficient is made in order to obtain an analytical solution for the Fourier heat conduction equation [20-21].
- *empirical methods*, do not require the rigorous solution of the Fourier equation, but they involve analyzing experimental data by means of semi-analytical formula [22].
- Finally, *numerical techniques*, (methods for solving the inverse heat conduction problem), are applied to determine the exact values of the time dependent interfacial heat fluxes, and the instantaneous heat transfer resistances at the metal/mold interface [23].

Garcia et al. [19] developed a mathematical heat transfer model by considering the solidification of metal under the superimposed effects of thermal conduction and Newtonian thermal contact. They assumed that the thermal properties of metal and mold are invariant during solidification including the heat transfer coefficient. Lead and aluminum alloys were used as cast metals and the Virtual Adjunct Method (VAM) was developed to predict the temperature profiles within the metal and cooling mold.

Lipton et al. [22] extended this concept to describe temperature distributions and the position of the solidus and liquidus isotherms. An Al-4.5%Cu melt was solidified in a water-cooled mold. They showed that the solidus and liquidus isotherm positions could be described by a quadratic polynomial function of temperature distribution in the solid, mushy zone, and liquid, by error functions.

Based on work with Al-Cu alloys and permanent copper molds, Prates et al. [23] evaluated the value of heat transfer coefficients as a function of the surface density of predendritic nuclei and heat extraction capacity. They also proposed a nucleation mechanism to explain the initial formation of a metal-mold interface with solid-solid contact. The postulation was based on the fact that, on a microscopic scale, the chill surface was not completely smooth and consisted of small asperities protruding from the surface profile. Their results showed that for a critical value of heat transfer coefficient larger than $2.5 \text{ kW /m}^2\text{K}$, the multiplication mechanism was not effective in the formation of the chill zone even in the presence of highly turbulent flow. A multiplication mechanism corresponds to the separation of crystals from the dendrites growing in a thermal or constitutionally super cooled liquid. For a coefficient lower than this, the laminar turbulent transition of fluid flow greatly improved the effectiveness of the multiplication mechanism.

4.2 Numerical analysis of interfacial heat transfer

As solidification progresses, the metal and mold either stay in contact at isolated asperities on the microscopically rough surfaces, or an interfacial gap separating the metal and mold gradually develop. One of the first significant works on this interfacial heat transfer mechanism for metal-mold systems was carried out by Beck et al [24] and Ho and Pehlke [25-27]. They determined the IHTC value via the two independent methods:

1. A computer solution of the inverse heat conduction problem (IHCP) using thermocouple measurement at selected locations in the casting and mold.
2. Measurements of the variation of interfacial gap size with time and deriving the IHTC values from heat transfer data across a static gap.

For both types, a rapid drop of interfacial heat transfer coefficient occurred during the initial stages of solidification due to changes in interfacial conformity. In the case of an interfacial gap, the heat transfer coefficient was affected by the magnitude of interfacial separation. On the other hand, provided that interfacial contact pressure remains relatively constant, the final thermal conductance for the case of a contacting metal-chill interface was principally a function of the mechanical finish of the mold as well as the material properties with respect to oxide formation and wetting.

Similar experiments were carried out by Nishida et al. [28] for cylindrical and flat castings of pure aluminum and Al-13.2%Cu alloy. The mold shape was found to affect the heat transfer coefficient and the formation of the air gap was detected by monitoring mold and casting movements during the solidification. In the case of cylindrical molds, the mold moves outwards away from the casting, while in rectangular molds, the mold surface

moves first inwards towards the casting, then outwards. It was also found that for the weakly constrained rectangular mold, the inward movement is even larger than for a strictly constrained one.

4.3 Interfacial heat transfer from various casting experiments

Taha [29] studied the solidification of Al-4.5Cu cylindrical castings with 12.5 mm diameter and length 95 or 230 mm in a vertical end-chill apparatus. IHTC values were assumed as a function of time and repeated computations were performed for varying IHTC values until experimental cooling curves matched those were computed. Then, the air gap and IHTC were computed using a numerical model which took into consideration metal and mould shrinkage and expansion, gas film formation, and metallostatic pressure.

Cho and Hong [30, 31] studied the IHTC for a squeeze casting process using Al- 4.5Cu alloy, and reported IHTC values of about 1000 W/m²K prior to pressurization which rapidly increased to around 4700 W/m²k at a pressure of 50 MPa for a cylindrical casting in a steel mould.

Michel [32] investigated the IHTC for Al-Si alloys in steel mould with and without coatings. They found that no coating or thin graphite coating resulted in the highest maximum IHTC. For pure aluminum, a 100µm vermiculite coating yielded higher IHTC values than a 300µm coating. They also found that the mould initial temperature had a greater impact on the IHTC than the coating.

Carroll [33] examined the effect of interfacial contact pressure on the IHTC for aluminum alloy casting against steel moulds. The average IHTC increased as the pressure was increased. The IHTC versus temperature curves were divided into three zones. The first zone saw a steady decrease in IHTC due to decreasing interfacial heat flux, and the IHTC increased in the second zone, which had 35% to 60% solid fraction. After casting surface reached 60% solid, the interface started to transform from a condition of high conformity to low conformity. In low pressure experiments, the IHTC dropped rapidly with temperature in the third zone while an approximate plateau was reached for the high pressure experiment.

Kim et al [34] conducted experiments of pure aluminum cast into a cylindrical copper mould to determine the effects of coating and superheat on the IHTC. While the cast alloy was liquid, the IHTC was influenced by mould surface roughness, the wettability of the alloy on the mould, and the physical properties of the coating layer. Due to the abrupt surface deformation of the casting, an IHTC drop was observed at the onset of solidification. The air gap and the direct contact between the casting and mould affected IHTC values. They claimed that when the cast metal was in the solid phase, the IHTC was not affected by the type or thickness of the mould coating, and only depended on the thermal conductivity and thickness of the air gap.

The accuracy of a solidification simulation depends on the accuracy of the heat transfer modeling. Modeling of the heat transfer at the metal/mold interface of a casting is very challenging due to a number of factors. One of the greatest modeling challenges is to properly handle air gap formation. Besides the different casting techniques, casting process

parameters, and casting geometry shapes, some additional influencing factors need to be also considered to determine IHTC accurately. These factors include:

- the pressure at the interface (the applied pressure during squeeze casting, the orientation of the casting with respect to gravity casting);
- alloy characteristics (superheat, composition, mushy zone, liquid surface tension);
- mold processing conditions (mold materials, roughness of contacting surface, coating type and thickness, preheat temperatures).

Since so many factors play a role in the heat transfer between the surface of the solidifying casting and the mould, determining accurate IHTC is very specific to a given casting shape and process. Most of the studies have been performed using cylindrical or plate castings, of which IHTC results cannot be easily applied to complex casting geometries. Griffiths [35] pointed out that small errors in experimental measurements of temperatures in a casting or mold could result in very large differences in IHTC calculation. Therefore, it is essential to explore an effective method to reduce the experimental measurement errors and consequently increase the accuracy of IHTC.

5. MATHEMATICAL MODELLING

5.1 Direct problem

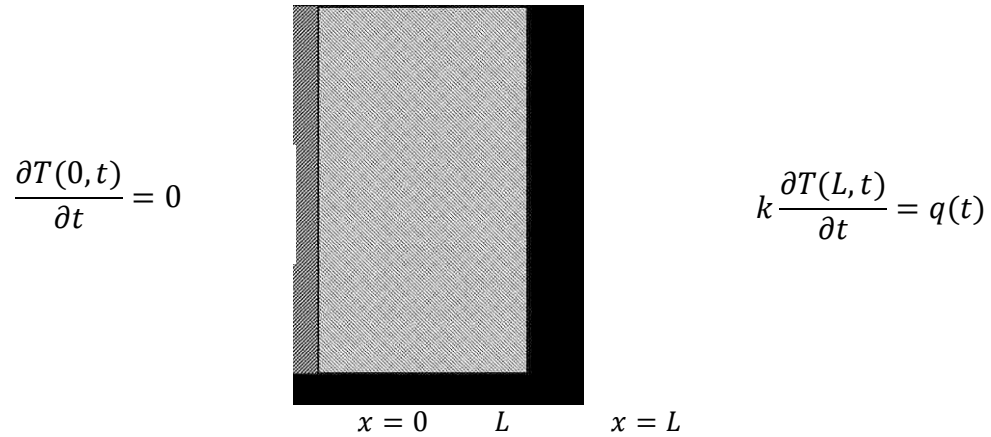


Figure 2- 3: One-dimensional wall with boundary conditions.

Direct heat conduction problems are the determination of temperature distribution inside a heat conducting body by applying the specified boundary conditions. For a one-dimensional heat conduction problem through a uniform wall, as show in Figure 2-3. On the left hand side, $x = 0$, the surface is insulated, on the right hand side, $x = L$, is subjected to heat flux $q(L, t)$. This problem can be described by the following equations:

$$\frac{\partial T(x, t)}{\partial t} = \alpha \frac{\partial^2 T(x, t)}{\partial x^2}, \text{ in } 0 < x < L, \text{ for } t > 0 \quad 2-2a$$

$$\frac{\partial T(0, t)}{\partial t} = 0, \text{ at } x = 0, \text{ for } t > 0 \quad 2-2b$$

$$k \frac{\partial T(L, t)}{\partial t} = q(t), \text{ at } x = L, \text{ for } t > 0 \quad 2-2c$$

$$T(x, 0) = T_0(x), \text{ for } t = 0, 0 < x < L \quad 2-2d$$

where,

α : thermal diffusivity

T : temperature

x : space coordinate k : thermal conductivity

L : thickness of the wall q : heat flux

For the case where the boundary condition at $x=L$, the initial condition $T_0(x)$, and the thermos-physical properties α , and k are all specified, the problem given by equations 2-2 is concerned with the determination of the temperature distribution $T(x, t)$ in the interior region of the solid as a function of time and location.

5.2 Inverse problem

Inverse problems are concerned with the estimation of boundary conditions from the knowledge of thermal history in the interior region of the solid. In many engineering problems, a precise determination of the thermal boundary condition may not be feasible [36, 37]. For instance, the application of a sensor unit may alter the thermal condition in the boundary region which could affect the actual values of the temperature measurements.

Since the temperature at interface is difficult or important to be directly measured, the inverse method in heat conduction is popular in the field of materials processing. By applying the inverse methods, thermal properties of materials or heat transfer at the surface of a body could be found. In the case of metal castings, the inverse method of heat conduction is useful in the determination of heat flux or interfacial heat transfer coefficient at the metal/mold interface. To characterize interfacial heat transfer with the inverse method, the temperature history at one or more points within the domain body need to be supplied [38].

The inverse methods are involved in the determination of the unknown function $q(t)$ at the surface $x=L$. To determine the heat flux $q(t)$, the measured temperature are given at an interior point, x_m at different times t_i ($i=1, 2, \dots, I$), over a specified time interval $0 < t < t_f$.

The mathematical formulation of the inverse problem could be expressed as below:

$$\frac{\partial T(x,t)}{\partial t} = \alpha \frac{\partial^2 T(x,t)}{\partial x^2}, \text{ in } 0 < x < L, \text{ for } 0 < t \leq t_f \quad 2-3a$$

$$\frac{\partial T(0,t)}{\partial t} = 0, \text{ at } x = 0, \text{ for } 0 < t \leq t_f \quad 2-3b$$

$$k \frac{\partial T(L,t)}{\partial t} = q(t) = (\text{unknown}), \text{ at } x = L, \text{ for } 0 < t \leq t_f \quad 2-3c$$

$$T(x, 0) = T_0(x), \text{ for } t = 0, 0 < x < L \quad 2-3d$$

where,

α : thermal diffusivity T : temperature

x : space coordinate k : thermal conductivity

L : thickness of the wall q : heat flux

The boundary surface function heat flux is unknown. Thus, this version of the problem is referred to as a boundary inverse heat conduction problem. The main objective of the direct problem is to construct the temperature field in the wall (Figure 2-3), when all parameters are specified, i.e. α , k , q , and T_0 . On the other hand, the objective of the inverse problem is to estimate heat flux from the measured temperature at some specified section of the medium ($x_m = 0$).

Inverse analysis is extensively used in materials modeling. However, the inverse heat conduction analysis is an ill-posed problem since it does not satisfy the general requirement

of existence, uniqueness, and stability under small changes to the input data. Furthermore, the output of an inverse solution to a heat conduction problem is very sensitive to measurement errors. To overcome such difficulties, many techniques for solving inverse heat conduction problems have been proposed [39]. In this work, Beck's nonlinear estimation technique [40, 41] was applied.

6. SUMMARY

Squeeze casting is an emerging casting technique for manufacturing of light alloys in the industry. More fundamental research is needed for a scientific understanding of the heat transfer at the metal/mold interface. As stated in the above sections, there are many published information on the study of the interfacial heat transfer coefficients between cast metal and the mold by using squeeze casting process, but there are few or no published work yet on casting complex shape with the variation in section thicknesses and applied pressures. Also, most of the works are studied on the conventional cast alloys, there are limited works on casting of wrought aluminums and magnesium alloys.

REFERENCE

- [1] Alexopoulos, N. D., Pantelakis, S. G. (2004). Quality evaluation of A357 cast aluminum alloy specimens subjected to different artificial aging treatment. *Materials & design*, 25(5), 419-430.
- [2] H. Shercliff, M. Ashby A process model for age hardening of aluminum alloys – I. The model *Acta Metall. Mater.*, 38 (1990), 1789–1802
- [3] Mitchell, I. Residual stress reduction during quenching of wrought 7075 aluminum alloy (Doctoral dissertation, WORCESTER POLYTECHNIC INSTITUTE). (2004).
- [4] Senkov, O. N., Shagiev, M. R., Senkova, S. V., & Miracle, D. B. (2008). Precipitation of Al₃ (Sc, Zr) particles in an Al–Zn–Mg–Cu–Sc–Zr alloy during conventional solution heat treatment and its effect on tensile properties. *Acta Materialia*, 56(15), 3723-3738.
- [5] Yue, T. M. Squeeze casting of high-strength aluminum wrought alloy AA7010. *Journal of materials processing technology*, 1997, 66(1), 179-185.
- [6] Zhong, Y., Su, G., Yang K. Microsegregation and improved methods of squeeze casting 2024 aluminium alloy. *J Mater Sci Technol*, 2003, 19(5), 413–6.
- [7] Kim, S.W., Durrant, G., Lee, J.H., Cantor, B. The microstructure of direct squeeze cast and gravity die cast 7050 (Al-6.2Zn-2.3Cu-2.3Mg) wrought Al alloy. *J Mater Synth Process* 1998, 6(2), 75–87.
- [8] Lee, J.H., Kim, H.S., Hong, S.I., Won, C.W., Cho, S.S., Chun, B. S. Effect of die geometry on the microstructure of indirect squeeze cast and gravity die cast 5083

- wrought Al alloy and numerical analysis of the cooling behavior. *J Mater Process Technol*, 1999, (96), 188–97.
- [9] Manson-Whitton, C.D.J., Cantor B, Clinch, M.O., Reilly, K.A., Schumacher, Q. P. Squeeze casting of a conventionally wrought aluminum alloy, *Light Metal – Warrendale – Proceedings*, 2003, 1023–32.
- [10] Higgins, R.A. *Engineering Metallurgy. Part I. Applied Physical Metallurgy*, 6th ed. ELBS with Edward Arnold, UK, 1983, 33-34
- [11] Franklin, J.R., Das, A. A. Squeeze casting: a review of the status *Brit. Foundryman*, March, 1983, 150–158
- [12] Das, A., Chatterjee, S. Squeeze casting of an aluminium alloy containing small amount of silicon carbide whiskers. *Metall. Mater. Technol.*, March, 1981, 137–142
- [13] Stevanovic, M., Sedmak, A., Markovic, S., Drobnyak, R. Numerical and experimental investigation of cooling rates in a spherical casting, *Technical Report, Foundry International*, December, 1994, 177–179.
- [14] Aniyi, J. A. Effects of die and stress relief temperatures on squeeze cast commercially pure aluminium. PhD Thesis. Mechanical Engineering Department, University of Ilorin, Nigeria. 1994.
- [15] Kim, T.-G., Lee, Z.-H., 1997. Time-varying heat transfer coefficients between tube-shaped casting and metal mold. *Int. J. Heat Mass Transfer* 40, 1997, (15), 3513–3525.
- [16] Browne, D.J., O’Mahoney, D. Interface heat transfer in investment casting of aluminium. *Metall. Mater. Trans. A* 32A, 2001, 3055–3063.

- [17] Maeng, D.Y., Lee, J.H., Won, C.W., Cho, S.S., Chun, B. S. The effect of processing parameters on the microstructure and mechanical properties of modified B390 alloy in direct squeeze casting. *Journal of Materials Processing Technology*, 2000, (105), 196-203.
- [18] Krishna, P., Bilkey, K.T., Pehlke, R. D. Estimation of interfacial heat transfer coefficient in indirect squeeze casting. *AFS Transactions*, 2001, (109), 131-139.
- [19] Hou, K., Pehlke, R. D. Transient methods for determination of metal-mold interfacial heat transfer, *AFS transactions*, 1983, (91), 689-698.
- [20] Gracia, A., Prates, M. Mathematical model for the unidirectional solidification of metals: 1. cooled molds, *Met. Trans.* 1978, (9B), 449 -457
- [21] Gracia, A., Clyne, T. W., Prates, M. Mathematical model for the unidirectional solidification of metals: II. Massive Molds, *Met. Trans. IOB.*, 1979, 85 - 92
- [22] Lipton, J., Garcia, A., Heinemann, W. An analytical solution of direct solidification with mushy zone, *Arch. Eisenhüttenwes.* 1982, (53) 469 - 473
- [23] Prates, M., Biloni, H. Variables affecting the nature of the chill zone. *Met. Trans.* 1972, (3B), 1501 - 1510
- [24] Beck, J. V., Blackwell, B., St. Clair Jr., C. R. *Inverse heat conduction: Ill-posed Problems*, Wiley Interscience, New York, 1985
- [25] Ho, K., Pehlke, R. D. Transient methods for determination of metal-mold interfacial heat transfer, *AFS Trans.*, 1983, 689 - 698
- [26] Ho, K., Pehlke, R. D. Mechanisms of heat transfer at a metal-mold interface, *AFS Trans.*, 1984, 587 - 597

- [27] Ho, K., Pehlke, R. D. Metal-mold interfacial heat transfer, *Met. Trans.* 1985, (16B), 585 – 594
- [28] Nishida, Y., Droste, W., Engler, S. The air-gap formation process at the casting-mold interface and the heat transfer mechanism through the gap, *Met. Trans.* 1986, (17B), 883 – 844
- [29] Taha, M. A., N.A., El-Mahallawy, A., Assar, R.M., Hammouda. Effect of melt superheat and chill material on interfacial heat-transfer coefficient in end-chill Al and Al-Cu Alloy castings. *Journal of Materials Science*, 1992, (27), 3467-3473.
- [30] Cho, I.S., Hong, C. P. Evaluation of heat-transfer coefficients at the casting/die interface in squeeze casting. *International Journal of Cast Metals Research*, 1996, (9), 227-232.
- [31] Cho, I.S., Hong, C. P. Modeling of microstructural evolution in squeeze casting of an Al-4.5mass% Cu Alloy. *ISIJ International*, 1997, (37)1098-1106.
- [32] Michel, F., Louchez, P.R., Samuel, F. H. Heat transfer coefficient during solidification of Al-Si alloys: Effects of mold temperature, coating type and thickness. *AFS Transactions*, 1995, (103) 275-283.
- [33] Carroll, M., Walsh, C., Makhlof, M. M. Determination of effective interfacial heat transfer coefficient between metal moulds and Al alloy castings. *AFS Transactions*, 1999, (107), 307-314.
- [34] Kim, H.S., Cho, I.S., Shin, J.S., Lee, S.M., Moon, B. M. Solidification parameters dependent on interfacial heat transfer coefficient between aluminum casting and copper mould. *ISIJ International*, 2005, (45), 192-198.

- [35] Griffiths, W. D. A model of the interfacial heat-transfer coefficient during unidirectional solidification of an aluminum alloy. *Metallurgical and Materials Transactions B*, 2000, (31B), 285-295.
- [36] Beck, J.V., Blackwell, B., Jr. St. Clair. *Inverse heat conduction: ill-posed problems*. Wiley Inter science: New York. 1985, 1-50.
- [37] Ozisik Necati, M. *Inverse heat conduction problem (IHCP)*. Heat Conduction; John Wiley & Sons Inc.: New York. 1993, 571-615.
- [38] Paray, F., Clements, J., Kulunk, B., Gruzleski, J. E. In-situ temperature measurement in low-pressure permanent-mold casting. *AFS Transactions*, 1997, (105), 791- 801.
- [39] Beck, J. V. Inverse problems in heat transfer with application to solidification and welding. In *Modeling of casting, welding and advanced solidification processes V*, ed. Rappaz M., Ozgu M.R., Mahin K.W., The Mineral, Metals and Materials society, 1991, 503-513.
- [40] Beck, J.V. Transient Sensitivity Coefficients for the Thermal Contact Conductance. *Int. J. Heat Mass Transfer*. 1967, (10), 1615–1616.
- [41] Beck, J.V. Non-linear Estimation Applied to the Non-linear Inverse Heat Conduction Problem. *J. Heat Transfer*. 1970, (13), 703–716.

CHAPTER 3

CHARACTERIZATION OF LOCAL CAVITY PRESSURES IN SQUEEZE CASTING OF MAGNESIUM ALLOY AM50

NOMENCLATURE	
<i>D</i>	Diameter
<i>E</i>	Young's modulus
<i>h</i>	Heat transfer coefficient
<i>H</i>	enthalpy
<i>k</i>	thermal conductivity
<i>L</i>	length
<i>P</i>	pressure
<i>q</i>	heat flux
<i>r, z</i>	cylindrical co-ordinate direction
<i>R</i>	radius
<i>T</i>	temperature
	<u>Greek Symbols</u>
	<i>α</i> Thermal expansion coefficient
	<i>ε</i> Strain
	<i>σ</i> stress
	<i>ν</i> Poisson's ratio
	<u>Subscripts</u>
	<i>1, 2, 3</i> Principal Stress directions
	<i>b</i> bulk
	<i>c</i> casting
	<i>d</i> die
	<i>w</i> mold wall
	<i>x, y, z</i> direction

1. INTRODUCTION

The most distinguished characteristic in squeeze casting process is that solidification starts and ends under an applied pressure. The effects of pressure include: reduction of porosity, change of the equilibrium diagram and reduction of grain size [1, 2]. Therefore, the cavity pressure during the squeeze casting process is one of the critical factors in making soundness casting. However, in practice, the cavity pressure usually is not listed as a process parameter, instead, the hydraulic pressure is measured and used as specific pressure, or the cavity pressure is even eliminated as a quality control variable by simply using big machine and providing more than the required press load [3]. The main reason was that the real characteristics of cavity pressure in squeeze casting had yet to be fully understood.

Due to the extreme hostile environment of squeeze casting cavity (the thermal, mechanical and chemical conditions in the die), there was rare reliable pressure sensor which can withstand such conditions. Therefore, it was almost impossible to measure the cavity pressure directly. So, it was not surprised that compared to total of about 1000 published papers related to squeeze casting, there are only very few research about the cavity pressure.

Matsubara et al [4] was probably one of the earliest published research related to topics of cavity pressure characteristics in squeeze casting. They measured the difference between the load applied and the load reached at the bottom of cavity in squeeze casting of pure aluminum, aluminum alloys and copper alloys, the friction force at the casting/mold interface was estimated.

Iwata et al [5] studied the transfer ability of molten metal pressure in the squeeze casting of Al-Si alloys, and found that the occurrence of shrinkage cavity depended on the duration of the transferred pressure, not so much as the value of the transferred pressure.

Krishna and Pehlke [6] tried using pressure transducer to directly measure cavity pressure in a squeeze casting, but only measured one location in the gate.

With the advent of new pressure transducers, several researchers have successfully carried out measurement of the cavity pressure in die casting [7-12]. In this study, an attempt has been made in characterizing the pressure distribution in the die cavity. A piezo-electric quartz pressure transducer was integrated into a die cavity with different geometrical shapes. The experiments have been carried out to reveal that the pressure distribution changes with the cavity geometry. Also, the change of the local cavity pressure at various locations in the duration of casting solidification was observed.

2. THEORETICAL CONSIDERATIONS

The magnesium alloy solidification process involves multiphase transforming from liquid to semi-solid, and then to solid. Different from most of other casting processing, a high pressure is applied during all the solidification process of squeeze casting, and casting deformation happens due to the external pressure. Therefore, it is necessary to analyze the deformation mechanism in every stage.

2.1 Thermal Contraction

During the solidification of squeeze casting, the temperature of molten metal decreases, consequently it results in a volume contraction ΔV_s , which can simply be expressed as:

$$\Delta V_s = \alpha \Delta T V \quad 3-1$$

where, α is coefficient of thermal expansion, ΔT is the change in temperature, and V is the original volume.

The speed of volume contraction v_s depends on the solidification rate. Therefore, for squeeze casting, the speed of pressure buildup v_p must be faster than v_s . Otherwise, the applied force could not be able to act on the casting surface, consequently, defects such as shrinkage porosity are generated in the casting [13].

2.2 Hydrostatic deformation

At the beginning of the solidification, the poured (filled) melt is in liquid state. Upon pressure being applied, it is typically under hydrostatic deformation if the melt temperature is still above the liquidus temperature. Under such a circumstance, all interfaces have the same pressure, and the only deformation is the volume change due to pressure, which is affected mainly by the bulk modulus or volumetric modulus of elasticity.

2.3 Plastic Deformation

As the melts continues to cool down, it first becomes mushy state and then solid forms from outside to inside. Since the yield stress of magnesium alloys at high temperature is very low, plastic deformation must be considered when it is within this temperature range.

Generally, the yield stress at high temperature can be expressed as:

$$\sigma = \sigma_m \exp[b(T_m - T)] \quad 3-2$$

where σ_m is the yield stress at melting temperature T_m , b is a temperature factor, T is the temperature of the material [13].

Levy-Mises Equations (Ideal Plastic Solid) describe the plastic deformation as following [14, 15]:

$$d\varepsilon_1 = \frac{d\bar{\varepsilon}}{\bar{\sigma}} [\sigma_1 - \nu(\sigma_2 + \sigma_3)] \quad 3-3$$

$$d\varepsilon_2 = \frac{d\bar{\varepsilon}}{\bar{\sigma}} [\sigma_2 - \nu(\sigma_1 + \sigma_3)] \quad 3-4$$

$$d\varepsilon_3 = \frac{d\bar{\varepsilon}}{\bar{\sigma}} [\sigma_3 - \nu(\sigma_2 + \sigma_1)] \quad 3-5$$

Where ε_1 , ε_2 , and ε_3 and principal stresses. ν is poisson's ratio. ε , σ is effective strain and stress.

The yield criteria for ductile metals (Von Mises criteria) is:

$$\sigma_o = \frac{1}{\sqrt{2}} [(\sigma_1 - \sigma_2)^2 + (\sigma_2 - \sigma_3)^2 + (\sigma_3 - \sigma_1)^2]^{1/2} \quad 3-6$$

where σ_o yield stress in uniaxial tension.

2.4 Elastic Deformation

When the solidified part temperature is low enough where the yield stress is higher than the pressure applied, only elastic deformation occurs. For elastic deformation, Hook's law is valid [14,15]:

$$\frac{\sigma}{\varepsilon} = E = \text{cons tan } t \quad 3-7$$

where E is the modulus of elasticity in tension or compression. The stress-strain relations are:

$$\varepsilon_x = \frac{1}{E} [\sigma_x - \nu(\sigma_y + \sigma_z)] \quad 3-8$$

$$\varepsilon_y = \frac{1}{E} [\sigma_y - \nu(\sigma_x + \sigma_z)] \quad 3-9$$

$$\varepsilon_z = \frac{1}{E} [\sigma_z - \nu(\sigma_y + \sigma_x)] \quad 3-10$$

ν is poisson's ratio, for A356 it is 0.3.

$$\varepsilon_y = \varepsilon_z = -\nu\varepsilon_x \quad 3-11$$

For two-dimensional problem in elasticity, Airy's stress function combines both equilibrium and compatibility equations together into an integration [16]:

$$\frac{\partial^4 \Phi}{\partial x^4} + 2 \frac{\partial^4 \Phi}{\partial x^2 \partial y^2} + \frac{\partial^4 \Phi}{\partial y^4} = 0 \quad \text{or} \quad \nabla^4 \Phi = 0 \quad 3-12$$

Where Φ is stress function, $\sigma_x = \frac{\partial^2 \Phi}{\partial y^2}$, $\sigma_y = \frac{\partial^2 \Phi}{\partial x^2}$, $\tau_{xy} = -\frac{\partial^2 \Phi}{\partial x \partial y}$

Considering the consequence of temperature change over the elastic body, we have:

$$\nabla^4 \Phi + \alpha E \nabla^2 T = 0 \quad 3-13$$

2.5 Friction between casting and the mold

(i) Coulomb Friction. Friction is proportional to the stress normal to the surface of the workpiece. The proportionality is defined by a coefficient of friction which is assumed to be constant throughout the metal forming operation.

$$t_f = m s_n \quad 3-14$$

where t_f = friction stress tangential to the surface

m = coefficient of friction

s_n = compressive stress normal to the surface (contact pressure)

This law is not applicable to bulk metal forming because high contact pressures are involved. At high contact pressures the Coulomb law predicts friction stresses greater than the shear strength of the metal and sticking rather than sliding is modeled at the interface. Coulomb friction is more applicable to sheet metal forming where surface pressures are lower.

(ii) Tresca Friction. Friction stress at the contact surface is equal to a fraction of the shear yield stress of the work piece material. It is calculated using a constant friction factor.

$$t_f = m k \quad 3-15$$

where m = friction factor

k = shear yield stress of the work piece

This law is applicable to bulk metal forming because, unlike Coulomb friction, the amount of friction is independent of the normal stress at the surface.

(iii) Viscoplastic Friction. Friction is rate dependent. It is calculated from a constant friction factor, the work piece velocity relative to the tool velocity, a power index and the consistency of the work piece material.

$$t_f = -\alpha K v^p \quad 3-16$$

where α = friction factor

v = relative velocity

p = sliding velocity sensitivity index

This law is very similar to the Norton–Hoff formulation used by FORGE2 to describe the metal flow.

3. EXPERIMENTAL SETUP AND PROCEDURES

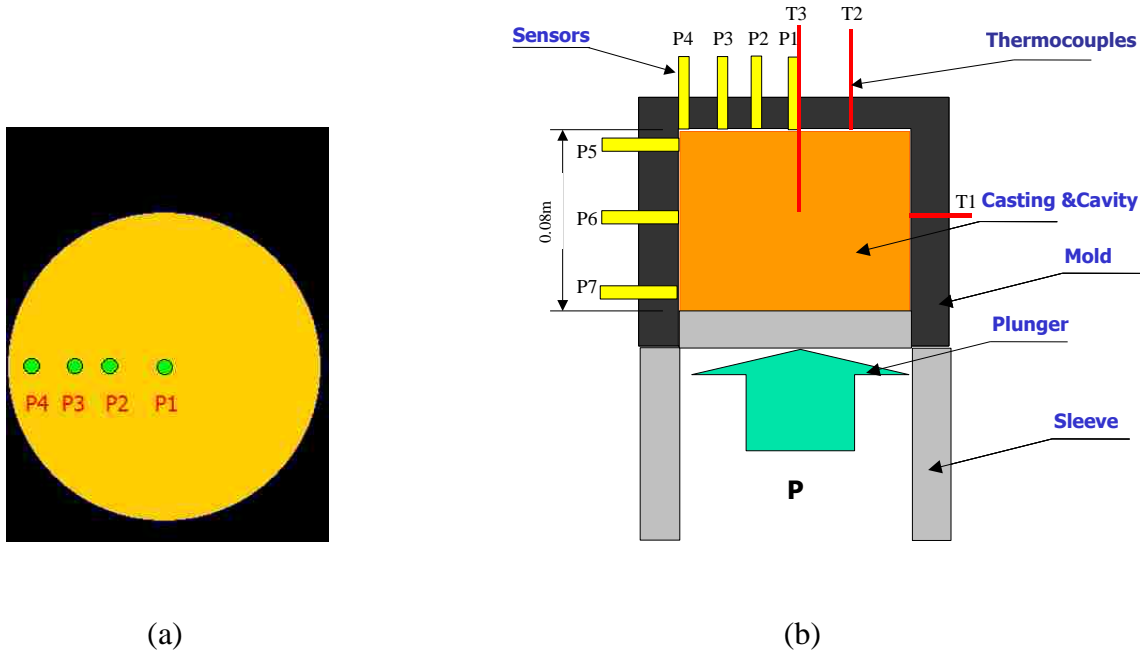


Figure 3- 1: Scheme diagram showing the locations in which pressure transducers and thermal couples are embedded in the system, (a) top view, and (b) cross-section view.

The squeeze casting system studied in this project is schematically shown in Figure 3-1, which consisted of a 75 tons hydraulic press, die, melting furnace and data acquisition system. The die assembly used to carry out the casting composed of two parts: the upper mold of casting cavity with a diameter of 0.1016 m and a height of 0.09652 m; and the bottom sleeve with a diameter of 0.1016 m and a height of 0.127 m and plunger. This combination enables to make a cylindrical casting with a diameter of 0.1016 m and a height of 0.08 m. Both the upper die and the bottom sleeve are heated by Acro-lab ceramic band

heaters, which are controlled by Shinko Temperature Controller separately. All experimental alloys were melted in a Lindberg electric resistance furnace. Magnesium alloy AM50 was held and melted in a mild steel crucible with a maximum holding capacity of 2 liters. Melting was carried out individually according to each casting. The temperature of the melt was regularly measured by an OMEGA digital thermometer during the melting. The molten metal was poured directly from the crucible into the sleeve to minimize the melts temperature drop. Protection gas (Sulfur Hexafluoride SF₆ 0.5% + carbon dioxide CO₂) was used during both melting and casting magnesium alloys to protect the melt from any excessive oxidation or possible burning. Pressure transducers (type 6175A2, Kistler) were mounted in the mold to measure directly the cavity pressure at different locations. The transducer type 6175A2 consists of a high temperature quartz sensor built into a rugged adapter. The transducer has a front diameter of 8 mm, is flush with the front of the adapter, separated by a cylindrical gap of <10 μm, and measures the pressure directly. The working range of this transducer is 0-200 MPa, it can stand an environment of 400°C, and the temperature of the melt touching the front of the sensor can be as high as 850°C. For the top surface, pressure sensors were incorporated into the die at 4 different locations (#1, #2, #3 and #4), as shown in Figure 1, to measure the local pressure variations during casting process. The purpose of those locations was to sense the ability of transferring the hydraulic pressure from the plunger head through the solidifying casting to the top end. For the side surface, although the sensor face is capable of being shaped with EDM machining to the cavity contour, in order to save the sensors, an indirect pressure measurement was chosen with a pin of 11mm diameter placed in the cavity, and the pressure sensor mounted behind the pin. Along the plunger moving direction, three

pressure sensors mounting locations (#5, #6 and #7), as also shown in Figure 3-1, were chosen to evaluate the pressure distribution on the die side surface. The purpose of those locations was to sense the ability of transferring the hydraulic pressure from the plunger head through the solidifying casting to the perpendicular surfaces. The thermocouple probes (KTSS-116U-12, OMEGA) were inserted into the cavity to measure the casting temperature. The data acquisition system (DAS) used in the testing was made by the Technical Support Center, which contains its own dedicated Processor: PCI-6033E (National Instrument). It consists of 8 temperatures (K-type) channels and 8 sensor channels. The analogue signals from the thermocouples and pressure transducers were sent to a data acquisition system through connector: SCB-100 (NI), and ultimately saved in a computer driver for permanent storage.

A software was developed based on Lab View so that it enables to program and monitor the process. The testing magnesium alloy AM50A, with chemical composition within the range of ASTM specification (Al4.5-5.3%, Mn0.28-0.50%, Zn<0.20%, Si<0.08%, Fe<0.004%, Cu<0.008%, Ni<0.001%, Be0.0005 – 0.0015% and Mg Balance), was used in this experimental investigation.

The operation procedure was: (a) Pre-heated the die to required casting temperature, and selected the operating parameters; (b) when the metal was ready, the molten metal was poured into shot sleeve; (c) the lower platen with the sleeve was moved up to close the upper die cavity, the melts was fed into the cavity by the piston; (d) a pressure was applied to the part right after the die cavity was filled, it was held down for a preset dwell time; (e) Piston retracted, and the lower platen returned to its original position, removed casting by an ejection pin. The cycle was repeated.

4. RESULTS AND DISCUSSIONS

4.1 Pressure distribution on the surface of a cylindrical casting

The initial pressure distribution on a cylindrical casting surface under applied pressure of 70 MPa and 35 MPa were shown in Figure 3-2. Obviously, the pressure distribution was not uniform either on the side or on the top surface.

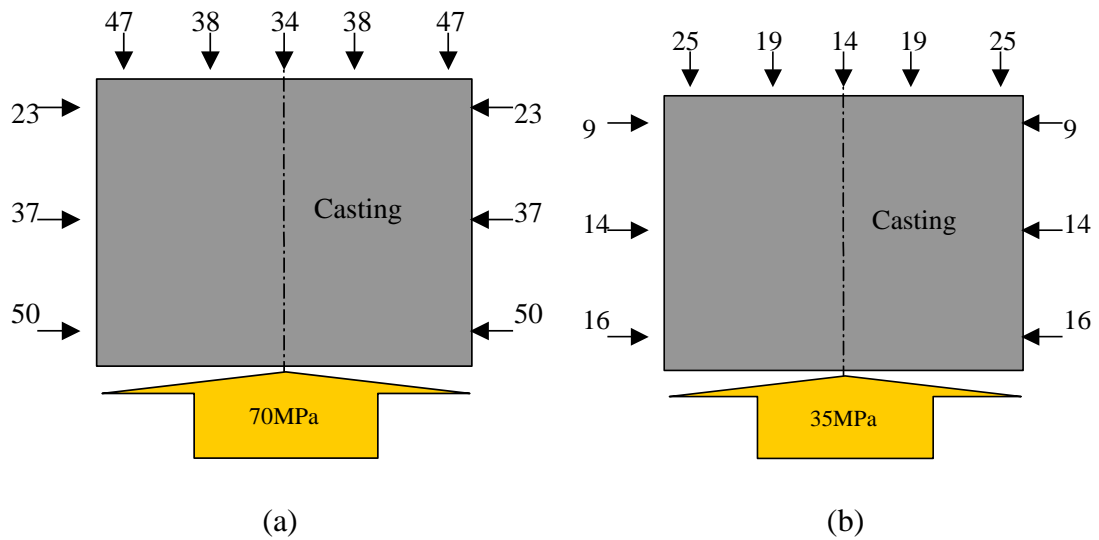


Figure 3- 2: Initial pressure distributions on the casting surface under applied pressure of (a) 70 MPa and (b) 35 MPa.

But, with checking the cooling curves at different locations in the casting, as shown in Figure 3-3, it was found that some area (outside) of the casting solidified when the filling was finished, which means a solid shell had already formed when the pressure was applied, therefore, it was impossible for the casting to be solidified under a hydrostatic pressure.

In Figure 3-2, the characteristics of pressure distribution on the side surface along the force direction can be explained that, in a closed cavity, for surface perpendicular to the direction of applying force, the force (pressure) was transferred by distortion as described in sections

2.3 & 2.4, basically, the larger the applied force the larger force transferred. The decrease trend of pressure along the force direct certainly should be attributed to the friction between the casting and the mold, which was also the main reason for degrading the applied force transferred to the top surface. Based on this, the relationship of applied force, side pressure and top pressure can be expressed as:

$$F_a \times \pi r^2 = \int_0^h f P_s(h) 2\pi r dh + \int_0^r P_t(r) 2\pi r dr \quad 3-17$$

where F_a is applied force, $P_s(h)$ and $P_t(r)$ pressure distribution on side and top surface respectively, f is the friction factor on casting/mold interface, h is the height of the casting and r is the radius of the casting.

Based on this equation and the experimental data of pressure distribution, it was estimated that friction factor at side casting/mold interface was around 0.2 for the initial, and about 0.45 when the pressure distribution was stable.

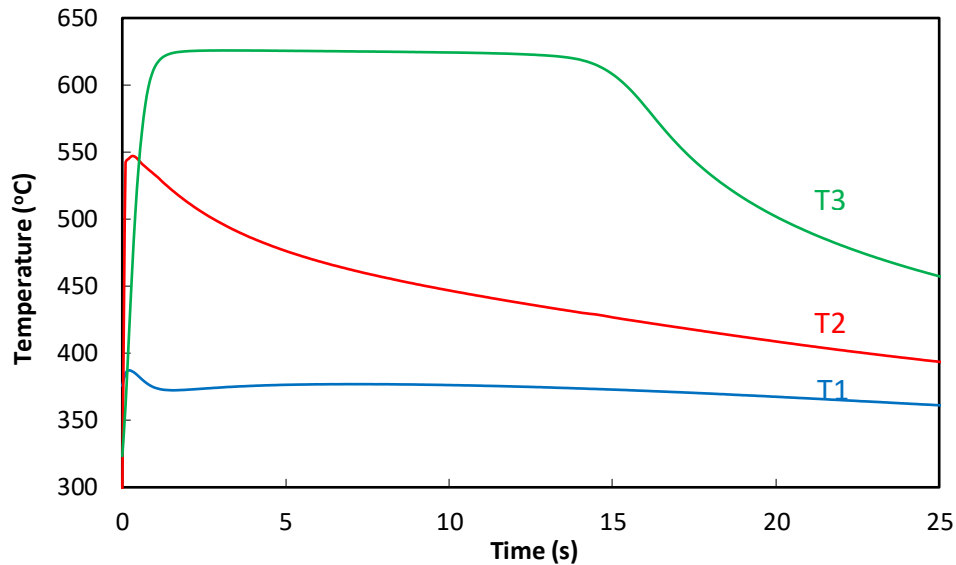


Figure 3- 3: Cooling curves at two locations in a cylindrical casting under applied pressure of 70 MPa.

It can also be found from Figure 3-2 that the pressure at the center top was lower than the rest of the top surface, this is due to the surface shape change caused by the delay of the filling. As described previously, after pouring, it took about 15s second to complete the filling, and during this time, solidification led contraction and shrinkage, and made the center level. Thus, the contact between the casting and the mold at top center should not be as close as other area.

4.2 Pressure distribution change with time

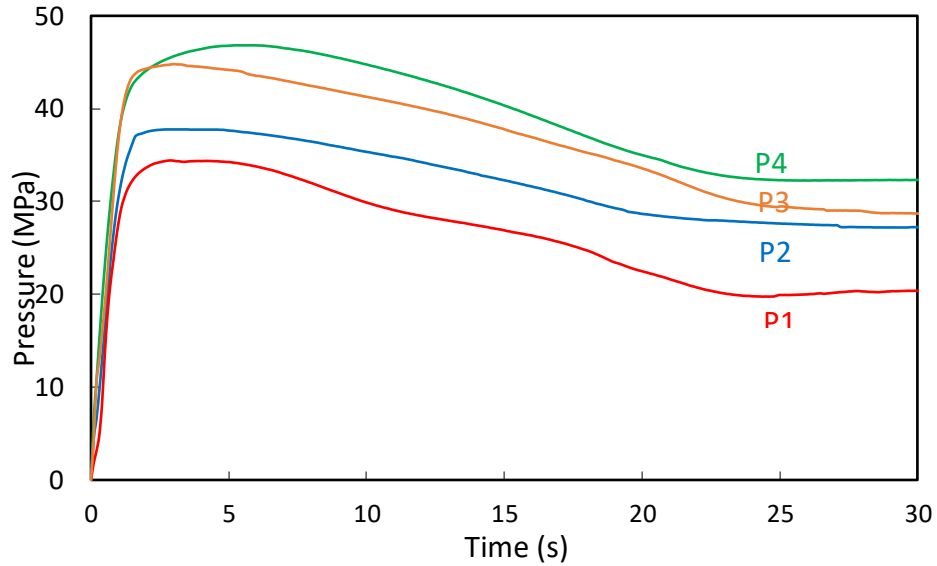
Figure 3-4 (a) & (b) show the pressure development curves at different locations of a cylindrical casting. As it can be seen that the cavity pressure built up quickly after the cavity filling completed and the external force applied. But, once it reached its peak, it began to decrease, after about 25 seconds, the curves became quite flat which means the pressure distribution was stable.

The reason for such an evolution on the top surface might be explained as (a) increase of friction at the casting/mold interface, because the friction factor is decided by the shear yield stress of the material (Tresca law, 2.5 (ii) above), which increases when the temperature decreases; (b) the contraction of the casting due to temperature decrease.

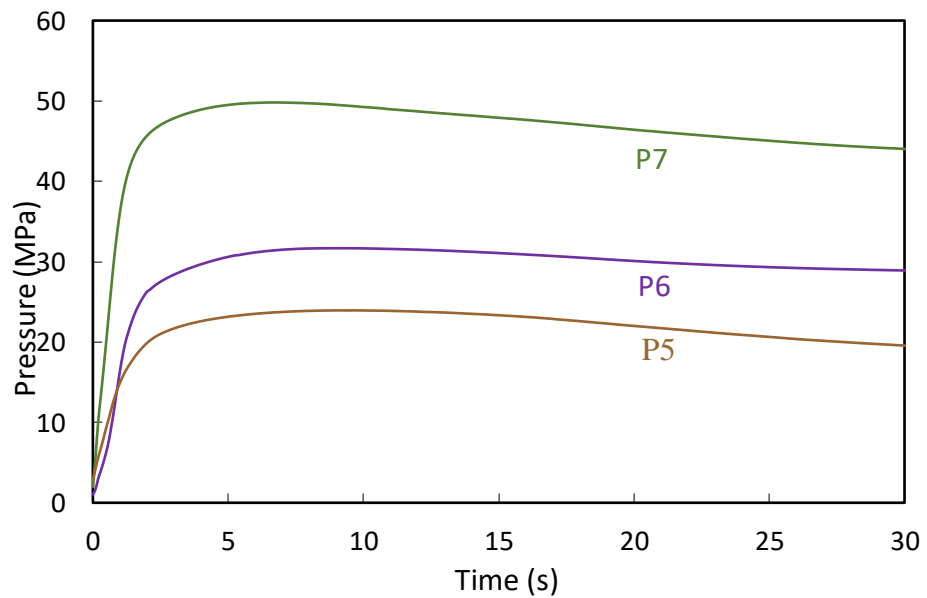
For the side surface, it should also be attributed to the increase of the metal strength with decrease of temperature, which means less distortion, therefore less force was transferred.

It can also be seen that the change trend (decrease) on top surface was more significant than on the side, this was mainly due to the temperature difference between the top and the side, as shown in Figure 3-3, the top surface temperature was much higher than the side, and the bigger the temperature drops the more contraction.

Cooling curves in Figure 3-3 reveals that the casting finished solidification about 25 seconds after completion of filling, this explained that the pressure curves became stable around the time.



(a)



(b)

Figure 3- 4: Local Pressure change with time on (a) the top surface, (b) side surface of a cylindrical casting under applied pressure of 70 MPa.

4.3 Variation of Pressure Transfer Rate and Temperature

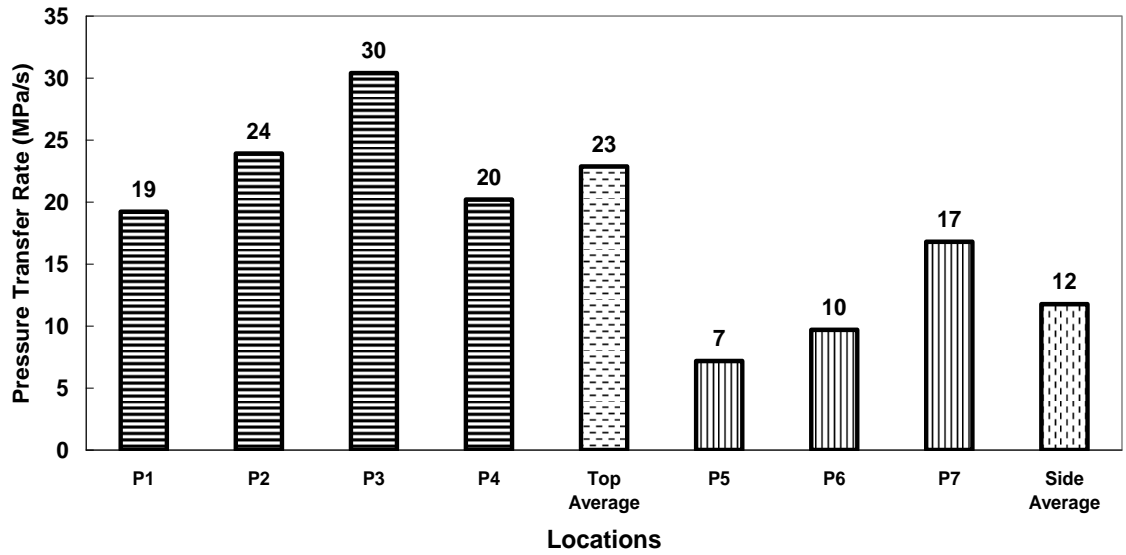


Figure 3- 5: Initial local pressure transfer rates on the top and side surfaces of a cylindrical squeeze casting of magnesium alloy AM50A.

Examination of Figure 3-4 manifests that, at the beginning of the external force application, the local pressures increased up to 95% of its peak value along the top surface in a much faster pace than that at the side surface of the casting despite that the local pressures along the top surface decrease considerably faster than those at the side surface after a certain period of time. For the clarification of discussion, the increasing rate of the local pressures up to 95% of its peak value is defined as an initial local pressure transfer rate thereafter in the text. Figure 3-5 compares the initial pressure transfer rates on the top surface to those at the side. The pressure transfer rate on the top surface varies from 19 to 30 MPa/s with an average of 23 MPa/s. But, at the side surface, the average pressure transfer rate is only around 12 MPa/s. This observation suggests that the pressure transfer in a direction perpendicular to the external force is faster than that in a parallel direction.

4.4 Pressure variation in different die cavity configurations

Figure 3-6 shows three different cavity configurations; experiments have been carried out to see how cavity shape may affect the pressure distribution. In Figure 3-7, the testing results show that in cavity A2, the pressure response was the largest, and became smaller from A3 to A1, it was evident that the influence of cavity shape was significant. It was possibly a result of solidification rate, as the surface/volume ratio of the casting increased from A2, to A3 and to A1. Also it might have related to the transfer distance of the applied force, as it could directly affect the distortion.

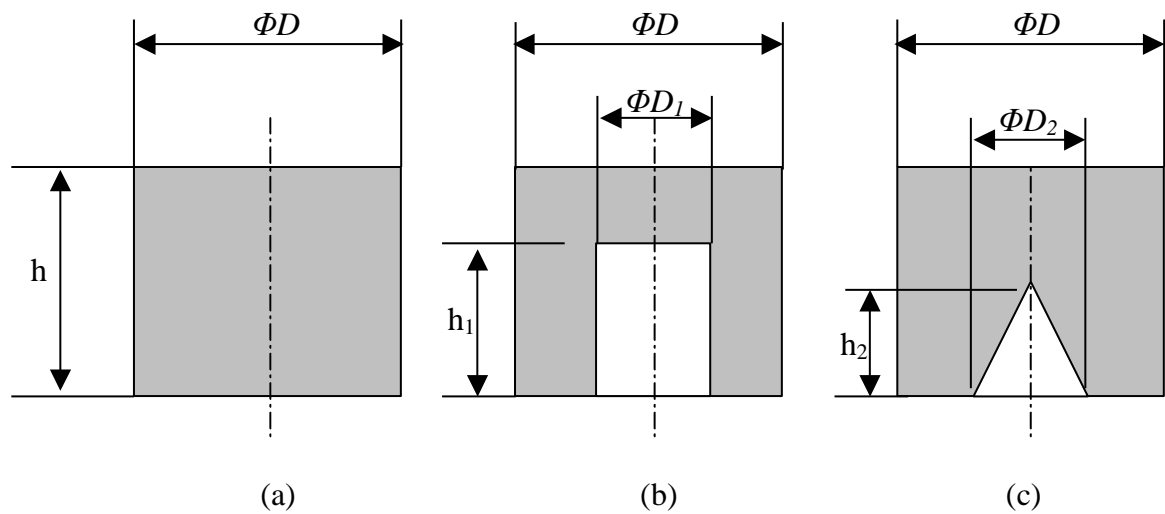


Figure 3- 6: Three different cavities, (a) A1, (b) A2, (c) A3.

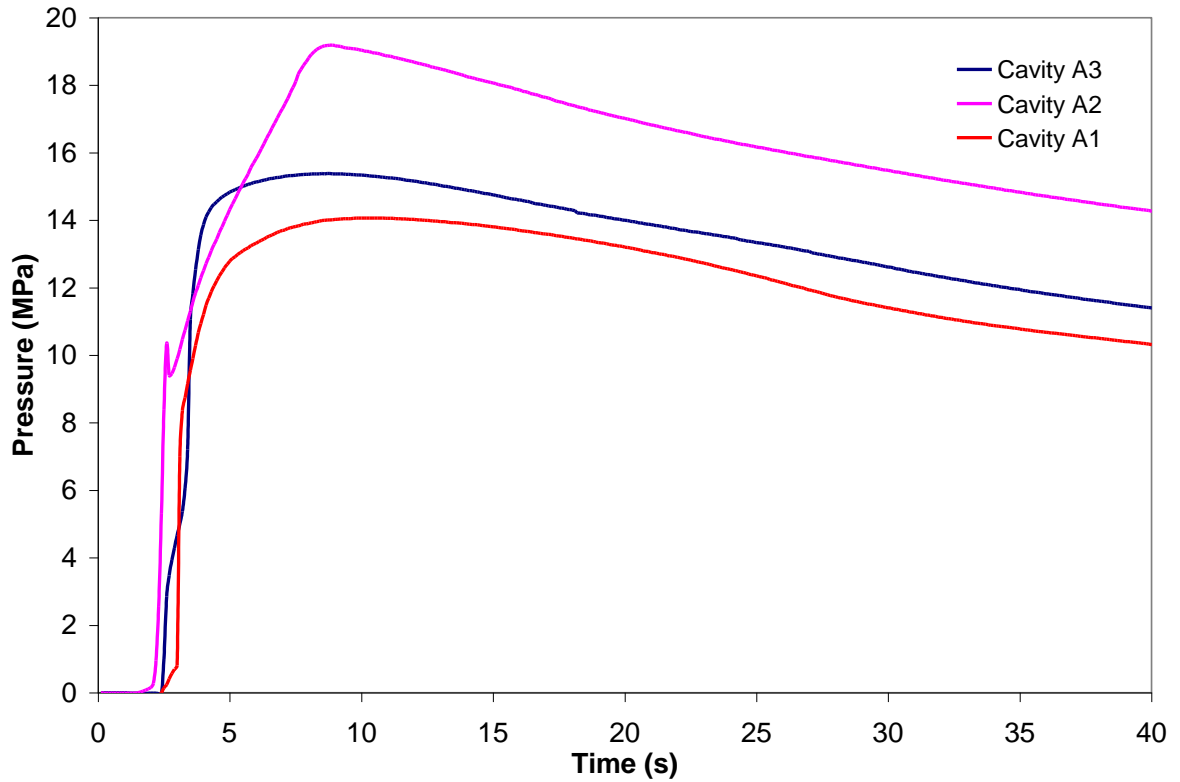


Figure 3- 7: Pressure development at the mid-side surface in different cavities under an applied pressure of 35 MPa.

5. CONCLUSIONS

1. Experiments have been taken to obtain an understanding of the cavity pressure phenomena in squeeze casting of magnesium alloy.
2. Measured casting surface temperatures show that while molten metal was pushed into cavity, instead of fully liquid, a solid shell was formed,
3. The pressure measurements indicated that the distribution of cavity pressure was non-uniform, it varied with locations and changes with time, but when the solidification of the casting was finished, the pressure distribution becomes stable.

4. The experimental data also revealed that cavity pressure was also strongly influenced by both cavity geometry and temperature.
5. Through experiments, it is possible to find out the friction factor at the casting/mold interface, which was essential for further simulation work.

REFERENCES

- [1] Rolland, Y., Squeeze Casting: A Literature Review. (Report Review). Gov. Res. Announc. Index. PB94-124575/XAB, 1993, 58.
- [2] Franklin, J. R., Das, A. A., Squeeze Casting--a Review of the Status. British Foundryman, Apr.1984, (77), 150-158.
- [3] Rajagopal, S., Squeeze Casting: a Review and Update. J. Appl. Metalwork. Jan. 1981, (1), 3-14
- [4] Matsubara, H., Nishida, Y., Suzuki, S., Measurement of Load Loss in Squeeze Casting. Rep. Gov. Ind. Res. Inst. Nagoya. July 1978, (3), 211-215.
- [5] Yasushi, I. W., Sugiyama, Y., Iwahori, H. and Awano, Y., Transferred pressure and shrinkage cavity of aluminum alloys on squeeze casting (Japanese). Casting Engineering, 2000, (72), 120-127.
- [6] Krishna, P., Pehlke, R.D., Theoretical and experimental of Indirect squeeze casting of A356 alloys. Light Metals, 2001, 377-390.
- [7] Venkatasamy, V.K., Analysis of in-cavity thermal and pressure characteristics in aluminum alloy die casting. Master Thesis, The Ohio State University, 1996.
- [8] Guthrie, B., and Whitbeck, R., Process optimization using in-cavity pressure transducers. NADCA Transaction, T99-073, Cleveland, 1999.
- [9] Tong, K.K., Steven, Hu, B.H., Niu, X.P.; Pinwill, I., Cavity pressure measurements and process monitoring for magnesium die casting of a thin-wall hand-phone component to improve quality. Journal of Materials Processing Technology, Sep 30, 2002, (127), 238-241.

- [10] Hu, B., Yong, J., Mun, C. C., and Kreij, J., Development of precision forming technologies for Magnesium Components. SIMTech Technical Report (PT/01/024/PMF), Precision Metal Forming Group, Process Technology Division, 2001.
- [11] Tanikawa, S., Asai, K., Yang, Y., Nomura, H., Kato, E., Effects of gate thickness on molten metal pressure transmission in high-pressure die cast cavity. *Journal of Japan Foundry Engineering*. Aug. 2003, (75), 525-531.
- [12] Kato, E., Nishiyama, N., Nomura, H., Asai, K., Tanikawa, S., Transferred pressure transfer relationship between mold filling flow of multi-piece aluminum die cast. *Japan Foundry Engineering*. 2002, (74), 370-376.
- [13] Xing, S.M., Ma, J., Chen, W.S., A rule for shrinkage prediction in squeeze casting process. *The Chinese Journal of Nonferrous Metals*. 1998, (8), 205-209.
- [14] Dieter, G.E., *Mechanical Metallurgy*, McGraw-Hill, New York, 1986
- [15] Meyera, M.A., a Chawla, K.K., *Mechanical Metallurgy*, Prentice-Hall, Inc., Englewood Cliffs, NewJersey, 1984.
- [16] Ugural, A.C., Fenster, S.K., *Advance strength and applied elasticity*, Prentice Hall, New Jersey, 2003.

CHAPTER 4

A STUDY OF SOLIDIFICATION AND MICROSTRUCTURE REFINING PHENOMENA OF SQUEEZE CAST MAGNESIUM ALLOY AJ62 WITH VARIATION IN APPLIED PRESSURES

1. INTRODUCTION

In order that squeeze casting process may become more widely used, not only the mechanical properties of the castings be fully evaluated, but also it is desirable to have a better understanding of the solidification behaviours of molten metal under an applied pressure [1, 2]. Mechanical properties of the castings are significantly affected by the casting structure which are depend on the casting conditions. The applied pressure during freezing could be considered as one of the most important casting parameters which has the greatest effects on the casting structure [3-5]. During squeeze casting process, the applied pressure eliminates air gap at the metal/die interface during solidification of the molten metal, thus enhances the heat transfer from the metal to the die, and consequently increases solidification rate [6]. In practice, there exists difference between the actual solidified microstructure and predicted form phase diagrams. This is mainly due to the fact

that the solidification taking place in most casting processes is under non-equilibrium conditions induced by the application of various solidification rate and/or pressures.

The effect of applied pressures on the melting point of an alloy system is given by the well-known Claucius-Clapeyron equation as follows.

$$\frac{dT}{dP} = \frac{T_m \Delta V}{H_f} \quad 4-1$$

where P is the applied pressure, T_m is the melting temperature under atmosphere conditions, H_f is the latent heat of fusion and ΔV is the volume change during freezing. During the solidification process, both ΔV and H_f are normally negative due to the shrinkage of metals and heat release, respectively. Thus, dT/dP is positive, which indicates that the applied pressure increases the melting point of a metal having a volume decrease tendency during solidification.

In the open literatures, many researches have been reported on squeeze casting of magnesium alloys. Yang et al. [7] optimized process parameters by investigating the effect of applied pressure, pouring temperature and die temperature on the microstructure of squeeze cast Mg-Nd alloy. Yong and Clegg [8] conducted a similar study and found that an applied pressure of 60 MPa was sufficient to eliminate all traces of shrinkage and gas porosity within the casting, the grain size reduced from 127 to 21um as the pressure increased from 0.1 to 60 MPa. Yue et al. [9] reported the influence of the grain size on mechanical properties of squeeze casting of magnesium alloy AZ91. Masoumi and Hu [10] reported the effect of applied pressure (3 to 90 MPa) on the tensile properties and microstructure of squeeze cast AX51 alloy. All of the above studies focused mainly on the relationship among process parameters and microstructure and properties. However, the

solidification behaviours of squeeze casting of magnesium alloys has not been systematically studied.

In this study, thermal and pressure sensors were employed to evaluate the evolutions of temperature and pressure distributions in a cylindrical squeeze casting. Investigation on the non-equilibrium solidification phenomena and microstructure of magnesium alloy AJ62 under various applied pressures has been carried out.

2. EXPERIMENTAL PROCEDURES

2.1 Material

The material used in this study was commercially-available magnesium alloy AJ62, of which chemical composition and thermal-physical properties are shown in Table 4-1 and 4-2.

Table 4- 1: Chemical composition of magnesium alloy AJ62 (wt. %)

Alloy	Mg	Al	Mn	Sr
AJ62	balance	6.1	0.34	2.1

Table 4- 2: Thermal-physical parameters of magnesium alloy AJ62

Material	Density	Specific heat	Thermal	Solidus	Liquidus
	P	C_p	Conductivity	Temperature	Temperature
	(g/cm ³)	(kJ/kg K)	k	T_s	T_l
			(W/m K)	(°C)	(°C)
AJ62	1.80	1.15	77	515	612

2.2 Squeeze casting

A 75-ton hydraulic press was used in the casting experiment. The metal was firstly melt in an electric resistance furnace with the protection of Sulfur Hexafluoride (SF_6) 0.5% + CO_2 gas mixture. The holding temperature of the furnace was 800°C . Both of the upper and bottom dies were preheated by band heaters. The upper die had a preheating temperature of 250°C , and 300°C for the lower die. The liquid metal was poured into the lower mold at 680°C . The liquid metal was squeeze casted in the upper die under a desired applied pressure and kept holding at that pressure for 25 seconds. Figure 4-1 shows a schematic drawing of the casting system. The casting was in round shape with diameter of 100 mm and a height of 80 mm. One Kistler pressure transducer was inserted into the cavity through the top wall of the die to measure the local cavity pressure. Meanwhile, local temperature in the casting was measured by Omega KTSS-116U thermocouple during solidification. As shown in Figure 4-2, the thermocouple was embedded in the casting center. Real time pressure and temperature data were recorded by a LabVIEW-based data acquisition system.

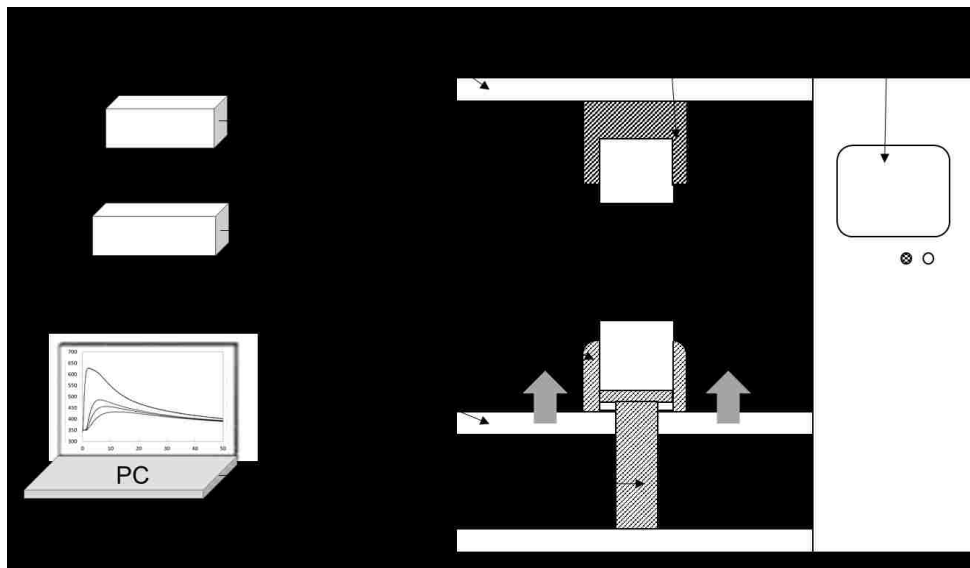


Figure 4- 1: Schematic diagram showing the squeeze casting and data acquisition system.

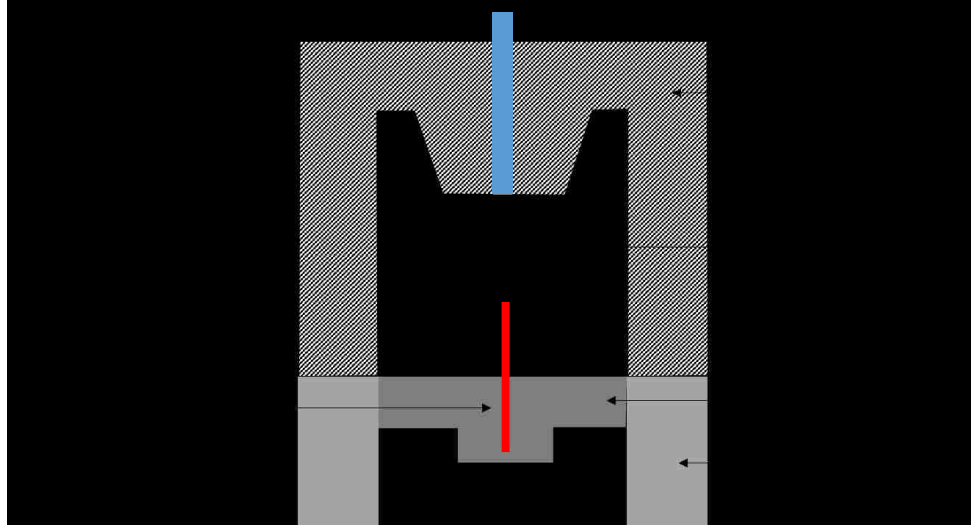


Figure 4- 2: schematic diagram showing the locations of pressure and temperature sensors in a cylindrical casting.

3. RESULTS AND DISCUSSION

3.1 Effect of applied pressure on liquidus and solidus temperature

Figure 4-3 shows a typical cooling curves measured in the center of the casting solidified under applied hydraulic pressures of 0, 30, 60 and 90 MPa. From the profiles of all the curves, the temperature decreased rapidly upon the molten metal was poured into the sleeve. Once the hydraulic pressure was applied, there was a significant increase in liquidus temperature. Then the temperature was kept almost constant for a certain period of time before starting to decrease to the solidus temperature. The increase in the liquidus and solidus temperature was in fully agreement with the Clausius-Clapeyron equation. As the applied pressure increased, the liquidus and solidus temperatures increased. Also, it can be seen from the temperature profile, the variation in applied pressures influences the holding duration of the liquidus temperature plateau. The measured liquidus temperature of

magnesium alloy AJ62 is 608.38, 609.67, 610.23 and 612.19°C for applied hydraulic pressures of 0, 30, 60 and 90 MPa, respectively. This observation indicates that the liquidus temperature of the alloy increased by 1.29, 1.85 and 3.81°C under the applied hydraulic pressure of 30, 60 and 90 MPa, respectively. The total solidification time for each casting was determined from the cooling curves as shown in Figures 4-3 & 4-4. The total solidification time was taken as the time required for the casting to go from its liquidus temperature to the end of the eutectic arrest at the solidus temperature. As for the case of the alloy solidified at atmospheric pressure where this solidus temperature was not clearly defined on the cooling curves, the completion of solidification was taken to be the moment when the temperature reached the theoretical solidus at 515°C. The results showed that when the pressures of 30, 60 and 90 MPa were applied to the casting, the total solidification time were reduced by 29.5, 30 and 33 seconds compared to that obtained under the atmospheric condition.

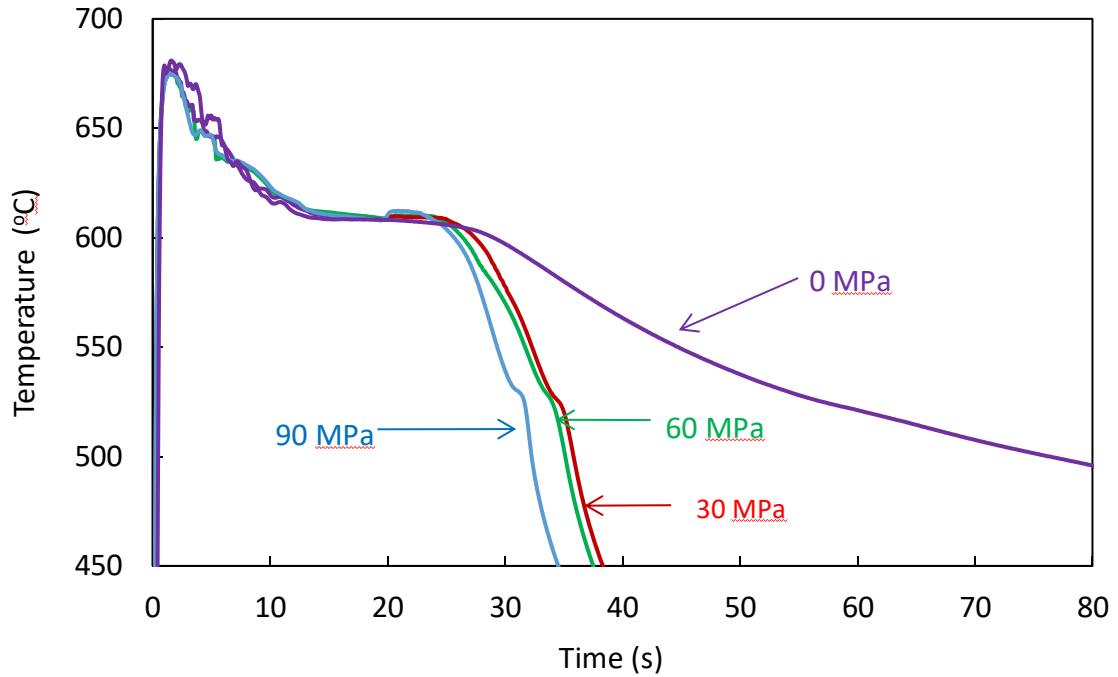


Figure 4- 3: Typical cooling curves of magnesium alloy AJ62 solidified under applied pressures of 0, 30, 60 and 90 MPa.

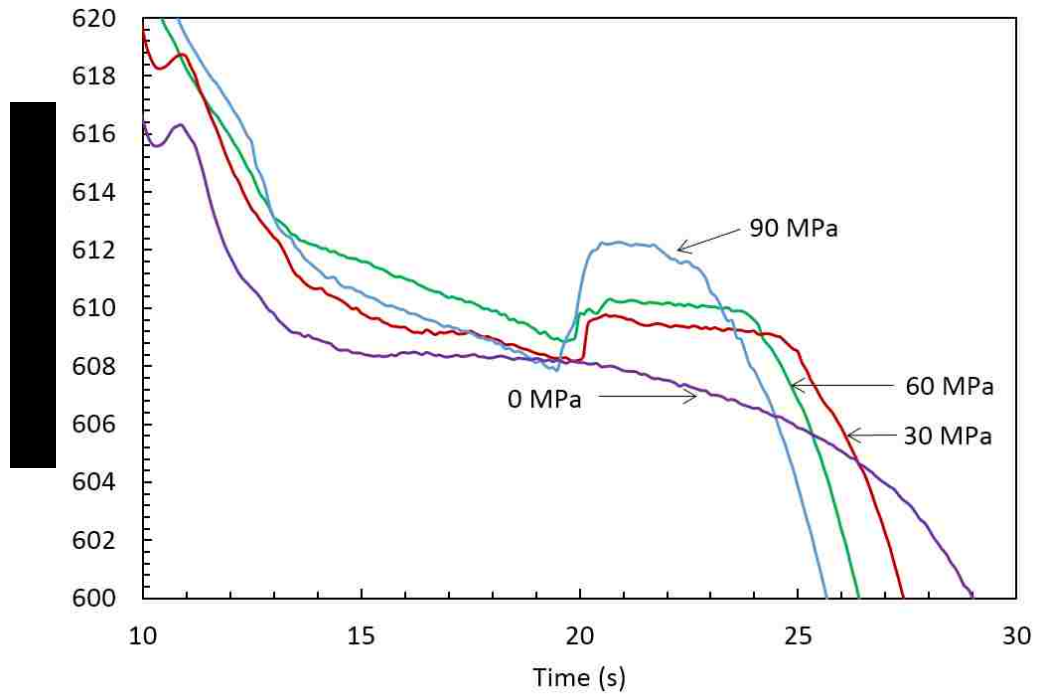


Figure 4- 4: Enlarged cooling curves showing the changes in liquidus temperatures of magnesium alloy AJ62 under applied pressures of 0, 30, 60 and 90 MPa.

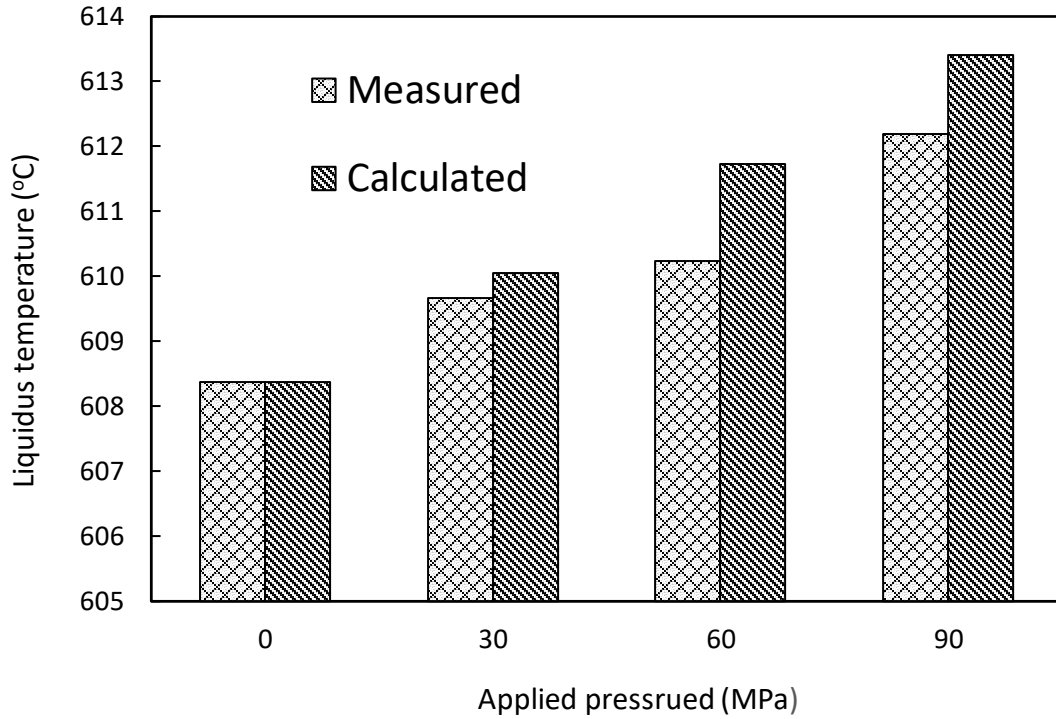


Figure 4- 5: Measured and calculated liquidus temperature of magnesium alloy AJ62 with variation in applied pressures.

Figure 4-5 shows the comparison of the measured and calculated liquidus temperature of magnesium alloy AJ62 with changing in applied pressures. The calculated liquidus temperature was obtained from the integration of Eq. 4-1, as shown below:

$$T_p = T_m \exp\left(\frac{\Delta V}{H_f} P\right) \quad 4-2$$

where T_p is the solidification temperature under an applied pressure, T_m is the equilibrium solidification temperature, ΔV is the volume change during solidification, H_f is the latent heat of fusion. P is the applied pressure. In comparison to the equilibrium liquidus temperature of the alloy, the calculated liquidus temperature increased by 1.67, 3.34, and 5.02°C for the applied pressure of 30, 60 and 90 MPa, respectively. The deviation between the measured and calculated results might be attributed to the fact that the hydraulic applied

pressures values used in the calculations since it is almost impossible to place the pressure sensor at the same location with the thermocouple which is at the center of the molten metal to measure the local pressures.

3.2 Pressure loss during solidification

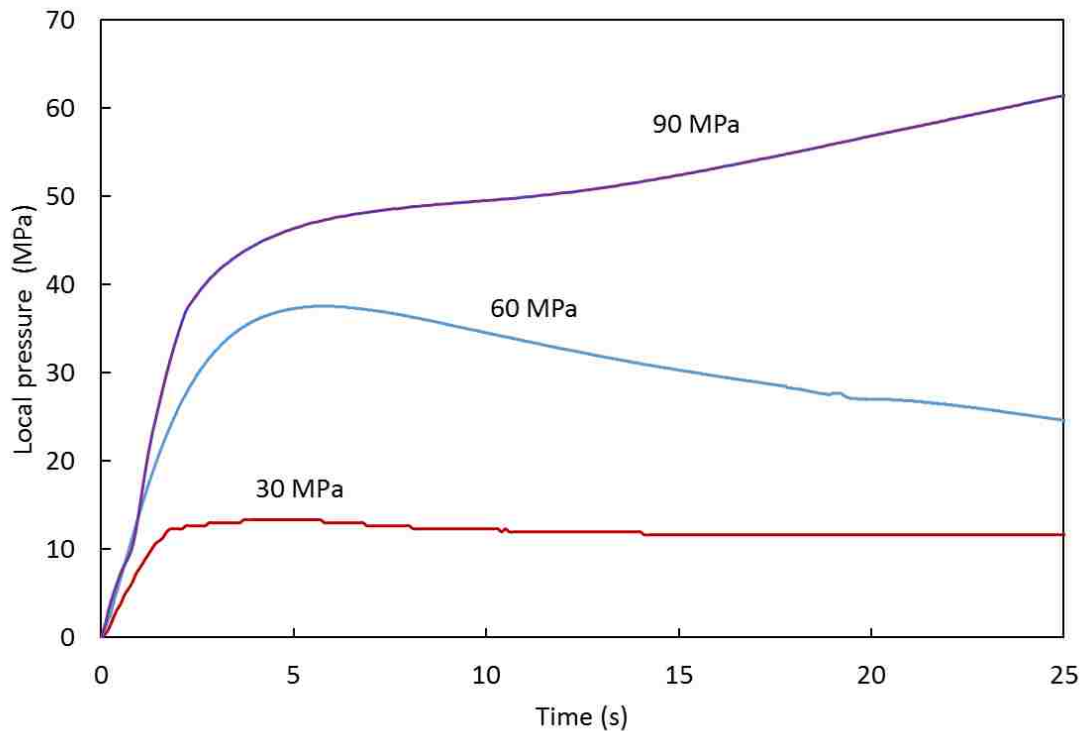


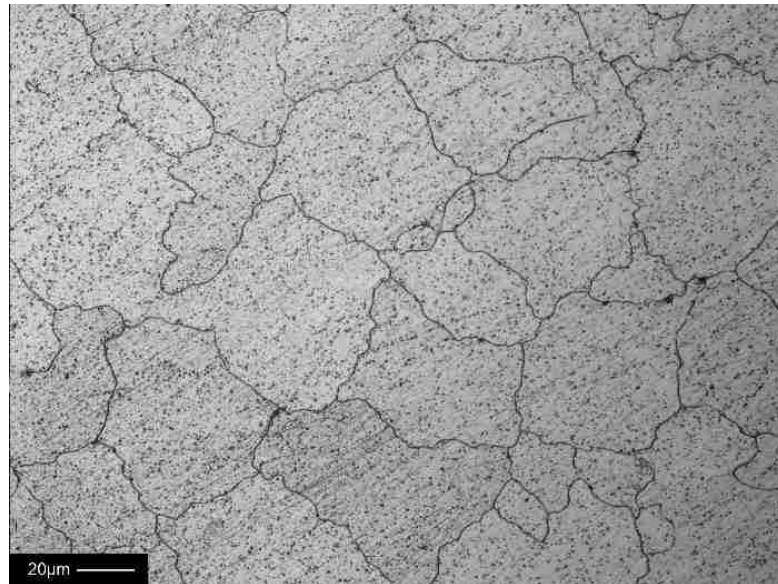
Figure 4- 6: Measured local pressure curves during the solidification of magnesium alloy AJ62 under applied hydraulic pressure of 30, 60 and 90 MPa.

Figure 4-6 shows the actual local pressures measured during the solidification of the alloy. The peak values of the local pressures are 13.33, 37.54 and 61.33 MPa. In comparison with the applied hydraulic pressures of 30, 60 and 90 MPa, it shows a significant pressure loss during the application of external pressures as the alloy solidifies. Mathematical, the pressure loss can be calculated by the following equation:

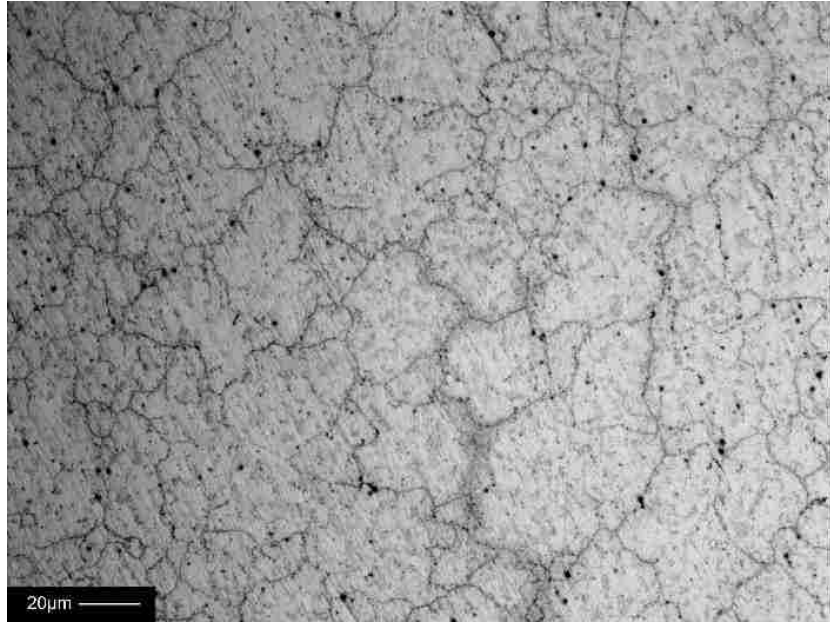
$$P_l(\%) = \left(\frac{P - P_i}{P} \right) \times 100 \quad 4-3$$

where P_l is the pressure loss, P the hydraulic pressure, and P_i is the peak value of experimentally measured instantaneous local pressure. As the hydraulic applied pressure increased from 30 to 90 MPa, the pressure loss during solidification were 55.6, 37.42 and 31.85 %, respectively. The pressure loss increased as the applied hydraulic pressure decreased. The phenomena of pressure loss might be due to the alloy densification and deformation induced by the applied pressure. This implies that, instead of using the local pressure, the direct employment of the applied pressure to calculate liquidus temperature led to the deviation between the calculated results and experimental measurements as shown in Figure 4-5.

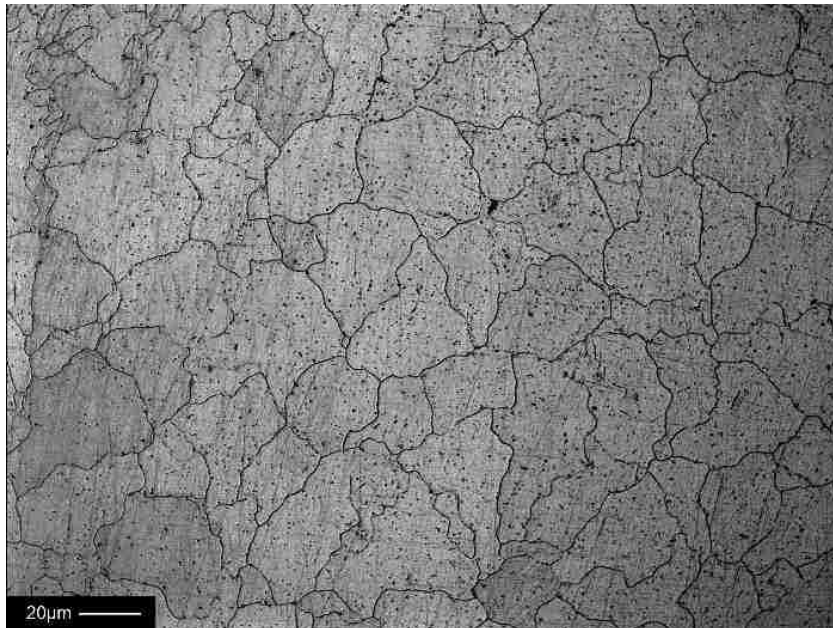
3.3 Effect of applied pressure on microstructure



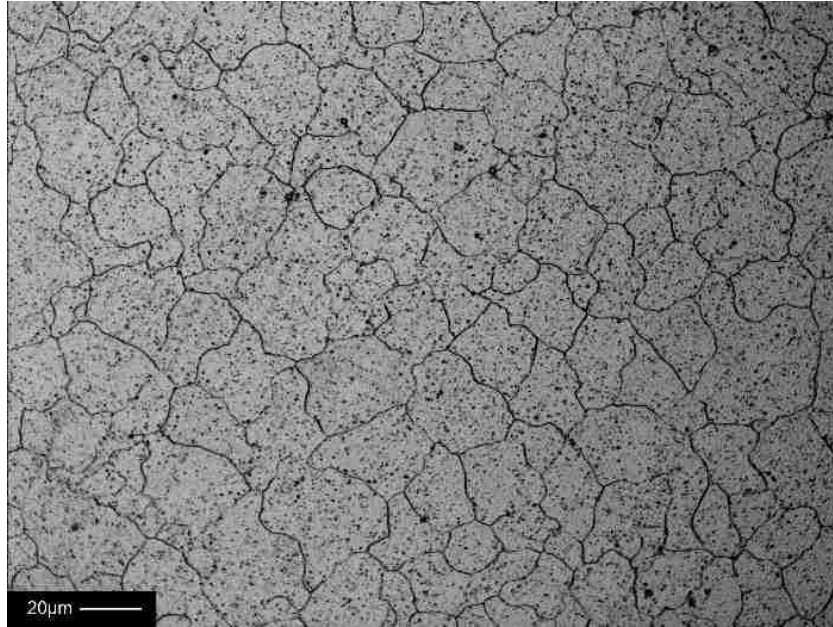
(a)



(b)



(c)



(d)

Figure 4- 7: Optical micrographs showing the grain size of the magnesium alloy AJ62 under applied hydraulic pressure of (a) 0 (b) 30 (c) 60 and (d) 90 MPa, the samples were heat treated (T4) and etched by 5% Nitric acid (HNO₃).

Figure 4-7 shows the grain structures of the squeeze casting magnesium alloy AJ62 under applied pressures of 0, 30, 60 and 90 MPa. As the pressure increased from the atmospheric pressure to 30, 60 and 90 MPa, the average grain size reduced by 21, 29 and 36 μm , respectively, compared to 64 μm at the atmospheric condition. The measured values of grain size were shown in Figure 4-8. This is because the applied high pressure increases the melting point of the alloy which was shown in Figure 4-3, and the molten metal was squeezed in close contact with the die surface to avoid the metal pulling out from the die surface at longer pressure duration (25 seconds) which kept the metal close to die cavity until the completion of solidification taking place. Consequently, the finer grain was obtained.

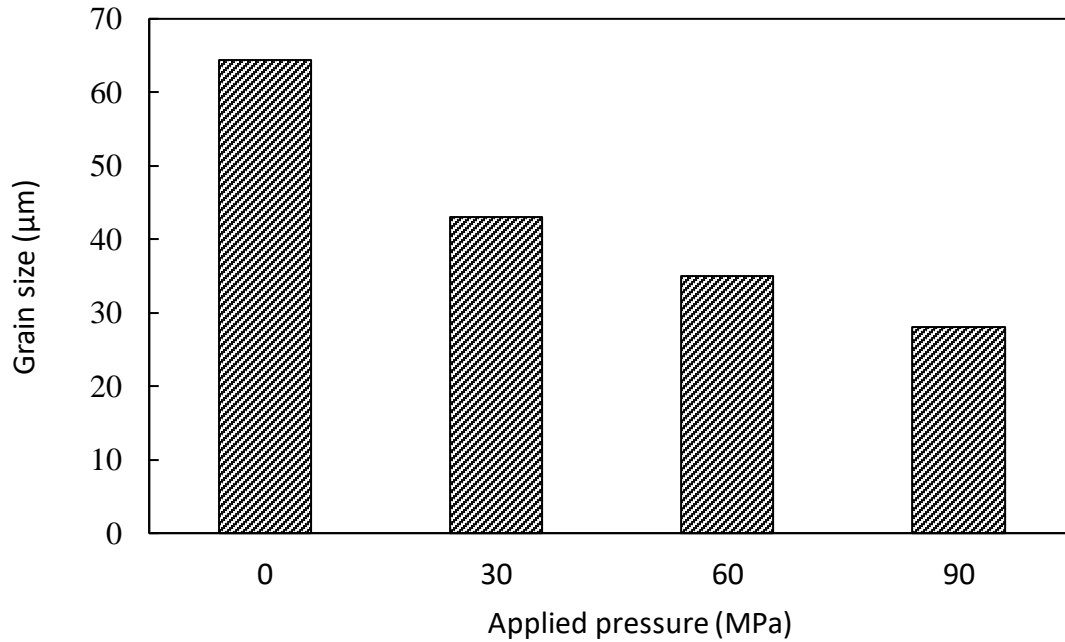


Figure 4- 8: Grain size measurements of the magnesium alloy AJ62 under applied pressure of 0, 30, 60 and 90 MPa.

4. CONCLUSIONS

It is evident from the experimental study that the solidification behaviour and microstructure of the magnesium alloy AJ62 depend on the external pressures during the solidification process. The following observations conclusions can be drawn from the current work,

1. The melting points of the alloy increased as applied pressures increased. The results show that the liquidus temperature of the alloy increased by 1.29, 1.85 and 3.81°C under the applied hydraulic pressure of 30, 60 and 90 MPa, respectively. Also, the

total solidification time were reduced by 29.5, 30 and 33 seconds compared to that obtained under the atmospheric condition.

2. By applying the Clausius-Clapeyron equation, the direct employment of the hydraulic pressure led to a reasonable overestimation in calculating the liquidus temperatures of the alloy.
3. The pressure loss increased as the applied hydraulic pressure decreased. As the hydraulic applied pressure increased from 30 to 90 MPa, the pressure loss during solidification were 55.6, 37.42 and 31.85 %, respectively. This phenomenon of pressure loss might be due to the alloy densification and deformation induced by the applied pressure.
4. The calculated liquidus temperatures increased as the applied pressure increased. The deviation between the measured and calculated results might be attributed to the local pressure loss since it is almost impossible to place the pressure sensor at the same location with the thermocouple at the center of the molten metal to measure the local pressures.
5. As the applied pressure increased, the grain structure was refined. As the pressure increased from the atmospheric pressure to 30, 60 and 90 MPa, the average grain size reduced by 21, 29 and 36 μm , respectively, in comparison to 64 μm at the atmospheric condition.

REFERENCES

- [1] M. R. Ghomashchi, A. Vikhrov, Squeeze casting: an overview. *Journal of Materials Processing Technology*. 2000, 101(1), 1-9.
- [2] H. Hu, Squeeze casting of magnesium alloys and their composites. *Journal of materials science*, 1998, 33(6), 1579-1589.
- [3] C. H. Caceres, C. J. Davidson, J. R Griffiths, C. L. Newton, Effects of solidification rate and ageing on the microstructure and mechanical properties of AZ91 alloy, *Materials Science and Engineering: A*, 2002, 325(1), 344-355.
- [4] N. A. El-Mahallawy, M. A. Taha, E. Pokora, F. Klein, On the influence of process variables on the thermal conditions and properties of high pressure die-cast magnesium alloys, *Journal of Materials Processing Technology*, 1998, 73(1), 125-138.
- [5] M. Zhang, W. W. Zhang, H. D. Zhao, D. T. Zhang, Y. Y. Li, Effect of pressure on microstructures and mechanical properties of Al-Cu-based alloy prepared by squeeze casting. *Transactions of Nonferrous Metals Society of China*, 2007, 17(3), 496-501.
- [6] Z. Sun, H. Hu, X. Niu, Determination of heat transfer coefficients by extrapolation and numerical inverse methods in squeeze casting of magnesium alloy AM60, *Journal of Materials Processing Technology*, 2011, 211(8), 1432-1440.
- [7] Y. Yang, L. Peng, P. Fu, B. Hu, W. Ding, B. Yu, Effects of Process Parameters on the Macrostructure of a Squeeze-Cast Mg-2.5 mass% Nd Alloy, *Materials transactions*, 2009, 50(12), 2820-2825.

- [8] M. S. Yong, A. J. Clegg, Process optimisation for a squeeze cast magnesium alloy, *Journal of Materials Processing Technology*, 2004, 145(1), 134-141.
- [9] T. M. Yue, H. U. Ha, N. J. Musson, Grain size effects on the mechanical properties of some squeeze cast light alloys, *Journal of materials science*, 1995, 30(9), 2277-2283.
- [10] M. Masoumi, H. Hu, Influence of applied pressure on microstructure and tensile properties of squeeze cast magnesium Mg–Al–Ca alloy, *Materials Science and Engineering: A*, 2011, 528(10) 3589-3593.

CHAPTER 5

DETERMINATION OF HEAT TRANSFER

COEFFICIENTS BY ENERGY BALANCE METHOD

IN SQUEEZE CASTING OF MAGNESIUM ALLOY

AJ62 WITH VARIATION IN WALL THICKNESSES

1. INTRODUCTION

Magnesium alloys have been widely used in today's automotive and aerospace industry due to its light weight characteristic. Magnesium is one-third lighter than aluminum and three-quarters lighter than zinc and four-fifths lighter than steel. Squeeze casting with the advantage of pressurized solidification, close dimensional tolerance and good surface finish has been widely used for complex shape casting. During the solidification process, the applied pressure feeds the liquid metal into the air or shrinkage porosities effectively. It makes castings free of porosity with excellent as-cast quality [1-3].

In today's foundry, numerical simulation improved the productivity significantly. However, one of the most important parameter, the interfacial heat transfer coefficients (IHTCs) at the metal-mold interface is usually roughly set in the available finite element method (FEM) or finite difference method (FDM)-based commercial codes [3-5]. To

ensure to accurately determine the solidification path, microstructure development and shrinkage porosity formation etc., it is necessary to have a precise prediction of boundary conditions. In the real-life casting process, the imperfection of the contact between the mold and liquid metal due to the air gap caused by the application of coating on die surface may decrease the heat transfer between metal and die as well as cooling rate of the casting surface. This thermal barrier could degrade casting quality and properties significantly. Therefore, an accurate prediction of IHTC is critical to simulate the solidification process. Many research works have been done to determine the interfacial heat transfer coefficient under different casting conditions. However, most of the attentions have been placed on permanent mold casting or high pressure die casting processes [6-9]. There is very limited knowledge about estimation of IHTC during squeeze casting.

In this work, squeeze casting experiments for fabricating a 5-step casting of magnesium alloy AJ62 were conducted. The metal/die interfacial heat transfer coefficient was determined based on the temperature gradient obtained at different locations inside of the die by using the energy balance method.

2. EXPERIMENTAL PROCEDURE

2.1 Experimental setup and sensor installation

Figure 5-1 graphically shows the installation of temperature sensor units (TSUs) and a data acquisition system. There were four thermocouples installed at each step. Three thermocouples were used to measure temperatures in the die, and one thermocouple for the

measurement of the casting surface temperature. All the thermocouples were connected to a data acquisition system to record the temperature history. Figure 5-2 shows the configuration of the 5-step die and the temperature sensor units. The dimensions for the five steps were 100x30x2, 100x30x4, 100x30x8, 100x30x12 and 100x30x20 mm, accordingly. Thermocouples A, B and C were inserted into the die at 2, 4 and 6 mm away from the inside die surface. Thermocouple D was inserted all the way through the die to the casting surface. The thermocouples used for all experiments were K-type thermocouple with 0.5 mm diameter and grounded sheathed for fast response time.

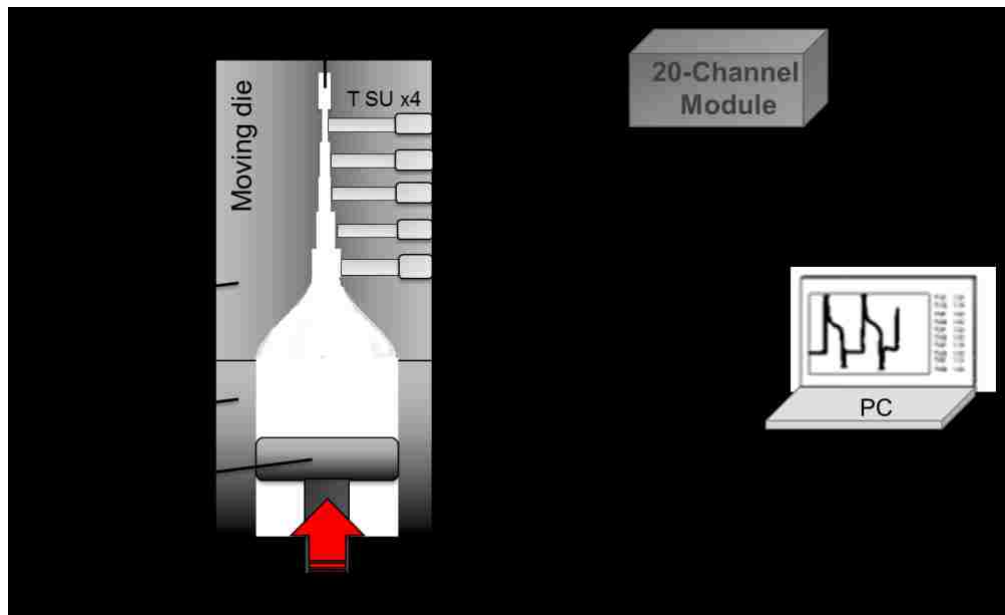
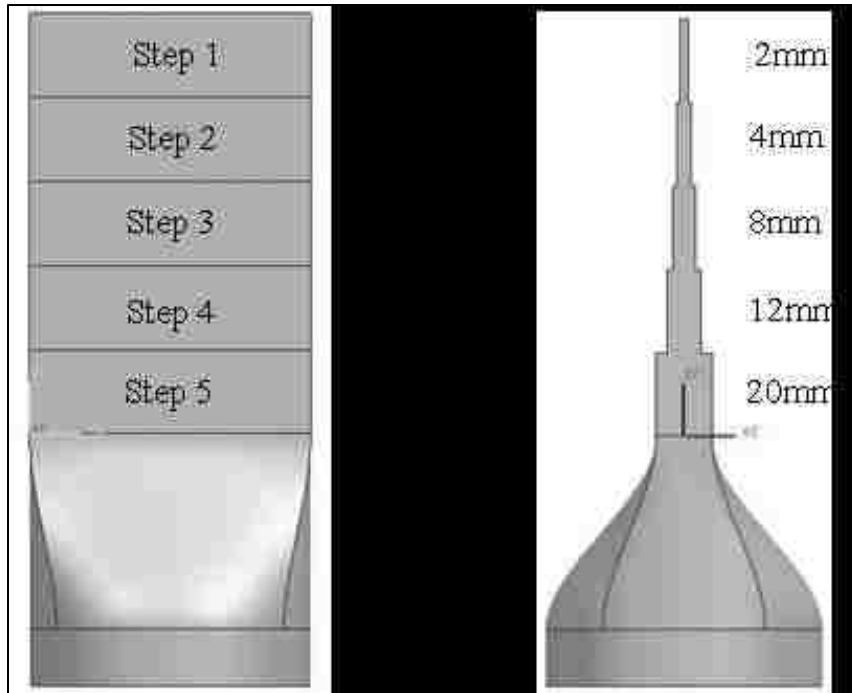
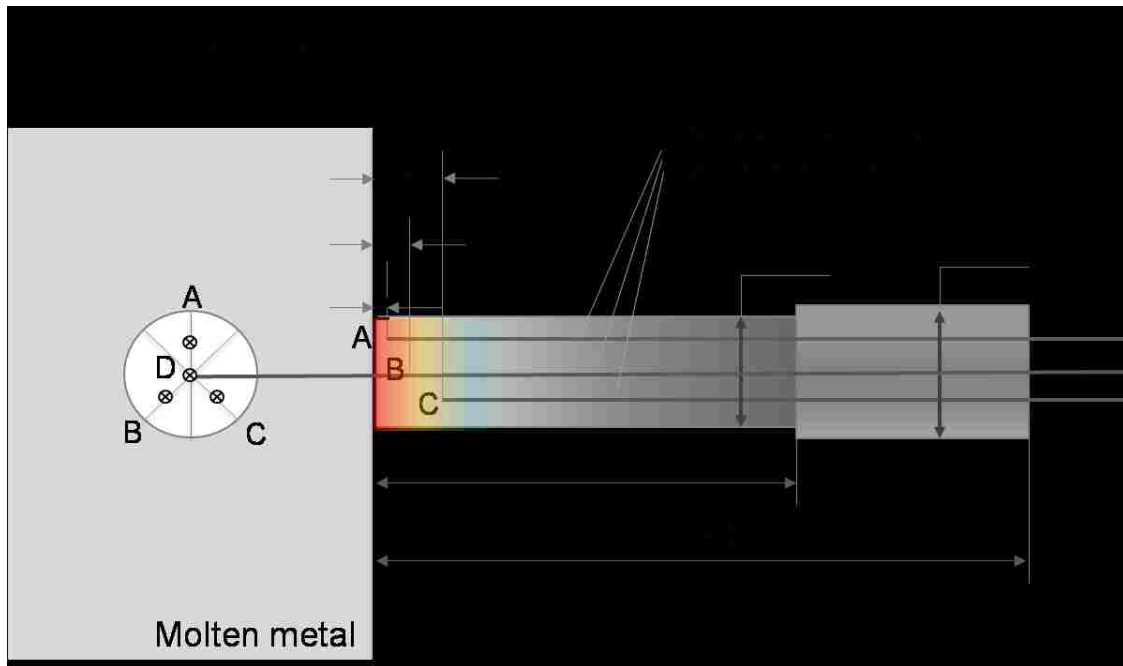


Figure 5- 1: Graphical illustrations showing a 5-step die connecting to temperature sensor units (TSUs) and a data acquisition system.



(a)



(b)

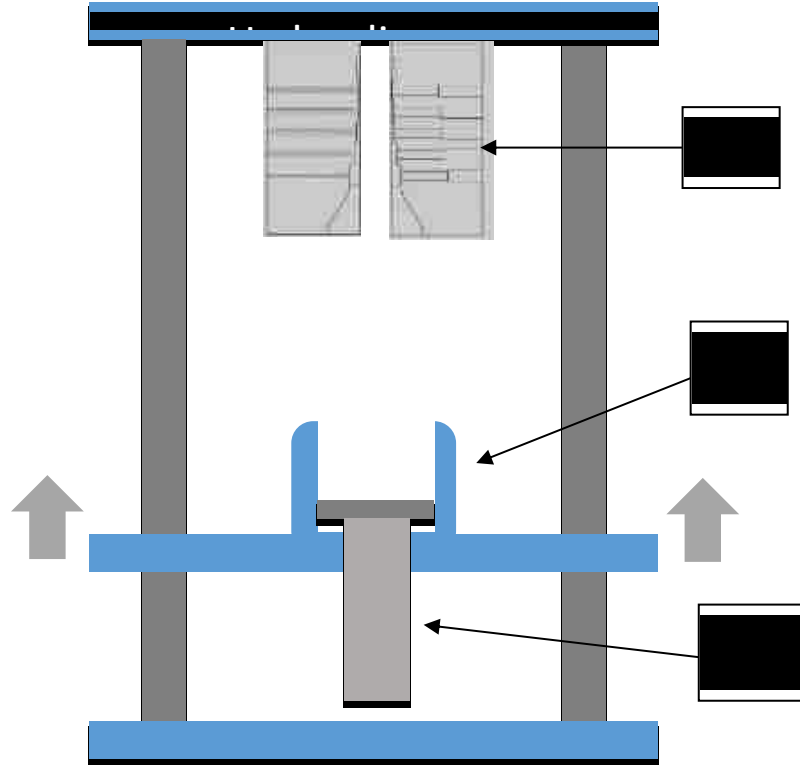
Figure 5- 2: Configuration of (a) a 5-step casting solid model and (b) a temperature sensor unit.

3.2 Casting Process

A 75-ton hydraulic press and magnesium alloy AJ62 were used in the experiment; the thermo-physical parameters for the alloy are summarized in Table 5-1. The metal was firstly melt in an electric resistance furnace with the protection of SF₆ gas. The holding temperature of the furnace was 800°C. As shown in Figure 5-3(b), the two half upper dies opened along the central parting line. The lower die had a diameter of 100 mm and a height of 200 mm. Both of the upper and lower dies were preheated by cartridge heaters. The upper die was preheated to 250°C and the lower die at 300°C. Liquid metal at 720°C was poured into the lower die. At last, the liquid metal was squeeze casted under an applied pressure of 60 MPa and kept holding under the applied pressure for 25 seconds.



(a)



(b)

Figure 5- 3: (a) a 75 tons hydraulic press and (b) schematic diagram of the squeeze casting machine, 1) upper die, 2) lower die and 3) piston.

Table 5- 1: Thermophysical properties of magnesium alloy AJ62

Material	Density (g/cm ³)	Specific heat (J/g K)	Thermo- conductivity (W/m K)	Solidus temperature (°C)	Liquidus temperature (°C)
AJ62	1.80	1.15	77	515	612

3.3 Determination of IHTC

The energy balance technique was employed to determine the interfacial heat transfer coefficient, in which attempts were made to monitor temperatures at the inner and outer surfaces of the interface. With the known short distance between temperature measuring surfaces, the temperature gradient adjacent to the die surface inside the die could be determined. Since the thickness was much smaller than the width at each step, the heat transfer coefficient could be solved as one-dimensional heat conduction problem. The governing equation for one-dimensional heat conduction in the die can be expressed as:

$$\rho c(T) \frac{\partial T(x,t)}{\partial t} = \frac{\partial}{\partial x} \left(k(T) \frac{\partial T(x,t)}{\partial x} \right) \quad 5-1$$

where k , c , and ρ are the heat conductivity, specific heat and density of the die, respectively.

The boundary condition at the metal/die interface was

$$q = h(T_c - T_d) \quad 5-2$$

where q and h were the heat flux and heat transfer coefficient at the metal/die interface and T_c was the casting temperature, and T_d was the die temperature.

With the experimental setup for determining the IHTC as described in the above configurations, the IHTC was estimated by performing an approximate energy balance based on the above equations, Eqs. 5-1 and 5-2.

$$h(T_c - T_d) = k_d \left(\frac{T_d - T_{d1}}{\Delta x_1} \right) + \frac{\Delta T_{d01} \Delta x_1 C_{pd} \rho_d}{\Delta t} \quad 5-3$$

$$k_d \left(\frac{T_d - T_{d1}}{\Delta x_1} \right) = k_d \left(\frac{T_{d1} - T_{d2}}{\Delta x_2} \right) + \frac{\Delta T_{d12} \Delta x_2 C_{pd} \rho_d}{\Delta t} \quad 5-4$$

where T_{d1} and T_{d2} were the local die temperature at location 1 and 2 respectively as shown in Figure 5-4, Δt was the time interval step of testing, Δt_{d01} and Δt_{d12} were the die temperature change for a time interval, and Δx_1 and Δx_2 were the distances between locations.

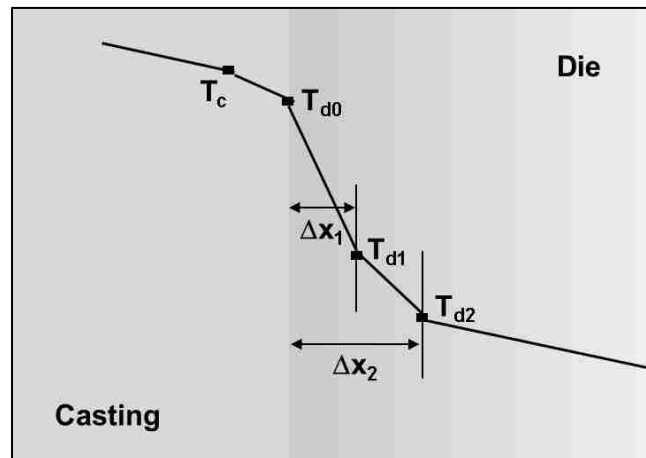


Figure 5- 4: Schematic drawing showing the temperature distribution at the metal/die interface.

4. RESULTS AND DISCUSSION

4.1 Experimental cooling curve

Figure 5-5 shows typical temperature versus time curves at the interface between the solidifying magnesium alloy AJ62 and steel die of step 5 with an applied hydraulic pressure of 60 MPa. The locations of the thermocouples were described in Figure 5-2, which included T_c (casting temperature) and T_{d1} and T_{d2} (die temperature). The following analysis of step 5 was based on this typical data with an applied pressure of 60 MPa. Since molten metal filled the cavity from the bottom of the lower die, the pre-solidification occurred upon the completion of cavity filling. No die temperatures exceeded 470°C, and the highest temperature of the casting surface was 632°C. To ease the result presentation and discussion, time zero was intentionally set at the instant when the cavity filling was completed and the applied pressure set in.

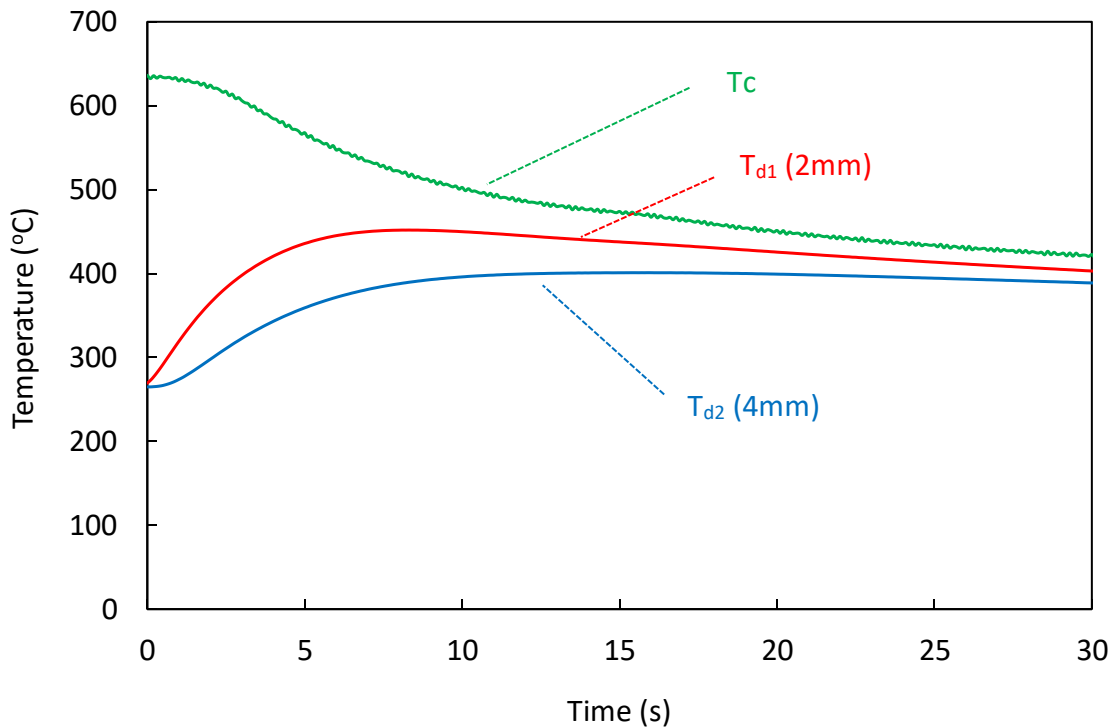


Figure 5- 5: Typical temperature versus time curves (Step 5, 60 MPa) at the metal surface and various positions inside the die (2 and 4 mm).

It can be seen from Figure 5-5 that the temperature curve at the casting surface (T_c) instantly increased to 632°C for an applied pressure of 60 MPa, due to the direct contact between thermocouple and the side layer of the casting. Then the casting surface temperature (T_c) kept almost unchanged for about three seconds. Meanwhile, the die temperature (T_{d1} and T_{d2}) increased by 60°C and 40°C respectively. After that, the casting surface temperature dropped rapidly. But, the die temperature still remained increasing for about another 7 seconds before it started to decrease. The temperature results of the casting surface showed that, at the beginning of the pressurized solidification, it took about three seconds for the applied pressure to force the casting surface in full and firm contact with the die.

4.2 Heat flux (q) and IHTC (h) curves

Figure 5-6 shows the change of interfacial heat flux (q) and heat transfer coefficient (IHTC) with the solidification time of step 5 with an applied hydraulic pressure of 60 MPa. The curves were estimated by the energy balance method based on the temperature gradient in Figure 5-5. At step 5 of the casting, the peak heat flux value was 6.02E+5 W/m², and the peak value of IHTC was 9,048 W/m² K. From the profile of the curves, it can be observed that the heat flux (q) reached its peak value abruptly within 4.6 seconds and decreased rapidly to a lower level (2.0E+04 W/m²) after 16 seconds. This significant increase in the heat flux should be attributed to the thermal contact at the metal/die interface and the large temperature difference at the beginning. The gradual decrease in heat flux was considered to be caused by a reduction in the thermal gradient.

The heat transfer coefficient (h) reached to its peak value (9,066 W/m² K) gradually at 11 seconds, and then decreased slowly to the lower level (2,164 W/m² K) after 40 seconds. This increase in the IHTC should result from the establishment firm thermal contact at the metal/die interface. The gradual loss of the good contact between the casting and the die gave rise to a slow drop of heat transfer coefficients for the rest of the process after the applied pressure was released.

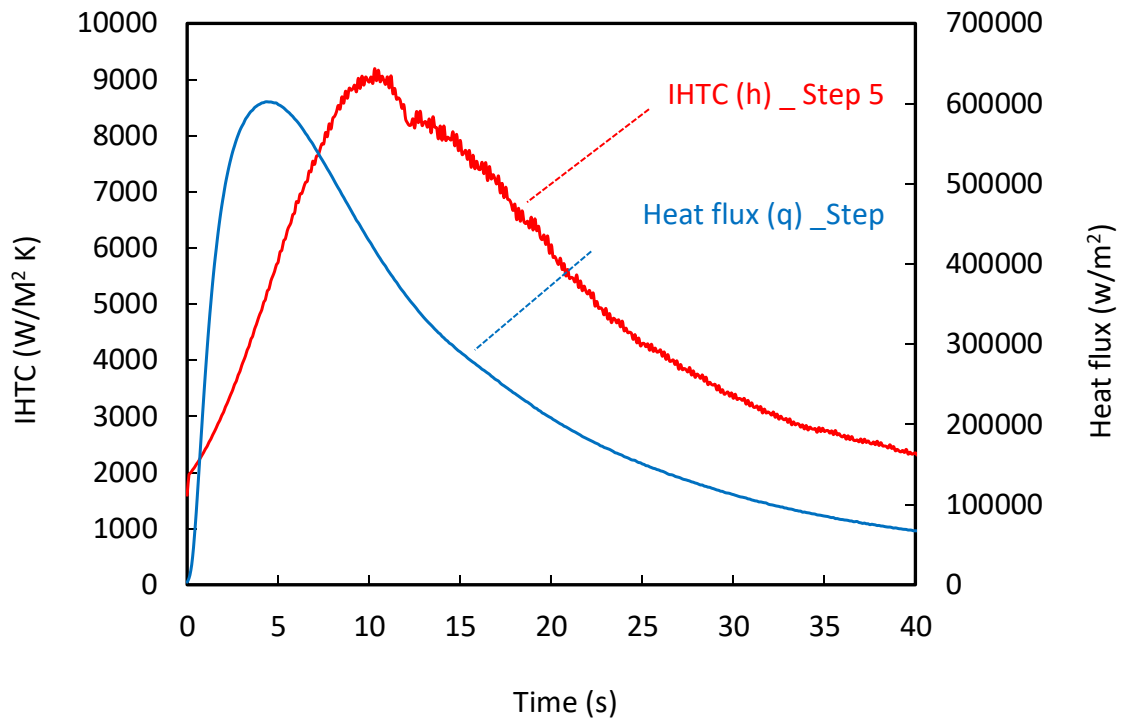


Figure 5- 6: Interfacial heat flux (q) and heat transfer coefficient (IHTC) curves for step 5 with an applied pressure of 60 MPa.

Figure 5-7 shows the heat flux (q) versus the solidification time of steps 1 to 5 with an applied pressure of 60 MPa. For these five steps, the peak heat flux values were 1.5E+05 W/m², 1.9E+05 W/m², 2.7E+05 W/m², 4.0E+05 W/m², and 6.0E+05 W/m², respectively. The curves of steps 1 to 4 exhibited similar profiles to step 5 which was described above.

They were all increased abruptly at the beginning as the liquid metal filled into the cavity and then dropped rapidly to their lower level.

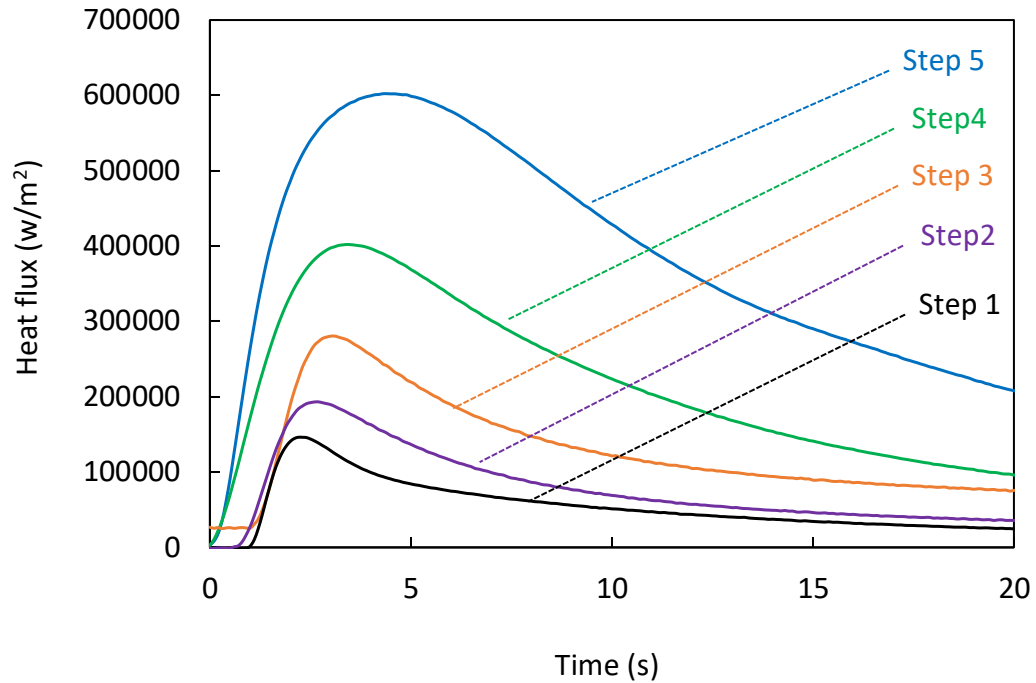


Figure 5- 7: Heat flux (q) curves for steps 1 to 5 estimated by the energy balance method.

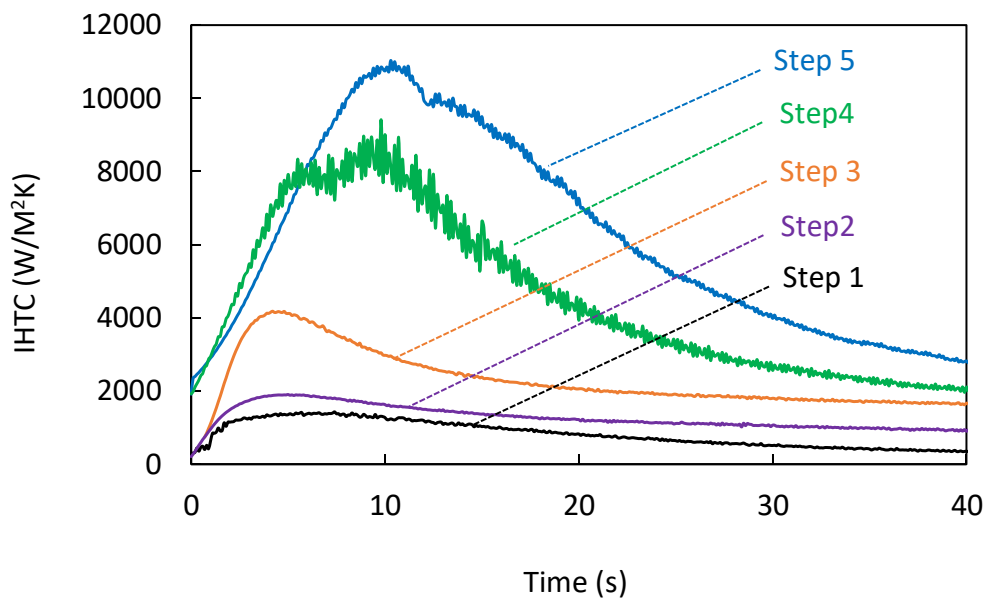


Figure 5- 8: Heat transfer coefficient (IHTC) curves for step 1 to step 5 estimated by the energy balance method for magnesium alloy AJ62 under an applied pressure of 60 MPa.

Figure 5-8 show the heat transfer coefficient (IHTC) curves of steps 1 to 5. For step 1, the IHTC began increasing and reached its peak value of 1,398 W/m² K at 7.53seconds, then decreased slowly to the level 200 W/m² K at 35 seconds. For step 2, the IHTC had a relatively low peak value of 1,876 W/m² K at 6.3 seconds, and then decreased slowly to the level 921 W/m² K at 40 seconds. However, for step 3, the IHTC increased rapidly at the beginning, and reached its peak value of 4,040 W/m² K at 5.5 seconds, and decreased slowly to the level 1,624 W/m²K at 40 seconds. The IHTC of step 4 rose sharply to its peak value of 6,383 W/m² K at 10.7 seconds, and then dropped quickly to the level 1,418 W/m² K at 40 seconds. The IHTC value for step 5 increased not as quickly as that of step 4 at the beginning. But, it reached the highest peak value of 9,066 W/m² K at 11 seconds among all five steps, and then decreased slowly to the level 2,164 W/m² K at 40 seconds.

5. CONCLUSIONS

In this work, the heat flux and IHTC at metal/die interface in squeeze casting were determined based on an energy balance method. The peak heat flux values for steps 1 to 5 were 1.5E+05 W/m², 1.9E+05 W/m², 2.7E+05 W/m², 4.0E+05 W/m², and 6.0E+05 W/m², respectively. For all steps, the IHTC values increased sharply at the beginning right after the liquid metal was pushed into the die cavity, and then dropped gradually after their peaks reached. The thickness of the step casting had a great influence on the IHTC values. The IHTC values increased as the section thickness increased. For the five steps from one to five, the peak IHTC were 1,398 W/m² K, 1,876 W/m² K, 4,040 W/m² K, 6,383 W/m² K, and 9,066 W/m² K, respectively. Also, the trend of changes of the IHTC was different as

the section thickness varies. The profile of the IHTC curve became wider as the casting section thickness increased.

REFERENCES

- [1] M. R., Ghomashchi and A.Vikhrov, Squeeze casting: an overview. *Journal of Materials Processing Technology*, 2000, (101)1, 1-9.
- [2] H. Hu, Squeeze casting of magnesium alloys and their composites. *Journal of Materials Science*, 1998, 33(6), 1579-1589.
- [3] H. Hu, and A. Yu, Numerical simulation of squeeze cast magnesium alloys AZ91D. *Modell. Simul. Mater. Sci. Eng.*, 2002, 10 (1) 1–11.
- [4] Z. Sun, H. Hu, and X. Niu, Determination of heat transfer coefficients by extrapolation and numerical inverse methods in squeeze casting of magnesium alloy AM60. *Journal of Materials Processing Technology*, 2011, (211)8, 1432-1440.
- [5] R. Rajaraman and R. Velraj, Comparison of interfacial heat transfer coefficient estimated by two different techniques during solidification of cylindrical aluminum alloys casting. *Heat and Mass Transfer*, 2008, (44)9, 1025-1034.
- [6] Z. Guo, S. Xiong, B. Liu, M. Li and J. Allison, Effect of Process Parameters, Casting Thickness, and Alloys on the Interfacial Heat-transfer Coefficient in the High-pressure Die Casting Process. *Metall. Mater. Trans.* 2008, A 39A, 2896-2905.
- [7] A. Hamasaiid, G. Dour, M. S. Dargusch, T. Loulou, C. Davidson, and G. Savage. Heat transfer coefficient and in-cavity pressure at the casting-die interface during high pressure die casting of magnesium alloy AZ91D. *Metall. Mater. Trans.* 2008, A 39A, 853-864.

- [8] S.W. Hao, Zhang, Z. Q, Chen, J. Y. Liu, Heat transfer at the metal-mold interface in ductile iron. AFS Transactions, 1987, (128), 601–608.
- [9] A. Hamasaiid, M. S. Dargusch, C. J. Davidson, S. Tovar, T. Loulou, F. Rezaei-Aria, and G. Dour, Effect of mold coating materials and thickness on heat transfer in permanent mold casting of aluminum alloys. Metall. Mater. Trans. 2007, A (38)6, 1303-1316.

CHAPTER 6

INTERFACIAL HEAT TRANSFER OF SQUEEZE

CASTING OF WROUGHT ALUMINUM ALLOY 5083

WITH VARIATION IN WALL THICKNESSES

1. INTRODUCTION

Aluminum alloys are increasingly used in today's automotive industry due to their low density, high strength-to-weight ratios, excellent formability and good corrosion resistance [1]. The expensive and low-productivity fabrication processes such as rolling, forging and machining are often involved to achieve the good mechanical properties for components with complex shapes. Wrought aluminum alloy 5083 is one of the highest strength non-heat treatable aluminum alloys, with excellent corrosion resistance, good weldability. This alloy can be found in applications of ship building, automobile and aircraft structures, tank containers, unfired welded pressure vessels, cryogenic applications, transmission towers, drilling rigs, transportation equipment, missile components and armour plates [2].

Casting processes have the advantages of low-cost and high productivity. However, wrought aluminum alloys are difficult to shape using conventional casting processes due to their limited castability, for example, their long freezing range, poor fluidity, high risk

of forming defects and high tendency for hot tearing, etc. [3]. Squeeze casting, also called liquid metal forging, extrusion casting, squeeze forming and pressure crystallization, as one of the best promising techniques has been emerging, and extensively studied in the past decade. This is because the fluidity is not a critical process parameter in squeeze casting, and liquid molten metal is solidified in the die cavity under applied pressures to reduce and minimize defects associated with shrinkage cavities and porosity formation in squeeze casting [4, 5].

In the open literature, most works on squeeze cast of wrought aluminum alloys focused only on their mechanical properties and microstructure development. There is limited work on the determination of the interfacial heat transfer coefficient (IHTC) at the metal/die interface during squeeze casting of wrought aluminum alloys. The previous study [6] indicated the contact interface between a casting aluminum alloy A356 and a carbon steel die coated with graphite had a great influence on cooling rates and solidification times. There is a considerable thermal resistance that exist between the castings and die due to the presence of air gap at the interface. The IHTC variation with time after pouring plays a notable role in controlling the solidification behaviours [6, 7]. In recent years, techniques such as computer-aided design and engineering have been rapidly developed. They are widely applied in the modeling and simulation of mold filling and alloy solidification during various casting processes. The numerical simulation enables the optimization of the casting processes and consequently saves enormous costs. However, these computers based techniques can only be beneficial when boundary conditions and material properties are well defined. The IHTC is believed to be one of the most important parameters during the computer simulation of the solidification process. Also, in the die casting practice,

difference in wall thickness of the casting significantly varies the local heat transfer coefficients [8]. It is critical to evaluate the effect of casting wall thickness, pressure levels and process parameters on the IHTC.

In this work, a special five-step casting was designed for numerical determination of casting thickness-dependant IHTCs, in which cross-section thicknesses of 2, 4, 8, 12 and 20 mm were included. Based on the temperature measurements of the casting at each step and the temperature at difference distance underneath the die surface (2, 4 and 6 mm) of each step, the inverse method of heat conduction was applied in determining of heat flux and heat transfer coefficient at the metal/die interface. The variation of the unknown boundary condition with time was assumed. This boundary condition was then applied with unknown coefficients, and the interior temperature field was determined in the domain by the finite-differences method (FDM). An objective function based on the measured and calculated temperature values at various internal points was then determined. It was minimized by correcting the values chosen for coefficients used in the boundary conditions. This was carried out iteratively until a stationary value of the objective function was obtained. Therefore, the measurement errors could be minimized by this numerical procedure.

2. EXPERIMENTAL PROCEDURE

2.1 Material and squeeze casting

2.1.1 Material

Table 6- 1: Chemical composition of wrought aluminum alloy 5083 (wt. %)

Mg	Mn	Fe	Si	Cr	Cu	Zn	Ti
4.5	0.7	0.4	0.4	0.25	0.1	0.25	0.15

Table 6- 2: Thermal-physical parameters of wrought aluminum alloy 5083

Material	ρ (g/cm ³)	C_p (J/g K)	k (W/m K)	T_s (°C)	T_l (°C)
Al 7075	2.66	0.9	117	591	638

The material used in this study was commercially-available wrought aluminum alloy 5083, of which chemical composition and thermal-physical properties are shown in Tables 6-1 and 6-2.

2.1.2 Squeeze casting

A 75-ton- hydraulic press was used in the casting experiment. The metal was firstly melt in an electric resistance furnace with the protection of nitrogen gas. The holding temperature of the furnace was 800°C. As shown in Fig. 6-1, the upper die opened along the center, which could form a five-step casting consisting of five steps with the dimensions

of $100 \times 30 \times 2$ mm (step 1), $100 \times 30 \times 4$ mm (step 2), $100 \times 30 \times 8$ mm (step 3), $100 \times 30 \times 12$ mm (step 4), $100 \times 30 \times 20$ mm (step 5), accordingly (Fig. 6-2). On top of step one, one extra step was designed as an overflow to entrap impurities in the upfront stream of the liquid melt during cavity filling. The vent was located on the top of the overflow, which could discharge the air inside the die. The lower die has a diameter of 100 mm and a height of 200 mm. Both of the upper and bottom dies were preheated by cartridge heaters. The upper die had a preheating temperature of 250°C , and 300°C for the lower die. Then, the liquid metal was poured into the lower mold at 680°C . At last, the liquid metal was squeeze casted in the upper die under a desired applied pressure and kept holding at that pressure for 25 seconds.

2.2 Experimental measurements of temperatures and pressures

The K-type thermocouples with 1.5 mm in diameter were used to determine the solidifying temperatures of the cast molten metal and heating temperatures of the P20 steel die at the various positions, as shown in Fig. 6-1. On the left side of the die, there were five pressure transducers (P SU) which were used to collect the pressure data for the five steps with section thicknesses of 2, 4, 8, 12, and 20 mm. There were four thermocouples located at each step. In total, twenty thermocouples were employed to collect the temperature data of all the five steps. At each step, one thermocouple (D) was inserted all the way through the die which was used to measure the casting temperature. The rest of three thermocouples (A, B and C) were 2, 4 and 6 mm away from the inside die surface to measure the die temperatures, as shown in Fig. 6-3. Real-time in-cavity local pressures and temperature

reading were recorded by a LabVIEW- based data acquisition system at regular intervals of 500 ms through the entire measurement period.

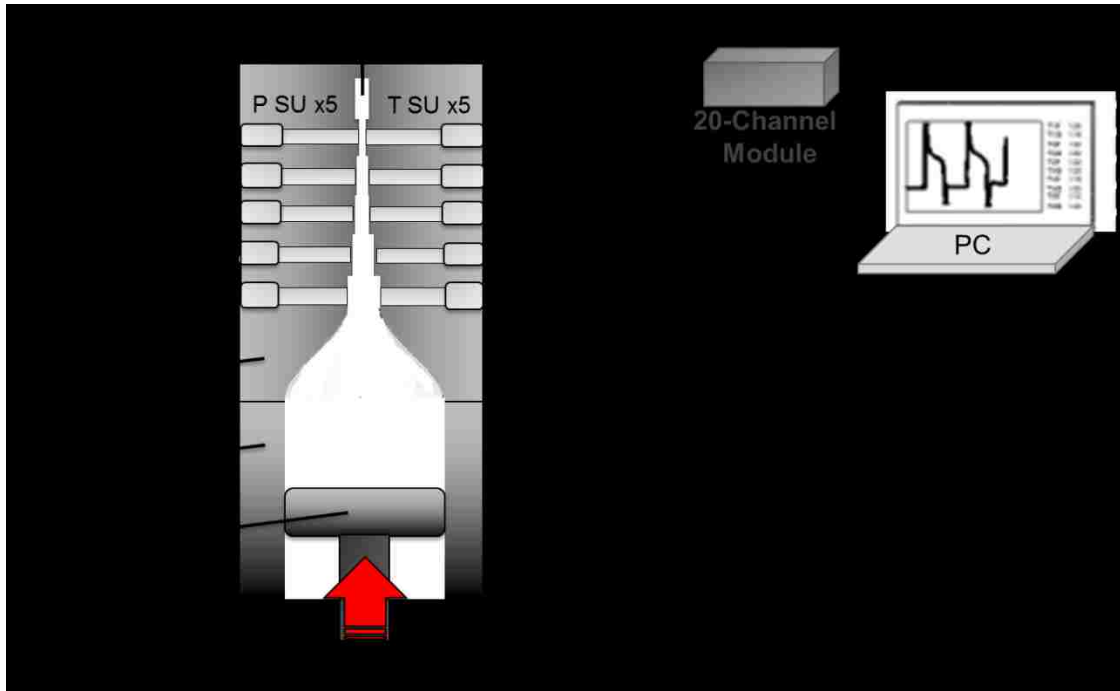


Figure 6- 1: Graphical installations of temperature sensor units (TSUs), pressure sensor units (PSUs) and data acquisition system.

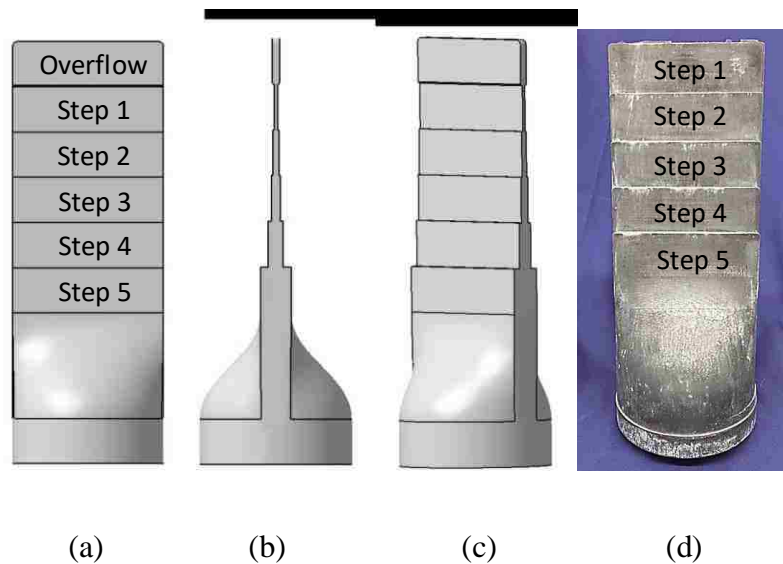


Figure 6- 2: (a) 3-D model showing the front view, (b) side view and (c) isometric view of the 5-step casting. (d) 5-step casting solidifying under applied pressure of 60 MPa.

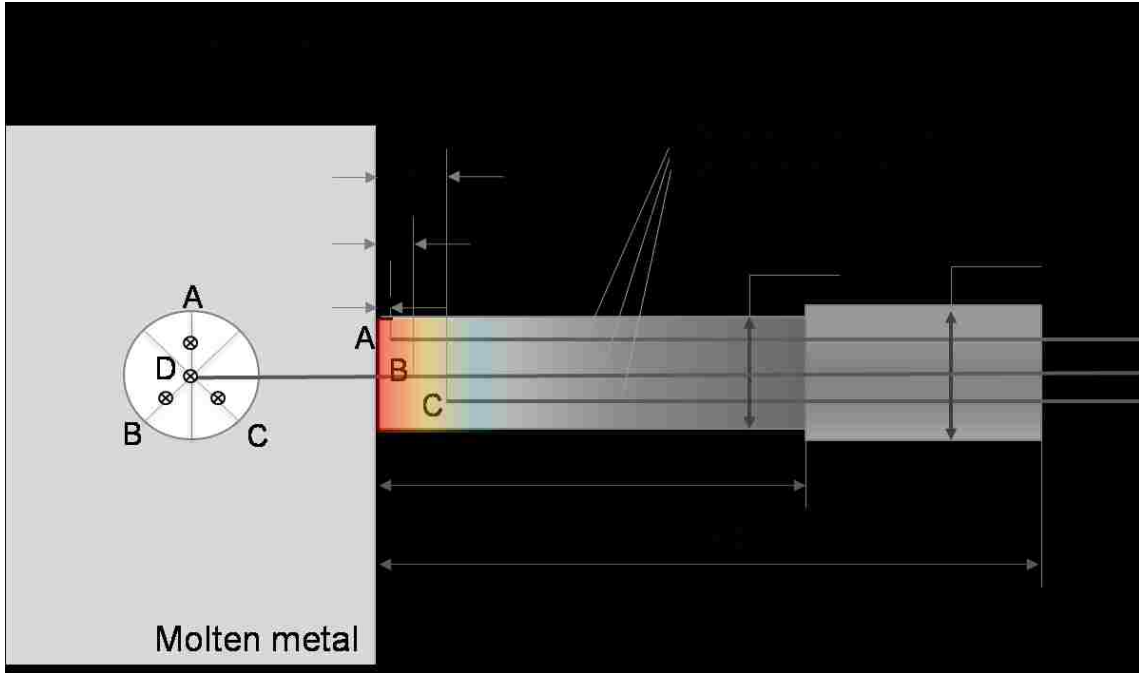


Figure 6- 3: Configuration of installation of the K-type thermocouples, the unit is in millimeters.

2.3 Inverse algorithm for the IHTC

The heat transfer inside the die at each step is transient conduction through on-dimensional step, which can be described by Eq. 6-1.

$$\rho c(T) \frac{\partial T(x,t)}{\partial t} = \frac{\partial}{\partial x} \left(k(T) \frac{\partial T(x,t)}{\partial x} \right) \quad 6-1$$

where ρ is the density of the conducting die, T is the temperature, t is the time, and x is the distance from the die surface to the sensor node, and $c(T)$, $k(T)$ are specific heat capacity and thermal conductivity of the die changed with temperature, respectively.

For the surface sensor node of the die, Eq. 6-1 can be rearranged as Eq. 6-2a:

$$(1 + 2F_0)T_0^{p+1} - 2F_0T_1^{p+1} = 2F_0 \frac{\Delta x}{k} q_0 + T_0^p \quad 6-2a$$

For any interior sensor node of the die, Eq. 6-1 can be solved as Eq. 6-2b:

$$(1 + 2F_0)T_n^{p+1} - (F_0T_{n-1}^{p+1} + T_{n+1}^{p+1}) = T_n^p \quad 6-2b$$

$$F_0 = \frac{\alpha \Delta t}{(\Delta x)^2} = \frac{k}{c\rho} \frac{\Delta t}{(\Delta x)^2} \quad 6-2c$$

where F_0 is the Fourier number, α is the thermal diffusivity, c is the heat capacity of the conducting die, p is the time step and n is the grid point.

As illustrated in Figure 6-4, the heat flux at the metal/die interface q_0 at each time step was determined at the following procedure: (1) at the first time step, a suitable initial value of heat flux q_0 was assumed, which was maintained constant for a definite integer number ($u = 2$ to 5) of the subsequent future time steps; (2) according to Eqs. 6-2a and b, with the measured initial die temperature ($p = 0$), the temperature distribution at each node of the next time step was calculated with this assumed q_0 ; (3) the assumed heat flux value is changed by a small value (εq_0); (4) the new temperature distribution value corresponding to $(q_0 + \varepsilon q_0)$ was determined accordingly; and (5) the sensitivity coefficient (\emptyset) was

calculated by Eq. 6-3, which was the partial derivative in Eq. 6-4, the Taylor's series approximation.

$$\phi^{p+j-1} = \frac{\partial T}{\partial q} = \frac{T^{p+j-1}(q_{n+1}^{p+j-1}(1+\varepsilon)) - T^{p+j-1}(q_{n+1}^{p+j-1})}{\varepsilon q_{n+1}^{p+j-1}} \quad 6-3$$

where j is the future time, the numerator was the difference in temperature calculated using a finite difference scheme at the monitored node at the same time step for temperature (Δt), using the boundary condition q and $q + \varepsilon$. the denominator was the difference in the q values, $\varepsilon = 0.0001$ was used in this work.

$$T_{n+i}^{p+j} \approx T_{n+i}^{p+j-1} + \frac{\partial T_{n+i}^{p+j-1}}{\partial q_{n+1}^{p+j}} (q_{n+1}^{p+j} - q_{n+1}^{p+j-1}) \quad 6-4$$

Eq. 6-5 was obtained by minimizing Eq. 6-2 with respect to q by setting the partial derivative to zero.

$$\frac{\partial F(q)}{\partial q} = \frac{\partial}{\partial q} \left(\sum_{i=1}^{l=mr} (T_{n+i} - Y_{n+i})^2 \right) = 0 \quad 6-5$$

Substituting Eqs. 6-3 and 6-4 in Eq. 6-5, the following equation was obtained

$$\frac{\partial}{\partial q} \left(\sum_{i=1}^{l=mr} (T_{n+1}^{p+j-1} + \phi_i^{p+j-1} (q_{M+1}^{p+j} - q_{M+1}^{p+j-1}) - Y_{n+i})^2 \right) = 0$$

which gave

$$\sum_{i=1}^{l=mr} \phi_i^{p+j-1} (T_{n+1}^{p+j-1} - Y_{n+i} + \phi_i^{p+j-1} (\nabla q_{n+1}^{p+j})) = 0 \quad 6-6$$

Rearranging Eq. 6-6, the correction term for the heat flux was calculated, given by Eq. 6-8.

$$\nabla q_{M+1}^p = \frac{\sum_{i=1}^l (Y_{n+i} - T_{n+1}^{p+j-1}) \phi_i^{p+j-1}}{\sum_{i=1}^{l=mr} (\phi_i^{p+j-1})^2} \quad 6-7$$

$$q_{corr}^p = q_{n+1}^p + \Delta q_{n+1}^p \quad 6-8$$

The corrected heat flux and the new temperature distribution were used as the initial value for next cycle of calculation. The calculation process was repeated until the following condition was satisfied.

$$\frac{\Delta q_{n+1}^p}{q_{n+1}^p} \leq \varepsilon \quad 6-9$$

Thus, for all time steps, the surface heat flux and die surface temperature were determined according to the above procedures. After the heat flux was computed, the heat transfer coefficient h was determined by the following equation, Eq. 6-10.

$$h = \frac{q}{A(T_c - T_d)} \quad 6-10$$

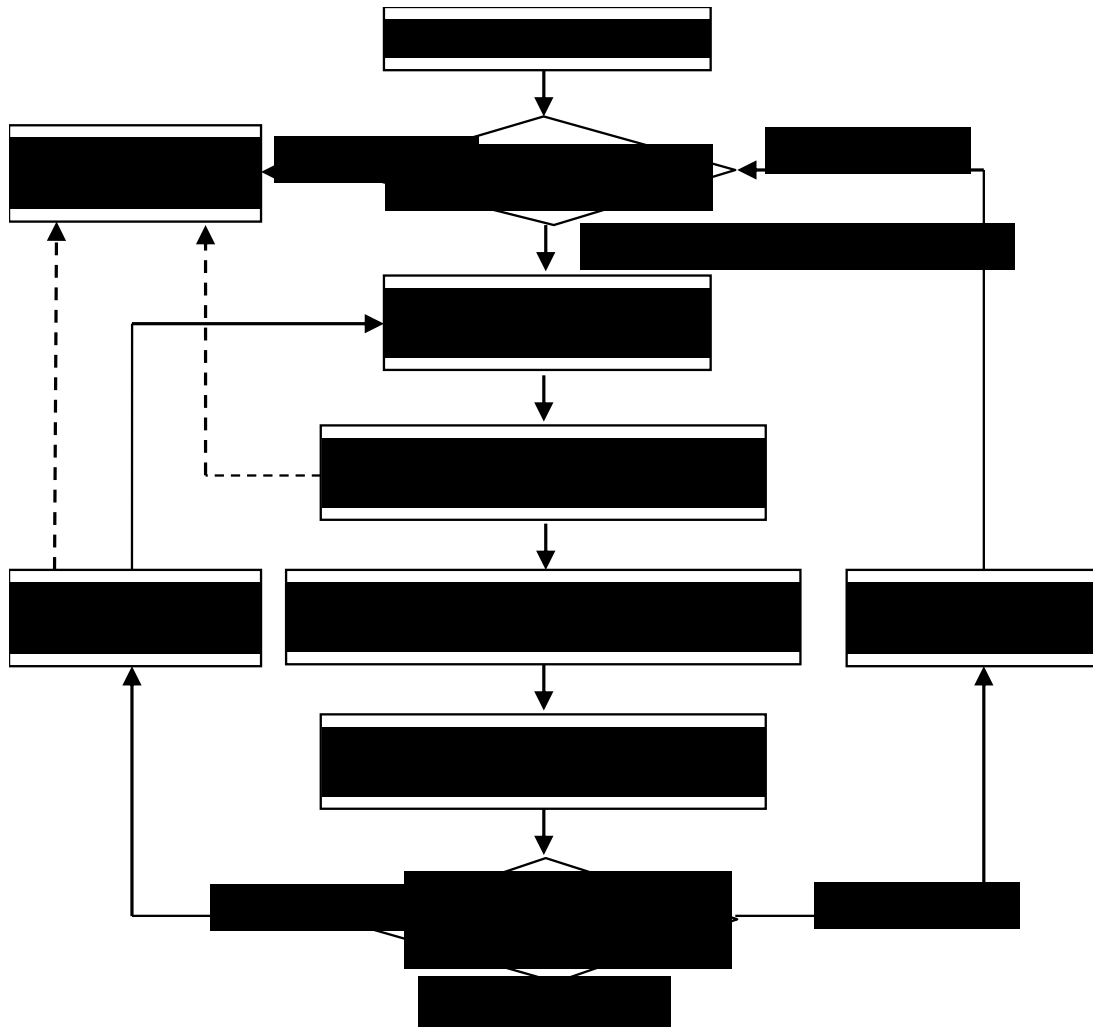


Figure 6- 4: Flow chart of the inverse algorithm for IHTC estimation at the metal die interface.

3. RESULTS AND DISCUSSIONS

Fig. 6-5 shows the temperature and local pressure measurement of step 5 with section thickness of 20 mm under an applied pressure of 60 MPa. It is noticed that the local pressure rose to its peak stage, 37.32 MPa, 2 seconds after the hydraulic pressure applied. After the pressure peak, the portion of the pressure profile was so-called the “shell establishment

stage”. The reason for pressure decreased from the peak was the strengthening of the solidified shell of the casting. This shell caused the metal/die interface to move apart. In other words, as the temperature started to decrease, the solid fraction increased and solidified shell strengthened, and the pressure finally could not overcome the resistance and then dropped linearly from the 2.4th second. Then, the pressure dropped to a negative value at the 10th second after sensing a positive pressure signal. This issue was confirmed by Kistler[®] that it caused by the ADA converter of the data acquisition system. The die surface temperature was estimated based on the temperature measured at different depth (2, 4 and 6 mm) inside of the steel die as shown in Fig. 6-6. Due to the design of the upper and lower die, pre-solidification occurred upon the completion of cavity filling. The highest temperature measured at casting surface was 625.9°C below the pouring temperature. The heat flux and IHTC values was calculated using the inverse method according to the estimated die surface temperature and casting surface temperature. For the thickest section (step 5, 20 mm), the peak value of heat flux was 9.84E+05 W/m², and the IHTC peak value was 8933 W/m²K.

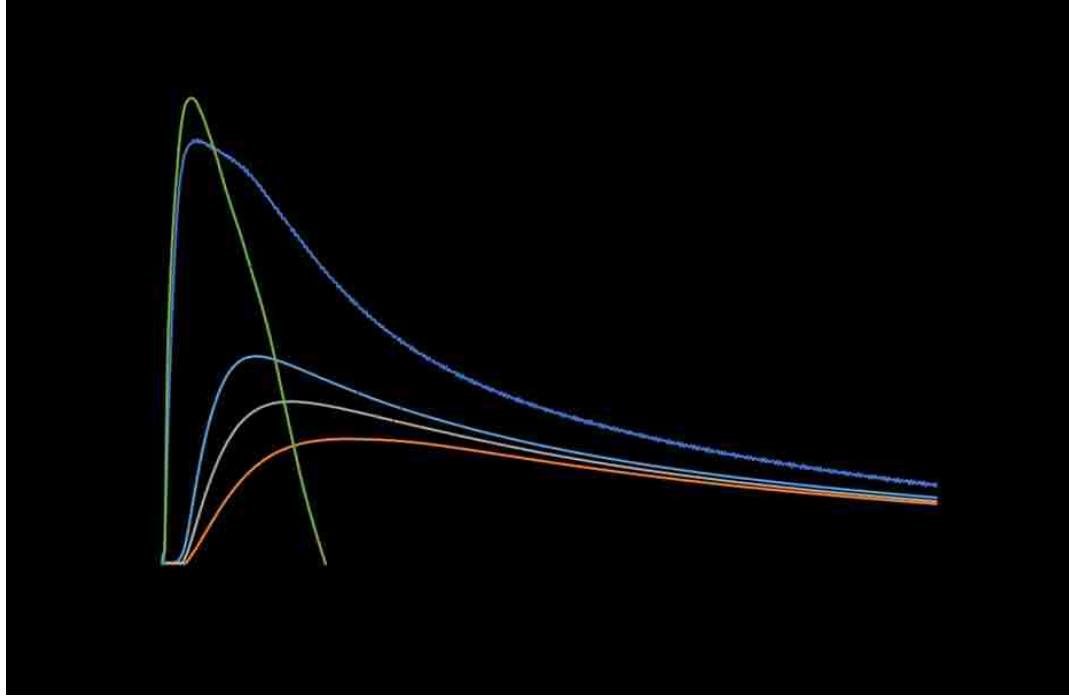


Figure 6- 5: Measured temperature and local pressure versus time curves for step 5 (20 mm) under applied pressure of 60 MPa.

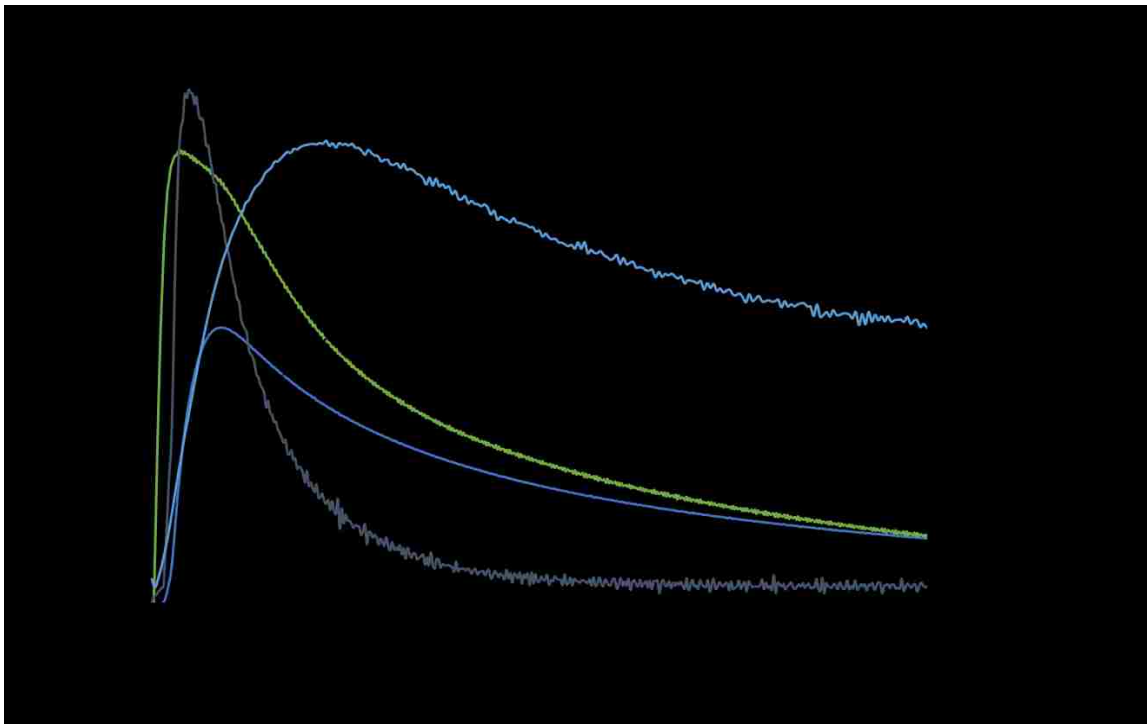


Figure 6- 6: Temperature, interfacial heat transfer coefficient (IHTC) and heat flux versus time curves for step 5 (20 mm) under applied pressure of 60 MPa.

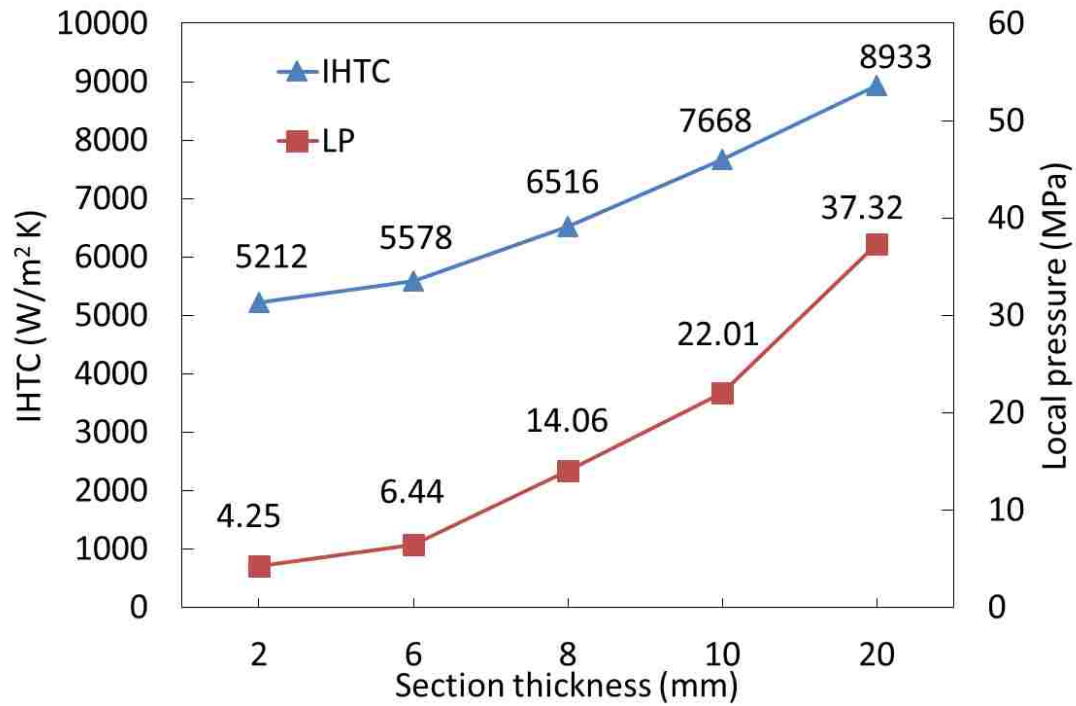


Figure 6- 7: Variation of interfacial heat transfer coefficient (IHTC) and local pressure (LP) peak values with different cross section thicknesses of the five step casting.

Fig. 6-7 shows the peak IHTC values and local pressure peak values with variation in cross section thicknesses of the 5-step casting. The in-cavity local pressures at the metal/die interface of each steps were measured using the Kistler pressure transducers. It can be observed that the local pressure at each steps (2 to 20 mm) were 4.25, 6.44, 14.06, 22.01 and 37.32 MPa. The pressure difference between the measured local pressure and the hydraulic applied pressure 60 MPa was a pressure loss.

$$P_{loss} = \frac{P - P_{local}}{P} \times 100\%$$

The pressure loss increased significantly as the section thickness decreased. As the liquid metal filled the cavity from the bottom (Step 5) to the top (Step 1), the pressure loss at the metal/die interface were 37.8%, 63.3%, 76.6%, 89.3% and 92.9%, respectively. The large

percentage of the pressure loss at thinner steps might due to the fast solidification rate of the casting and the solidified metal formed a solid barrier at the metal/die interface which blocked the pressure transfer path at the interface.

Fig. 6-8 shows the IHTC curves of all five steps which were estimated by the inverse method. From the profile of the five curves, the IHTCs started with a relatively rapid increasing stage. After their peaks were reached, the IHTCs decreased gradually until they were reached to their lower level (a relatively constant stage). From step 1 to 5, the peak IHTC values varied from 5212, 5578, 6516, 7668 to 8933 W/m² K. It indicated that a firmer contact was formed at the metal/die interface as the section thickness became thicker and the section thickness significantly influenced the values of IHTC. To obtain the relationship between casting wall thickness and IHTCs, the values of IHTC in the 10th second have been selected. As shown in Fig. 6-9 the empirical equation, relating IHTC to the wall thickness is:

$$h = 1977.7 \ln(x) + 2587.1$$

where h is the interfacial heat transfer coefficient and x is the wall thickness of each steps.

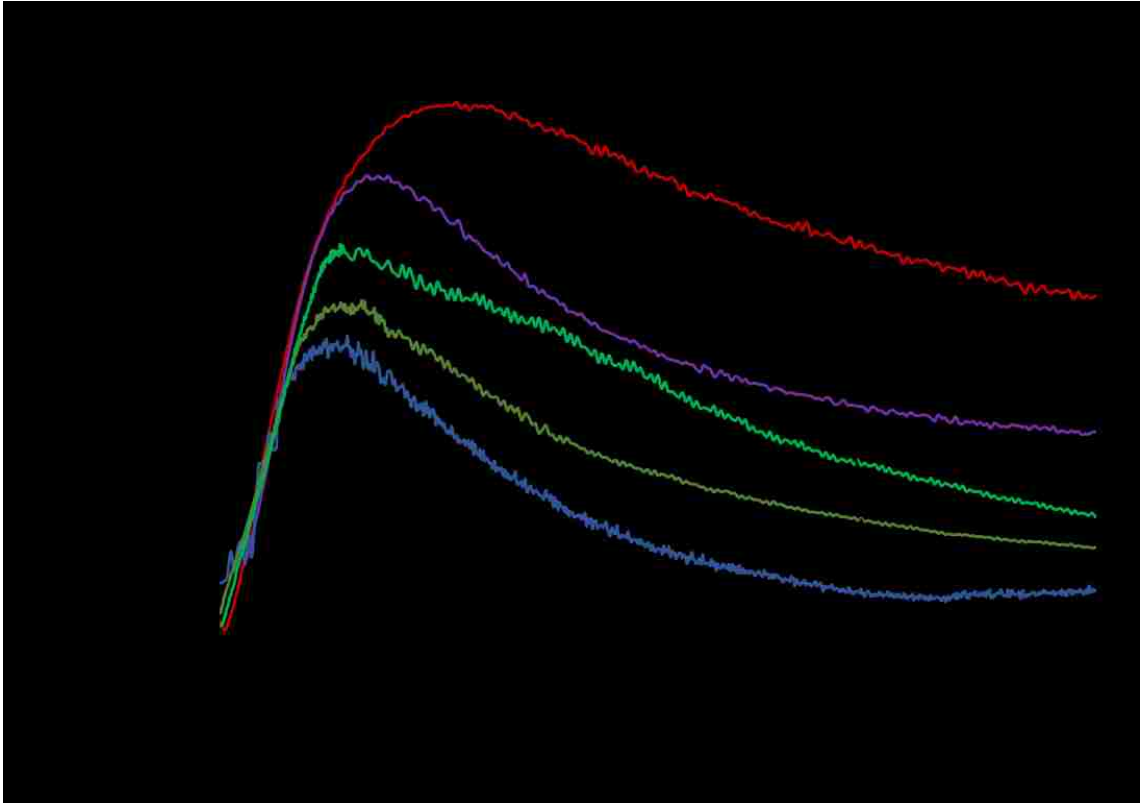


Figure 6- 8: Interfacial heat transfer coefficient (IHTC) versus time curves for all five steps (2, 4, 8, 10 and 20 mm) under applied pressure of 60 MPa.

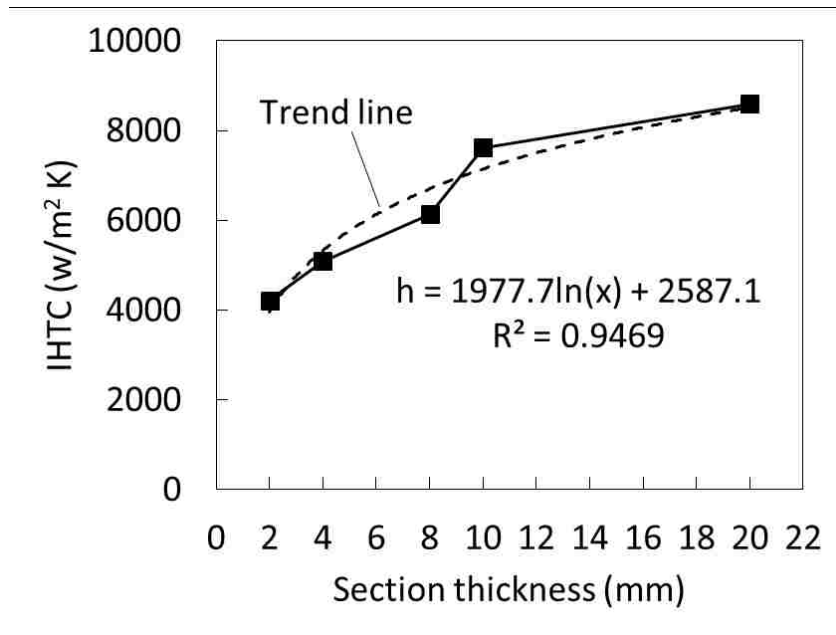


Figure 6- 9: Interfacial heat transfer coefficient curve versus section thickness in 10 second.

4. CONCLUSIONS

A 5-step casting with the various cross-section thicknesses was successfully fabricated under an applied hydraulic pressure of 60 MPa. The heat flux and IHTC were successfully determined based on the finite difference-based inverse method. Based on the experimental measurements and calculated results, the following conclusions were drawn.

- 1) The peak IHTC values varied from 5212, 5578, 6516, 7668 to 8933 W/m² K for the casting with section thicknesses of 2, 4, 8, 10 and 20 mm, respectively, under an applied pressure of 60 MPa. The increases in IHTC indicated that the solid contact could be reached at the metal/die interface for the thicker steps, since the thicker step required longer time to reach the peak values due to the additional time needed for the pressure transfer.
- 2) The pressure loss was significantly influenced by the wall thicknesses. As the section became thinner, the pressure loss rose significantly which was due to the pressure-transfer path blocked by the fast solidified metal at the metal/die interface of the thin sections after the molten metal travelled to the thinner section from the bottom thicker section.
- 3) The casting wall thickness influenced IHTC significantly. The large temperature differences and relatively high local pressures should be responsible for high IHTC peak value at the thicker step.
- 4) The empirical equation, relating IHTCs to the wall thickness of the casting is:

$$h = 1977.7 \ln(x) + 2587.1$$

REFERENCES

- [1] Ducker World LLC, North America Light Vehicle Aluminum Content, <http://www.drivealuminum.org/research-resources/PDF/Research/2014/2014-ducker-report>, June, 2014 (2015).
- [2] Mutombo, K., and Toit, M. D. Corrosion fatigue behaviour of aluminium 5083-H111 welded using gas metal arc welding method. InTech (2011).
- [3] Souissi, N., Souissi, S., Lecompte, J. P., Amar, M. B., Bradai, C., & Halouani, F. Improvement of ductility for squeeze cast 2017 A wrought aluminum alloy using the Taguchi method. The International Journal of Advanced Manufacturing Technology, 2015, 78(9-12), 2069-2077.
- [4] Ghomashchi, M. R., & Vikhrov, A. Squeeze casting: an overview. Journal of Materials Processing Technology, 2000, 101(1), 1-9.
- [5] Hu, H. Squeeze casting of Magnesium alloys and their composites, Journal of materials science, 1998, (33), 1579-1589.
- [6] Ilkhchy, A. F., Jabbari, M., & Davami, P. Effect of pressure on heat transfer coefficient at the metal/mold interface of A356 aluminum alloy. International Communications in Heat and Mass Transfer, 2012, 39(5), 705-712.
- [7] Zhang, L., and Li, L. Determination of heat transfer coefficients at metal/chill interface in the casting solidification process. Heat and Mass Transfer, 2013, 49(8), 1071-1080.

- [8] Guo, Z., Xiong, S., Cho, S., & Choi, J. Interfacial heat transfer coefficient between metal and die during high pressure die casting process of aluminum alloy. *Frontiers of Mechanical Engineering in China*, 2007, 2(3), 283-287.

CHAPTER 7

INTERFACIAL HEAT TRANSFER IN SQUEEZE CASTING OF MAGNESIUM ALLOY AM60 WITH VARIATION OF APPLIED PRESSURES AND CASTING WALL-THICKNESSES

1. INTRODUCTION

The mechanical properties of magnesium castings are strongly dependent on the rates of heat extraction that occurs during solidification. The heat transfer coefficient for high pressure die casting (HPDC) can be expected to be much higher than that for gravity permanent mold casting processes. Compared to other conventional casting processes, the most attractive features of squeeze casting are slow filling velocities and the pressurized solidification. Before the solid fraction of the casting becomes high enough, the applied pressure squeezes liquid metal into the air or shrinkage porosities effectively. Therefore, squeeze casting can make castings virtually free of porosity and usually have excellent as-cast quality, and are heat treatable, which is difficult to achieve with other conventional casting processes.

The accuracy of a solidification simulation depends on the accuracy of the heat transfer modeling. The critical portion of heat transfer in the casting is that at the metal/mold interface. Modeling of the interfacial heat transfer coefficient (IHTC) is very challenging due to a number of factors, such as air gap, casting geometry, alloy characteristics, mold material, coating, preheat temperature, and other process parameters. For the squeeze casting process, the applied hydraulic and local pressures, pouring temperatures, and die initial temperatures, are believed to strongly influence the pressure-transfer behavior inside the casting [1]. In various casting processes, the contact between the liquid metal and mold die is imperfect because of coating applied on the die surface and air gap caused by shrinkage. These thermal barriers may decrease the heat transfer between metal and die and cooling rates of the casting surface, which influences microstructure and quality of the casting significantly. Hence, precise determination of heat transfer coefficients at the metal-mold interface is essential to accurately simulate solidification process.

The interfacial heat transfer depends on actual contact situation between the rough surface of the mold and the casting. In the case of relatively low melting temperature light alloys, the mechanism of heat transfer would be by conduction through the points of interfacial contact, and by conduction through the interfacial gas in the regions between the contact points. Radiation would not be expected to be a significant heat transfer mechanism in the case of Al or Mg alloys [2].

The effect of many casting parameters on the interfacial heat transfer coefficient have been studied experimentally. Browne and O'Mahoney [3] examined the effect of alloy freezing range and head height during solidification of an aluminum alloy in investment casting. Ferreira et al. [4, 5] analyzed the effect of alloy composition, melt superheat, mold material,

mold roughness, mold coatings, and mold initial temperature distribution on the interfacial heat transfer coefficient. Arun et al. [6] examined two-dimensional heat transfer in gravity die casting, and studied how the initial non-uniform temperature field that typically results after filling of the mold caused the distribution of heat flux and initiation of air-gap formation around a casting-mold interface non-uniformly.

Other researchers aimed at examining the effect of increased pressure on interfacial heat transfer. Meneghini and Tomesani [7] concluded that increased metal height increased the interfacial heat transfer coefficient and delayed the onset of air-gap formation during gravity aluminum alloy die casting. Chattopadhyay [8] simulated the squeeze casting process numerically on A-356 with variable heat transfer coefficients, and used heat transfer coefficient values 20,000 to 40,000 W/m²K for applied pressures of 25-100 MPa, respectively, and suggested that pressures of up to 60-100MPa were optimal for the squeeze casting process. Aweda and Adeyemi [9] found only a small (14%) increase in interfacial heat transfer coefficient on pure aluminum with applied pressure 86MPa. Guo et al. [10] found that heat transfer coefficient initially reached a maximum value of about 10,000 to 20,000 W/m²K on ADC12 aluminum alloy with 2 to 14 mm section thickness, followed by a rapid decline to low values of about a few hundred W/m²K. In the case of high pressure die casting of Mg alloy(AM50) in H13 tool steel dies, an initial peak heat transfer coefficient value reached 12,000 W/m²K, then decreased to less than 1,000 W/m²K over 7 seconds. Dour et al. [11] measured the interfacial heat transfer coefficient values of 45,000-60,000 W/m²K on Al-12%Si alloy within the 33-90MPa pressure range, but observed that the pressure variation did not have a significant impact on the heat transfer. A “saturation effect” where increased pressure did not lead to increased heat transfer, was

suggested to occur above 5MPa local in-cavity pressure at the interface of H13 die and aluminum alloy. Hamasaiid et al. [12] and Dargusch et al. [13] reported the peak heat transfer coefficient value of 90,000-112,000 W/m²K during the HPDC of magnesium alloy AZ91D with section thickness 2-5mm, declining to low values within 2 seconds. In high pressure die casting (HPDC), the typical behavior of the heat transfer coefficient was to increase to a peak value, then followed by a rapid decline. This may be explained by increasing solidification and fraction solid in the mold cavity causing a reduction in the pressure transmitted from the piston to the casting-mold interface.

Although the IHTC has been studied extensively by many researchers for light alloys, these studies only focused on castings with simple geometries. Little attention has been paid to variation of casting thicknesses and hydraulic pressures. Actually, in the die casting practice, the different thicknesses at different locations of castings results in significant variation of the local heat transfer coefficients. Therefore, it is essential to investigate the influence of casting thickness, local pressure levels, and process parameters on the IHTC. In this study, a special 5-step squeeze casting was designed for numerical determination of casting thickness-dependent IHTCs. The temperature measuring units to hold multiple thermocouples simultaneously and the pressure transducers were employed to accurately measure the temperatures and the local pressures during squeeze casting of magnesium alloy AM60.

2. EXPERIMENTAL DESIGN

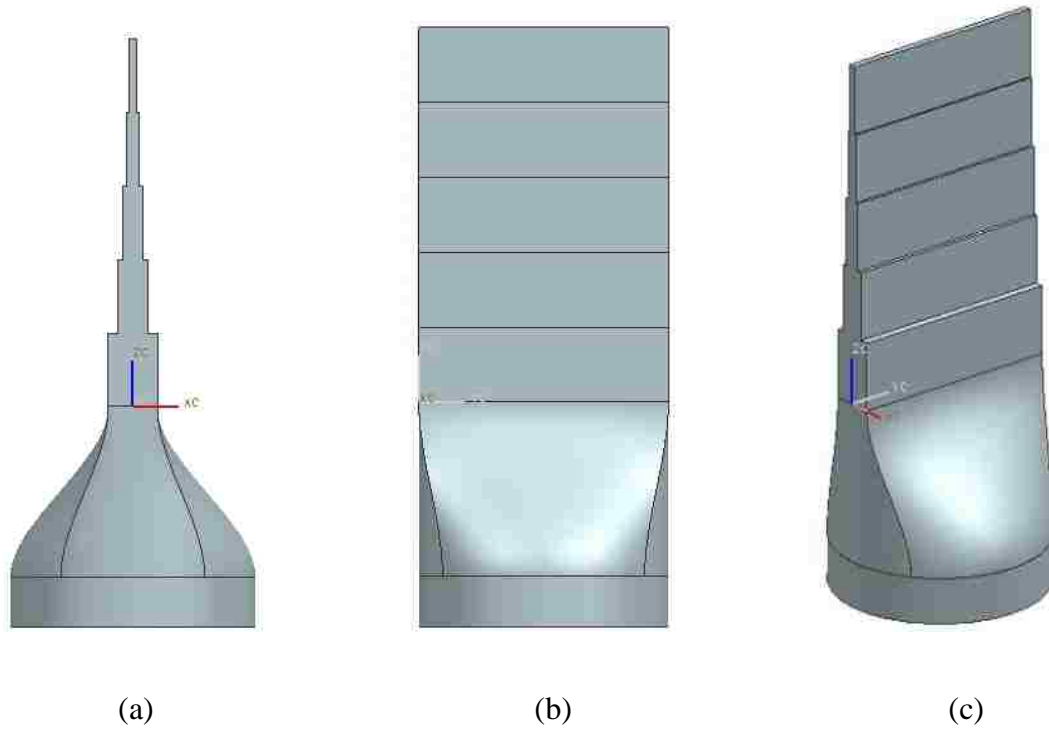


Figure 7- 1: a) side view, b) front view and c) isometric view of 5-step casting 3-D model with the round-shape gating system.

Figure 7-1 shows the 3-D model of 5-step casting, which consists of 5 steps (from top to bottom designated as steps 1 to 5) with dimensions of $100 \times 30 \times 2$ mm, $100 \times 30 \times 4$ mm, $100 \times 30 \times 8$ mm, $100 \times 30 \times 12$ mm, $100 \times 30 \times 20$ mm accordingly. The molten metal was filled the cavity from the bottom cylindrical shape sleeve with a diameter of 100 mm.



(a)



(b)

Figure 7- 2: (a) An electric resistance furnace with SF₆ gas protection, and (b) a 75-ton vertical hydraulic press.

Table 7- 1: Thermophysical properties of magnesium alloy AM60

Properties	Mg Alloy AM60	
	Solid	Liquid
Thermal Conductivity (W/m K)	62	90
Specific Heat (J/kg K)	1020	1180
Density (kg/m ³)	1790	1730
Latent Heat (kJ/kg)	373	
Liquidus Temperature at 0MPa (°C)	621	
Solidus Temperature at 0MPa (°C)		451.6

The integrated casting system consisted of a 75 tons laboratory hydraulic press, a two-halve split upper die forming a 5-step cavity, one cylindrical sleeve lower die, an electric resistance furnace and a data acquisition system (Figure 7-2). The electric furnace was protected by a gas mixture of Sulfur Hexafluoride (SF₆) 0.5% + CO₂ in balance. The die material was P20 steel. Commercial magnesium alloy AM60 was used in experiment with

chemical composition (6% Al-0.13% Mn-0.5% Si-0.35% Cu-0.22% Zn-balance Mg). Table 7-1 gives the thermal properties of the related materials in this study.

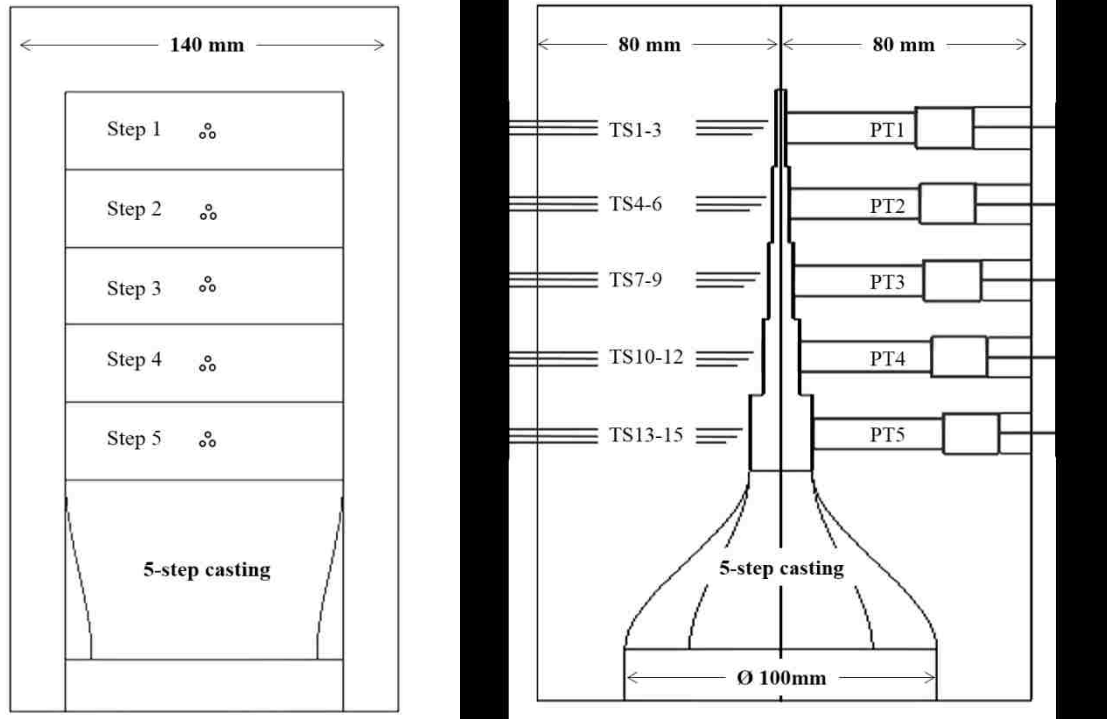


Figure 7- 3: Configuration of upper-dies and geometric installation of thermocouples and pressure transducers.

To measure the temperatures and pressures at the casting-die interface accurately and effectively, a special thermocouple holder was developed. It hosted 3 thermocouples simultaneously to ensure accurate placement of thermocouples in desired locations of each step. The thermocouple holders were manufactured using the same material P20 as the die to ensure that the heat transfer process would not be distorted. Figure 7-3 illustrates schematically the configuration of the upper die (left and right parts) mounted on the top ceiling of the press machine. It also revealed the geometric installation of pressure transducers and thermocouple holders. Pressures within the die cavity were measured

using Kistler® pressure transducers 6175A2 with operating temperature 850°C and pressures up to 200 MPa.

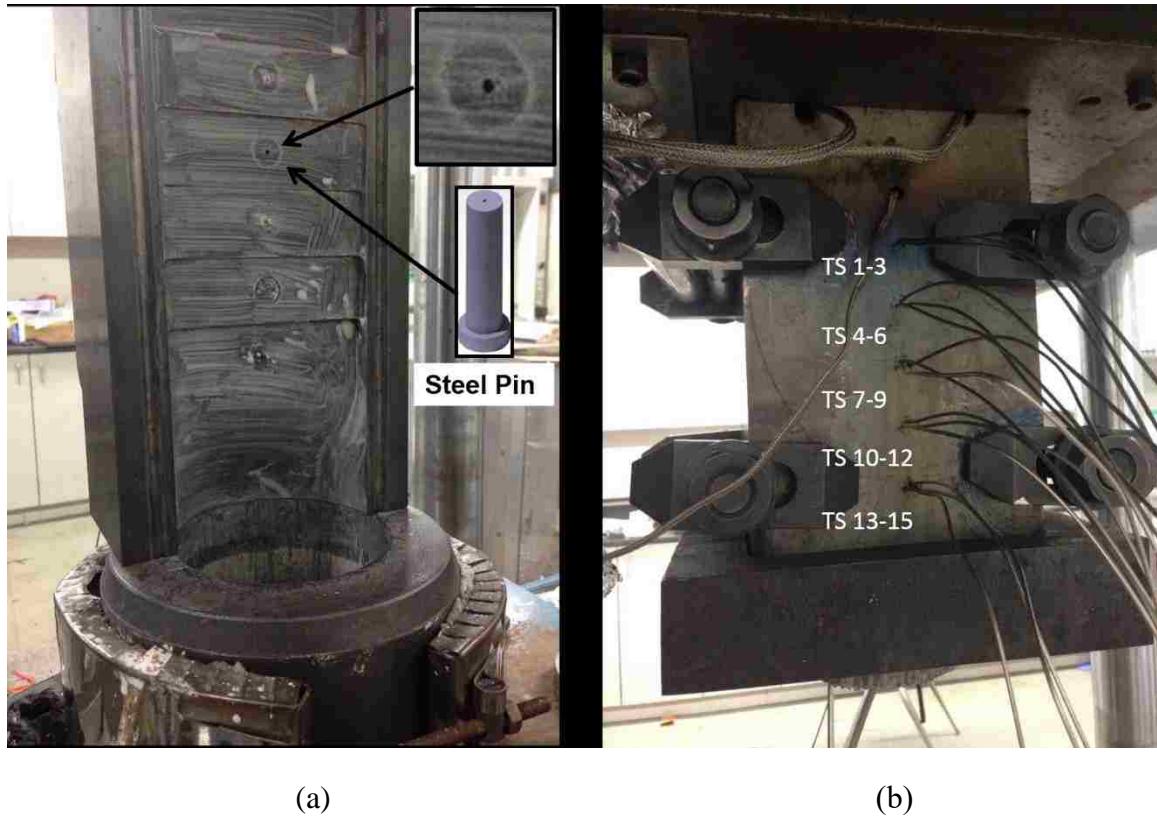


Figure 7- 4: The left and right halves of the 5-step squeeze casting die, (a) five steel pins with the holes in their center for the insertion of the thermocouples to measure the casting temperatures, and (b) the installation of the fifteen thermocouples (TS 1-15) for the die temperature measurement.

The experiments were designed to measure both in-cavity local pressure and heat flux simultaneously at the die-casting interface of each step. As shown in Figure 7-3, pressure transducers and temperature thermocouples were located opposite each other so that measurements from sensors could be directly correlated due to the symmetry of the step casting. Five pressure transducers and fifteen temperature measuring units were designated as PT1 through PT5, TS1 through TS15, respectively. The thermocouple unit was inserted

into the die and adjusted until the front wall of the sensor approached the cavity surface. The thermocouples installed inside the 5-step squeeze casting mold were type K with 1/16 inch diameter, stainless steel sheath, ungrounded junction, and 24 inches sheath length. To measure the temperature at the center of each step, a thermocouple was inserted into the cavity through a center hole in a steel pin, which was exchangeable with the pressure transducer. The installation of the thermocouples is shown in Figure 7-4.

Before molten metal was poured, the dies were pre-heated to 210°C by four heating cartridges installed inside the dies. The casting procedure included pouring molten magnesium alloy AM60 into the bottom sleeve at 720°C, closing the dies, filling cavity, holding the applied pressure for 25 seconds, lowering the sleeve lower die, splitting the two parts of the upper die. Finally, the 5-step casting was shaken out from the cavity. The temperatures inside the die and casting were measured by Omega® KTSS-116U-24 thermocouples with response time below 10 ms. Real-time in-cavity local pressures and temperature data were recorded by a LabVIEW- based data acquisition system.

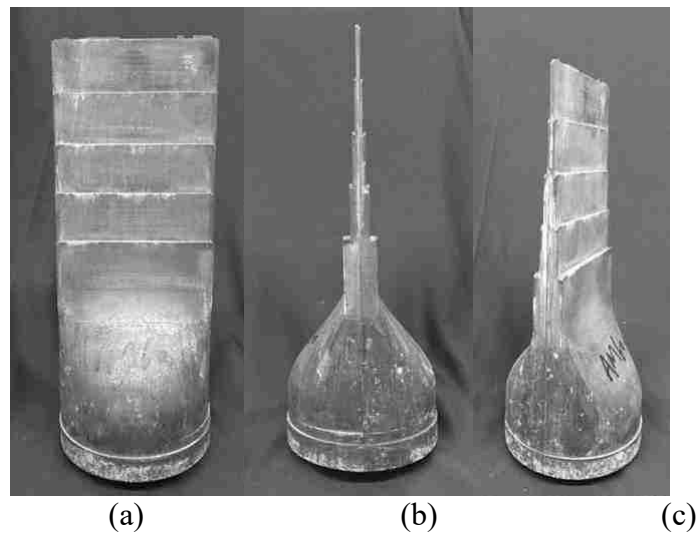


Figure 7- 5: A typical 5-step squeeze casting solidifying under an applied pressure of 60MPa, (a) front view, (b) side view and (c) isometric view.

The mold coating used in step castings is Boron Nitride lubrication (Type S_f) which was sprayed manually onto the surface of the mold cavity before heating the dies to the initial temperature. To minimize the thermal barrier effect of mold coating, the coating thickness applied in this study was relatively thin (below 50um). Figure 7-5 shows a typical squeeze casting of AM60 alloy under an applied pressure of 60 MPa. The chill vent and all five steps were filled completely. The soundness of the 5-step casting was evaluated via real-time X-ray inspection with a GE X-Cube radiosopic inspection system.

3. INVERSE ALGORITHM FOR THE IHTC

The heat transfer inside the die at each step during squeeze casting of AM60 alloy is transient conduction through one-dimensional steps which can be described by Equation 7-1:

$$\rho c(T) \frac{\partial T(x,t)}{\partial t} = \frac{\partial}{\partial x} \left(k(T) \frac{\partial T(x,t)}{\partial x} \right) \quad 7-1$$

where ρ is density of conducting die, T is the temperature, t is the time and x is the distance from the die surface to the node point; $c(T)$, $k(T)$ are specific heat capacity and thermal conductivity of the die changed with temperature, respectively. The details on the inverse algorithms incorporating the finite difference method as a numerical solution are given in chapter 6.

4. NUMERICAL SIMULATION FOR IHTC VERIFICATION

By applying the IHTC values determined by the inverse algorithm to casting simulation, the cooling curves at the center of Step 5 were compared between numerical predictions and experimental results. The finite difference method-based commercial simulation package (MAGMASoft®) was employed as the numerical simulation tool and the application pressure of 60 MPa was taken as an example to conduct the verification.

Before the simulation was performed, casting process parameters were defined, including the thermophysical properties of the casting and mold material and their initial temperature conditions. The heat transfer coefficients also had to be input as the boundary condition for the casting configuration. Specifications for the filling and solidification processes included the filling time or pouring rate, the filling direction, the feeding effectivity, criterion temperatures and the solver types. The feeding effectivity defined the maximum ratio of the volume available for feeding and the actual volume of the top chill vent. The filling time was determined based on the casting size and the hydraulic plunger moving speed. The fill direction indicates the flow of metal into the mold and is defined here in the positive Z direction to match the orientation of the squeeze casting system. The filling and solidification simulation parameters used in this study are listed in Tables 7-2 and 7-3 [15, 16].

Table 7- 2: Parameters for filling simulation

Filling Definition	
Parameter	Value
Solver	Solver 5
Filling Depends on	Time
Filling Time	1.8 s
Storing Data	10% increments of % Filled
Fill Direction-X	0
Fill Direction-Y	0
Fill Direction-Z	+1

Table 7- 3: Parameters for solidification simulation

Solidification Definition	
Parameter	Value
Temperature from Filling	Yes
Solver	Solver 5
Stop Simulation	Automatic
Stop Value	433°C
Calculate Feeding	Yes
Feeding Effectivity	70%
Criterion Temperature 1# (solidus)	451.6°C
Criterion Temperature 2# (liquidus)	621.0°C
Storing Data	10% increments of % Solidified

Simulation of the mold filling and solidification process required geometrical models of the casting, the gating system and the mold. The preprocessor module of simulation software then read the STL files as geometry. After the establishment of the full casting models, the whole geometry was enmeshed automatically with about 200,000 elements.

Three different heat transfer coefficients were applied to the prediction calculation: (1) a constant IHTC of $7000 \text{ W/m}^2 \text{ K}$ (C7000) [15]; (2) the heat transfer coefficient calculated from Yu's research [17]; (3) the heat transfer coefficients calculated by the inverse algorithms in this study. The thermophysical properties of the magnesium alloy AM60 were selected from the database of the employed simulation software. The initial and boundary conditions for simulation are listed in Table 7-4.

Once the meshed geometries and the necessary process parameters were established, the actual filling and solidification simulations were carried out. The type of numerical calculations employed based on the finite difference algorithm (Solver) was selected for accuracy and computational time.

Table 7- 4: Initial and boundary conditions for simulation

1	Material definitions (Initial Temperature) [0 °C]	Cast Alloy (AM60) Mould (HPDC)	620 210
2	Boundary definitions (Heat Transfer Coefficient) [W/ m ² K]	Casting – Mould	(1) C7000 (2) Yu’s Curve (3) Inverse algorithms
3	Filling definitions (pouring time) [s]	Use solver 5	1.8

5. RESULTS AND DISCUSSION

5.1 Pressure Effect on IHTCs

The results of the real-time X-ray radiograph examination are shown in Figure 7-6. It is evident from Figure 7-6 (a) that the 5-step squeeze cast AM60 under an applied pressure of 60 MPa was virtually free of gas and shrinkage porosities. However, the typical porosities were easily found in the 5-step casting while no external pressures were applied as shown in Figure 6-6 (b). Figure 7-7 shows typical temperatures versus time curves at the metal-die interface of Step 4 for solidifying magnesium alloy AM60 and inside the steel die with an applied hydraulic pressure of 30MPa. The results include the measured temperature of casting surface and temperature measurements obtained at different depths underneath the die surface (T1-2 mm, T2-4 mm, and T4-6 mm). Since molten metal filled

the cavity from the bottom, pre-solidification occurred upon the completion of cavity filling. No die surface temperatures exceeded 340°C, and the highest temperature of the casting surface was 532.97°C.

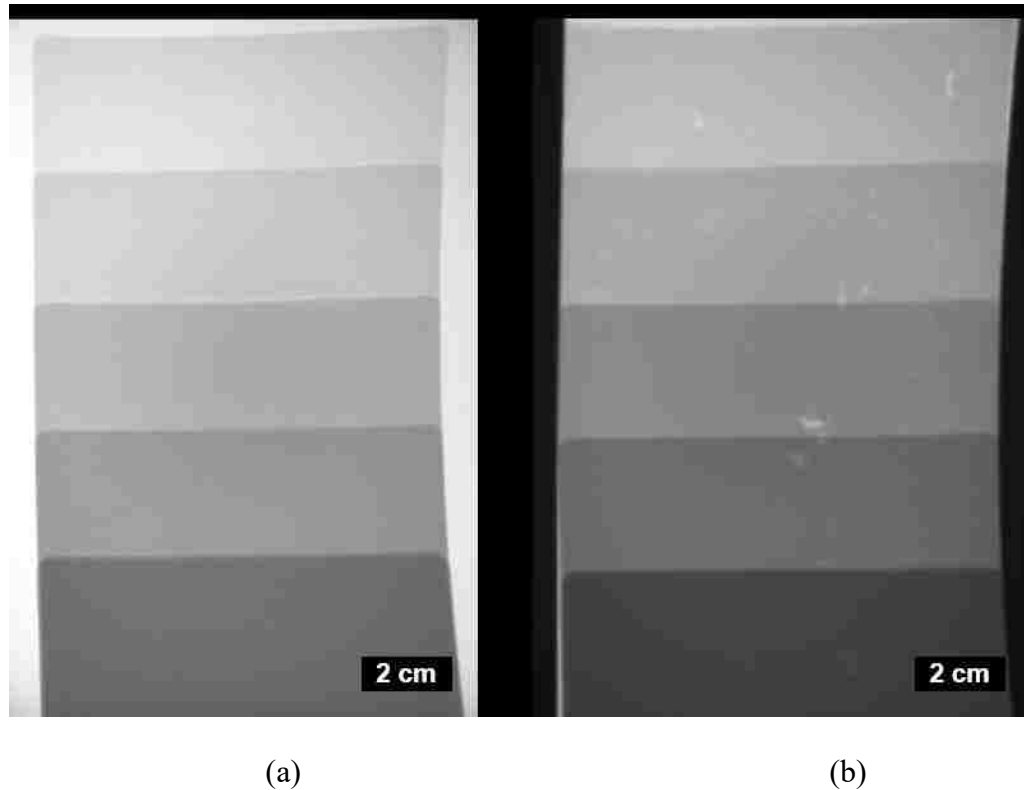


Figure 7- 6: X-ray radioscopic examination showing the soundness of the step castings under the applied pressures of (a) 60 MPa and (b) 0 MPa.

The die surface temperature (T_0) and the heat flux (q) transferred at the interface between the molten metal and die were determined by the inverse method. Figure 7-7 shows the estimated result of the interfacial heat flux (q) and the heat transfer coefficient (IHTC) versus solidification time. The peak heat flux value was $7.38E+05$ W/m², and the peak value of IHTC was 6005 W/m²K. It can be observed that the heat flux and IHTC curves reached to their peak value promptly and then dropped gradually until their values dropped to a low level, respectively.

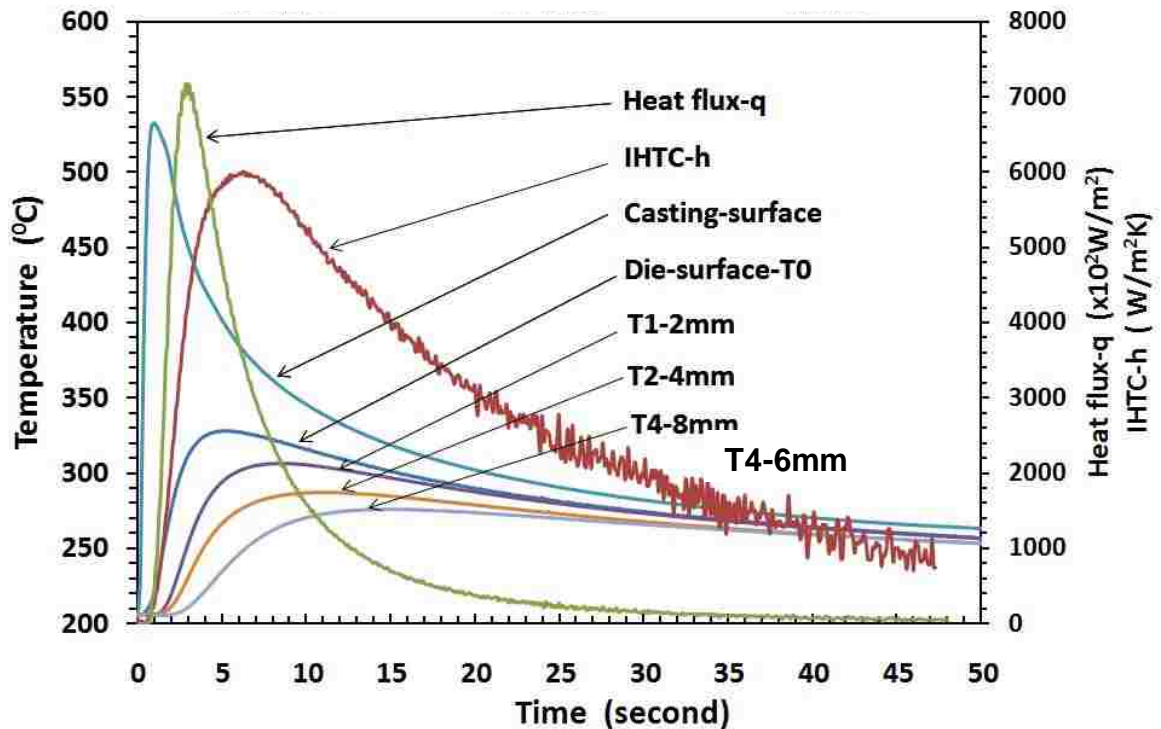


Figure 7- 7: Typical temperature versus time curves (Step 4, 30 MPa) at metal surface, die surface, and various positions inside the die; The interfacial heat flux(q) and the heat transfer coefficient (IHTC) curves estimated by inverse method (Step 4, 30 MPa).

The in-cavity local pressures at the interface of step casting and die were measured using the Kistler® pressure transducers of which calibration was conducted before the experiment. Figure 7-8 shows the local pressure distributions at the casting-die interface of step 4 under the applied hydraulic pressures of 30, 60, 90 MPa. Upon the completion of the cavity filling, the local pressure increased abruptly to reach its peak value, then decreased gradually until the pressure-transfer path died out. For the hydraulic pressures of 30, 60, and 90 MPa, the local pressure peak values were 12.1, 21.7, and 35.2 MPa, respectively. With the applied hydraulic pressure increased from 30 to 90 MPa, the IHTC peak value of step 4 was increased from 6005 to 9418 W/m²K, accordingly. This effect can

be associated to greater local pressure application experienced for higher applied hydraulic pressure.

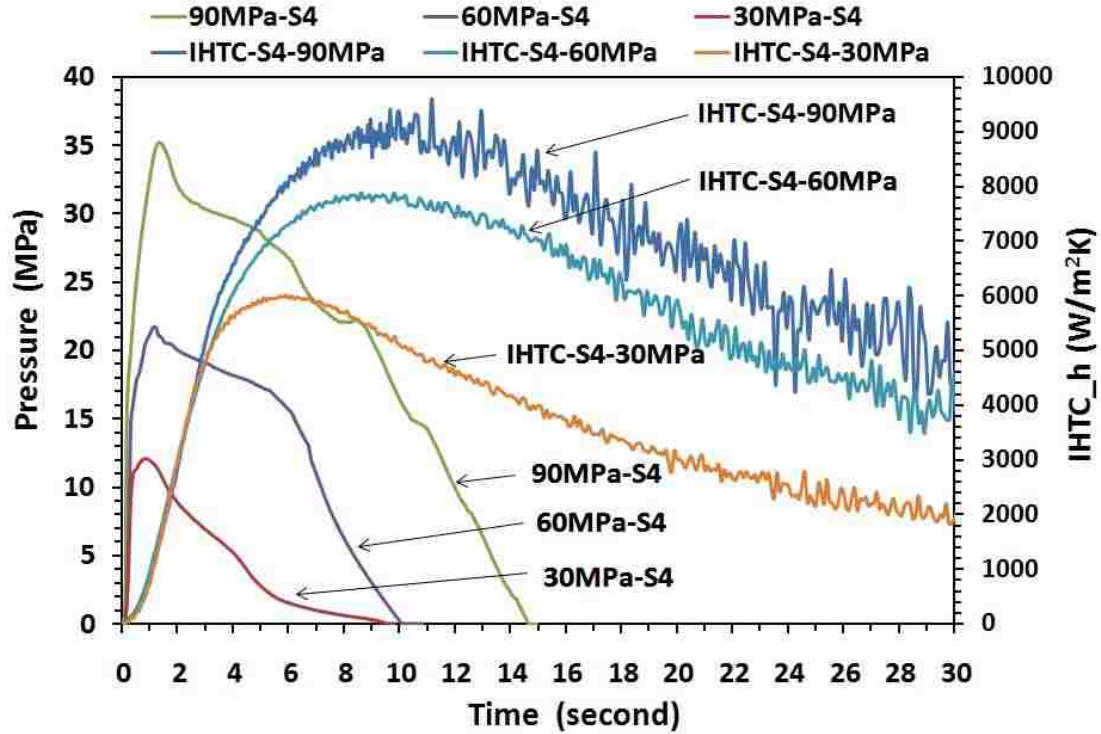


Figure 7- 8: Typical local pressure distributions and IHTC curve at the casting-die interface of step 4 under the applied hydraulic pressures of 30, 60, 90 MPa.

Under the applied hydraulic pressure of 30 MPa, the pressure-transfer path inside the casting shrank quickly (9.1 s) as the solidification proceeded. The pressure-transfer path existed longer (14.6 s) when the applied hydraulic pressure increased to 90 MPa, indicating that a good heat transfer condition can be achieved. From the hydraulic pressure 30 to 90 MPa, the local pressure peak value at step 5 casting-die interface was varied from 20 to 50 MPa.

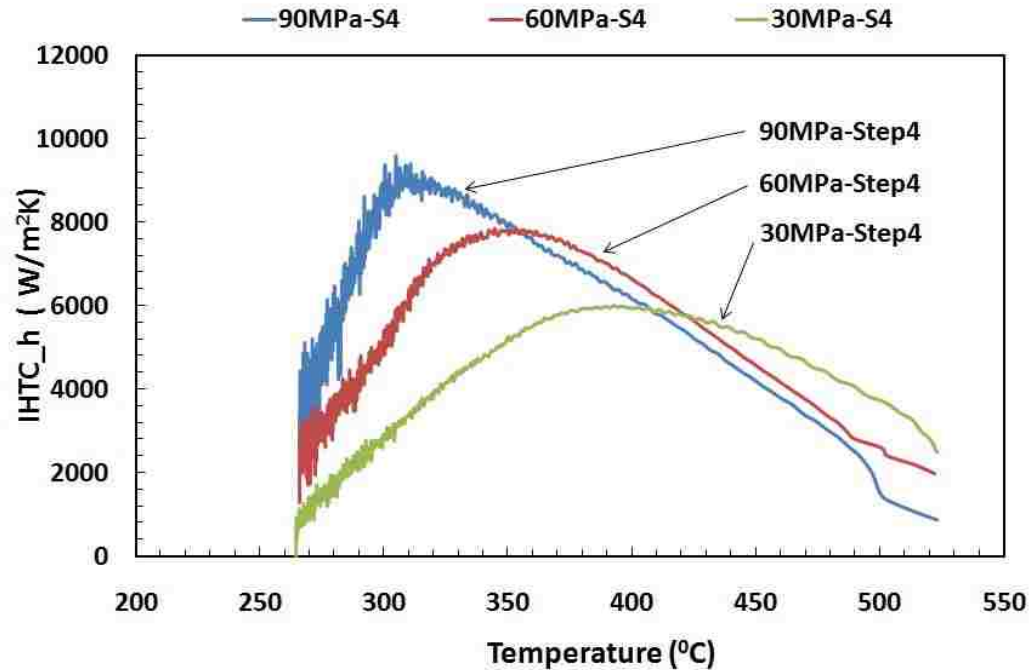


Figure 7- 9: Typical effects of applied pressures on the heat transfer coefficients varying with casting surface temperature at the step 4.

Figure 7-9 shows the variation of interfacial heat transfer coefficients as a function of casting surface solidifying temperature at the step 4 under applied hydraulic pressures 30, 60, and 90 MPa. It can be observed that the values of the interfacial heat transfer coefficients increased gradually after the cavity filled. When the maximum IHTC values reached at different casting surface temperatures under various applied pressures, the IHTC values decreased to a low value level. For the applied pressures of 30, 60, and 90 MPa, the peak IHTC values (6005, 7871, and 9418 W/m²K) were found at 392, 353, and 304°C, respectively. As the applied pressure was relatively small (30 MPa), the peak value of the IHTC was low (6005W/m²K) and appeared at a high die surface temperature (392°C). However, under the high applied pressure (90 MPa), the peak value of the IHTC was increased to 9418 W/m²K and occurred at a low die surface temperature (304°C). This

observation should be attributed to the presence of long pressure transfer path as the high pressure was applied.

5.2 Effect of Casting Wall Thicknesses on IHTCs

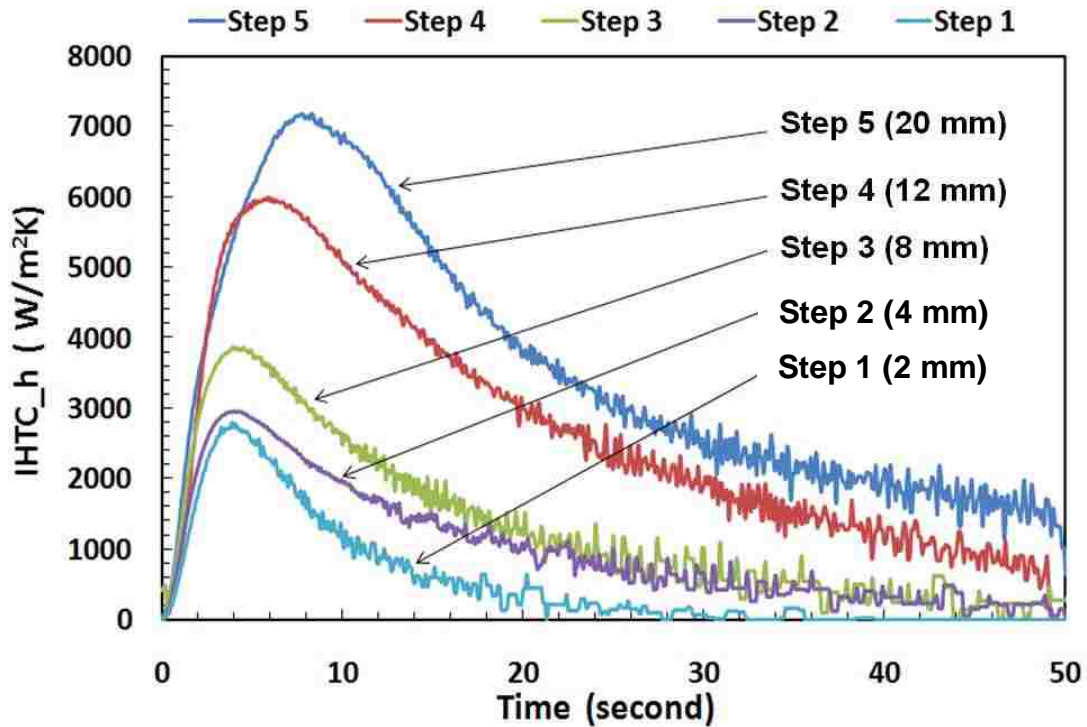


Figure 7- 10: Interfacial heat transfer coefficients (IHTC) curves of 5 steps under the applied pressure of 30 MPa.

Figure 7-10 shows that the heat transfer coefficient (IHTC) curves of 5 steps determined by the inverse method under an applied pressure of 30 MPa. For all the steps, the IHTCs began with an increasing stage and reached their peak values, then dropped gradually until the value became a low level. From steps 1 to 5 with 30 MPa pressure, the peak IHTC values varied from 2807W/m²K, 2962W/m²K, 3874W/m²K, 6005W/m²K to 7195W/m²K, indicating the closer contact between the casting and die surface at thicker steps. Therefore,

the wall thickness affected IHTC peak values significantly. The peak IHTC value increased as the step became thicker. This effect can be associated to greater local pressure application experienced at the thicker step.

For the steps 1, 2, 3, 4 and 5, it took 4.1, 4.2, 4.7, 6.1, and 8.2 seconds respectively to reach their peak values, respectively. Besides the different peak values, the time for IHTC to obtain the peak value during the initial stage increased as the step became thicker. The thicker steps needed relatively long time to reach the high peak IHTC values since additional time was required for pressure transfer.

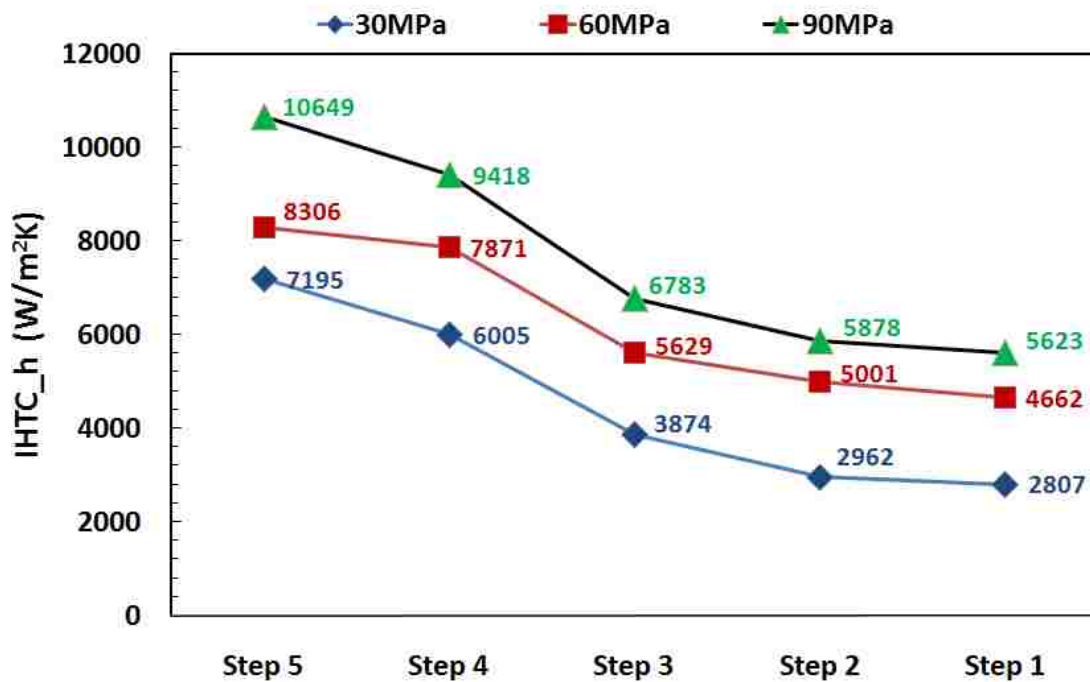


Figure 7- 11: The peak IHTC values of 5 steps estimated by the inverse method with the applied pressures of 30, 60 and 90 MPa.

Figure 7-11 shows the IHTC peak values at step 1 through 5 with the applied pressures of 30, 60 and 90 MPa. Similar characteristics of IHTC peak values can be observed at 30, 60

and 90MPa. Under the applied pressure of 60 MPa, the peak IHTC values at steps 1, 2, 3, 4, and 5 varied from 4662 W/m²K, 5001 W/m²K, 5629 W/m²K, 7871 W/m²K and 8306 W/m²K. As the applied pressure became 90 MPa, the peak IHTC values varied from 5623 W/m²K, 5878 W/m²K, 6783 W/m²K, 9418 W/m²K to 10649 W/m²K at steps 1, 2, 3, 4, 5, respectively.

With increasing the applied hydraulic pressures, the IHTC peak value of each step was increased accordingly. This is because the pressure exerted locally at each step became larger as the high hydraulic pressure applied. The wall thickness affected IHTC peak values significantly. It also can be observed that the peak IHTC value and heat flux increased as the step became thick. The large difference in temperatures between the melt and the die with the thick cavity section as well as relatively high localized pressure should be responsible for the high peak IHTC values observed at the thick steps.

5.3 IHTC Empirical Equations

From the above interfacial heat transfer coefficient (IHTC) curves obtained with temperatures and pressures, the peak IHTC value(h) empirical equation as a function of local pressures and solidification temperatures can be derived for all steps by multivariate linear and polynomial regression.

- *For the step 5 with thickness 20mm,*

$$h_{step5} = (0.000044P - 0.0028)T^3 + (3.118 - 0.0633P)T^2 + (25.66P - 1053.33)T - 3131P + 112616$$

$$(0\text{MPa} < P < 50\text{MPa}, \quad 20^\circ\text{C} < T < 540^\circ\text{C},$$

the correlation coefficient $R = 0.9026$)

- For the step 4 with thickness 12mm,

$$h_{\text{step4}} = (0.00017P - 0.0022)T^3 + (2.297 - 0.2048P)T^2 + (76.17P - 738.08)T - 8983P + 75045$$

$$(0\text{MPa} < P < 36\text{MPa}, \quad 20^\circ\text{C} < T < 540^\circ\text{C},$$

the correlation coefficient $R = 0.9586$)

- For the step 3 with thickness 8mm,

$$h_{\text{step3}} = (0.000014P + 0.0011)T^3 - (1.35 + 0.0178P)T^2 + (8.44P + 506.66)T - 623P - 68705$$

$$(0\text{MPa} < P < 25\text{MPa}, \quad 20^\circ\text{C} < T < 510^\circ\text{C},$$

the correlation coefficient $R = 0.8625$)

- For the step 2 with thickness 5mm,

$$h_{\text{step2}} = (0.0039 - 0.00003P)T^3 + (0.016P - 3.473)T^2 + (945 - 0.87P)T - 185P - 89714$$

$$(0\text{MPa} < P < 15\text{MPa}, \quad 20^\circ\text{C} < T < 450^\circ\text{C},$$

the correlation coefficient $R = 0.8563$)

- For the step 1 with thickness 3mm,

$$h_{\text{step1}} = (0.000087P + 0.0015)T^3 - (0.075P + 1.24)T^2 + (20.13P + 344)T - 1632P - 30051$$

$$(0\text{MPa} < P < 10\text{MPa}, \quad 20^\circ\text{C} < T < 360^\circ\text{C},$$

the correlation coefficient $R = 0.8694$)

where P is the local pressure with the range from 0 MPa to 50 MPa (hydraulic pressure from 0 MPa to 90 MPa), T is the solidification temperatures with the range from 0°C to 540°C, and the correlation coefficient R varies from 0.85 to 0.95.

5.4 IHTC Verification

A 5-step casting of magnesium alloy AM60 was squeezed under an applied pressure of 60 MPa with a melt temperature of 620°C and a die temperature of 210°C. The temperature history at the center of the fifth step of the 5-step casting is represented in Figure 7-12.

During experiments, after the commencement of the process, the temperature increased at the center of Step 5 was recorded by the first segment of cooling curve till the melt was filled into cavity. Before the filling was completed, the center of the casting as the last solidification area was cooled at a slower rate than its outer portion. The highest temperature of 614.8 °C just around the liquidus temperature (615°C) at the center was able to maintain at the liquidus-solidus mush state and then dropped quickly. This observation indicates that pre-solidification occurred in the 5-step casting adjacent to the casting/die interface during filling. As solidification time further increased, the temperature at the center of Step 5 decreased toward the solidus temperature within 6 seconds and the temperature decreased below 300°C after 60 second.

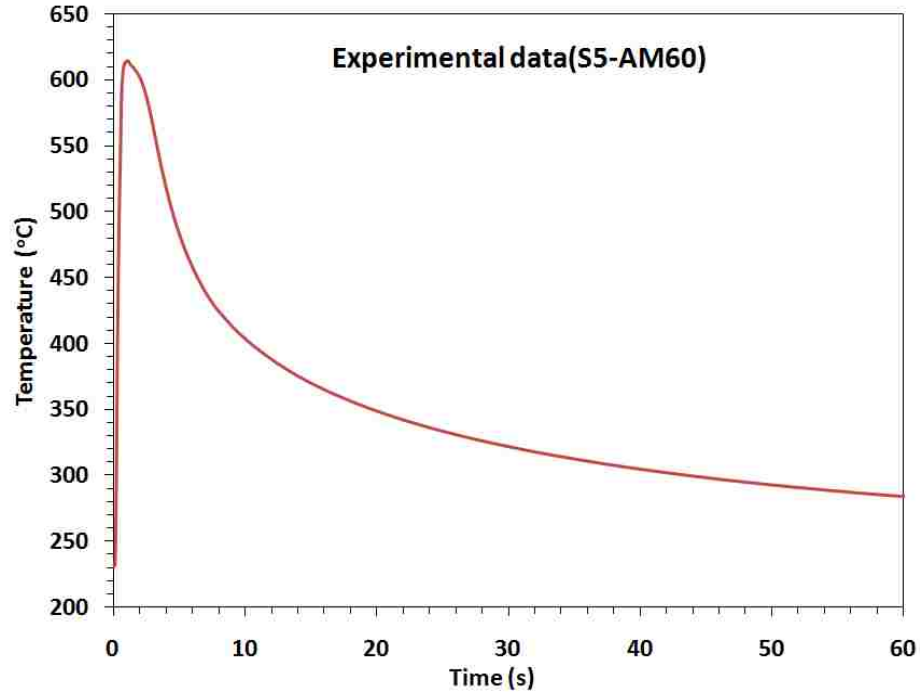


Figure 7- 12: A typical experimental cooling curve at the center of Step 5 (AM60) under an applied pressure of 60 MPa.

For the verification of the identified IHTC, the temperature distribution was calculated by feeding the different IHTCs into the simulation package with the same materials and process parameters, and then compared to the measured temperatures at the corresponding location.

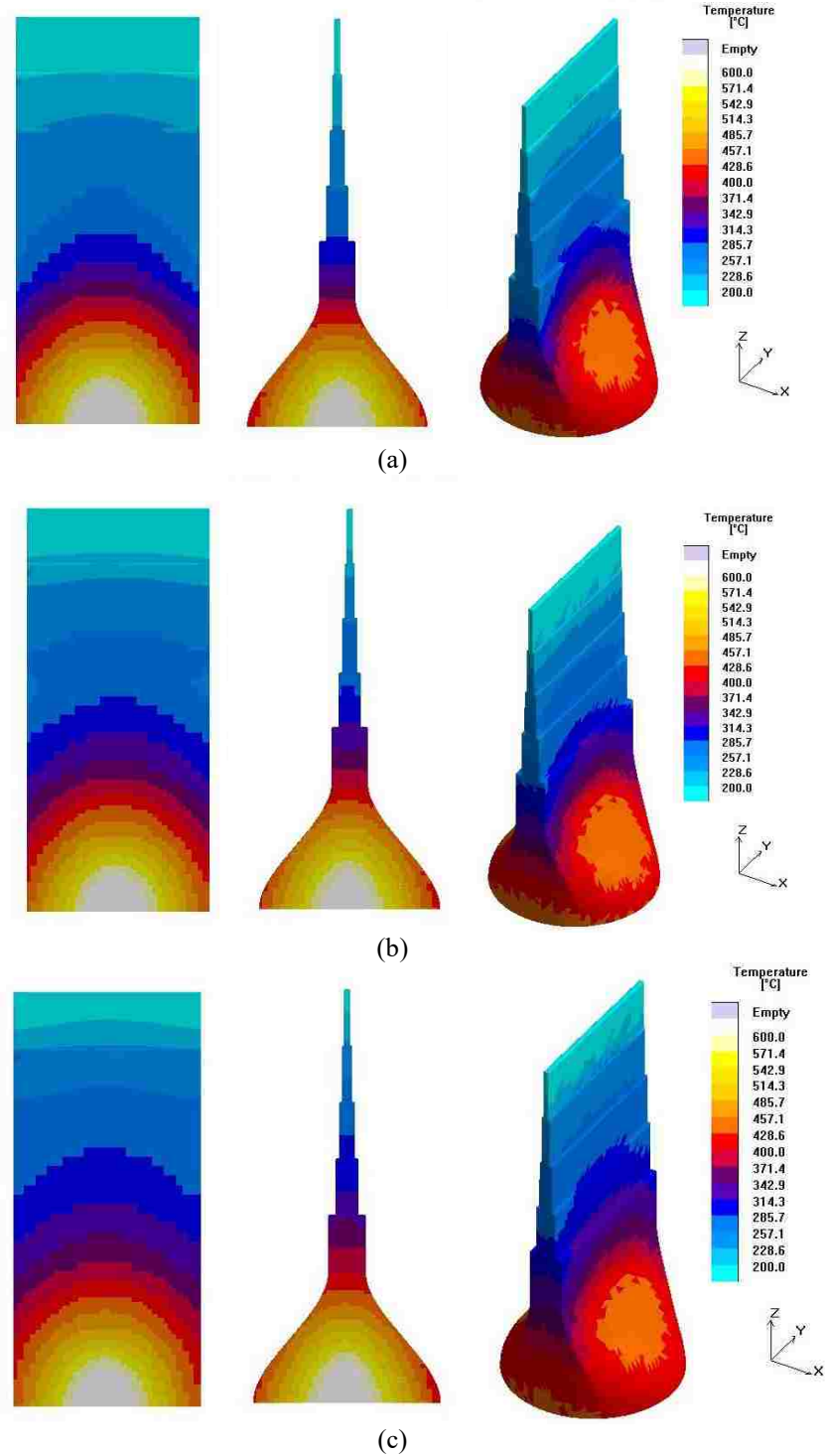
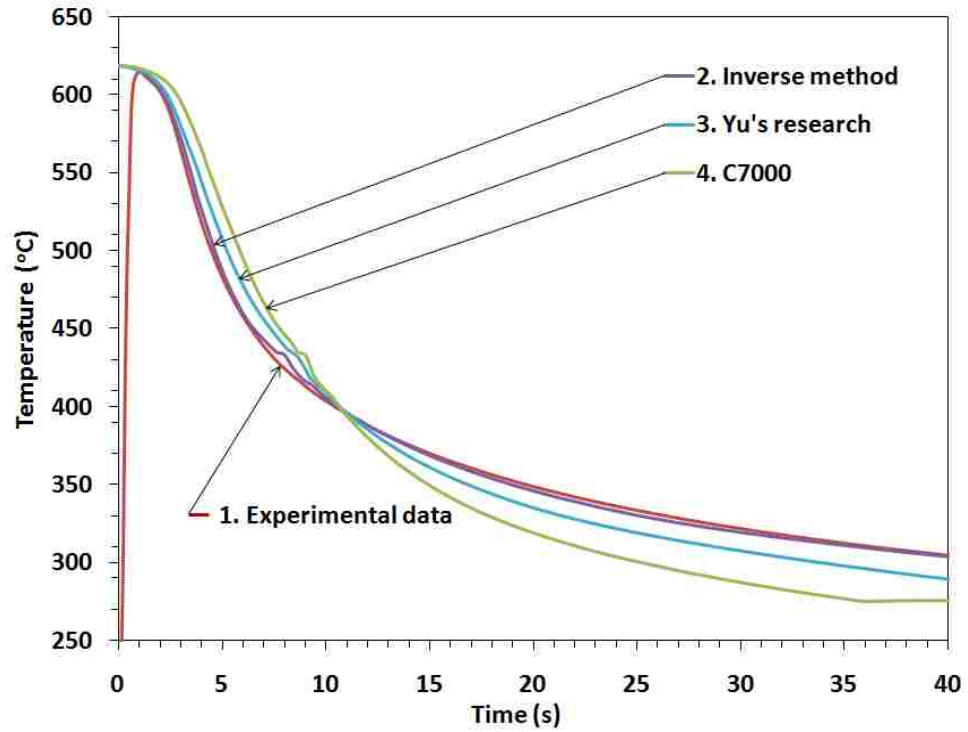
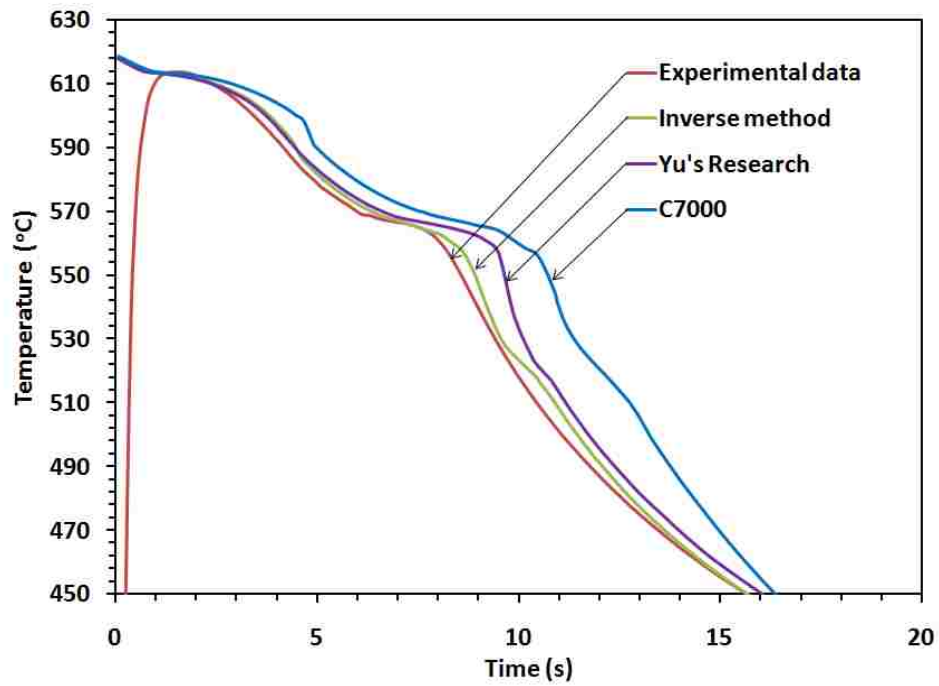


Figure 7- 13: Temperature distribution inside the 5-step casting (80% solidified) of AM60 simulated with the input of HTCs, (a) 7000 W/m²K, (b) Yu's research, and (c) the Inverse algorithms.



(a)



(b)

Figure 7- 14: Comparison of the experimental and computational cooling curves at the center of Step 5 under an applied pressure of 60 MPa, (a) the entire cooling period, and (b) the enlarged solidification region.

Figure 7-13 shows the temperature distribution inside the 5-step casting simulated with the input of three selected different HTCs when 80% volume of the casting was solidified. As shown in Figure 7-14, the curve 4 presented the computed results by applying the constant IHTC ($7000 \text{ W/m}^2\text{K}$). It appeared that, an underestimation of the IHTC ($7000 \text{ W/m}^2\text{K}$) occurred at the early stage of the solidification process since the computed temperatures were quite higher than the experimental measurements. As the solidification proceeded after 11 seconds, however, the measured temperature history moved upward and stayed above the numerical prediction. The input of $7000 \text{ W/m}^2\text{K}$ seemed to be overestimated.

The curve 3 in Figure 7-14 was predicted by applying Yu's research data. It can be observed that a small deviation between the prediction and experimental data. The simulation was improved by Yu's research data over the adoption of a simple constant ($7000 \text{ W/m}^2\text{K}$). But, the underestimation and overshooting of the IHTCs also took place at the early and later stages of the solidification process, respectively.

The curve 2 in Figure 7-14 represents the predicted temperatures by applying the IHTC data derived from the inverse algorithms in this study. A little deviation between the experimental measurements and the computed temperatures was observed in the region of the solidus temperature. This may be attributed to the fact that the inverse calculated the HTCs based on the temperatures measured in the mold, and at the casting surface which might be slightly outside the casting. Also, it was almost impossible to precisely measure the temperatures right at the casting center.

The computational output from the inverse method has the best agreement with experimental data compared to those resulting from other methods. The maximal temperature differences were less than 90°C and the mean temperature differences were less than 3.80°C between the numerical calculation of the inverse algorithms and experimental measurements. The results confirm that the inverse algorithms can be applied to determine the IHTC between the castings and mold accurately and reliably.

6. CONCLUSIONS

1. The 5 step casting of magnesium alloy AM60 with different wall-thicknesses (2, 4, 8, 12 and 20 mm for Steps 1, 2, 3, 4, 5) were prepared under various hydraulic pressures (30, 60, and 90 MPa) using in-directed squeeze casting process. The IHTC versus time and temperature curves have been successfully determined by the inverse method. The heat fluxes and IHTCs reached to their peak values promptly and then dropped gradually to a low level.
2. The in-cavity local pressures at the interface of the step casting and die rose abruptly to its peak value, then decreased gradually until the pressure-transfer path died out. The pressure-transfer path extended longer as the applied hydraulic pressure increased.
3. As the applied hydraulic pressure increased, the high IHTC peak value of each step was obtained accordingly. This effect can be attributed to the exertion of greater pressure locally at each step for higher applied hydraulic pressure.

4. Similar characteristics of IHTC peak values can be observed at 30, 60 and 90 MPa applied pressures. With an applied pressure of 60 MPa, the peak IHTC values at steps 1, 2, 3, 4, and 5 were 4662 W/m²K, 5001 W/m²K, 5629 W/m²K, 7871 W/m²K and 8306 W/m²K respectively. As the applied pressure increased to 90 MPa, the peak IHTC values were 5623 W/m²K, 5878 W/m²K, 6783 W/m²K, 9418 W/m²K and 10649 W/m²K respectively.
5. The wall thickness affected IHTC peak values significantly. The peak IHTC values and heat fluxes increased as the steps became thick. The large difference in temperatures between the melt and the die with thick cavity sections as well as relatively high localized pressure should be responsible for the high peak IHTC values observed at the thick steps.
6. The empirical equations of all steps relating IHTC to the local pressures and solidification temperature at the casting surface were developed.

REFERENCES

- [1] Sun, Z., Zhang, X., Niu, X., Yu, A., Hu, H. Numerical simulation of heat transfer in pressurized solidification of Magnesium alloy AM50. *Heat and Mass Transfer*. 2011, (47), 1241-1249.
- [2] Griffiths, W., Kawai, K. The effect of increased pressure on interfacial heat transfer in the aluminium gravity die casting process. *J. Mater. Sci.* 2010, (45), 2330-2339.
- [3] Browne, D., O' Mahoney, D. Interface heat transfer in investment casting of aluminum. *Metall. and Mater. Trans. A*, 2001, (32A), 3055-3063.
- [4] Ferreira, I. L., Spinelli, J. E., Nestler, B., Garcia, A. Influences of solute content, melt superheat and growth direction on the transient metal/mold interfacial heat transfer coefficient during solidification of Sn–Pb alloys. *Mat. Chem. Phys.* 2008, (111), 444-454.
- [5] Ferreira, IL, Spinelli, J. E., Pires, L. C., Garcia, A. The effect of melt temperature profile on the transient metal/mold heat transfer coefficient during solidification. *Mat. Sci. Eng. A*. 2005, (408), 317-325.
- [6] Arun, K. S., Sreenivas, R.K.V., Prasanna, K. T. S. Spatial Variation of Heat Flux at the Metal-Mold Interface due to Mold Filling Effects in Gravity Die Casting. *Int. J. Heat Mass Transf.* 2008, (51), 2676-2685.
- [7] Meneghini, A., Tomesani, L. Chill material and size effects on HTC evolution in sand casting of aluminium alloys, *J Mat Proc Technol.* 2005, 534-539.

- [8] Chattopadhyay, H. Simulation of transport process in squeeze casting. *J Mat Proc Technol.* 2007, (186), 174-178.
- [9] Aweda, J., Adeyemi, M. Experimental determination of heat transfer coefficients during squeeze casting of aluminum. *J. Mater. Process. Technol.* 2009, (209), 1477-1483.
- [10] Guo, Z.P., Xiong, S.M., Liu, B.C., Li, M., Allison, J. Effect of Process Parameters, Casting Thickness, and Alloys on the Interfacial Heat-transfer Coefficient in the High-pressure Die Casting Process. *Metall. and Mater. Trans.* 2008, (39A), 2896-2905.
- [11] Dour, G., Dargusch, M., Davidson, C. and Nef, A. Development of a non-intrusive heat transfer coefficient gauge and its application to high pressure die casting. *J. Mater. Process. Technol.* 2005, (169), 223-233.
- [12] Hamasaiid, A., Dargusch, M., Davidson, C., Tovar, S., Loulou, T., Rezai-aria, F. and Dour, G. Effect of mold coating materials and thickness on heat transfer in permanent mold casting of aluminum alloys. *Metall. and Mater. Trans. A*, 2007, (38A), 1303-1316.
- [13] Dargusch, M., Hamasaiid, A., Dour, G., Loulou, T., Davidson, C., and StJohn, D. The accurate determination of heat transfer coefficient and its evolution with time during high pressure die casting of Al-9% si-3% Cu and Mg-9% Al-1% Zn alloys. *Advanced Engineering Materials.* 2007, 9(11), 995-999.
- [14] Sun, Z., Hu, H., Niu, X. Experimental Study and Numerical Verification of Heat Transfer in Squeeze Casting of Aluminum Alloy A443. *Metallurgical and Materials Transactions B*, 2001, (43B), 1676-1683.

- [15] MAGMASOFT® (version 4.4) Release Notes and Manual, (2006).
- [16] Magnesium and Magnesium Alloys. ASM Speciality Handbook, ed. M.M. Avedesian and H. Baker. ASM International, 2000.
- [17] Yu, A. Mathematical modeling and experimental study of squeeze casting of magnesium alloy AM50A and aluminum alloy A356. Ph.D. dissertation, Dept. of mechanical, automotive & materials engineering, University of Windsor. 2007.

CHAPTER 8

ESTIMATION OF HEAT TRANSFER COEFFICIENT IN SQUEEZE CASTING OF WROUGHT ALUMINUM ALLOY 7075 BY THE POLYNOMIAL CURVE FITTING METHOD

1. INTRODUCTION

Wrought aluminum alloys with their high strength properties have achieved widespread use in today's aerospace and automotive industries. Aluminum alloys of 7075 are known for its high strength and other good characteristics which allow them suitable for applications such as structural component or tooling plates [1]. Squeeze casting has the advantage of pressurized solidification, close dimensional tolerance and good surface finish. During the solidification process, the applied pressure feed the liquid metal into the air or shrinkage porosities effectively. It makes castings free of porosity and excellent as-cast quality [2-3]. There is limited open literatures or research activities that focus on casting wrought aluminums. It is interesting to combine the advantages of wrought aluminum with its excellent properties and squeeze casting process with its novel shaping

techniques. The cast version of wrought aluminum might fill the gap between wrought and cast components.

In today's foundry, numerical simulation improved the productivity significantly. However, one of the most important parameter, the interfacial heat transfer coefficients (IHTCs) at the metal-mold interface is usually roughly set in the available finite element method (FEM) and finite difference method (FDM) commercial code [4]. To accurately determine the solidification path, microstructure development and shrinkage porosity formation etc., it is necessary to have a precise prediction of boundary conditions. In the real-life casting process, the imperfection of the contact between the mold and liquid metal due to the air gap caused by the application of coating on die surface may decrease the heat transfer between metal and die as well as cooling rate of the casting surface. These thermal barriers could degrade casting quality and properties significantly [5, 6]. Therefore, an accurate prediction of the IHTC is critical to simulate the solidification process.

For decades, researchers have done extensive works to obtain heat transfer coefficients for different metal-mold interfaces by different kind of casting processes experimentally or analytically. Dour et al. [7] reported their work to evaluate IHTC of a thin wall aluminum casting by the application of HPDC technique. The results showed that the lower preheat die temperature and a faster shot velocity led to a higher IHTC value. Rajaraman and Velraj [8] estimated IHTC by the Beck's and control volume methods. The results indicated that the calculated results by these two methods have a maximum percentage deviation of around 40 and 57%, respectively. The control volume technique produced more accurate and reliable results, since it does not involve iteration and step by step

computation. Hao et al. [9] used FDM to solve thermal conduction equation. They used the temperature recovery method to calculate the latent heat of fusion. They found that the IHTC of ductile iron increased gradually and it indicated that the metal-die interface stay in close contact condition. This showed a different result in comparison to those estimated in steel and other nonferrous alloy castings. Also, most of the casting products involve various section thicknesses, difference in section thicknesses could result in significant variation of the heat transfer coefficient. Also, as the section became thinner, the evaluation of IHTC was vital due to the limitation in solidification time. Thus, it was important to examine the influence of casting section thickness on the IHTC [10-12].

However, most of the work has been focused on permanent mold casting processes and casting aluminum alloys. There is very limited knowledge about IHTC during squeeze casting by using wrought aluminum alloys.

In this work, 5-step squeeze casting mold was designed for evaluation casting thickness-dependent IHTC. The temperature at the die surface was estimated by the polynomial extrapolation method, which required the temperature values at different locations inside the die. With the temperature measurements and the estimated die surface temperatures, the heat flux and interfacial heat transfer coefficient were calculated at the casting /die interface.

2. EXPERIMENTAL PROCEDURES

2.1 Die Design

Table 8- 1: Thermo-physical parameters of Al 7075-T6 alloy

Material	Density	Specific	Thermal	Solidus	Liquidus
	g/cm ³	heat	conductivity	temperature	temperature
		J/g K	130 W/m K	°C	°C
Al 7075	2.81	0.96	130	477	635

Table 8- 2: Chemical composition of Al7075 alloy (in weight percent)

Al	Zn	Mg	Cu	Cr	Fe	Si	Mn	Ti
88~92	5.1~6.1	2.1~2.9	1.2~2.0	0.18~0.28	Max	Max	Max	Max
					0.50	0.40	0.30	0.20

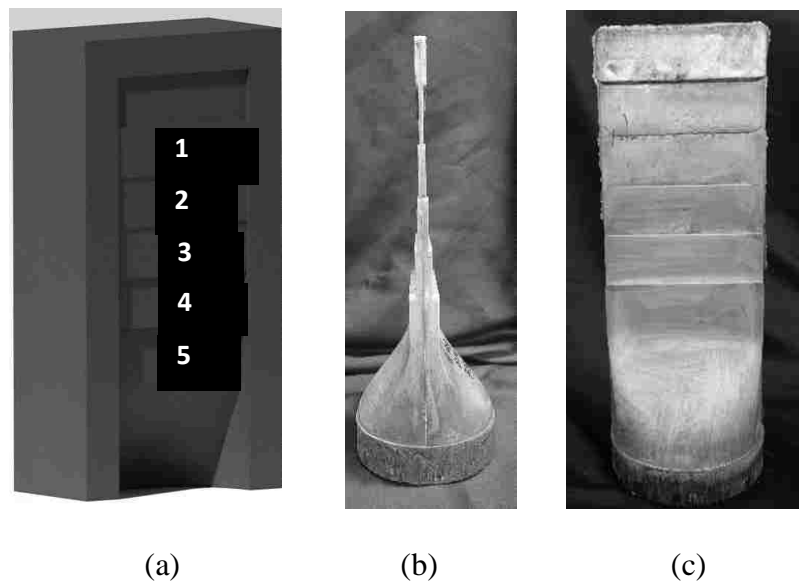


Figure 8- 1: a) 3-D model of step casting mold, and b) side view and c) front view of 5-step casting sample of Al 7075 by squeeze casting under an applied pressure of 60 MPa.

Figure 8-1(a) illustrates the 3-D model of a 5-step casting die. There were totally six steps, of which the first step (top step) was designed as an overflow to entrap impurities in the upfront stream of the liquid melt during cavity filling. The vent was located on the top of the overflow, which could discharge the air inside the die. The dimensions for the rest of the 5 steps (from the second top) were 100x20x2 mm, 100x30x4 mm, 100x30x8 mm, 100x30x12 mm and 100x30x20 mm, accordingly. Figure 1(b) gives the side view of a 5-step casting sample of Al7075, of which chemical composition is given in Table 8-2.

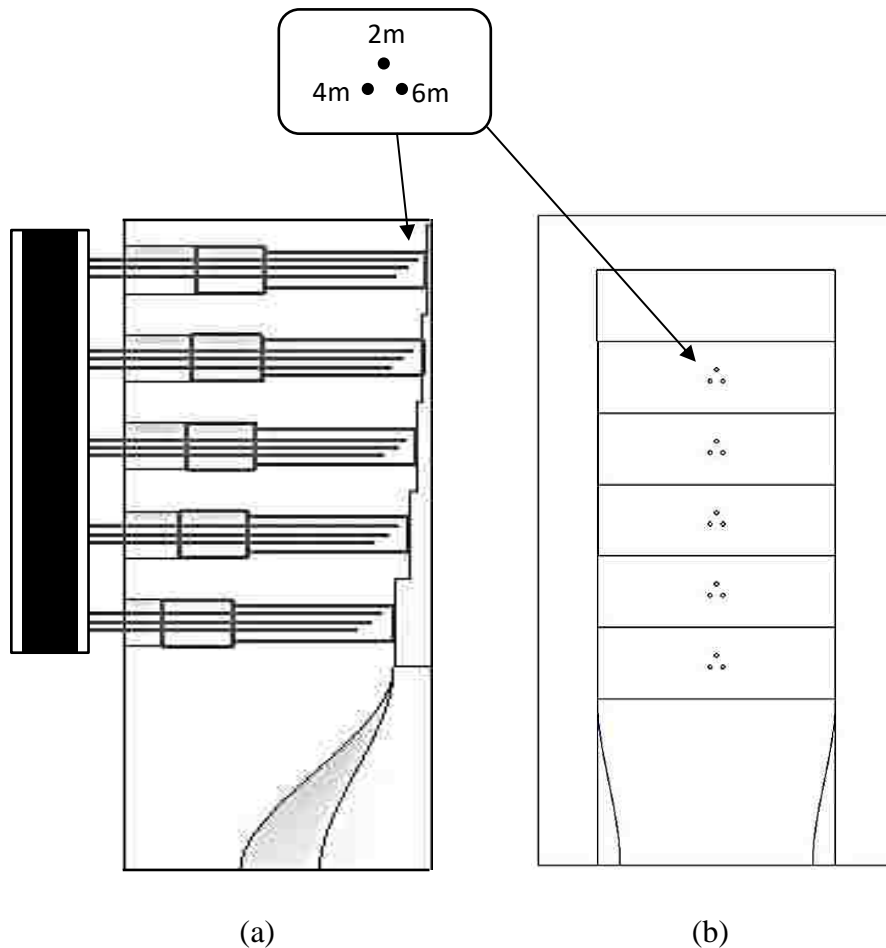


Figure 8- 2: a) side view and b) front view of the step die illustrating the locations of the thermocouples in each step.

To acquire the temperature history of each step, three K-type thermocouples (totally 15 thermocouples) were placed at each steps with the distance of 2 mm, 4 mm, and 6 mm away from the cavity surface, as shown in Figure 8-2. The cavity was filled from the bottom sleeve (with diameter of 100 mm) to the top.

2.2 Casting Process

A 75-ton- hydraulic press and wrought aluminum 7075 were used in the experiment, the thermo-physical parameters for the alloy are summarized in Table 8-1. The metal was firstly melt in an electric resistance furnace with the protection of nitrogen gas on the top. The holding temperature of the furnace was 800°C. As shown in Figure 8-3, the two half upper dies opened along the central parting line. The lower die had a diameter of 100 mm and a height of 200 mm. Both of the upper and lower dies were preheated by cartridge heaters. The upper die was preheated to 250°C and the lower die at 300°C. Liquid metal at 710°C was poured into the lower die. At last, the liquid metal was squeeze casted under an applied pressure of 60 MPa and kept holding at this pressure for 25 seconds.

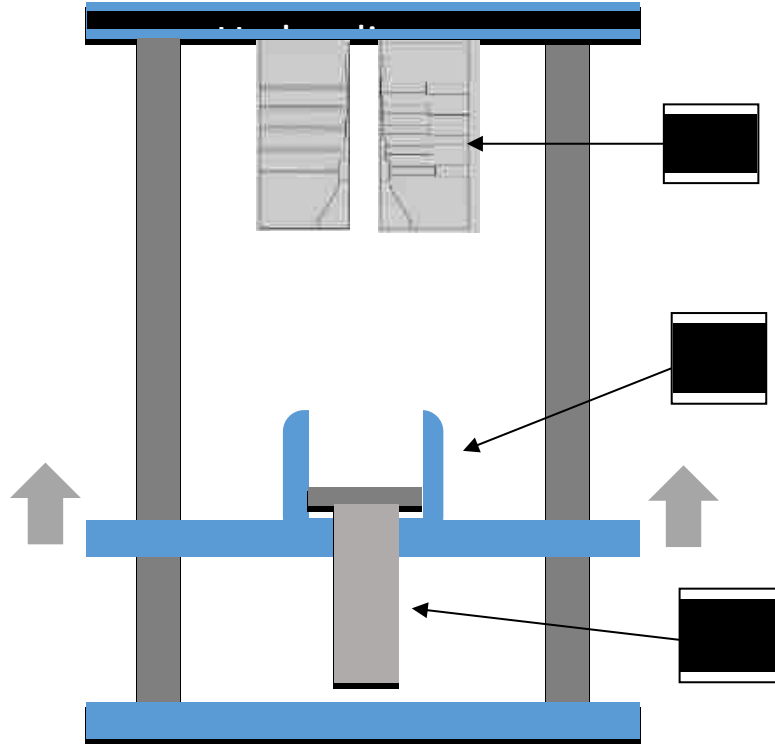


Figure 8- 3: Schematic diagram of squeeze casting machine 1) upper die, 2) lower die and 3) piston.

2.3 Heat Transfer Model

Since the thickness of each steps was much smaller than the width, it could be assumed that the heat transfer was one dimensional at each step. The IHTC can be characterized by the following equation (Eq. 8-1).

$$h(t) = \frac{q(t)}{T_c - T_d} \quad 8-1$$

where h is IHTC, q is average heat flux at the metal-mold interface, A is the cross section area, T_c is casting temperature and T_d is die surface temperature, respectively. The heat flux for both of the casting and die interface could be evaluated from Eq. 8-2 with the temperature gradient at the surface and sub-surface nodes (2, 4, and 6mm from the surface).

$$q(t) = -k(T) \frac{dT}{dx} = -k(T) \frac{T_m^t - T_{m-1}^t}{\Delta x} \quad 8-2$$

where k is thermal conductivity of the casting or die materials. The superscript t is solidification time. The subscript m is the number of the discrete nodal points. The heat transfer at each step is unsteady conduction transfer through one-dimensional body which can be described by Eq. 8-3.

$$\rho c(T) \frac{\partial T(x,t)}{\partial t} = \frac{\partial}{\partial x} \left(k(T) \frac{\partial T(x,t)}{\partial x} \right) \quad 8-3$$

For the heat transfer at the surface of the die, Eq. 8-3 could be rearranged as Eq. 8-4:

$$(1 + 2F) T_0^{p+1} - 2F T_1^{p+1} = 2F \frac{\Delta x}{k} q_0 + T_0^p \quad 8-4$$

For the heat transfer inside of the die, Eq. 8-3 could be rearranged as Eq. 8-5:

$$(1 + 2F) T^{p+1} - F (T_{m-1}^{p+1} + T_{m+1}^{p+1}) = T_m^p \quad 8-5$$

where the superscript p denotes the time dependent of T . F is a finite different form of the Fourier number:

$$F = \frac{\alpha \Delta t}{(\Delta x)^2} = \frac{k}{c\rho} \frac{\Delta t}{(\Delta x)^2} \quad 8-6$$

The heat flux at the metal-die interface at each time step was obtained by applying Equations 8-4 and 8-5.

2.4 Polynomial Curve Fitting

The metal-die interface temperature T_c was estimated by the polynomial curve fitting method. Thus, the IHTC values can be calculated by Eq. 8-1 with the measured casting temperature. Three K-type thermocouples were located at $X_1= 2$ mm, $X_2= 4$ mm and $X_3= 6$ mm away from the inside die surface for each steps. Using the temperature reading from thermocouples at different locations, a temperature versus time curve can be obtained. The temperature at the inside die surface ($X_0= 0$ mm) can be estimated by using the polynomial curve fitting method.

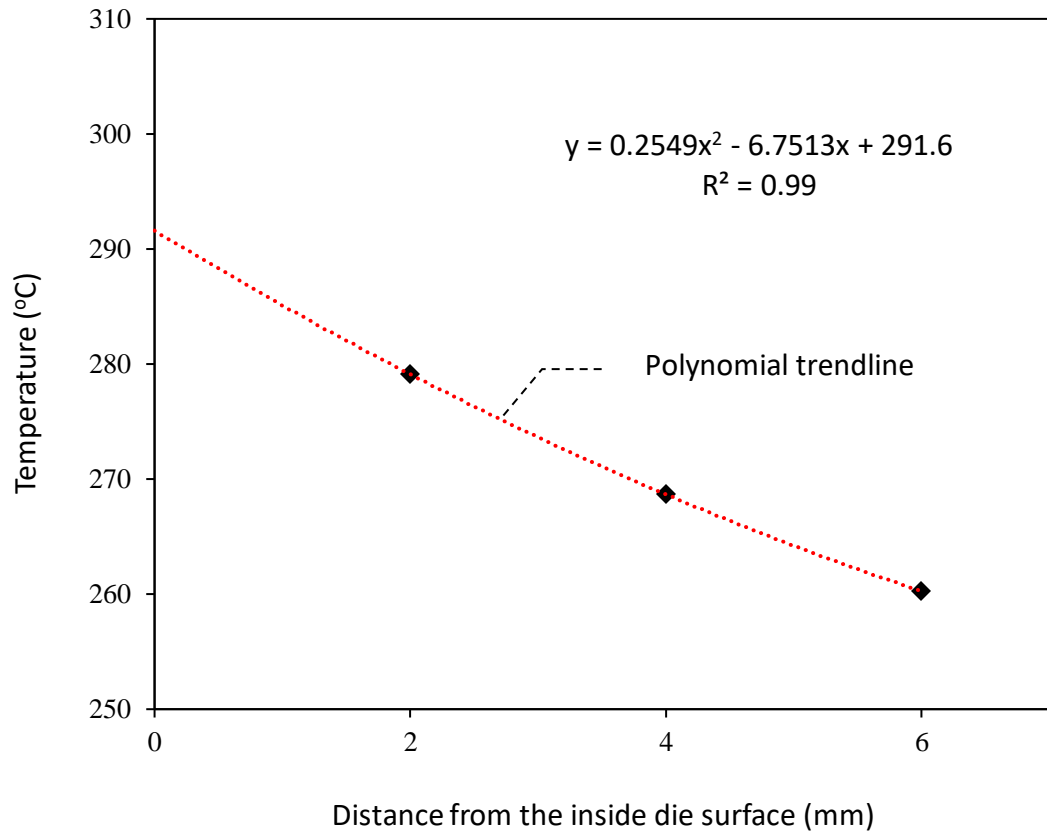


Figure 8- 4: Polynomial curve fitting with the temperature readings from step 2 at 1.1 seconds after pressurized solidification.

During solidification (after completion of filling), the data could be plotted on a temperature versus time plot by selection of the temperatures readings from the three thermocouples at the same time step, for example $t=1.1$ second, as shown in Figure 8-4. The temperature values versus distance X were then fitted by the polynomial trendline. To obtain the temperature at the inside die surface, the value $X_0=0$ mm was substituted in the polynomial curve fitting equation (Eq. 8-7).

$$y = 0.2549x^2 - 6.7513x + 291.6$$

8-7

This procedure was repeated for different time increments to obtain a series of die surface temperature data.

3. RESULTS AND DISCUSSION

3.1 Cooling curves

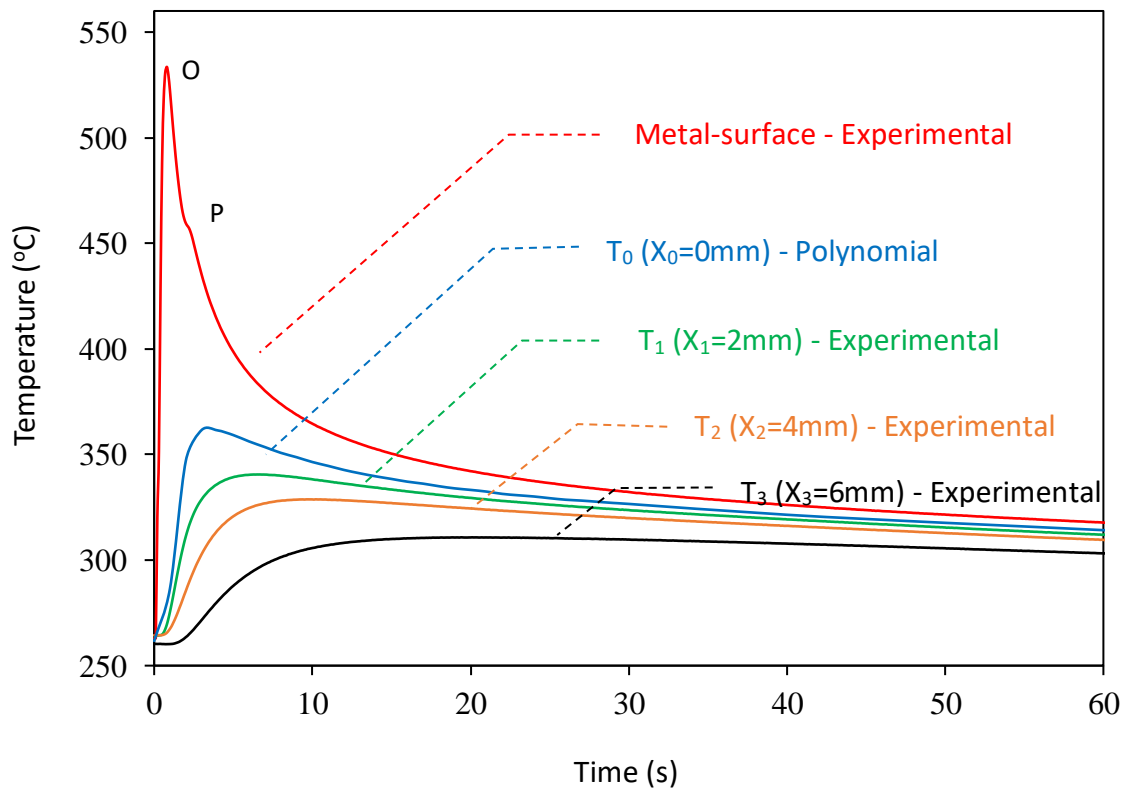


Figure 8- 5: Typical temperature versus time curve (step 2, 60 MPa) at the casting metal surface, die surface and various positions inside the die.

Figure 8-5 shows an example of the typical temperature versus time curve (at step 2), which includes estimated die surface temperature T_0 by polynomial curve fitting, measured temperature at the casting surface and T_1 , T_2 and T_3 at distances of $X_1= 2$ mm, $X_2= 4$ mm

and $X_3 = 6$ mm away from the inside die surface. The molten metal was poured at 710 °C. As the molten metal filled from the bottom to the top of the die, the temperature was decreased to 529 °C at step 2. From Figure 8-5, a dynamic temperature change occurred at the metal-die interface, since the temperatures of the casting surface increased and dropped much faster than the temperatures in the locations at different depths under the die surface. Segment OP of metal-surface temperature curve represented the period immediately after liquid metal pouring. The abrupt negative slope indicates a fast heat transfer behavior at the metal-die interface. Also, the rapid decrease in temperature took only 0.9 s after metal solidification which indicates a high cooling rate occurs at step 2. Corresponding to the decrease in metal surface temperature, there was an increase in die surface temperature T_0 ($X_0 = 0$ mm) which was estimated by the polynomial curve fitting method. The casting continued to lose heat until it reached the solidus temperature and completely solidified.

3.2 Heat Flux and IHTC Curves

Figure 8-6 presents the determined step-2 heat flux (q) and IHTC (h) profiles associated with the results in Figure 8-5. The rapid decrease in temperature at segment OP of the metal surface led to an abrupt increase in heat flux until its maximum value (3.08×10^5 W/m²) was reached. Corresponding to the rapid decrease in temperature at segment OP, the abrupt increase in IHTC was observed at segment EF on IHTC curve. Then, the IHTC kept increasing until reaches its maximum 2300 W/m² K. Once the peak was reached (point G), the IHTC values started to fluctuate until point J was reached, after which the IHTC fell rapidly to point K. The uncertainty and error of the polynomial extrapolated method should

be responsible for the fluctuation presented in IHTC or heat flux values. The rapid decrease in IHTC (segment JK) at step 2 could be caused the fact that the casting surface was not firmly contact with the die surface due to the lack of pressure present at step 2 as the solidification process proceeded.

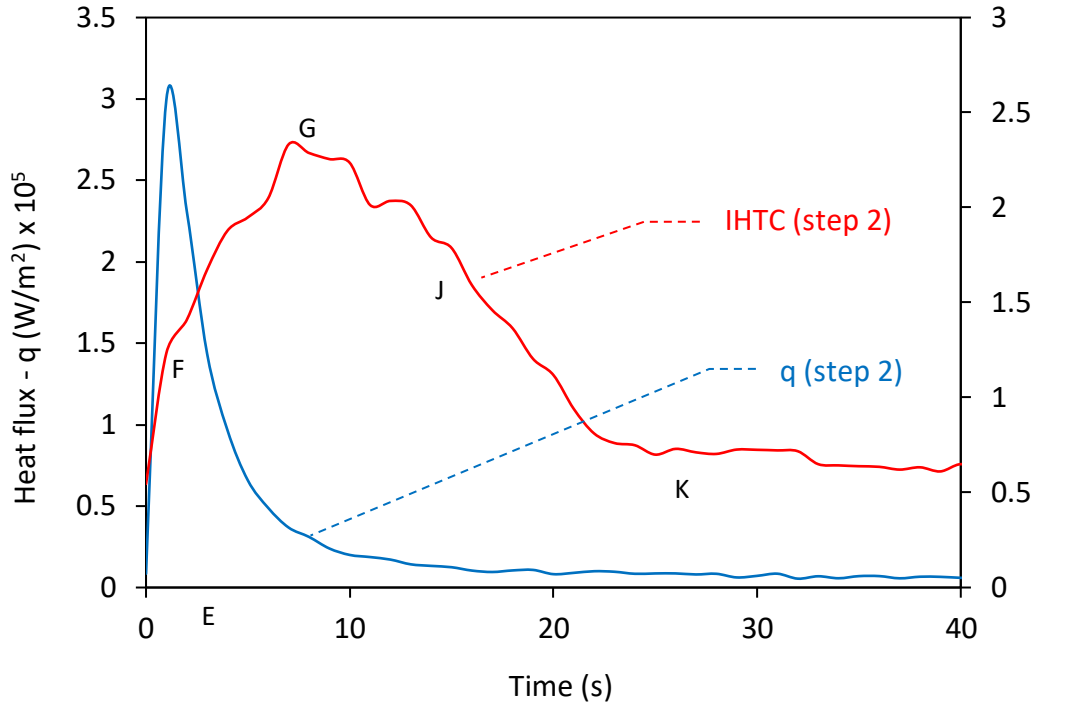


Figure 8- 6: Interfacial heat flux (q) and interfacial heat transfer coefficient (IHTC) curves for step 2 with the applied pressure of 60 MPa.

Figures 8-7 and 8-8 show the estimated heat flux and IHTC at step 1 to step 5 by the extrapolated fitting, respectively. All the q and IHTC profiles varies in a similar manner with step 2 as discussed before. They all initially increased abruptly right after the pressure was applied until the peaks were reached and then decreased until their values became steady state.

The casting step thickness influenced the IHTC significantly. For step 1, with the section thickness of 2 mm, IHTC reached its peak ($1.33 \text{ Ex}10^3 \text{ W/m}^2 \text{ K}$) 5s after the pressure applied. And then, it decreased to its lower level ($444.32 \text{ W/m}^2 \text{ K}$) at 21s. For step 2, with the section thickness of 4 mm, IHTC reached its peak ($2.33 \text{ Ex}10^3 \text{ W/m}^2 \text{ K}$) 7s after the pressure applied. It then decreased to its lower level ($699.4 \text{ W/m}^2 \text{ K}$) at 25s. For step 3, with the section thickness of 8 mm, IHTC reached its peak ($4.36 \text{ Ex}10^3 \text{ W/m}^2 \text{ K}$) 8s after the pressure applied. It decreased to its lower level ($1.69\text{Ex}10^3 \text{ W/m}^2 \text{ K}$) at 30s. For step 4, with the section thickness of 12 mm, IHTC reached its peak ($8.2 \text{ Ex}10^3 \text{ W/m}^2 \text{ K}$) 10s after the pressure applied. It decreased to its lower level ($4.12\text{Ex}10^3 \text{ W/m}^2 \text{ K}$) at 23s. For step 5, with the section thickness of 20 mm, IHTC reached its peak ($11.7 \text{ Ex}10^3 \text{ W/m}^2 \text{ K}$) 11s after the pressure applied. It decreased to its lower level ($4.5\text{Ex}10^3 \text{ W/m}^2 \text{ K}$) at 31s.

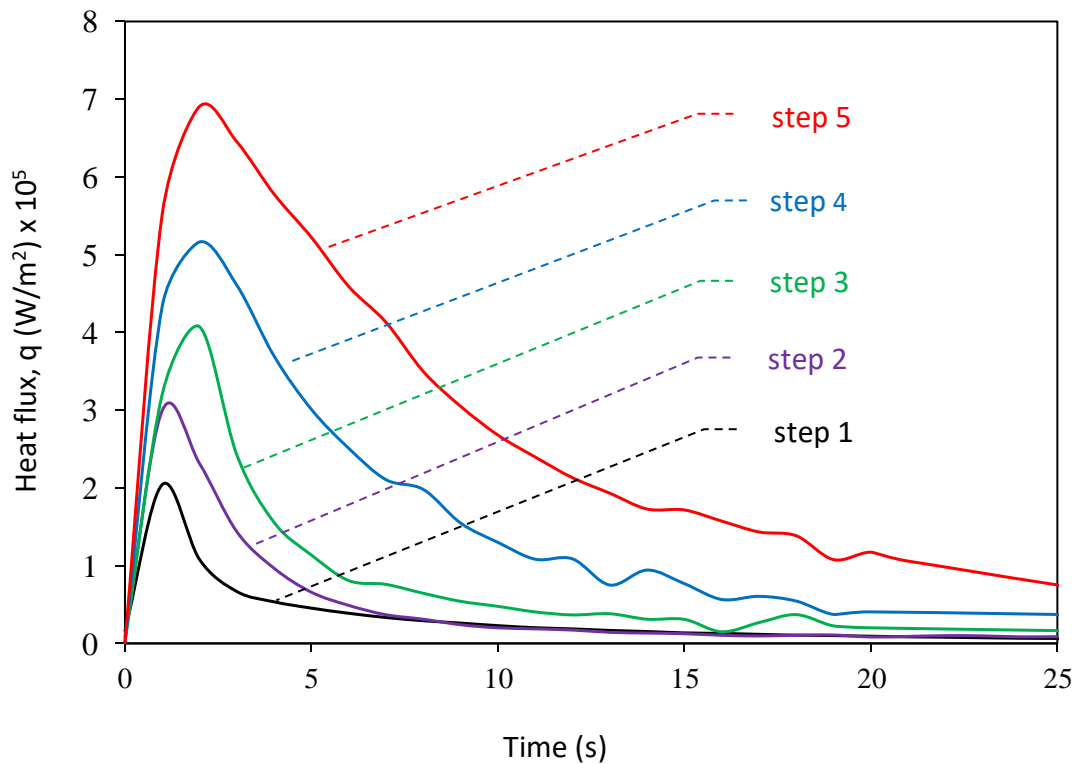


Figure 8- 7: Heat flux (q) curves for steps 1-5 estimated by the extrapolated fitting method.

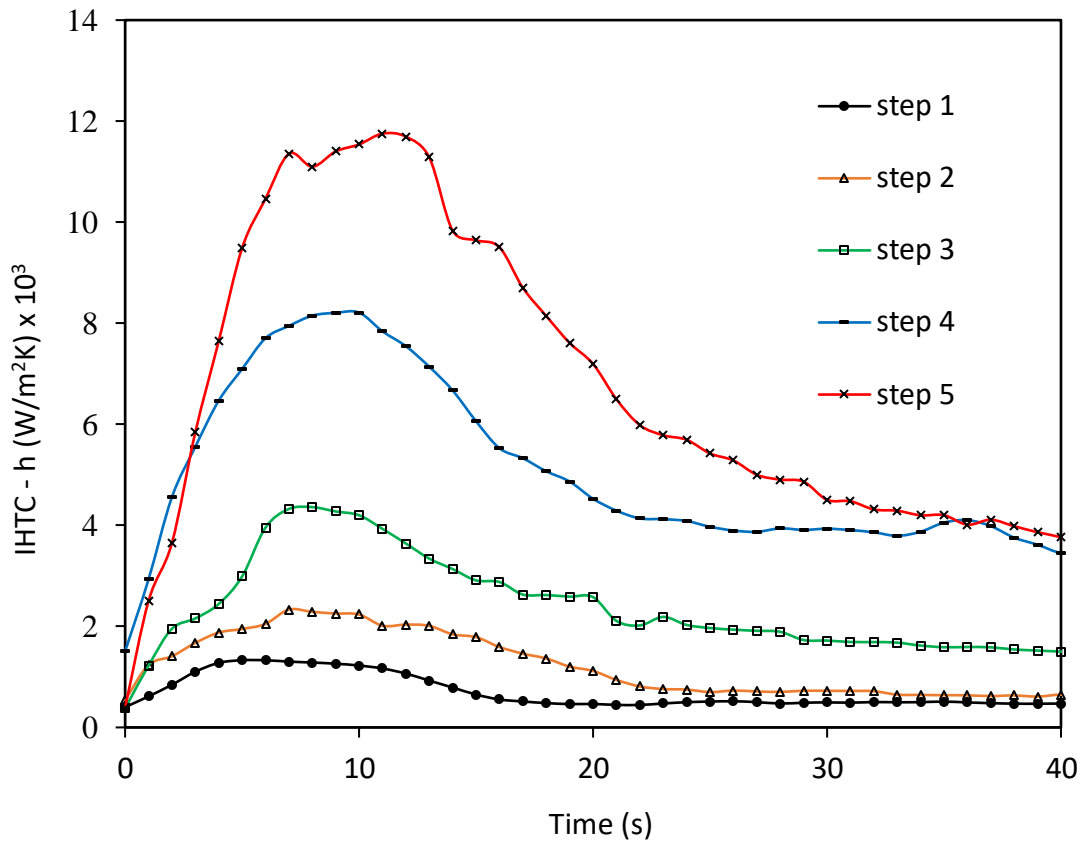


Figure 8- 8: Interfacial heat transfer coefficient (IHTC) curves for step 1-5 estimated by extrapolated fitting method.

Also, the IHTC curve profiles expanded vertically, were elevated, and became tall and steep as the step thickness increased. Also, as the step thickness increased, it took more time for the IHTC to climb to its maximum value. For example, it took almost 3s longer for step 5 to reach its peak ($11.75 \times 10^3 \text{ W/m}^2 \text{ K}$) in comparison with step 3.

4. CONCLUSION

The wrought aluminum 7075 alloy was successfully cast by the squeeze casting technique under an apply pressure of 60 MPa. The IHTC between the wrought alloy and steel die was estimated by the extrapolation method based on the temperature measurements during squeeze casting.

All the IHTC curves presented a similar pattern. After the pressure was applied, the curves increased rapidly until their peak were reached and then decreased until they arrived at their plateaus. The step thickness had a significant influence on the shape of the IHTC curves. Their profiles became expanded, tall and steep as the step thicknesses increased. The step thickness also varied the IHTC values. It increased as the section thickness increased. Comparing the IHTC curves for step1 to step 5, the IHTC values varied form $1.33 \times 10^3 \text{ W/m}^2 \text{ K}$ to $11.75 \times 10^3 \text{ W/m}^2 \text{ K}$. It took almost 6s longer for step 5 to reach its peak compared with step 1.

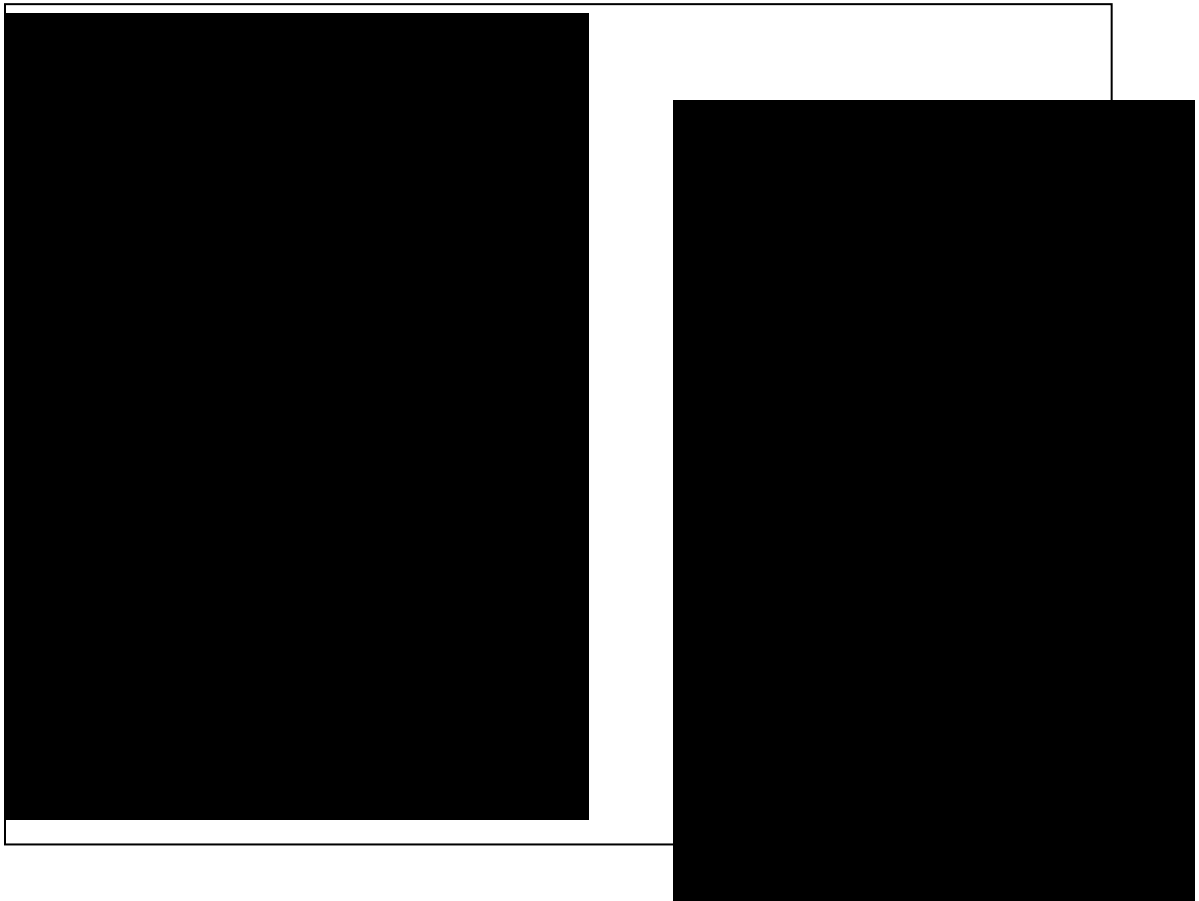
REFERENCES

- [1] Kobayashi, T. Wrought Aluminum Alloys. Strength and Toughness of Materials. Springer Japan, 2004, 111-140.
- [2] Ghomashchi, M. R., and Vikhrov, A. Squeeze casting: an overview. Journal of Materials Processing Technology, 2000, (101.1), 1-9.
- [3] Hu, H. Squeeze casting of magnesium alloys and their composites. Journal of materials science, 1998, (33.6), 1579-1589.
- [4] Hu, H and Yu, A. Numerical simulation of squeeze cast magnesium alloy AZ91D, Modell. Simul. Mater. Sci. Eng., 2002, 10 (1), 1–11.
- [5] Aweda, J. O., and Adeyemi, M. B. Experimental determination of heat transfer coefficients during squeeze casting of aluminium. Journal of Materials Processing Technology, 2009, (209.3), 1477-1483.
- [6] Griffiths, W. D. The heat-transfer coefficient during the unidirectional solidification of an Al-Si alloy casting. Metallurgical and Materials Transactions B 30.3 (1999) 473-482.
- [7] Dour, G and Dargusch, M and Davidson, C. Recommendations and guidelines for the performance of accurate heat transfer measurements in rapid forming processes, Int. J. Heat Mass Transfer, 2006, 49 (11–12), 1773–1789.
- [8] Rajaraman, R., & Velraj, R. Comparison of interfacial heat transfer coefficient estimated by two different techniques during solidification of cylindrical aluminum alloy casting. Heat and Mass Transfer, 2008, 44(9), 1025-1034.

- [9] Hao, S. W, Zhang, Z. Q, Chen, J. Y, Liu, P. C. Heat transfer at the metal–mold interface in ductile iron. AFS Trans., 1987, (128), 601–608.
- [10] Sun, Z., Hu, H., and Niu, X. Determination of heat transfer coefficients by extrapolation and numerical inverse methods in squeeze casting of magnesium alloy AM60. Journal of Materials Processing Technology, 2011, (211.8), 1432-1440.
- [11] Hamasaiid, A. Effect of mold coating materials and thickness on heat transfer in permanent mold casting of aluminum alloys. Metallurgical and materials Transactions A, 2007, (38.6), 1303-1316.
- [12] Guo, Z. Effect of process parameters, casting thickness, and alloys on the interfacial heat-transfer coefficient in the high-pressure die-casting process. Metallurgical and Materials Transactions A, 2008, (39.12), 2896-2905.

CHAPTER 9

DETERMINATION OF METAL/DIE INTERFACIAL HEAT TRANSFER COEFFICIENTS IN SQUEEZE CASTING OF WROUGHT ALUMINUM ALLOY 7075 WITH VARIATIONS IN SECTION THICKNESSES AND APPLIED PRESSURES



1. INTRODUCTION

Aluminum and its alloys have the advantages of low melting points, rapid heat transfer, high strength-to-weight ratio, and good corrosion resistance. For this reason, aluminum alloys are widely used in the automotive industry [1]. Comparing to casting alloys, wrought aluminum alloys typically employ lower alloying constituents such as silicon, which contains around 1.5% comparing to 3-15% of the casting alloys. Wrought alloys are typically not castable, and they usually gain their shape and high-strength property in the mechanical deformation processes of rolling, hammering or milling [2]. The major problem associated with casting these wrought alloys is their high tendency to form casting defects such as porosity, shrinkage, and hot tearing resulting from their inherent solidification characteristics, i.e., long freezing ranges and poor fluidities [3].

To make better use of wrought aluminum alloys for various potential engineering applications, squeeze casting, also called liquid metal forging, extrusion casting, squeeze forming and pressure crystallization, as one of the best promising techniques, has been emerging, and extensively studied in the past few decades. This is because the fluidity is not a critical process parameter in squeeze casting, and liquid molten metal is solidified in the die cavity under applied pressures to reduce and minimize defects associated with shrinkage cavities and porosity formation in squeeze casting [4, 5].

Yue et al. [3] compared the tensile properties of AA7010 alloy fabricated by squeeze casting process under applied pressure of 50 MPa and its wrought counterpart. They found that when the pouring temperature was near the liquidus temperature of the alloy, fine cellular grains formed. The tensile properties of the squeeze cast alloy heat-treated to the

peak-aged condition were all above the specified minimum set for the die forgings of the material. Souissi et al. [6] used the Taguchi method to establish the relationship between the yield strength, ultimate tensile strength and microhardness and process parameters in direct squeeze casting of 2017A wrought aluminum alloy. Their statistical results revealed that the squeeze pressure had a major effect on the mechanical properties, followed by the melt temperature. Hajjari et al. [7] successfully cast the 2024 aluminum alloy by a direct squeeze casting process. The effect of squeeze pressure on the microstructure and tensile of the alloy was investigated. It was found that squeeze casting of 2024 aluminum alloy gave rise to the refinement of the microstructure and the reduction of dendrite arm spacing (DAS) of the alloy over the gravity cast counterpart. The elimination of porosities was the primary reason for increasing the ultimate tensile strength of the alloy up to the applied pressure of 50 MPa. But, above 50 MPa applied pressure, finer microstructure due to higher cooling rates appeared to be the cause of an increase in tensile properties. Guo et al. [8] applied a combination of low superheat pouring and a shear field to the direct squeeze casting technique to rheoform wrought aluminum alloy 2024. The innovated squeeze casting process improved the microstructures and mechanical properties of the 2024 alloy under an applied pressure of 60 MPa or 90 MPa. An increase in the applied pressure increased the density of the alloy and its mechanical properties. Skolianos et al. [9] used squeeze casting technique to cast aluminum AA6061 alloy under different pressure levels ranging from 20 to 100 MPa. They found that squeeze casting decreased both the volume fraction porosity and the micropore size as well as the size of the dendrites and of the interdendritic areas, and the ultimate tensile strength of the as-cast and heat-treated castings increased with increasing applied pressures. Their results also showed that the property

increase appeared to be independent of the magnitude of the applied pressure. The elongation was seen to reach a maximum at the pressure of 60-80 MPa for all as-cast and heat-treated samples. Lee et al. [10] applied a finite element model to simulate indirect squeeze-casting with different die geometries involving solidification under applied pressures. The temperature profile and porosity locations were predicted with the model, in which pressure-dependent and casting section thickness-independent heat transfer coefficients were employed. They found that the macro shrinkage cavities that were formed at the hot spot were completely eliminated with an applied pressure of 100 MPa.

Most works on squeeze casting of wrought aluminum alloys were focused only on their mechanical properties and microstructure development. There is limited work on the determination of the interfacial heat transfer coefficient (IHTC) at the metal/die interface during squeeze casting of wrought aluminum alloys. The previous study [11] indicated the contact interface between a casting aluminum alloy A356 and a carbon steel die coated with graphite had a great influence on cooling rates and solidification times. There was a considerable thermal resistance that exist between the castings and die due to the presence of air gap at the interface. The IHTC variation with time after pouring played a notable role in controlling the solidification behaviours [11, 12]. In recent years, techniques such as computer-aided design and engineering have been rapidly developed. They were widely applied in the modeling and simulation of mold filling and alloy solidification during various casting processes, the numerical simulation enabled design and casting engineers to optimize casting processes and consequently save enormous manufacturing costs. However, these computers based techniques could only be beneficial when boundary conditions and material properties were well defined. The IHTC is believed to be one of

the most important parameters during the computer simulation of the solidification process during casting. Also, in the casting practice, differences in wall thickness of the casting significantly varied the local heat transfer coefficients [13]. It is critical to evaluate the effect of casting wall thickness, pressure levels and other process parameters on the IHTC.

In this work, a special five-step casting was designed for numerical determination of casting thickness-dependant IHTCs, in which cross-section thicknesses of 2, 4, 8, 12 and 20 mm were included. Based on the temperature measurements of the casting at each step and the temperatures at difference depths underneath the die surface (2, 4 and 6 mm) of each step, the inverse method was applied in determining of heat fluxes and heat transfer coefficients at the metal/die interface when heat conduction took place during the pressurized solidification of wrought aluminum alloy 7075. The variation of the unknown boundary condition with time was assumed. This boundary condition was then applied with unknown coefficients, and the interior temperature field was computed in the domain by the finite-differences method (FDM). An objective function based on the measured and calculated temperature values at various internal points was then determined. It was minimized by correcting the values chosen for coefficients used in the boundary condition. This was carried out iteratively until a stationary value of the objective function was obtained. Therefore, the measurement errors were minimized by this numerical procedure.

2. EXPERIMENTAL PROCEDURE

2.1 Material and squeeze casting

2.1.1 Material

The material used in this study was commercially-available wrought aluminum alloy 7075, of which chemical composition is shown in Table 9-1. The thermophysical properties are given in Table 9-2.

Table 9- 1: Chemical composition of wrought aluminum alloy 7075 (wt. %)

Zn	Mg	Cu	Cr	Fe	Si	Mn	Ti
5.6	2.5	1.6	0.23	Max	Max	Max	Max
				0.50	0.40	0.30	0.20

Table 9- 2: Thermal-physical parameters of wrought aluminum alloy 7075

Material	ρ	C_p	k	T_s	T_l
	(kg/m ³)	(J/kg K)	(W/m K)	(°C)	(°C)
Al 7075	2810	960	130	477	635

2.1.2 Squeeze casting

A 75-ton- hydraulic press was used in the casting experiment. The metal was melt in an electric resistance furnace with the protection of nitrogen gas. The holding temperature of the furnace was 800°C. As shown in Figure 9-1, the upper die opened along the center, which could form a step casting, however, the very top step was designed as an overflow which entrapped impurities in the upfront stream of the liquid melt formed during pouring. The vent was located on the top of the overflow, which could discharge the air inside the

die. The dimensions of the five casting steps were $100 \times 30 \times 2$ mm (step 1), $100 \times 30 \times 4$ mm (step 2), $100 \times 30 \times 8$ mm (step 3), $100 \times 30 \times 12$ mm (step 4), $100 \times 30 \times 20$ mm (step 5), and they were named steps 1-5 accordingly (Figure 9-2). The lower die had a diameter of 100 mm and a height of 200 mm. Both of the upper and lower dies were preheated by cartridge heaters. The upper die had a preheating temperature of 250°C , and 300°C for the lower die. The liquid metal was poured into the lower mold at 680°C . The liquid metal was squeeze casted in the upper die under a desired applied pressure, and kept holding at that pressure for 25 seconds.

2.2 Experimental measurements of temperatures and pressures

The K-type thermocouples with 1.5 mm in diameter were used to determine the solidifying temperatures of the cast molten metal and heating temperatures of the P20 steel die at the various positions, as shown in Figure 9-1. On the left side of the die, there were five pressure transducers which were used to collect the pressure data for the five steps with section thicknesses of 2, 4, 8, 12, and 20 mm. They were Kistler pressure transducers 6175A2 with operating temperature 850°C and pressures up to 200 MPa. There were five thermocouples located at each step. At each step, one thermocouple (D) was inserted all the way through the die which was used to measure the casting temperature and one thermocouple was used to measure the temperatures of the casting surface. The other three thermocouples (A, B and C) were 2, 4 and 6 mm away from the inside die surface to measure the die temperatures, as shown in Figure 9-3. In total, twenty-five thermocouples were employed to collect the temperature data of all the five steps. Real-time in-cavity

local pressures and temperature reading were recorded by a LabVIEW- based data acquisition system at regular intervals of 500 ms through the entire measurement period.

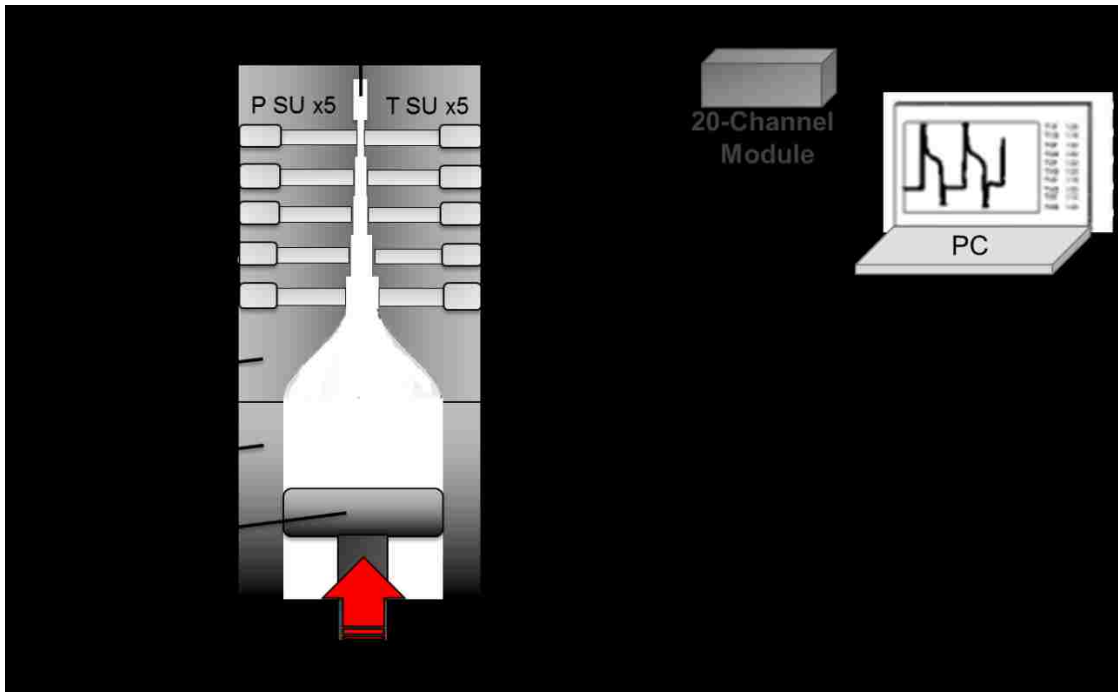


Figure 9- 1: Graphical installations of temperature sensor units (TSUs), pressure sensor units (PSUs) and data acquisition system.

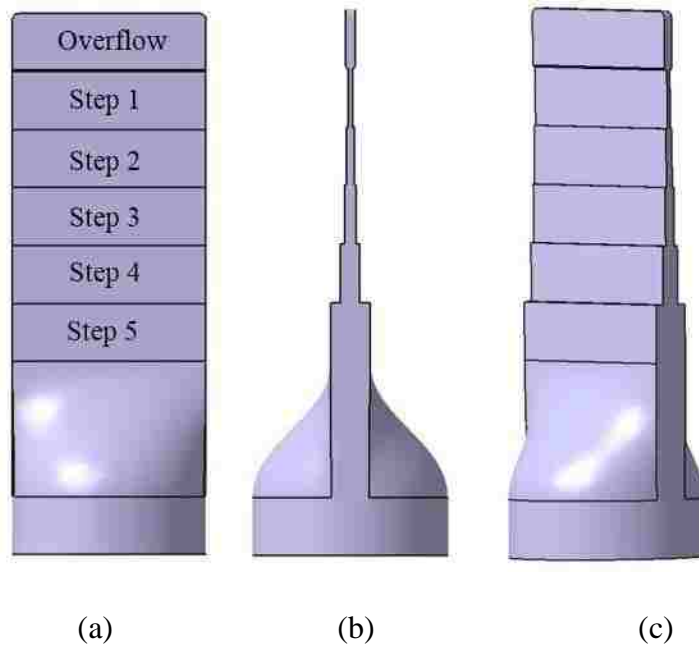


Figure 9- 2: 3-D model showing the (a) front view (b) side view and (c) isometric view of the 5-step casting.

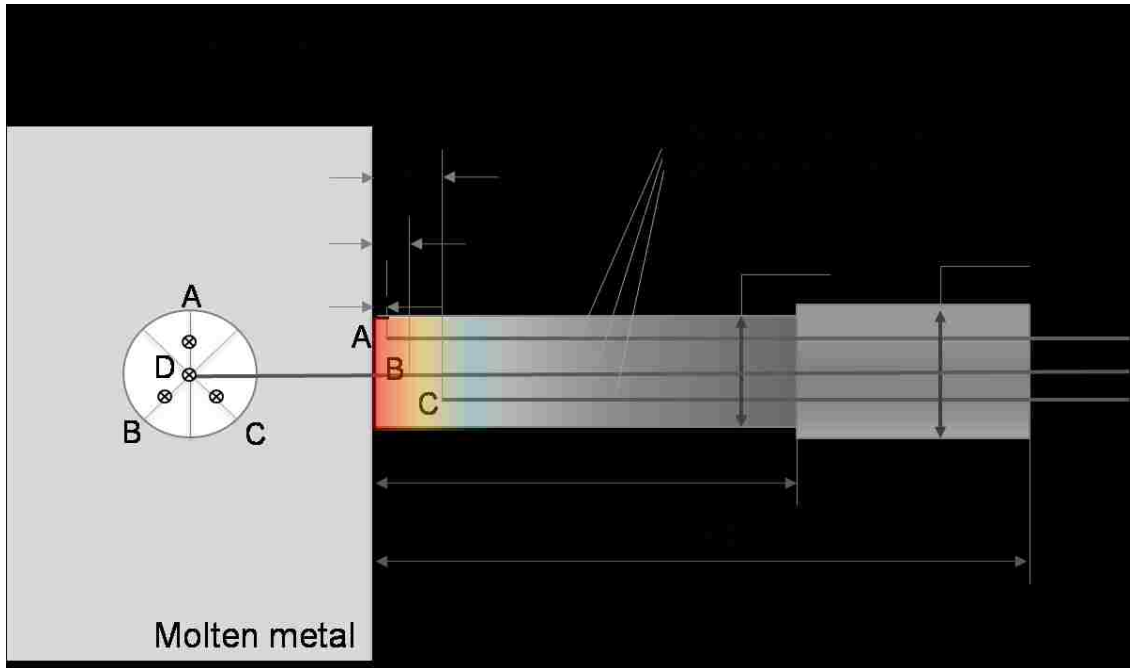


Figure 9- 3: Configuration of installation of the K-type thermocouples, the unit is in millimeters.

3. INVERSE ALGORITHM

The heat transfer inside the die can be estimated by the following equation (Eq. 9-1) which could be applied for transient heat conduction through one-dimensional problem. As shown in Figure 9-4, one-dimensional object was subjected to unknown time-dependent heat transfer coefficient at one end, whereas the other end was the heat source that was assumed constant throughout the time period considered.

$$\rho c(T) \frac{\partial T(x,t)}{\partial t} = \frac{\partial}{\partial x} \left(k(T) \frac{\partial T(x,t)}{\partial x} \right) \quad 9-1$$

This one-dimensional transient heat conduction equation was solved subjected to the following boundary and initial conditions.

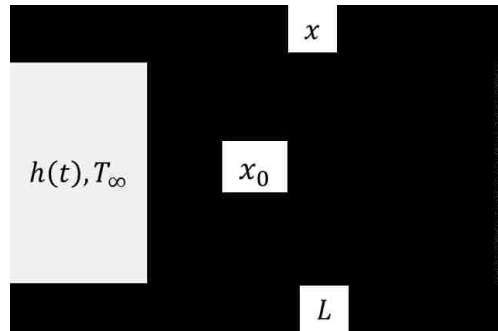


Figure 9- 4: One-dimension inverse heat conduction problem to be solved for heat transfer coefficient.

$$T(x_0, t) = Y(t)$$

$$T(L, t) = B(t)$$

$$T(L, 0) = T_i(x)$$

To find the heat flux at $L=0$, the following function based on least squares was minimized.

$$S(q) = \sum_{i=1}^{l=mr} (T_{n+i} - Y_{n+i})^2 \quad 9-2$$

$$m = \frac{\Delta\theta}{\Delta t}$$

The unknown heat flux q was represented by a vector of elements $q(q_1, q_2, \dots, q_n)$ and the heat flux $q(0, t)$ was approximated by q_n by letting each one represent a step.

$$q(0, t) = q_n \text{ for } \theta_{n-1} < t < \theta_n$$

For the surface sensor node of the die, where the boundary condition was unknown, Eq. 9-1 can be rearranging as Eq. 9-3a.

$$(1 + 2F_0)T_0^{p+1} - 2F_0T_1^{p+1} = 2F_0 \frac{\Delta x}{k} q_0 + T_0^p \quad 9-3a$$

For any interior sensor node, the problem was solved from Eq. 9-3b which is rearranged form Eq. 2.

$$(1 + 2F_0)T_n^{p+1} - (F_0T_{n-1}^{p+1} + T_{n+1}^{p+1}) = T_n^p \quad 9-3b$$

$$F_0 = \frac{\alpha \Delta t}{(\Delta x)^2} = \frac{k}{c\rho} \frac{\Delta t}{(\Delta x)^2} \quad 9-3c$$

As illustrated in Figure 9-5, the heat flux at the metal/die interface q_0 at each time step was determined at the following procedure: (1) at the first time step, a suitable initial value of heat flux q_0 was assumed, which was maintained constant for a definite integer number ($u = 2$ to 5) of the subsequent future time steps; (2) according to Eqs. 9-3a and 9-3b, with the measured initial die temperature ($p = 0$), the temperature distribution at each node of the next time step was calculated with this assumed q_0 ; (3) the assumed heat flux value is changed by a small value (εq_0); (4) the new temperature distribution value corresponding to $(q_0 + \varepsilon q_0)$ was determined accordingly; and (5) the sensitivity coefficient (\emptyset) was calculated by Eq. 9-4, which was the partial derivative in Eq. 9-5, the Taylor's series approximation.

$$\phi^{p+j-1} = \frac{\partial T}{\partial q} = \frac{T^{p+j-1}(q_{n+1}^{p+j-1}(1+\varepsilon)) - T^{p+j-1}(q_{n+1}^{p+j-1})}{\varepsilon q_{n+1}^{p+j-1}} \quad 9-4$$

where the numerator was the difference in temperature calculated using a finite difference scheme at the monitored node at the same time step for temperature (Δt), using the boundary condition q and $q + \varepsilon$. the denominator was the difference in the q values, $\varepsilon = 0.0001$ was used in this work.

$$T_{n+i}^{p+j} \approx T_{n+i}^{p+j-1} + \frac{\partial T_{n+i}^{p+j-1}}{\partial q_{n+1}^{p+j}} (q_{n+1}^{p+j} - q_{n+1}^{p+j-1}) \quad 9-5$$

Eq. 9-6 was obtained by minimizing Eq. 9-2 with respect to q by setting the partial derivative to zero.

which gave

$$\sum_{i=1}^{I=mr} \phi_i^{p+j-1} (T_{n+1}^{p+j-1} - Y_{n+i} + \phi_i^{p+j-1} (\nabla q_{n+1}^{p+j})) = 0 \quad 9-7$$

Rearranging Eq. 9-7, the correction term for the heat flux was calculated, given by Eq. 9-8.

$$\nabla q_{M+1}^p = \frac{\sum_{i=1}^I (Y_{n+i} - T_{n+1}^{p+j-1}) \phi_i^{p+j-1}}{\sum_{i=1}^{I=mr} (\phi_i^{p+j-1})^2} \quad 9-8$$

$$q_{corr}^p = q_{n+1}^p + \Delta q_{n+1}^p \quad 9-9$$

The corrected heat flux and the new temperature distribution were used as the initial value for next cycle of calculation. The calculation process was repeated until the following condition was satisfied.

$$\frac{\Delta q_{n+1}^p}{q_{n+1}^p} \leq \varepsilon \quad 9-10$$

Thus, for all time steps, the surface heat flux and die surface temperature were determined according to the above procedures. After the heat flux was computed, the heat transfer coefficient h was determined by the following equation, Eq. 9-11.

$$h = \frac{q}{A(T_c - T_d)}$$

9-11

4. RESULTS AND DISCUSSION

4.1 Determination of heat fluxes and IHTCs

Figure 9-6 shows three representative 5-step castings of which overflows were trimmed, fabricated by the squeeze casting process under the applied pressures of 30, 60 and 90 MPa, respectively. Figure 9-7 shows the typical temperature versus time curves for step 2 (section thickness of 4 mm) of the solidifying step casting of wrought aluminum alloy 7075. This demonstrating 5-step casting was fabricated under an applied hydraulic pressure of 60 MPa. The results included the measured casting temperature and measured temperatures at different depths underneath the die surface (T1-2mm, T2-4mm, and T4-8mm). The measured temperature at 2 and 8 mm from the cavity surface were used to evaluate the heat flux, IHTC and the die surface temperature. The inversely calculated temperature at 4 mm from the cavity surface was compared to the measured temperature at the same distance to validate the inverse modeling. As depicted in the Figure 9-8, there was a very good fit between the measured and calculated temperatures at 4 mm, indicating that the inverse estimation results were quite reliable.

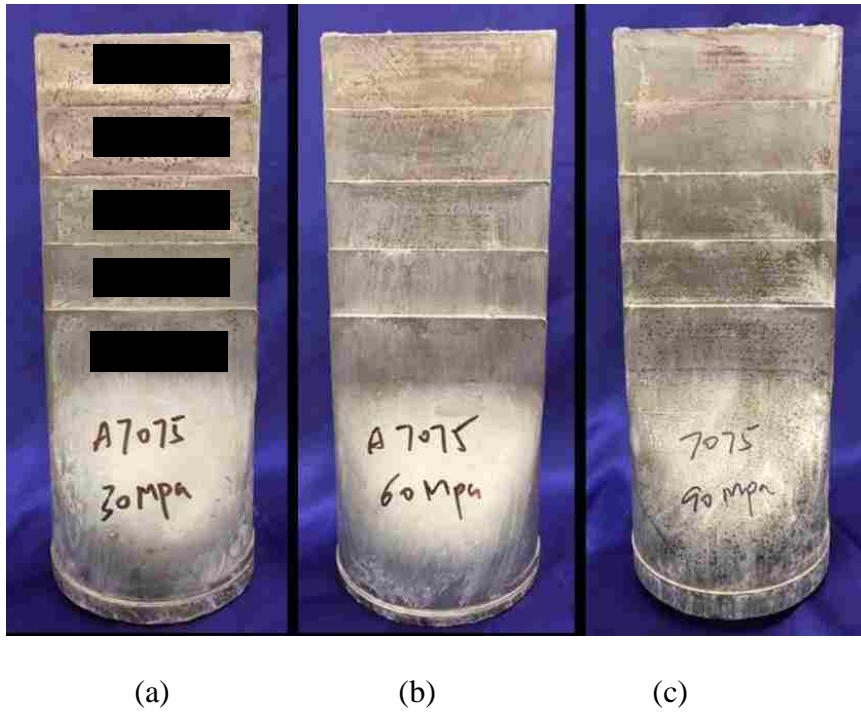


Figure 9- 6: 5-step squeeze castings with the applied pressures of (a) 30, (b) 60 and (c) 90 MPa.

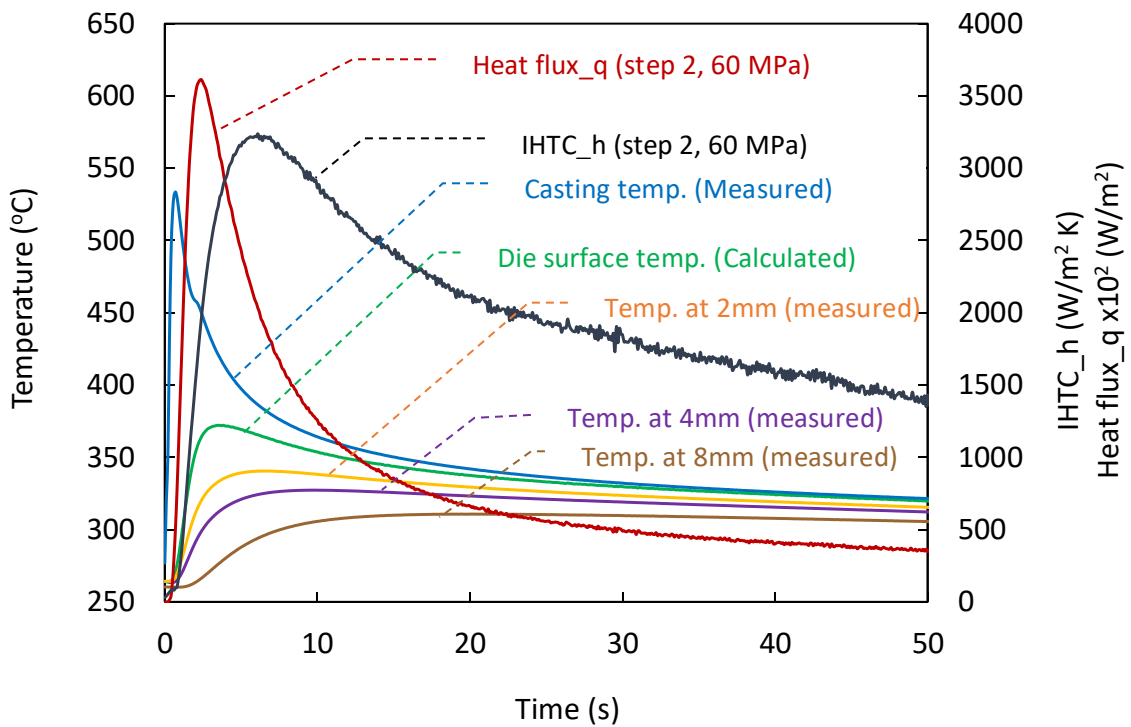


Figure 9- 7: Typical temperature, heat flux and IHTC versus time curves of step 2.

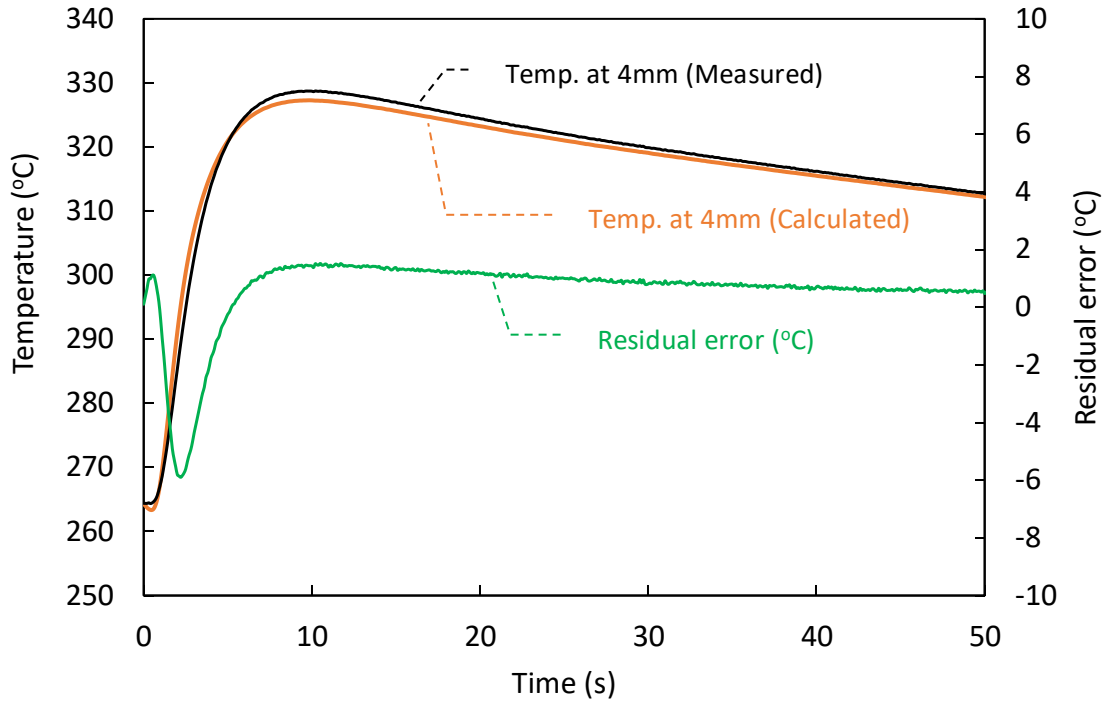


Figure 9- 8: The residual error between the measured and calculated temperatures evaluated by the inverse method at position $T_2=4$ mm.

Since molten metal filled the cavity from the bottom of the die, pre-solidification occurred upon the completion of the cavity filling. The temperature of the die surface at step-2 was 372.2 °C, and the casting surface temperature was only 529.6 °C. The casting temperature dropped abruptly after the filling process was completed. This indicated that the molten metal immediately lost its heat after contacting the die surface upon the commencement of the cavity filling. A fast heat transfer at the metal/die interface occurred, which resulted in a prompt rise of the die surface temperature and then reached its peak. Once the cavity filling finished, the casting temperature continuously decreased. The decreasing slope of the casting temperature curve indicated that the cooling rate of the casting decreased as the solidification process proceeded.

While the casting surface temperature rapidly decreased, the IHTC immediately increased after the shot was performed. This abrupt increase was associated with the rapid increase in the heat flux until the peak value of $3.61 \times 10^5 \text{ W/m}^2$ was reached. After the peak was reached, the heat flux began to decrease rapidly. This phenomenon was due to the fact that the close contact previously achieved at the metal/die interface deteriorated. This deterioration might be caused by the lack of the required local pressure inside the die as the solidification process progressed. The IHTC kept increasing until reaching the peak of $3238.54 \text{ W/m}^2\text{K}$ and then dropped to a low level.

4.2 Effect of local pressures and section thicknesses

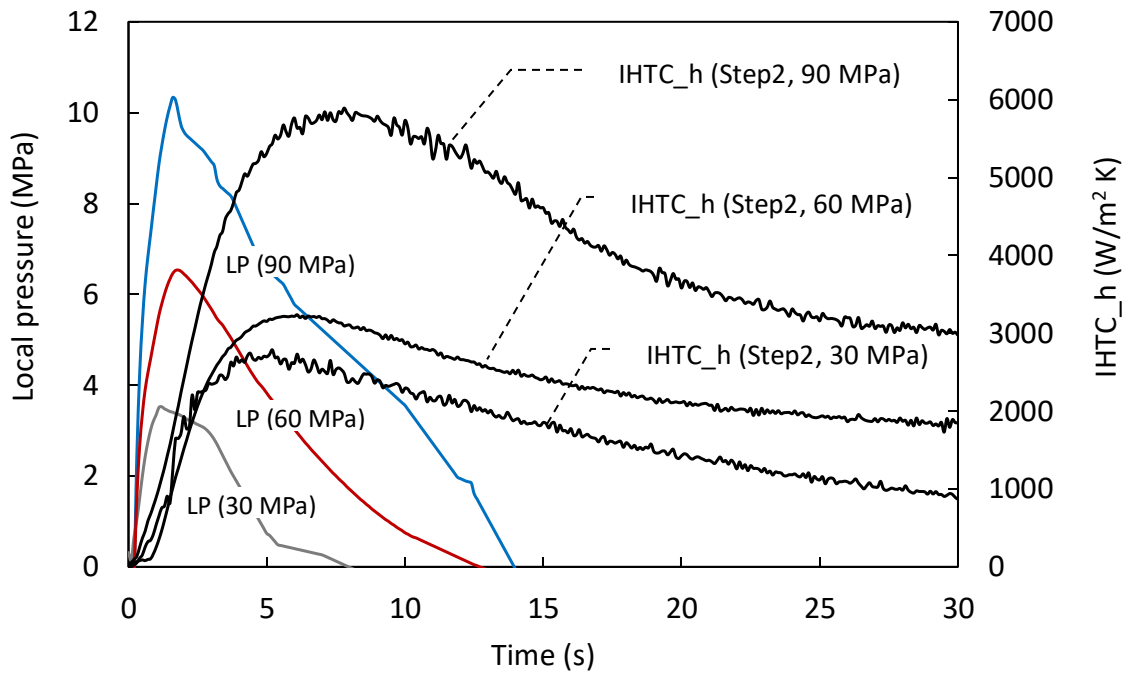


Figure 9- 9: Local pressure and IHTC versus time curves, with the applied pressures of 30, 60 and 90 MPa for step 2 with the section thickness of 4 mm.

The local pressure (LP) at the interface of the step casting and die were also measured during the casting process. Figure 9-9 shows the local pressure distributions at the metal/die interface of step 2 under the applied hydraulic pressures of 30, 60 and 90 MPa, respectively. As the cavity filling was performed, the local pressure increased rapidly to reach its peak and then dropped gradually until the pressure-transfer path died out. The local pressure peaks were 3.35, 6.51, and 10.28 MPa for the applied hydraulic pressures of 30, 60 and 90 MPa, respectively. The IHTC peak increased as the applied pressure increased. For step 2, the IHTC peak value rose from 3238.54 to 5832.39 W/m²K, accordingly with increasing the applied pressure from 30 to 90 MPa.

The variation of the applied pressures led to the different pressure transfer times. For the applied pressure of 30 MPa, the pressure-transfer path shrank faster (8.1s) as the solidification process proceeded. The pressure-transfer path kept longer (13.7s) when the applied pressure increased to 90 MPa. The extended pressure-transfer path indicated that a good heat transfer condition was achieved.

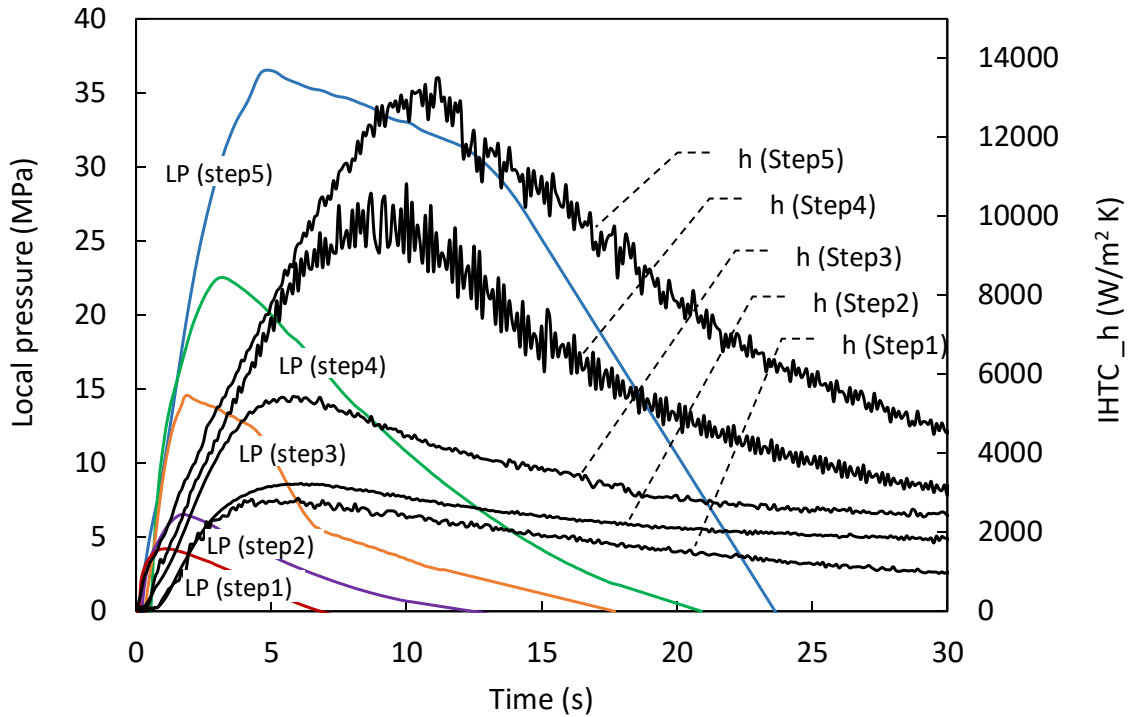


Figure 9- 10: Typical IHTC and local pressure curves for 5-step casting under the applied pressure of 60 MPa.

Figure 9-10 shows the IHTC curves for all the five steps (60 MPa) determined by the inverse method. From their profiles of the five steps, the IHTCs started with a rapid increasing stage and reached their peak, then decreased gradually until the values fell to their lower level. For the section thicknesses of 2, 4, 8, 12 and 20 mm with the applied pressure of 60 MPa, the peak IHTC varied as 2174.78, 3238.54, 5436.21, 10826.27 and 13494.05 W/m²K, respectively. The higher IHTC values indicated the firm contact between the casting and die surface was available at the thicker section of the step casting, which could be mainly attributed to the presence of the greater local pressure at the thicker section. This observation implied that the IHTC values were significantly influenced by the wall thickness of the casting,

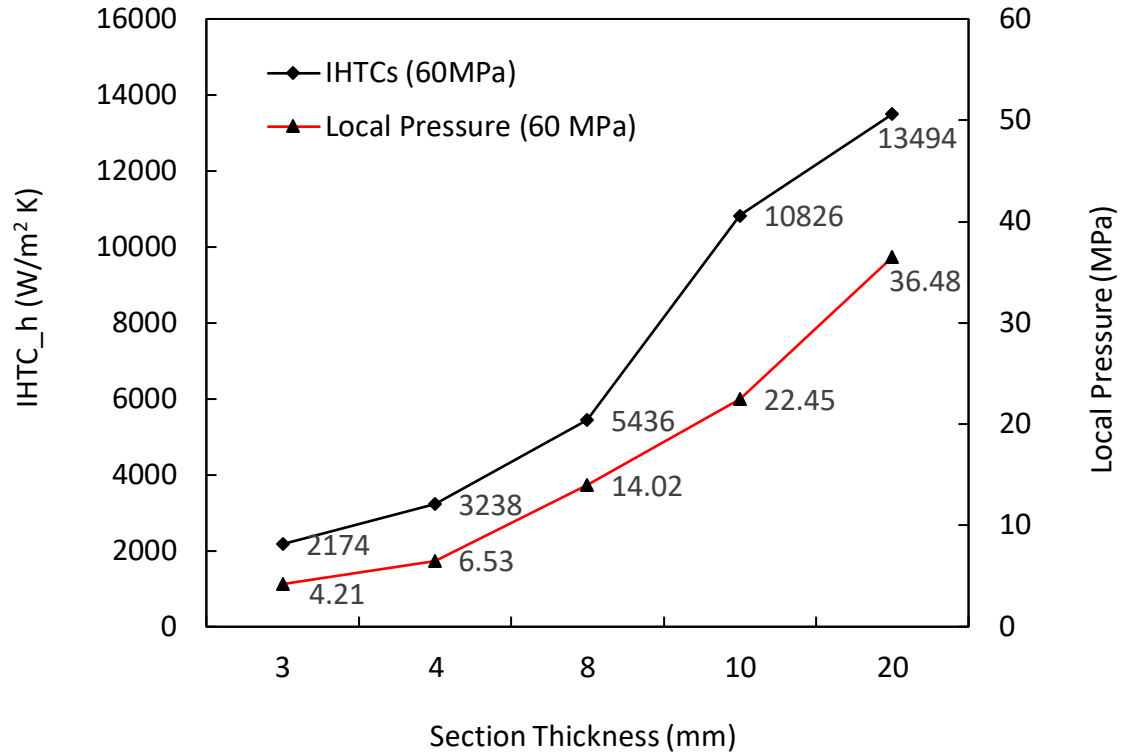


Figure 9- 11: The peak IHTC values and local pressures for the casting under the applied hydraulic pressure of 60 MPa varied with the different wall thickness of steps 1 to 5.

As depicted Figure 9-11, the peak IHTC values and local pressures for the casting under the applied hydraulic pressure of 60 MPa varied with the different wall thicknesses of steps 1-5. As the wall thickness increased from 2 to 20 mm, the peak IHTC values increased from 2174.78 to 13494.05 W/m²K, accordingly. With increasing the casting wall thicknesses from 2, 4, 8, 12 to 20 mm, the local pressure peak values were increased from 4.21 to 36.48 MPa, respectively. The pressure loss between the instantaneous experimental measurements and the hydraulic applied pressure can be calculated by the following formula,

$$P_{loss}(\%) = \frac{P_{applied} - P_{local}}{P_{applied}} \quad 9-12$$

As the molten metal was filled the cavity from the bottom with the applied pressure of 60 MPa, the pressure loss at the casting surface was 93%, 89.1%, 76.6%, 62.6% and 39.2% from step 1 (top) to step 5 (bottom) of the casting, respectively. A great percentage of pressure loss happened at the upper thinner section in comparison to that of the lower thicker section. As the section thickness became thinner, this significant increase in the pressure loss should mainly attributed to the fast shrink of the pressure-transfer path inside the casting during the filling process.

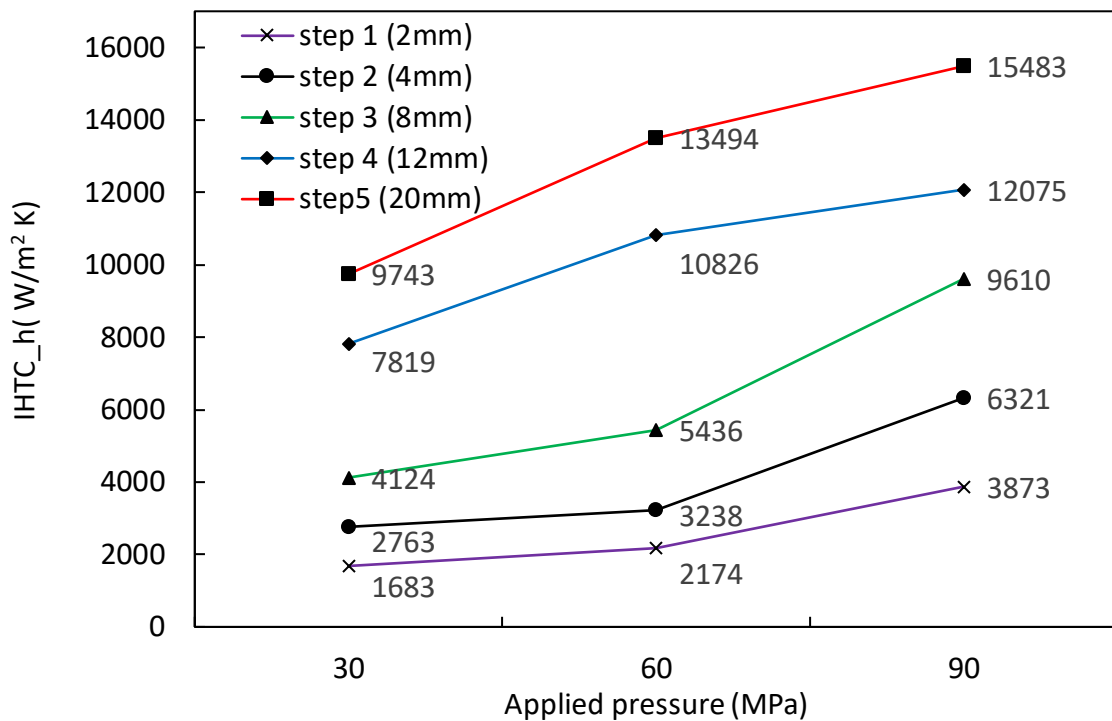


Figure 9- 12: The peak IHTC values versus applied pressures for steps 1 to 5.

Figure 9-12 shows the IHTC peak value versus pressure curves for all the five steps. The IHTC peak values for each step increased with increasing the applied pressures. As the pressures and section thicknesses increased, the IHTC peak values increased significantly. The large temperature difference between the casting and the die as well as the relatively high local pressure at the thicker steps should be responsible for the high IHTC peak values for the thicker steps.

4.3 Application of the determined IHTCs

To demonstrate the applicability of the determined IHTCs, MAGMASoft®, a commercial software, was employed to conduct the solidification simulation of the step casting. During the simulation, the temperature distribution was calculated by feeding the different IHTCs into the MAGMASoft with the same materials and process parameters, and then compared to the measured temperature data at the corresponding location. There are two different types of IHTC value were applied to the simulation: (1) a constant IHTC value of 7000 W/m² K (C7000) from MAGMASoft database for all the five steps. The constant value was selected based on the calculated average IHTC peak value of the five steps with the applied pressure of 60 MPa; (2) the IHTC values calculated by the inverse method, and the five steps were assigned the different determined IHTC curves as inputs in the MAGMASoft. Figures 9-13 and 9-14 show the input IHTC curves in the MAGMASoft for steps 2 and 5.

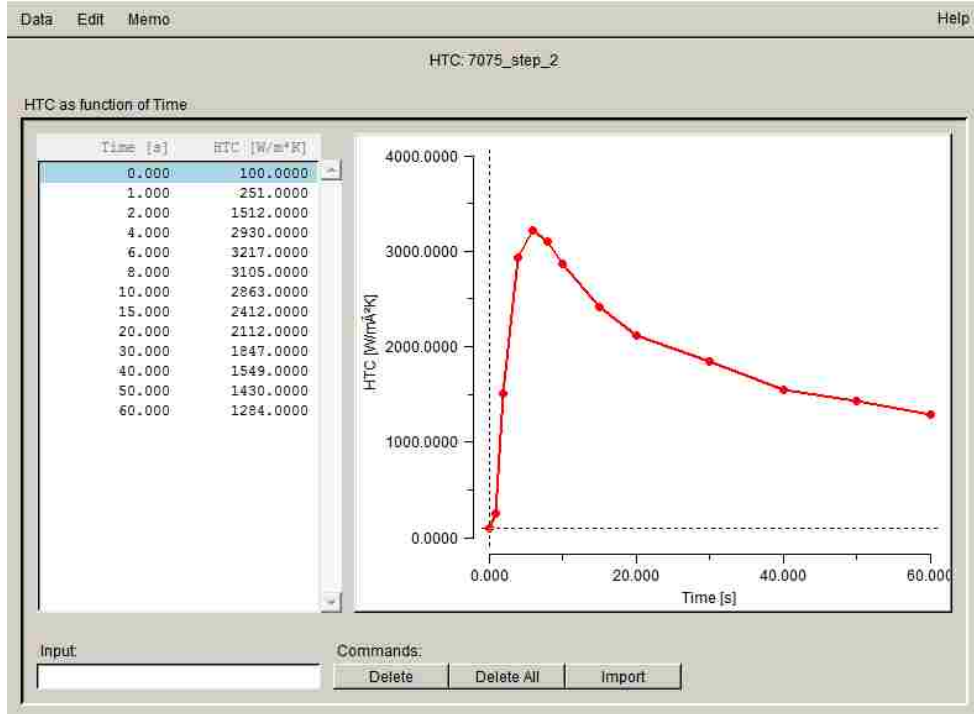


Figure 9- 13: IHTC derived from the inverse method data applied to MAGMAsoft simulation for step 2.

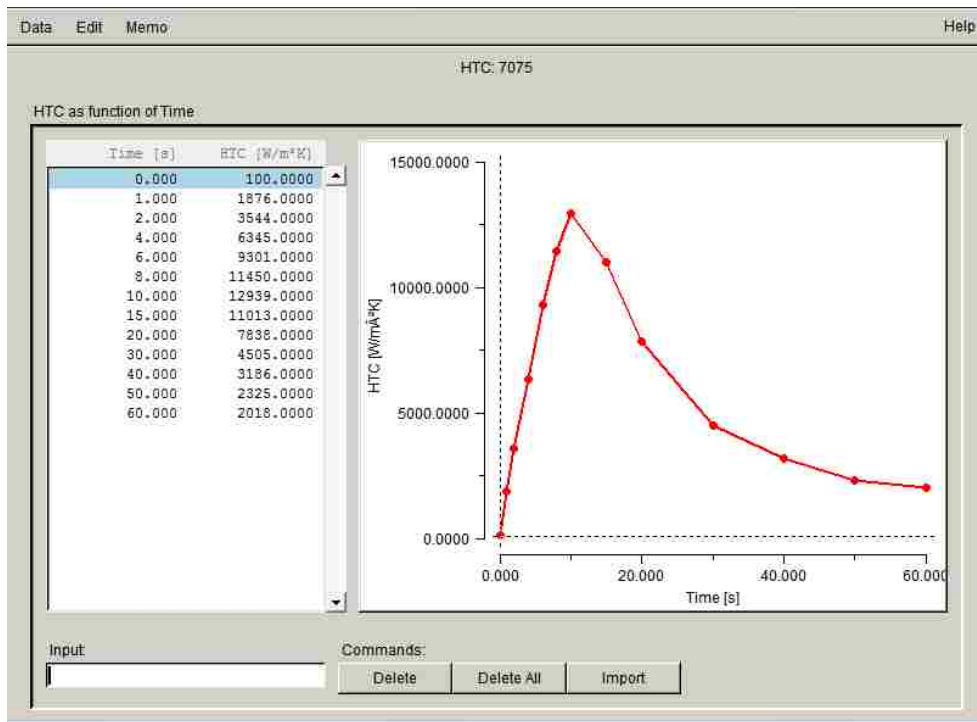


Figure 9- 14: IHTC derived from the inverse method data applied to MAGMAsoft simulation for step 5.

Figures 9-15 and 9-16 show the comparison of the measured and computational cooling curves at the center location of the casting at step 2 and step 5. The recorded temperature was experimentally measured by thermocouple D. Before the filling process was completed, the casting center as the last solidified location was cooled at a slower rate than its outer portion. For steps 2 and 5, the highest temperature of 535.3°C (step 2) and 632.6°C (step 5) were below the liquidus temperature 635°C. This observation indicated that the pre-solidification occurred in the five step casting adjacent to the metal/die interface during filling. As solidification time further increased, the temperature at the center of steps 2 and 5 decreased toward the solidus temperature at 1.1 s and 15.2 s, respectively.

For step 2, an overestimation of the IHTC ($7000 \text{ W/m}^2 \text{ K}$) occurred throughout the whole solidification process, since the computed temperatures were lower than the measured temperature. For the actual step casting, there was pre-solidification occurred at step 2 and the highest temperature was only 535.3°C. For the MAGMA simulation, the pouring temperature value was set to be higher than the liquidus temperature of aluminum 7075. Thus, there was a 115°C temperature drop at the early stage of the solidification process. For step 5, it appeared that, an underestimation occurred at the stage before reaching the solidus temperature. As the solidification proceeded, the calculated temperature curve moved downward and stayed below the measured temperature curve. The input of the constant IHTC ($7000 \text{ W/m}^2 \text{ K}$) seemed to be overestimated. With the input of the IHTC values calculated by the inverse method for steps 2 and 5, the predicted cooling curves showed a good fit to the measured temperature curves. The small deviation between the experimental measurements and the computed temperatures might result from the presence

of the inherent residual error in the inverse calculation of the IHTCs based on the temperature measurements in the die. The results the IHTC comparative study verified that the inverse method could be applied to determine the IHTCs between the castings and mold reliably. To achieve the accuracy in casting simulation, IHTC variations at different casting geometric locations must be taken into consideration.

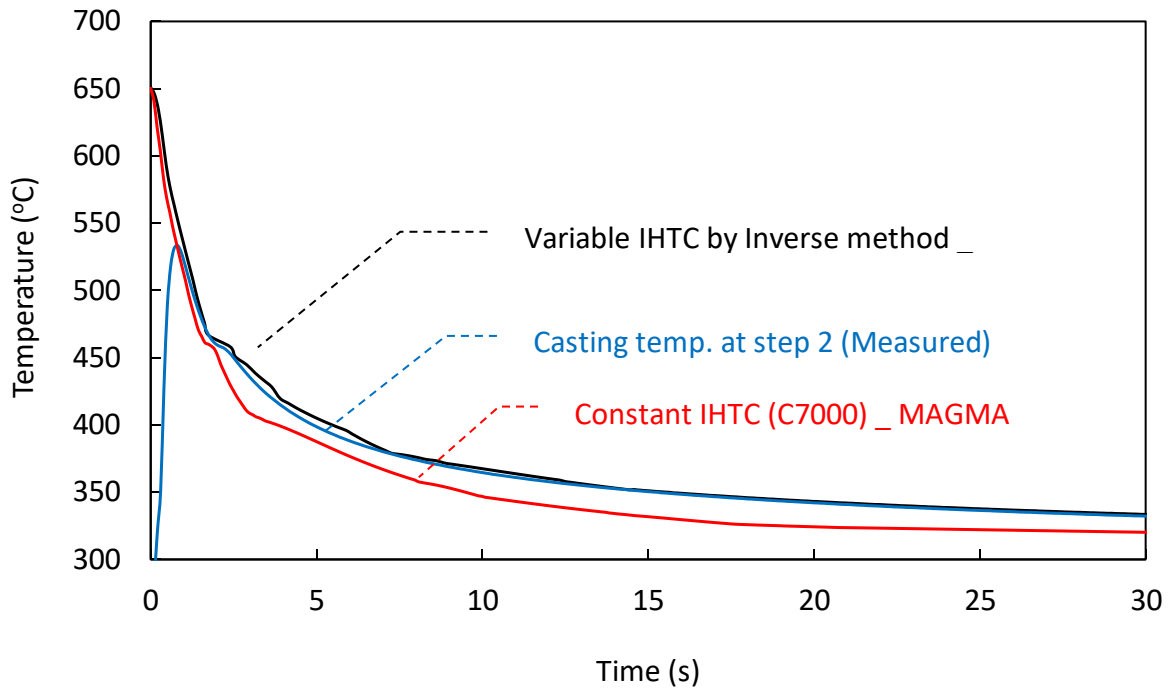


Figure 9- 15: Comparison of the experimental and computational cooling curve at the center of step 2 under an applied pressure of 60 MPa.

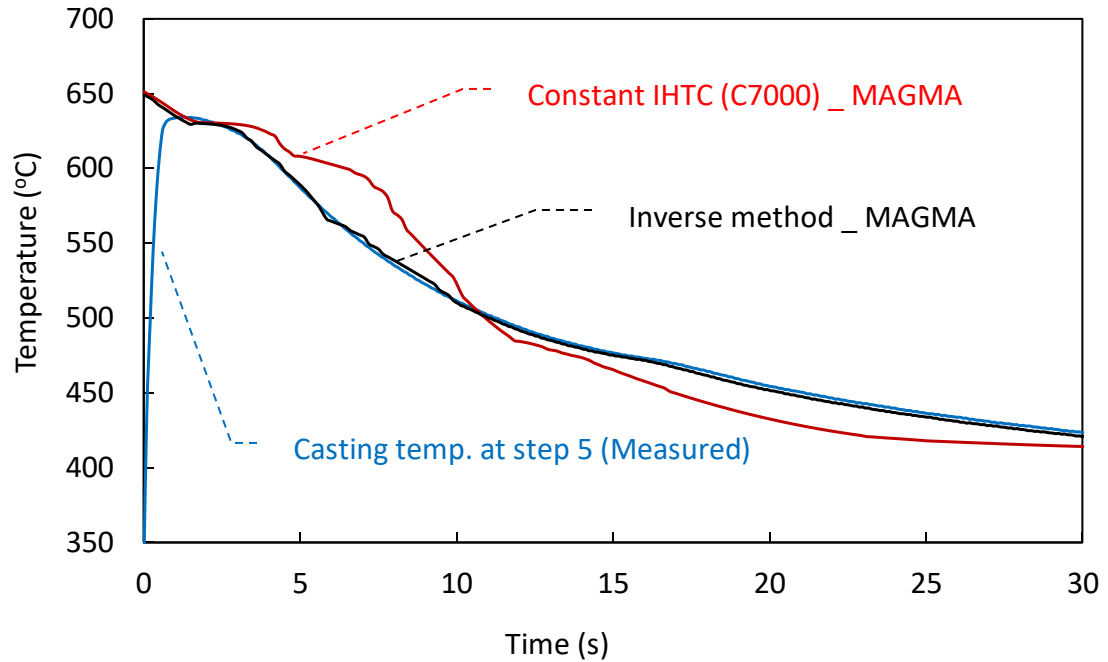


Figure 9- 16: Comparison of the experimental and computational cooling curve at the center of step 5 under an applied pressure of 60 MPa.

5. CONCLUSIONS

A detailed methodology for the numerical understanding of heat transfer phenomena taking place during squeeze casting of wrought aluminum alloy 7075 has been developed. A 5-step squeeze casting with the various cross-section thicknesses was successfully fabricated under the different applied hydraulic pressures (30, 60 and 90 MPa). The heat fluxes and IHTCs were successfully determined based on the finite difference-based inverse method. Based on the experimental temperature and pressure measurements and calculated results, the following conclusions were drawn.

- 5) From steps 1 to 5, the peak IHTC values varied from 1683.46 W/m²K to 9473.23 W/m²K, 2174.78 W/m²K to 13494.05 W/m²K and 3873.45 W/m²K to 15483.01

W/m²K for the applied hydraulic pressures of 30, 60 and 90 MPa, respectively. The increases in IHTC indicated that the solid contact between the metal and die surface could be reached under the higher applied pressures at thicker steps. The thicker step required longer time to reach the peak values due to the additional time needed for the pressure transfer.

- 6) The in-cavity local pressures at the metal/die interface rose rapidly to their peak and then dropped gradually until the pressure transfer path died out. Also, the pressure transfer path experienced longer time as the applied hydraulic pressure increased from 30 to 90 MPa.
- 7) The pressure loss was significantly influenced by the casting section thicknesses. As the section became thinner, the pressure loss rose significantly which was due to the pressure-transfer path inside the casting shrank rapidly as the molten metal travelled to the thinner section from the bottom thicker section.
- 8) The casting wall thickness influenced IHTC significantly. The peak values of the IHTC increased as the steps became thicker. The high IHTC peak value for the thicker step should mainly attributed to the large temperature differences and relatively high local pressures.
- 9) The comparison between the measured temperature data and the temperature profiles predicted by MAGMASoft simulation, indicated that the accurate and reliable results of the step casting simulation were obtained when the varied IHTC values calculated by the inverse method were assigned to each step, in comparison to the input of the constant IHTC value applied to all the five steps.

REFERENCES

- [1] Ducker World LLC, North America Light Vehicle Aluminum Content, <http://www.drivealuminum.org/research-resources/PDF/Research/2014/2014-ducker-report>, June, 2014 (2015).
- [2] Zheng, C. Q., & Simard, A. Optimization of casting parameters on an improved AA6061 aluminum alloy for semi-solid die casting. SP-2294: Advances in Light Weight Materials–Aluminum, Casting Materials, and Magnesium Technologies, (SP-2294), 2010, 1-12.
- [3] Yue, T. M. Squeeze casting of high-strength aluminum wrought alloy AA7010. *Journal of materials processing technology*, 1997, (66), 179-185.
- [4] Ghomashchi, M. R., & Vikhrov, A. Squeeze casting: an overview. *Journal of Materials Processing Technology*, 2000, 101(1), 1-9.
- [5] Hu, H. Squeeze casting of Magnesium alloys and their composites, *Journal of materials science*, 1998, (33), 1579-1589.
- [6] Souissi, N., Souissi, S., Niniven, C. L., Amar, M. B., Bradai, C., & Halouani, F. An experimental design and theoretical analysis of squeeze casting parameters for 2017A aluminium alloy. *International Journal of Materials Engineering Innovation*, 2015, 6(1), 59-73.
- [7] Hajjari, E., & Divandari, M. An investigation on the microstructure and tensile properties of direct squeeze cast and gravity die cast 2024 wrought Al alloy. *Materials & Design*, 2008, 29(9), 1685-1689.

- [8] Guo, H. M., Yang, X. J., & Zhang, M. Microstructure characteristics and mechanical properties of rheoformed wrought aluminum alloy 2024. *Transactions of Nonferrous Metals Society of China*, 2008, 18(3), 555-561.
- [9] Skolianos, S. M., Kiourtsidis, G., & Xatzifotiou, T. Effect of applied pressure on the microstructure and mechanical properties of squeeze-cast aluminum AA6061 alloy. *Materials Science and Engineering: A*, 1997, 231(1), 17-24.
- [10] Lee, J. H., Kim, H. S., Hong, S. I., Won, C. W., Cho, S. S., & Chun, B. S. Effect of die geometry on the microstructure of indirect squeeze cast and gravity die cast 5083 wrought Al alloy and numerical analysis of the cooling behavior. *Journal of Materials Processing Technology*, 1999, 96(1), 188-197.
- [11] Ilkhchy, A. F., Jabbari, M., & Davami, P. Effect of pressure on heat transfer coefficient at the metal/mold interface of A356 aluminum alloy. *International Communications in Heat and Mass Transfer*, 2012, 39(5), 705-712.
- [12] Zhang, L., and Li, L. Determination of heat transfer coefficients at metal/chill interface in the casting solidification process. *Heat and Mass Transfer*, 2013, 49(8), 1071-1080.
- [13] Hamasaiid, A., Dour, G., Dargusch, M. S., Loulou, T., Davidson, C., & Savage, G. Heat transfer at the casting/die interface in high pressure die casting-experimental results and contribution to modelling. In the Eleventh International Conference on Modeling of Casting, Welding and Advanced Solidification Processes. The Minerals, Metals & Materials Society (TMS) (2006).

CHAPTER 10

DISSERTATION CONCLUSIONS

In order to fulfil the objectives of this work which stated in Chapter 1, a new 5-step casting mold was developed. The interfacial heat transfer coefficients, local pressurises in mold cavity and heat transfer phenomena taking place in squeeze casting of wrought aluminum alloys 5083, 7075 and magnesium alloys AJ62 and AM60 were characterized. To precisely determine the interfacial heat transfer coefficient, the inverse modeling method was developed and applied. The main conclusions from this work could be drawn as following:

1. The influences of applied pressure and casting section thicknesses on the IHTCs of the wrought aluminum alloys and cast magnesium alloys were successfully determined by applying the concept of 5-step casting.
2. The polynomial and energy balance methods have been used to estimate the IHTCs for the wrought aluminum alloys 5083 and magnesium alloy AJ62.
3. A mathematical model based on the finite difference method and inverse method has been developed for numerical determination of IHTCs of the magnesium alloy AM60 and wrought aluminum alloy 7075 by using squeeze casting technique.
4. By applying the energy balance method on determination of the IHTC of magnesium alloy AJ62. It could be concluded that the peak heat flux values for steps 1 to 5 were $1.5\text{E}+05 \text{ W/m}^2$, $1.9\text{E}+05 \text{ W/m}^2$, $2.7\text{E}+05 \text{ W/m}^2$, $4.0\text{E}+05 \text{ W/m}^2$, and $6.0\text{E}+05 \text{ W/m}^2$, respectively. For all steps, the IHTC values increased sharply at the beginning right after the liquid metal was pushed into the die cavity, and then

dropped gradually after their peaks reached. The thickness of the step casting had a great influence on the IHTC values. The IHTC values increased as the section thickness increased. For the five steps from one to five, the peak IHTC were 1,398 W/m² K, 1,876 W/m² K, 4,040 W/m² K, 6,383 W/m² K, and 9,066 W/m² K, respectively. Also, the trend of changes of the IHTC was different as the section thickness varies. The profile of the IHTC curve became wider as the casting section thickness increased.

5. For magnesium alloy AM60M, the IHTC peak values were observed under applied pressures of 30, 60 and 90 MPa. With an applied pressure of 60MPa, the peak IHTC values at steps 1, 2, 3, 4, and 5 were 4662 W/m²K, 5001 W/m²K, 5629 W/m²K, 7871 W/m²K and 8306 W/m²K respectively. As the applied pressure increased to 90MPa, the peak IHTC values were 5623 W/m²K, 5878 W/m²K, 6783 W/m²K, 9418 W/m²K and 10649 W/m²K respectively.
6. For wrought aluminum alloy 5083, the IHTC was investigated under applied pressure of 60 MPa. The peak IHTC values varied from 5212, 5578, 6516, 7668 to 8933 W/m² K for the casting with section thicknesses of 2, 4, 8, 10 and 20 mm, respectively, under an applied pressure of 60 MPa. The increases in IHTC indicated that the solid contact could be reached at the metal/die interface for the thicker steps, since the thicker step required longer time to reach the peak values due to the additional time needed for the pressure transfer.
7. For wrought aluminum 7075 alloy, the IHTC between the wrought alloy and steel die was estimated by the extrapolation method based on the temperature measurements during squeeze casting under the applied pressure of 60 MPa. All

the IHTC curves presented a similar pattern. After the pressure was applied, the curves increased rapidly until their peak were reached and then decreased until they arrived at their plateaus. The step thickness had a significant influence on the shape of the IHTC curves. Their profiles became expanded, tall and steep as the step thicknesses increased. The step thickness also varied the IHTC values. It increased as the section thickness increased. Comparing the IHTC curves for step1 to step 5, the IHTC values varied from 1.33×10^3 W/m² K to 11.75×10^3 W/m² K. It took almost 6s longer for step 5 to reach its peak compared with step 1.

8. For wrought aluminum alloy, the IHTC was also determined by applying the inverse method. From steps 1 to 5, the peak IHTC values varied from 1683.46 W/m²K to 9473.23 W/m²K, 2174.78 W/m²K to 13494.05 W/m²K and 3873.45 W/m²K to 15483.01 W/m²K for the applied hydraulic pressures of 30, 60 and 90 MPa, respectively. The increases in IHTC indicated that the solid contact between the metal and die surface could be reached under the higher applied pressures at thicker steps. The thicker step required longer time to reach the peak values due to the additional time needed for the pressure transfer.
9. The in-cavity local pressures at the metal/die interface rose rapidly to their peak and then dropped gradually until the pressure transfer path died out. Also, the pressure transfer path experienced longer time as the applied hydraulic pressure increased from 30 to 90 MPa.
10. The pressure loss was significantly influenced by the casting section thicknesses. As the section became thinner, the pressure loss rose significantly which was due

to the pressure-transfer path inside the casting shrank rapidly as the molten metal travelled to the thinner section from the bottom thicker section.

11. The casting wall thickness influenced IHTC significantly. The peak values of the IHTC increased as the steps became thicker. The high IHTC peak value for the thicker step should mainly attributed to the large temperature differences and relatively high local pressures.
12. For magnesium alloy AM60 and wrought aluminum 7075, a comparison was carried out between the measured temperature data and the temperature profiles predicted by MAGMASoft simulation. The results indicated that the accurate and reliable results of the step casting simulation were obtained when the varied IHTC values calculated by the inverse method were assigned to each step, in comparison to the input of the constant IHTC value applied to all the five steps.

CHAPTER 11

FUTURE WORKS

This study carried out in this thesis provides the groundwork to pursue further investigations in the future. The following aspects are worth exploring.

- To evaluate mechanical properties of squeeze cast wrought aluminum and magnesium alloys influenced by casting section thicknesses and processing parameters;
- To investigate the relations between the mechanical properties and the interfacial heat transfer coefficients and cooling behaviours of the squeeze cast wrought aluminum and magnesium alloys.
- To optimize squeeze casting process parameters including applied pressure levels, die temperatures, liquid metal pouring temperatures and pressure holding times.
- To establish a standardized data bank for material properties and boundary conditions in simulation software (MAGMASoft). Based on the author's survey, it is found that, with the advent of the modern and powerful computer, the computer simulation software has rapidly been developed and produced very impressive results. However, the application of the simulation software is limited by the available data for certain materials. Hopefully, a universal data bank for the simulation software will be built in the near future and accessible to all users.

APPENDICES

APPENDIX A

COPYRIGHT RELEASES FROM PUBLICATIONS

CHAPTER 3



Xuezhi Zhang <zhang11w@uwindsor.ca>

Permission for including article in graduation dissertation

2 messages

Xuezhi Zhang <zhang11w@uwindsor.ca>
To: info@scientific.net

Mon, Jan 25, 2016 at 12:18 PM

Dear Sir or Madam,

In order to complete my PhD study at the university, I would like to include my research paper, "*Characterization of Local Cavity Pressures in Squeeze Casting of Magnesium Alloy AM50*" in my dissertation.

May I have your permission to include my published paper to my graduation dissertation?

--

Xuezhi (John) Zhang
Ph.D. Student



Dept. of Mechanical, Materials & Automotive Engineering
University of Windsor
401 Sunset Ave.
Windsor, Ontario
Canada N9B 3P4

Tel: 519-253-3000 (x4155)
Cell: 519-817-0836
E-mail: zhang11w@uwindsor.ca

authors@scientific.net <authors@scientific.net>
To: Xuezhi Zhang <zhang11w@uwindsor.ca>

Tue, Jan 26, 2016 at 2:32 AM

Dear Xuezhi Zhang,

Thank you for your request. As author you are able to include your paper into dissertation. Please, take into account that you should mention already published paper as one of references.

Best regards,
Ksenia Indeykina,
Scientific Team

[Quoted text hidden]

CHAPTER 4

Permission for including article in graduation dissertation

2 messages

Xuezhi Zhang <zhang11w@uwindsor.ca>
To: smsaconf@yeah.net

Mon, Jan 25, 2016 at 12:37 PM

Dear Dr. Zhao,

In order to complete my PhD study at the university, I would like to include my research paper in my dissertation.

"Solidification and Microstructure Refining Phenomena of Squeeze Cast Mg Alloy AJ62" (2016)

May I have your permission to include my published paper to my graduation dissertation?

Thanks,

Best regards,

--

Xuezhi (John) Zhang
Ph.D. Student



University
of Windsor

Dept. of Mechanical, Materials & Automotive Engineering
University of Windsor
401 Sunset Ave.
Windsor, Ontario
Canada N9B 3P4

Tel: 519-253-3000 (x4155)
Cell: [519-817-0836](tel:519-817-0836)
E-mail: zhang11w@uwindsor.ca

SMSA2016 Committee <smsaconf@yeah.net>
To: zhang11w@uwindsor.ca

Tue, Jan 26, 2016 at 8:17 PM

Dear Zhang,

You can do that.

Best regards,

SMSA2016 Committee

Email: smsaconf@yeah.net

Tel: [+86-13311791280](tel:+86-13311791280)

Secretary: Dr. Zhao

CHAPTER 5

Re:FW: Permission for including article in graduation dissertation

1 message

박성수 <sspark@unist.ac.kr>
To: zhang11w@uwindsor.ca

Fri, Jan 29, 2016 at 12:48 AM

Dear Xuezhi Zhang,

Thank you for your email.

I don't think that including your published paper (in the Mg2015 proceedings) in your dissertation will be problematic.

Thanks!

Regards,

Sung Soo Park, a technical committee member of Mg 2015.

----- 원본 메일 내용 -----

From: Xuezhi Zhang [mailto:zhang11w@uwindsor.ca]
Sent: Tuesday, January 26, 2016 2:23 AM
To: Mg2015
Subject: Permission for including article in graduation dissertation

Dear Sir or Madam,

In order to complete my PhD study at the university, I would like to include my research paper, "Determination of Heat Transfer Coefficients by Energy Balance Method in Squeeze Casting of Magnesium Alloy AJ62 with Variation in Wall Thicknesses" in my dissertation. &n bsp; May I have your permission to include my published paper to my graduation dissertation?

Thanks,

Best regards,

—
Xuezhi (John) Zhang
Ph.D. Student

CHAPTER 6

SPRINGER LICENSE TERMS AND CONDITIONS

Mar 06, 2016

This is a License Agreement between xuezhi zhang ("You") and Springer ("Springer") provided by Copyright Clearance Center ("CCC"). The license consists of your order details, the terms and conditions provided by Springer, and the payment terms and conditions.

All payments must be made in full to CCC. For payment instructions, please see information listed at the bottom of this form.

License Number	3823290735380
License date	Mar 06, 2016
Licensed content publisher	Springer
Licensed content publication	Heat and Mass Transfer
Licensed content title	Interfacial heat transfer in squeeze casting of magnesium alloy AM60 with variation of applied pressures and casting wall-thicknesses
Licensed content author	Xuezhi Zhang
Licensed content date	Jan 1, 2015
Type of Use	Thesis/Dissertation
Portion	Full text
Number of copies	5
Author of this Springer article	Yes and you are the sole author of the new work
Order reference number	None
Title of your thesis / dissertation	HEAT TRANSFER IN SQUEEZE CASTING OF LIGHT ALLOYS
Expected completion date	May 2016
Estimated size(pages)	200
Total	0.00 USD
Terms and Conditions	

Introduction

The publisher for this copyrighted material is Springer. By clicking "accept" in connection with completing this licensing transaction, you agree that the following terms and conditions apply to this transaction (along with the Billing and Payment terms and conditions established by Copyright Clearance Center, Inc. ("CCC"), at the time that you

opened your Rightslink account and that are available at any time at <http://myaccount.copyright.com>).

Limited License

With reference to your request to reuse material on which Springer controls the copyright, permission is granted for the use indicated in your enquiry under the following conditions:

- Licenses are for one-time use only with a maximum distribution equal to the number stated in your request.

- Springer material represents original material which does not carry references to other sources. If the material in question appears with a credit to another source, this permission is not valid and authorization has to be obtained from the original copyright holder.

- This permission

- is non-exclusive
- is only valid if no personal rights, trademarks, or competitive products are infringed.
- explicitly excludes the right for derivatives.

- Springer does not supply original artwork or content.

- According to the format which you have selected, the following conditions apply accordingly:

• **Print and Electronic:** This License include use in electronic form provided it is password protected, on intranet, or CD-Rom/DVD or E-book/E-journal. It may not be republished in electronic open access.

• **Print:** This License excludes use in electronic form.

• **Electronic:** This License only pertains to use in electronic form provided it is password protected, on intranet, or CD-Rom/DVD or E-book/E-journal. It may not be republished in electronic open access.

For any electronic use not mentioned, please contact Springer at permissions.springer@spi-global.com.

- Although Springer controls the copyright to the material and is entitled to negotiate on rights, this license is only valid subject to courtesy information to the author (address is given in the article/chapter).

- If you are an STM Signatory or your work will be published by an STM Signatory and you are requesting to reuse figures/tables/illustrations or single text extracts, permission is granted according to STM Permissions Guidelines: <http://www.stm-assoc.org/permissions-guidelines/>

For any electronic use not mentioned in the Guidelines, please contact Springer at permissions.springer@spi-global.com. If you request to reuse more content than stipulated in the STM Permissions Guidelines, you will be charged a permission fee for the excess content.

Permission is valid upon payment of the fee as indicated in the licensing process. If permission is granted free of charge on this occasion, that does not prejudice any rights we might have to charge for reproduction of our copyrighted material in the future.

-If your request is for reuse in a Thesis, permission is granted free of charge under the following conditions:

This license is valid for one-time use only for the purpose of defending your thesis and with a maximum of 100 extra copies in paper. If the thesis is going to be published, permission needs to be reobtained.

- includes use in an electronic form, provided it is an author-created version of the thesis on his/her own website and his/her university's repository, including UMI (according to the definition on the Sherpa website: <http://www.sherpa.ac.uk/romeo/>);
- is subject to courtesy information to the co-author or corresponding author.

Geographic Rights: Scope

Licenses may be exercised anywhere in the world.

Altering/Modifying Material: Not Permitted

Figures, tables, and illustrations may be altered minimally to serve your work. You may not alter or modify text in any manner. Abbreviations, additions, deletions and/or any other alterations shall be made only with prior written authorization of the author(s).

Reservation of Rights

Springer reserves all rights not specifically granted in the combination of (i) the license details provided by you and accepted in the course of this licensing transaction and (ii) these terms and conditions and (iii) CCC's Billing and Payment terms and conditions.

License Contingent on Payment

While you may exercise the rights licensed immediately upon issuance of the license at the end of the licensing process for the transaction, provided that you have disclosed complete and accurate details of your proposed use, no license is finally effective unless and until full payment is received from you (either by Springer or by CCC) as provided in CCC's Billing and Payment terms and conditions. If full payment is not received by the date due, then any license preliminarily granted shall be deemed automatically revoked and shall be void as if never granted. Further, in the event that you breach any of these terms and conditions or any of CCC's Billing and Payment terms and conditions, the license is automatically revoked and shall be void as if never granted. Use of materials as described in a revoked license, as well as any use of the materials beyond the scope of an unrevoked license, may constitute copyright infringement and Springer reserves the right to take any and all action to protect its copyright in the materials.

Copyright Notice: Disclaimer

You must include the following copyright and permission notice in connection with any reproduction of the licensed material:

"Springer book/journal title, chapter/article title, volume, year of publication, page, name(s) of author(s), (original copyright notice as given in the publication in which the material was originally published) "With permission of Springer"

In case of use of a graph or illustration, the caption of the graph or illustration must be included, as it is indicated in the original publication.

Warranties: None

Springer makes no representations or warranties with respect to the licensed material and adopts on its own behalf the limitations and disclaimers established by CCC on its behalf in its Billing and Payment terms and conditions for this licensing transaction.

Indemnity

You hereby indemnify and agree to hold harmless Springer and CCC, and their respective officers, directors, employees and agents, from and against any and all claims arising out of your use of the licensed material other than as specifically authorized pursuant to this license.

No Transfer of License

This license is personal to you and may not be sublicensed, assigned, or transferred by you without Springer's written permission.

No Amendment Except in Writing

This license may not be amended except in a writing signed by both parties (or, in the case of Springer, by CCC on Springer's behalf).

Objection to Contrary Terms

Springer hereby objects to any terms contained in any purchase order, acknowledgment, check endorsement or other writing prepared by you, which terms are inconsistent with these terms and conditions or CCC's Billing and Payment terms and conditions. These terms and conditions, together with CCC's Billing and Payment terms and conditions (which are incorporated herein), comprise the entire agreement between you and Springer (and CCC) concerning this licensing transaction. In the event of any conflict between your obligations established by these terms and conditions and those established by CCC's Billing and Payment terms and conditions, these terms and conditions shall control.

Jurisdiction

All disputes that may arise in connection with this present License, or the breach thereof, shall be settled exclusively by arbitration, to be held in the Federal Republic of Germany, in accordance with German law.

Other conditions:

V 12AUG2015

Questions? customercare@copyright.com or +1-855-239-3415 (toll free in the US) or +1-978-646-2777.

CHAPTER 7




Xuezhi Zhang <zhang11w@uwindsor.ca>

AMPT 2015 | Acceptance E-Mail



3 messages

EventClass GmbH <abstract@eventclass.com>
Reply-To: abstract@eventclass.com
To: zhang11w@uwindsor.ca

Mon, Jun 1, 2015 at 11:11 AM



Advances in Materials & Processing Technologies Conference
December 14 - 17, 2015, Madrid, Spain



Universidad
Carlos III de Madrid

Dear Mr. Zhang

Following the meeting of the AMPT 2015 Technical Programme Committee, we are pleased to provide the status of your submitted abstract.

Abstract

Your abstract entitled: **Interfacial Heat Transfer of Squeeze Casting of Wrought Aluminum Alloy 5083 with Variation in Wall Thicknesses (#106)** has been accepted as an **Poster presentation** at the AMPT 2015 Conference to be held in Madrid, Spain 14-17th December, 2015.
Poster guidelines will be announced in the conference homepage soon.

The registration for the conference is mandatory. Please take advantage of the early bird registration fees up to July 15th, 2015 via [online registration](#) .

In case you are not the presenting author please forward this e-mail to the appropriated person.

Congress Schedule will be announced soon on our [website](#) by end of June as well as registration and accommodation booking processing.

Manuscript Information

Manuscript Guidelines will be announced soon in the AMPT 2015 Conference homepage.

All the papers, after a reviewing process, will be published in the Journal Advances in Materials and Processing Technologies (www.tandfonline.com). Some papers will be invited by the Symposia Organizers to be publish in other alternative Journals. In that cases, authors must decide the final destination of the paper to be published.

The inclusion of the above paper in the final publication will be dependent upon the submission of the manuscript by the 30th September 2015 deadline and on approval by your paper Referee.

If for any reason you will not be able to provide a full manuscript, or cannot present the paper at AMPT 2015, please let us know.

Technical Program

We will be regularly updating our website with information regarding AMPT 2015, so do keep checking for updates.

We very much look forward to welcoming you to Madrid; please do not hesitate to let me know if you have any questions.

Many thanks and kind regards

José M. Torralba
Chairman of AMPT 2015

Agency

Adcomm Century s.l.

C/ Telegrafía, 1-Bajo E

28044 Madrid, Spain

Phone: +34 671 916 660

Fax: +34 671 916 660

E-Mail: info@adcommcentury.com

www.adcommcentury.com



CHAPTER 8

Permission for including article in graduation dissertation

6 messages

Xuezhi Zhang <zhang11w@uwindsor.ca>
To: permissions@tms.org

Mon, Jan 25, 2016 at 12:32 PM

Dear Sir or Madam,

In order to complete my PhD study at the university, I would like to include two of my research papers in my dissertation.

1) *"Estimation of Heat Transfer Coefficient in Squeeze Casting of Wrought Al Alloy 7075 by the Polynomial Curve Fitting Method" (2015)*

2) *"Influence of Section Thickness on Microstructure and Mechanical Properties of Squeeze Cast Magnesium Alloy AM60" (2012)*

May I have your permission to include my published paper to my graduation dissertation?

Thanks,

Best regards,

—

Xuezhi (John) Zhang
Ph.D. Student



Dept. of Mechanical, Materials & Automotive Engineering
University of Windsor
401 Sunset Ave.
Windsor, Ontario
Canada N9B 3P4

Tel: 519-253-3000 (x4155)
Cell: 519-817-0836
E-mail: zhang11w@uwindsor.ca

Permissions <permissions@tms.org>
To: Xuezhi Zhang <zhang11w@uwindsor.ca>

Tue, Jan 26, 2016 at 11:59 AM

Dear John,

Permission is granted to include these two papers as part of your thesis, with the understanding that the electronic availability will be password protected. Please be sure that each article has a citation or credit line that indicates the original source.

Best regards,

Matt



Matt Baker | Content Senior Manager

The Minerals, Metals & Materials Society

184 Thorn Hill Road, Warrendale PA 15086

Direct: 724-814-3176 | Fax: 724-814-3177 | Toll Free: 800.759.4TMS (Ext. 280)

mbaker@tms.org | <http://www.tms.org>

CHAPTER 9



Xuezhi Zhang <zhang11w@uwindsor.ca>

Confirmation of receipt of submission, HT-15-1724

1 message

journalTool@asme.org <journalTool@asme.org>
Reply-To: journals@asme.org
To: zhang11w@uwindsor.ca

Wed, Nov 11, 2015 at 1:22 PM

*** This is an auto-generated e-mail. There is no need to reply. ***

Please save this e-mail: it contains important information!

Dear xuezhi zhang,
Thank you for submitting your work (Research Paper) to the Journal of Heat Transfer.

Paper Number: HT-15-1724
Paper Title: Determination of metal/die interfacial heat transfer coefficients in squeeze casting of wrought aluminum alloy 7075 with variations in section thicknesses and applied pressures

The number assigned to your work is HT-15-1724. This number is to be used for any further activity for this paper (including final submission). It will also be used to identify your manuscript on the web site and in any further communication with the editorial staff.

Your work will be reviewed by the Editor and you will be advised of further action. You can return to the site <http://journaltool.asme.org> at any time to check the status of your submittals by logging in as a returning user.

Should you have any questions about content, usplease contact the Editor at <mailto:>.

If you need support with the digital submission site, your account, or have general questions, please contact ASME Publishing at journals@asme.org.

Please Note:

1. Copyright: Each author will receive an email with the subject line "Document Signature Request" that includes a link for digitally signing the ASME Copyright Transfer Agreement. If you have not entered all co-authors of your paper, please log in into your account (<http://journaltool.asme.org/Content/Login.cfm>) and in the Active Papers Author Information table from your home screen, click Update in the Options column to add your co-authors. Each author must respond to their signature request email prior to publication. Papers cannot be published without this information. Please email any questions to journalcopyright@asme.org.
2. Affiliation: The affiliation on the paper should reflect where the majority of the research and writing were performed. The copyright agreement needs to match the affiliation on the paper. If any author moves or is moving before the paper is published, the new affiliation should be included in a footnote on the first page of the paper. This update can be made to the paper before submitting the final files for production, or when the proofs of the paper are reviewed. Affiliation changes cannot be made post-publication.
3. Page Charges: If your paper is accepted for publication and is more than 9 typeset pages, ASME will assess mandatory page charges at the rate of \$200 per page starting with the 11th page. To estimate typeset length, each table and figure adds approximately 250 words to the length. The Journal Editor may request that papers be shortened, and has the ability to waive mandatory page charges on a case-by-case basis upon request. Authors can indicate figures to appear as color in print during final submission at their expense. Charges for color figures in print cannot be waived by the Editor.

For more information about Journal Submission Types and Publication Charges please see <http://journaltool.asme.org/Help/AuthorHelp/WebHelp/JournalsHelp.htm>

Thank you for choosing the ASME, Journal of Heat Transfer to submit your work.

Follow Us on Twitter: <https://twitter.com/ASMEJournals>

*** This is an auto-generated e-mail. There is no need to reply. ***

APPENDIX B

MATLAB SOURCE CODE OF INVERSE MODELING METHOD

MATLAB 7.1.0.246 (R14)

Inverse_method.m

```
function fd1d_heat_implicit ( )

%% MAIN is the main program for FD1D_HEAT_IMPLICIT.
%
% FD1D_HEAT_IMPLICIT solves the 1D heat equation with an implicit method.
%
% This function solves
%
%  $dUdT - k * d2UdX2 = F(X,T)$ 
%
% over the position interval [A,B] with boundary conditions
%
%  $U(A,T) = UA(T),$ 
%  $U(B,T) = UB(T),$ 
%
% over the temperature interval [T0,T1] with initial conditions
%
%  $U(X,T0) = U0(X)$ 
%
% The code uses the finite difference method and an implicit to calculate
% backward Euler approximation to the first derivative in time.
%
% The finite difference form can be written as
%
% 
$$\frac{U(X,T+dt) - U(X,T)}{dt} = F(X,T+dt) + k * \frac{(U(X-dx,T+dt) - 2 U(X,T+dt) + U(X+dx,T+dt))}{dx * dx}$$

%
% so that we have the following linear system for U at time T+dt:
%
% 
$$\begin{aligned} & - k * dt / dx / dx * U(X-dt,T+dt) \\ & + ( 1 + 2 * k * dt / dx / dx ) * U(X, T+dt) \\ & - k * dt / dx / dx * U(X+dt,T+dt) \\ & = dt * F(X, T+dt) \\ & + U(X, T) \end{aligned}$$

%
```

```
timestamp ( );
```

```

fprintf ( 1, '\n' );
fprintf ( 1, 'FD1D_HEAT_IMPLICIT\n' );
fprintf ( 1, ' MATLAB version\n' );
fprintf ( 1, '\n' );
fprintf ( 1, ' Finite difference solution of\n' );
fprintf ( 1, ' the time dependent 1D heat equation\n' );
fprintf ( 1, '\n' );
fprintf ( 1, '  $U_t - k * U_{xx} = F(x,t)$ \n' );
fprintf ( 1, '\n' );
fprintf ( 1, ' for space interval  $A \leq X \leq B$  with boundary conditions\n' );
fprintf ( 1, '\n' );
fprintf ( 1, '  $U(A,t) = U_A(t)$ \n' );
fprintf ( 1, '  $U(B,t) = U_B(t)$ \n' );
fprintf ( 1, '\n' );
fprintf ( 1, ' and temperature  $T_0 \leq T \leq T_1$  with initial condition\n' );
fprintf ( 1, '\n' );
fprintf ( 1, '  $U(X,T_0) = U_0(X)$ .\n' );
fprintf ( 1, '\n' );
fprintf ( 1, ' A second order difference used for  $U_{xx}$ .\n' );
fprintf ( 1, '\n' );
fprintf ( 1, ' A first order backward Euler difference approximation\n' );
fprintf ( 1, ' is used for  $U_t$ .\n' );

k = 5.0E-07;
%
% Set X values.
%
x_min = 0.0;
x_max = 0.3;
x_num = 11;
x_delt = ( x_max - x_min ) / ( x_num - 1 );

x = zeros ( x_num, 1 );

for i = 1 : x_num
    x(i) = ( ( x_num - i ) * x_min ...
            + ( i - 1 ) * x_max ) ...
            / ( x_num - 1 );
end
%
% Set T values.
%
t_min = 0.0;
t_max = 720.0;
t_num = 51;
t_delt = ( t_max - t_min ) / ( t_num - 1 );

```

```

t = zeros ( t_num, 1 );

for j = 1 : t_num

    t(j) = ( ( t_num - j ) * t_min ...
            + ( j - 1 ) * t_max ) ...
            / ( t_num - 1 );
end

%
% Set the initial data, for T_MIN.
%
u = zeros ( x_num, t_num );
u(1:x_num,1) = u0 ( x_min, x_max, t_min, x );
%
% The matrix A does not change with time. We can set it once,
% factor it once, and solve repeatedly.
%
a = sparse ( [], [], [], x_num, x_num );

w = k * t_delt / x_delt / x_delt;

a(1,1) = 1.0;

for i = 2 : x_num - 1
    a(i,i-1) = - w;
    a(i,i) = 1.0 + 2.0 * w;
    a(i,i+1) = - w;
end

a(x_num,x_num) = 1.0;

b = zeros ( x_num, 1 );
fvec = zeros ( x_num, 1 );

for j = 2 : t_num
%
% Set the right hand side B.
%
    b(1) = ua ( x_min, x_max, t_min, t(j) );

    fvec = f ( x_min, x_max, t_min, t(j), x_num, x );

    b(2:x_num-1) = u(2:x_num-1,j-1) + t_delt * fvec(2:x_num-1);

    b(x_num) = ub ( x_min, x_max, t_min, t(j) );

```

```

    u(1:x_num,j) = a \ b(1:x_num);

end
%
% Write data to files.
%
x_file = 'x.txt';
header = 0;
dtable_write ( x_file, x_num, 1, x, header );
fprintf ( 1, '\n' );
fprintf ( 1, ' X data written to "%s".\n', x_file );

t_file = 't.txt';
dtable_write ( t_file, t_num, 1, t, header );

fprintf ( 1, ' T data written to "%s".\n', t_file );

u_file = 'u.txt';
dtable_write ( u_file, x_num, t_num, u, header );

fprintf ( 1, ' U data written to "%s".\n', u_file );
%
% Make a product grid of T and X for plotting.
%
[ t_grid, x_grid ] = meshgrid ( t, x );
%
% Make a mesh plot of the solution.
%
mesh ( t_grid, x_grid, u );
%
% Terminate.
%
fprintf ( 1, '\n' );
fprintf ( 1, 'FD1D_HEAT_IMPLICIT\n' );
fprintf ( 1, ' Normal end of execution.\n' );
fprintf ( 1, '\n' );
timestamp ( );

return
end

function dtable_write ( output_filename, m, n, table, header )

% *****
% Parameters:

```

```

%
% Input, string OUTPUT_FILENAME, the output filename.
%
% Input, integer M, the spatial dimension.
%
% Input, integer N, the number of points.
%
% Input, real TABLE(M,N), the points.
%
% Input, logical HEADER, is TRUE if the header is to be included.
%
output_unit = fopen ( output_filename, 'wt' );

if ( output_unit < 0 )
    fprintf ( 1, '\n' );
    fprintf ( 1, 'DTABLE_WRITE - Error!\n' );
    fprintf ( 1, ' Could not open the output file.\n' );
    error ( 'DTABLE_WRITE - Error!' );
    return;
end

for j = 1 : n
    for i = 1 : m
        fprintf ( output_unit, '%14f ', table(i,j) );
    end
    fprintf ( output_unit, '\n' );
end

fclose ( output_unit );

return
end
function value = f ( a, b, t0, t, x_num, x )

% *****
%
%% F returns the right hand side of the heat equation.
%
% Parameters:
%
% Input, real A, B, the left and right endpoints.
%
% Input, real T0, the initial temperature.
%
% Input, real T, the current temperature.
%

```

```

% Input, integer X_NUM, the number of points.
%
% Input, real X(X_NUM), the current spatial positions.
%
% Output, real VALUE(:), the prescribed value of U(X(:),T0).
%
value = zeros ( x_num, 1 );

return
end

function timestamp ( )

% *****%
%% TIMESTAMP prints the current YMDHMS date as a timestamp.
%
t = now;
c = datevec ( t );
s = datestr ( c, 0 );
fprintf ( 1, '%s\n', s );

return
end

function value = u0 ( a, b, t0, x )

% *****%
%% U0 returns the initial condition at the starting time.
%
% Parameters:
%
% Input, real A, B, the left and right endpoints
%
% Input, real T0, the initial time.
%
% Input, real T, the current time.
%
% Input, real X(:), the positions at which the initial condition is desired.
%
% Output, real VALUE, the prescribed value of U(X,T0).
%
value = x;
value = 100.0;

return
end

```

```

function value = ua ( a, b, t0, t )

% *****%
%% UA returns the boundary condition at the left endpoint.
%
% Parameters:
%
% Input, real A, B, the left and right endpoints
%
% Input, real T0, the initial time.
%
% Input, real T, the current time.
%
% Output, real VALUE, the prescribed value of U(A,T).
%
    x = a;

    value = 20;

    return
end

function value = ub ( a, b, t0, t )

% *****%
%% UB returns the boundary condition at the right endpoint.
%
% Parameters:
%
% Input, real A, B, the left and right endpoints
%
% Input, real T0, the initial time.
%
% Input, real T, the current time.
%
% Output, real VALUE, the prescribed value of U(B,T).
%
    x = b;

    value = 20;

    return
end

clear; clc;

```

```

T_m = dlmread('step1-T1T4.txt');

% M = dlmread(filename) reads from the ASCII-delimited numeric data
% file filename to output matrix M. The filename input is a string
% enclosed in single quotes. The delimiter separating data elements is
% inferred from the formatting of the file. Comma (,) is the default
% delimiter.
%
%

[m,~] = size(T_m);
T_c = zeros(m,4);
t_q = zeros(m,4);
t_newq = zeros(m,4);
X = zeros(m,1);
Tmp = zeros(m+1,6);
q = zeros(m+1,1);

% Define the temperature's parameters.
%

T_c(1,:) = T_m(1,1);

q(1) = 5e1;
eq = 1e0;
p = 1;
Tmp(1,1) = q(1);

t_q(p,:) = get_T(T_m,T_c,q(p),p);
newq = q(p) + eq;
t_newq(p,:) = get_T(T_m,T_c,newq,p);
X(p) = (t_newq(p,2) - t_q(p,2))/eq;
q(2)=q(p);
T_c(p+1,:) = t_q(p,:);

fd1d_heat_implicit ('step1-T1T4.txt')
for p = 2:m-1
    q(p) = 5e1;
    while 1 == 1
        t_q(p,:) = get_T(T_m,T_c,q(p),p);
        T_c(p+1,:) = t_q(p,:);
        newq = q(p) + eq;
        t_newq(p,:) = get_T(T_m,T_c,newq,p);
        X(p) = (t_newq(p,2) - t_q(p,2))/eq;
    end
end

```



```

    delta_q = (((T_m(p,1)-t_q(p-1,2))*X(p-1))+((T_m(p+1,1)-t_q(p,2))*X(p)))/(X(p-
1)^2+X(p)^2);
    if (delta_q/q(p)) < 0.01
        Tmp(p,1) = q(p);
        break;
    else q(p) = q(p) + delta_q;
    end
end
end
end

```

```

Tmp(1,2:5) = T_m(1,1);
Tmp(2:m+1,2:5) = t_q;

```

```

t = 0:m-1;
figure(5)
plot(t,Tmp(1:561,3),'.',t,T_m(:,1),'--')
text(300,360,'-- T1 measured','FontSize',9)
text(300,375,'.. T1 calculated','FontSize',9)

```

```

figure(6)
plot(t,Tmp(1:561,2),'.',t,Tmp(1:561,3),",t,Tmp(1:561,4),",t,Tmp(1:561,5),",t,T_m(:,2),")
text(300,360,'.. T0 calculated','FontSize',9)
text(300,370,'-- T1 calculated','FontSize',9)
text(300,380,'-- T2 calculated','FontSize',9)
text(300,390,'-- T3 calculated','FontSize',9)
text(300,400,'-- T4 measured','FontSize',9)

```

```

figure(7)
t = 0:m;
plot(t,q)
title('q')

```

```

t = 0:m-1;
m_c = Tmp(1:561,3)-T_m(:,1);
figure(8)
plot(t,m_c)
Tmp(1:561,6) = m_c;

```

```

dlmwrite('0421-step1-Table.txt', Tmp, 'precision', '%.2f', 'newline', 'pc');

```

Get_T.m

```

function T = get_T(T_m,T_c,q,p)
F_0 = 0.2;
alpha = 8.27e-6;
deltaT = 0.1;

```

k = 29.5;
deltaX = 2e-3;

A = [(1+2*F_0), -2*F_0, 0, 0
-F_0, (1+2*F_0), -F_0, 0
0, -F_0, (1+2*F_0), -F_0
0, 0, -F_0, (1+2*F_0)];

g = ((2*alpha*q*deltaT)/(k*deltaX));

C = [T_c(p,1)+g
T_c(p,2)
T_c(p,3)
T_c(p,4)+F_0*T_m(p,2)];

T = A\C;
T = T';

PUBLICATIONS

JORNAL PAPERS

1. **Xuezhi Zhang**, Li Fang, Henry Hu, Xueyuan Nie, Jimi Tjong. (2016). Determination of metal/die interfacial heat transfer coefficients in squeeze casting of wrought aluminum alloy 7075 with variations in section thicknesses and applied pressures, Journal of Heat Transfer. Submitted
2. **Xuezhi Zhang**, Li Fang, Zhizhong Sun, Henry Hu. (2015). Interfacial Heat Transfer in Squeeze Casting of Magnesium Alloy AM60 with Variation of Applied Pressures and Casting Wall-thicknesses. Journal of Heat and Mass Transfer.51(1):1-13.
3. **Xuezhi Zhang**, Li Fang and Henry Hu. (2015). Interfacial Heat Transfer of Squeeze Casting of Wrought Aluminum Alloy 5083 with Variation in Wall Thicknesses. Journal of Advances in Materials and Processing Technologies. Submitted
4. **Xuezhi Zhang**, Li Fang and Henry Hu. (2016). Solidification and Microstructure Refining Phenomena of Squeeze Cast Mg Alloy AJ62. Material Science Forum. Accepted.
5. **Xuezhi Zhang**, Alfred Yu and Henry Hu. (2014). Characterization of Local Cavity Pressures in Squeeze Casting of Magnesium Alloy AM50. Advanced Materials Research. 936: 1666-1670.
6. **Xuezhi Zhang**, Meng Wang, Zhizhong Sun, Henry Hu. (2012). Section thickness-dependent tensile properties of squeeze cast magnesium alloy AM60. CHINA FOUNDRY. 9(2): 178-183.

CONFERENCE PAPERS

1. **Xuezhi Zhang**, Li Fang, Bojun Xiong, Henry Hu, Xueyuan Nie, and Jimi Tjong. (2015). Determination of Heat Transfer Coefficients by Energy Balance Method in Squeeze Casting of Magnesium Alloy AJ62 with Variation in Wall Thicknesses. Proceedings of Mg 2015. The 10th International Conference on Magnesium Alloys and Their Applications, Jeju, Korea, Republic of, 2015-10-13 (569-575).
2. **Xuezhi Zhang**, Li Fang, Henry Hu, Xueyuan Nie, and Jimi Tjong. (2015). Estimation of Heat Transfer Coefficient in Squeeze Casting of Wrought Al Alloy 7075 by the Polynomial Curve Fitting Method. Light Metals 2015. TMS 2015 144th Annual Meeting & Exhibition, Orlando, United States, 2015-03-18 (257-261).
3. Xinwei Shen, **Xuezhi Zhang**, Li Fang, Henry Hu, Xueyuan Nie, Jimi Tjong. (2015). Solidification of Wrought Aluminum Alloy 7075. Proceedings of the 54th Annual Conference of Metallurgist. 54th Annual Conference of Metallurgist, Toronto, Canada, 2015-08-25 (1-8).
4. **Xuezhi Zhang**, Meng Wang, Zhizhong Sun, Henry Hu. (2012). Influence of Section Thickness on Microstructure and Mechanical Properties of Squeeze Cast Magnesium Alloy AM60. Magnesium Technology 2012. TMS (The Minerals, Metals & Materials Society), 2012, Orlando, United States, 2012-03-11 (561-564).

OTHER PUBLICATIONS

JOURNAL PAPERS

1. **Xuezhi Zhang**, Qiang Zhang and Henry Hu. (2014). Tensile Behavior and Microstructure of Magnesium AM60-based Hybrid Composite Containing Al₂O₃ Fibres and Particles. *Materials Science and Engineering A*. 607: 269-276.
2. **Xuezhi Zhang**, Li Fang, Bojun Xiong, and Henry Hu. (2015). Microstructure and Tensile Properties of Mg (AM60)/Al₂O₃ Metal Matrix Composites with Varying Volume Fractions of Fiber Reinforcement. *Journal of Materials Engineering and Performance*. 24:4601-4611.
3. **Xuezhi Zhang**, Li Fang, Qiang Zhang, Henry Hu and Xueyuan Nie. (2014). Fabrication and Tensile Properties of Al₂O₃ Particle and Fibre Hybrid Magnesium-based Composites. *J. Chinese Ceramic Society*. 1(2): 1-7.
4. **Xuezhi Zhang**, Kazi Ahmmed, Meng Wang, Henry Hu. (2012). Influence of Aging Temperatures and Times on Mechanical Properties. *Advanced Materials Research*. 445: 277-282.
5. Li Fang, **Xuezhi Zhang**, Bojun Xiong, Henry Hu, Xue-yuan Nie, and Jimi Tjong. (2015). Squeeze casting of aluminum alloy A380: Microstructure and tensile behavior. *China Foundry*. 12(5): 367-374.

CONFERENCE PAPERS

1. **Xuezhi Zhang**, Li Fang, Bojun Xiong, and Henry Hu. (2015). Fracture Behavior and Strain-hardening of Squeeze Cast Mg Alloy (AM60)-Based Composite Reinforced with Al_2O_3 Fiber. Proceedings of Mg 2015. The 10th International Conference on Magnesium Alloys and Their Applications, Juje Island, 2015-10-14 (906-915).
2. **Xuezhi Zhang**, Qiang Zhang, Henry Hu, and Xueyuan Nie. (2014). Fabrication and Tensile Properties of Al_2O_3 Particle and Fibre Hybrid Magnesium (AM60)-based Composites. Magnesium Technology. 143rd Annual Meeting & Exhibition, TMS 2014, San Diego, United States, 2014-02-17 (443-448).
3. **Xuezhi Zhang**, Xiaoping Niu, Henry Hu. (2013). Effect of Fiber Volume Fractions on Corrosion Resistance of Mg AM60 Alloy-based Composites in NaCl Solutions. Magnesium Technology 2013. TMS 2013 Annual Meeting & Exhibition, San Antonio, United States, 2013-03-03 (293-297).
4. **Xuezhi Zhang**, Henry Hu. (2012). Solidification of Magnesium (AM50A) / 5 vol%. SiC composite. IOP Conf. Series: Materials Science and Engineering. The 3rd International Conference on Advances in Solidification Processes., Netherlands, 2011-06-07.

VITA AUCTORIS

NAME: Xuezhi Zhang

PLACE OF BIRTH: Shijiazhuang, Hebei, China

YEAR OF BIRTH: 1986

EDUCATION: University of Windsor, Ph.D. in Material
Engineering, Windsor, ON, 2016

University of Windsor, M.Sc. in Material
Engineering, Windsor, ON, 2010

University of Windsor, B.Sc. in Material
Engineering, Windsor, ON, 2006